

**Quantitative detection of trace gas species in the atmosphere
using LED Broadband Cavity Enhanced Absorption Spectroscopy**

**Thesis submitted for the degree of
Doctor of philosophy
At the University of Leicester**

**By
Anna Hollingsworth
Atmospheric Chemistry Group
Department of Chemistry
University of Leicester**

September 2010

Abstract

A broadband version of cavity enhanced absorption spectroscopy (BBCEAS) has been applied to measure the ambient concentrations of reactive trace gases, particularly nitrogen dioxide (NO_2) in the polluted urban environment and molecular iodine (I_2) in the marine boundary layer. The spectrometer's light source, a light emitting diode (LED), enables absorption spectra of gas samples to be acquired over 50 nm bandwidths at visible and near-ultraviolet wavelengths. Differential optical absorption spectroscopy (DOAS) is then applied to unambiguously identify and quantify the various absorbers present in the samples.

Especially difficult operating conditions were encountered during the instrument's first field deployment onboard the research vessel RRS Discovery. As a result, the instrument did not achieve the I_2 detection limits it had demonstrated in laboratory testing and was unable to detect any I_2 signal in the mid-Atlantic Ocean during the Reactive Halogens in the Marine Boundary Layer Experiment. However, iodine was detected around many night-time low tides during the BIOFLUX II campaign at the Mace Head Atmospheric Research Station in County Galway, Ireland. The maximum I_2 concentration of 608 pptv (parts per trillion by volume) correlated with the campaign's lowest tide, and is three times greater than any previous report of atmospheric I_2 concentrations. The BIOFLUX observations support current understanding that coastal I_2 derives from seaweed (particularly kelp species) exposed to air around low tide.

LED-BBCEAS measurements of NO_2 made on the University campus during the Leicester Air Quality Measurement Project are compared with data from two chemiluminescence instruments. The need to closely co-locate instruments during comparisons of the various techniques is discussed, and evidence of a possible interference in the chemiluminescence measurements has been found.

Acknowledgements

I would like to thank the following institutes and organisation who provided funding:
BIOFLUX II: an exchange visit sponsored by the European Science Foundation's
Research Networking Programme "Interdisciplinary Tropospheric Research: from the
Laboratory to Global Change (INTROP)". Academic host: Harald Berresheim, National
University of Ireland, Galway. Thanks also to the staff at the Mace Head Atmospheric
Research Station, and those fellow scientists measuring alongside me, particularly
Roisin Commane and Katja Seitz who kindly shared their data with me.

RHaMBLe: D319 cruise funded by The Natural Environment Research Council, grant
award NE/D00652X/1. The Discovery crew, they got me through the seasickness,
Gordon McFiggans (as principal investigator on the RHaMBLe Consortium), and the
other scientists onboard for making the experience truly one of a kind!

LAMP was organised by Dr Roland Leigh at the University of Leicester, SRC.

The Department of Chemistry, University of Leicester for my PhD studentship.

I also wish to thank my supervisor Dr S Ball, for his guidance, patience and general
loveliness over the last few years.

Finally I wish to thank my family for their continued support and encouragement. Mum
for always being on the end of the phone, a listening ear. My wonderful husband, Tim,
who has been my rock and friend since the day we first met.

Contents

1 Introduction	22
1.1 The Earth's atmosphere	23
1.2 Chemistry in the troposphere: OH and NO ₃	26
1.3 Air pollution and air quality control	29
1.3.1 Controlled atmospheric pollutants: PM, O ₃ and NO ₂	32
1.3.2. Current NO ₂ measurement across the UK	33
1.4 Nitrogen oxide chemistry in the troposphere	34
1.5 Iodine chemistry in the troposphere	35
1.5.1 Atmospheric iodine sources: seawater and terrestrial sources	38
1.5.2 Atmospheric iodine sources: biological, organic sources	40
1.5.3 Iodine sinks in the troposphere	43
1.5.4 Iodine and ozone destruction	44
1.5.5 Iodine and HO ₂ /OH chemistry	47
1.5.6 Iodine and dimethyl sulphide chemistry	49
1.5.7 Iodine and particle formation	50
1.5.8 Field measurements and their implications	54
1.6 Motivation for this work	57

2 Introduction to spectroscopy and cavity based spectroscopic techniques	58
2.1 Introduction to spectroscopy	58
2.1.1 Energy levels in atoms and molecules	60
2.2 Spectroscopic methods	64
2.2.1 Absorption spectroscopy	65
2.3 Cavity based spectroscopy techniques	69
2.3.1 A brief history of cavity techniques	70
2.3.2 Cavity Ring Down Spectroscopy	71
2.3.3 Cavity enhanced absorption spectroscopy (CEAS)	75
2.4 Broad Band Cavity Enhanced Absorption Spectroscopy (BBCEAS)	76
2.4.1 BBCEAS for atmospheric samples	78
2.4.2 Mirror reflectivity determination: theory	79
2.4.3 Differential Optical Absorption Spectroscopy	80
2.5 Summary	84
3 LED BBCEAS instrument: development and operation	87
3.1. Introduction	87
3.2. The BBCEAS instrument: general overview	88
3.3 BBCEAS light source: Light emitting diode (LED)	92

3.3.1 Light source investigations: LED emission spectrum	93
3.3.2 LED investigations: Temperature effects on LED emission spectra	96
3.4 The BBCEAS optical cavity	100
3.5. Detectors: spectrometers and CCD imaging	102
3.5.1 Chromex 250is and Wright Instruments CCD camera	103
3.5.2 Ocean Optics high resolution spectrometer	108
3.6 BBCEAS instrument stability	109
3.6.1 Vibrational stability	109
3.6.2 Thermal stability	111
3.7 Analysis of BBCEAS data to obtain absorber concentration	117
3.7.1 File import to analysis routine	118
3.7.2 Definition of cavity parameters and λ selection	119
3.7.3 Mirror reflectivity determination	121
3.7.4 Spectral analysis for trace gas quantification	122
3.8. Mirror reflectivity determination measurements	123
3.9. Lab measured spectra	129
3.9.1 Nitrous acid detection by BBCEAS	130
3.9.2 Survey of absorbers species in the visible region	132

3.10. Instrument adaptations for field deployment	137
4 Iodine measurements during D319: part of the Reactive Halogens in the Marine Boundary Layer (RHaMBLe) project	141
4.1. Introduction to RHaMBLe	141
4.2. D319 cruise track and air mass origin	142
4.3. D319 measurement instrumentation	146
4.3.1 Location of the BBCEAS instrument during D319	146
4.3.2 Operating parameters BBCEAS during D319	148
4.3.3 BBCEAS measurements on RSS Discovery	150
4.3.4. Cavity Mirror reflectivity measurement ($R(\lambda)$)	152
4.4. BBCEAS trace gas measurements during D319	155
4.4.1 BBCEAS of ambient water vapour during D319	155
4.4.2 BBCEAS of ambient NO_2 and I_2 during D319	159
4.5 Challenges of operating the BBCEAS instrument during D319	162
4.6 Summary and conclusion	165
5 Iodine measurements at Mace Head: the BIOFLUX II campaign	167
5.1 Introduction	167
5.2 Iodine chemistry and Mace Head	168

5.3. Aims & instrumentation for BIOFLUX II	174
5.4. Meteorological data during BIOFLUX II	177
5.5. The I ₂ BBCEAS INSTRUMENT and MEASUREMENTS during BIOFLUX II	180
5.5.1. Operating parameters BBCEAS during BIOFLUX II	181
5.5.2. Acquisition of I(λ) sample spectra and I ₀ (λ) nitrogen flush spectra	186
5.5.3 In situ calibration of mirror reflectivity using O ₄ absorption	187
5.5.4. Mathcad analysis routine details	189
5.5.5. Errors in retrieved concentrations for absorber species	192
5.6. Spectral analysis: water vapour retrievals and time series	194
5.7. Spectral analysis: Molecular Iodine retrievals and time series	200
5.7.1 BBCEAS derived iodine concentrations: 10 minute time series	201
5.7.2 Iodine correlation with tide and wind directions and discussion	204
5.7.3 Comparison of 10 minute BBCEAS analysis to Long Path DOAS data	213
5.7.4 Analysis of night of 30 th – 31 st August 2007 on 2 minute resolution	217
5.8 Summary and conclusion	219
6 BBCEAS measurements of NO₂ during the Leicester Air Quality Measurement Project	222
6.1 Introduction to LAMP	222

6.1.1 LAMP project aims	222
6.2 Review of NO ₂ instrumentation	223
6.2.1 Chemiluminescence detectors	223
6.2.2. TDLAS: Tuneable diode laser absorption spectroscopy	
detection of NO ₂	227
6.2.3 Cavity techniques to measure atmospheric NO ₂	229
<i>6.2.3.1 Cavity Attenuated Phase-shift Spectroscopy (CAPS).</i>	229
<i>6.2.3.2 Incoherent broadband CEAS</i>	231
<i>6.2.3.3 Pulsed cavity ring down</i>	234
6.2.4 Laser induced fluorescence (LIF) detection of NO ₂	235
6.2.5 Gas chromatography with luminol chemiluminescence detection (GC/LCD)	
for NO ₂	237
6.3. Instruments participating in the LAMP campaign	239
6.3.1 NO ₂ instrumentation and sampling positions during LAMP	241
6.4 LAMP site information and meteorological data	243
6.4.1 LAMP site information	243
6.4.2 LAMP meteorological data	244
6.5 BBCEAS instrument and measurements during LAMP	246

6.5.1 Operating parameters of the BBCEAS instrument during LAMP	247
6.5.2 BBCEAS measurements during LAMP	251
6.5.2.1 Operating parameters for ambient measurements	252
6.5.2.2 Operating parameters for O ₄ calibration measurements to determine mirror reflectivity curve	254
6.5.3 Mathcad analysis routine details	255
6.6. Spectral analysis: NO ₂ retrievals and time series	257
6.6.1 Weekday and weekend trends in NO ₂ concentration	263
6.7 Comparison of NO ₂ measurements from BBCEAS and other in situ monitors	266
6.7.1 Comparison of BBCEAS NO ₂ measurements to NO _{xy} photolysis-chemiluminescence instrument NO ₂ measurements	267
6.7.1.1 Exploring the correlation of O ₃ with NO _x data.	271
6.7.2 Comparison of BBCEAS NO ₂ measurements to the commercial chemiluminescence	275
6.7.3 Correlation of BBCEAS NO ₂ with other NO ₂ data sets	276
6.8 Summary and conclusions	279
6.9 Further work with the LAMP BBCEAS dataset	280
7 Conclusions	282
References	286

LIST OF FIGURES

Figure 1.1 The structure of the Earth's atmosphere	24
Figure 1.2 The Chapman cycle	25
Figure 1.3 Schematic of the atmospheric oxidation processes of OH and HO ₂	28
Figure 1.4 Measurement sites comprising the AURN monitoring system	33
Figure 1.5 Simplified scheme of tropospheric iodine photo oxidation	37
Figure 1.6 Time series of IO at Ein Bokek during 2 weeks of measurement	39
Figure 1.7 Accumulation and release of iodous species in Laminarias	41
Figure 1.8 Mixing ratio of I ₂ , IO and OIO by DOAS at Mace Head	43
Figure 1.9 The fractional importance of HO ₂ loss and OH formation reactions in the Coastal marine environment	48
Figure 1.10 Experimental set up from the study linking seaweed emissions to new particle formation	54
Figure 2.1 Absorption and emission processes	60
Figure 2.2. The electromagnetic spectrum	62
Figure 2.3. An illustration of a two electronic state system	63
Figure 2.4 Basic absorption of radiation incident onto a single absorber species gas sample	66
Figure 2.5. Light behaviour from a pulsed source inside an optical cavity	72

Figure 2.6. Light intensity within an optical cavity over time	72
Figure 2.7 Differential optical absorption spectroscopy for one absorber	82
Figure 2.8 Differential optical absorption spectroscopy for two absorbers	83
Figure 3.1. Schematic diagram of the optical layout of the LED BBCEAS	89
Figure 3.2 The BBCEAS instrument in the laboratory	91
Figure 3.3 Schematic of LED investigations	94
Figure 3.4 LED output from UV LEDs	96
Figure 3.5 The emission spectra of a near-UV LED recorded as a function of TEC mount's temperature set point	98
Figure 3.6 Cavity mirror surface structure	101
Figure 3.7 Optical layout of an imaging spectrograph, Chromex 250is	102
Figure 3.8 Mercury lamp emission for wavelength calibration of Chromex 250is	105
Figure 3.9 Schematic of part of the CCD array	106
Figure 3.10 View across UVIZEN data file to assign limits used for averaging for illuminated and dark sections CCD array	107
Figure 3.11 Scaffold mounting for field LED BBCEAS instrument	111
Figure 3.12 Measured dark current on CCD with Chromex spectrometer following power up.	113

Figure 3.13 Ocean optics HR2000 measured scans for illuminated and non-illuminated detector.	114
Figure 3.14 Dark current measurements made at different temperatures for the HR4000 Ocean Optics spectrometer	116
Figure 3.15 Outline of mathcad analysis routine used to for quantitative analysis of BBCEAS spectra	118
Figure 3.16 Fitting of oxygen absorption, 23 rd July 2007	127
Figure 3.17 Fitting of NO ₂ absorption 23 rd July 2007	128
Figure 3.18 Fitted spectrum of HONO, measured on 29 th November 2006	130
Figure 3.19 Fitting of oxygen absorption, 7 th November 2006	134
Figure 3.20 Fitting of NO ₂ absorption bands, 7 th November 2006	134
Figure 3.21 Fitted I ₂ BBCEAS spectrum, 7 th November 2006.	135
Figure 3.22 Fitted water vapour BBCEAS spectrum, 7 th November 2006	135
Figure 3.23 Fitted Br ₂ BBCEAS spectrum, 7 th November 2006.	136
Figure 3.24 The 19" rack housing the electronic components of the BBCEAS	138
Figure 3.25 BBCEAS cavity enclosures	139
Figure 4.1 RSS Discovery ship track during D319 cruise 2007	143
Figure 4.2. The 5 day back trajectories of air masses reaching RSS Discovery	145

Figure 4.3. Track of RHaMBLe Discovery Cruise D319 showing the MODIS retrieved chlorophyll a averaged for the month of May 2007	145
Figure 4.4 Diagram to illustrate positioning of BBCEAS on RSS Discovery	147
Figure 4.5. BBCEAS instrument cavity mounted on the gantry on the deck of RSS Discovery	147
Figure 4.6 Operation hours of BBCEAS I ₂ instrument during D319 cruise.	149
Figure 4.7. Fitting the O ₂ -O ₂ absorption, 1st June 2007.	154
Figure 4.8. Fitting of NO ₂ absorption 23 rd July 2007, 1 st June 2007	154
Figure 4.9 Fitted water vapour BBCEAS spectrum, 26 th May 2007	157
Figure 4.10. Time series from BBCEAS fitting of water vapour	158
Figure 4.11. Fitted NO ₂ BBCEAS spectrum, 28 th May 2007.	159
Figure 4.12. Time series of NO ₂ concentration from Green and Blue BBCEAS and NO _x instrument sampling on 28 th May 2007.	161
Figure 4.13. Time series of standard deviation of residual spectrum from Green and Blue BBCEAS instrument sampling on 28 th May 2007.	161
Figure 4.14 Cavity mirror surface with salt deposits, following a period of sampling ambient airflow during D319.	163
Figure 5.1 Particle formation pathway in the gas phase involving Iodine species	171
Figure 5.2 Map of the atmospheric research station site at Mace Head.	173

Figure 5.3. The locations of high density Laminaria populations at Mace Head	173
Figure 5.4 Meteorological data for Mace Head during BIOFLUX II BBCEAS measurements	179
Figure 5.5. Differential spectral structure due to molecular absorbers at green wavelengths	180
Figure 5.6 BBCEAS instrument cavity mounted on gantry at Mace Head.	181
Figure 5.7 Light intensity throughput at Mace Head on 26 th August 2007	184
Figure 5.8 Light intensity throughput variation with temperature measured at Mace Head on 26 th August 2007	185
Figure 5.9 Fitting the O ₂ -O ₂ absorption bands, 26 th August 2007	189
Figure 5.10 The fitted BBCEAS of water vapour absorption, 26 th August 2007	197
Figure 5.11 BIOFLUX II BBCEAS derived water vapour concentration, averaged to 10 minutes	199
Figure 5.12 One day section of BIOFLUX time series	200
Figure 5.13. BBCEAS determined Iodine concentration and tide height with photolysis rate for iodine	202
Figure 5.14 The fitted amount of iodine is 280.6 +/- 11.3pptv, 30 th August 2007	203
Figure 5.15 The fitted amount of iodine is 50ppt +/- 4.86ppt, 27 th August 2007	204
Figure 5.16. Time series showing the BBCEAS retrieved iodine concentrations peaks observed during BIOFLUX II.	206

Figure 5.17 Correlation of BBCEAS determined I ₂ concentration with tide height, wind direction and hour of the day.	211
Figure 5.18 LIF IO data from BIOFLUX II, plot from R Commane	212
Figure 5.19 Illustration of DOAS light path from Mace Head to the retro reflector sited at Roundstone	215
Figure 5.20 Iodine Correlation plots between BBCEAS and DOAS data recorded during BIOFLUX II	216
Figure 5.21 BBCEAS determined Iodine concentration analysed at 2 minute resolution on night of the 30 th August 2007.	218
Figure 5.22 The fitted amount of iodine is 608ppt +/- 17ppt, 30 th August 2007	218
Figure 6.1. Schematic NO and NO ₂ detector: a chemiluminescence detector	224
Figure 6.2. Time series of NO ₂ measurements from a standard chemiluminescence monitor and a TILDAS instrument during the 2002 [MCMA] campaign.	227
Figure 6.3 Schematic of dual channel TDLAS system used to measure formaldehyde, nitrogen dioxide, and sulfur dioxide in New York during 2002	228
Figure 6.4 Attenuated phase shift spectroscopy for ambient NO ₂ measurement	230
Figure 6.5. Optical layout of the LED based broadband cavity enhanced absorption instrument used for quantifying NO ₂ in laboratory trials	232
Figure 6.6. Fitted BBCEAS spectra of NO ₂ samples prepared from the thermal decomposition of N ₂ O ₄	232

Figure 6.7. Time series of measurements of NO ₂ in ambient laboratory air made by the BBCEAS spectrometer and a commercial chemiluminescence detector.	233
Figure 6.8 Schematic of pulsed Cavity Ring-Down Spectrometer	235
Figure 6.9. Correlation plot of CRDS data with P-CL data averaged to 1 minute and recorded at Boulder	235
Figure 6.10 One-minute average NO ₂ mixing ratios measured by the P-CL and LIF and DOAS instruments for 18 June–14 July 1999	236
Figure 6.11. NO ₂ concentrations derived from collocated DOAS (upper) and GC/LCD (lower) during MCMA 2003	238
Figure 6.12. Instrument locations at the LAMP measurement site SRC building, University of Leicester	241
Figure 6.13 LAMP measurement site	243
Figure 6.14. Temperature, relative humidity and wind direction during LAMP measured at 10m sampling height.	245
Figure 6.15 Wind direction occurrences in specified directions throughout the LAMP campaign	246
Figure 6.16 BBCEAS cavity location on SRC roof top	247
Figure 6.17. Absorption spectra of molecular absorbers in the blue wavelength region for reasonable atmospheric concentrations	248

Figure 6.18 Light intensity throughput of the BBCEAS cavity measured at LAMP on 24 th July 2007	249
Figure 6.19. Calibration of cavity mirror reflectivity by fitting the O ₂ -O ₂ absorption, 24 th July 2007.	255
Figure 6.20. BBCEAS spectrum of ambient NO ₂ (red) and spectral fit (black) from the evening of 24 th July 2007. 20.4ppb +/- 0.182ppb	257
Figure 6.21. BBCEAS spectrum of ambient NO ₂ (red) and spectral fit (black) from the evening of 24 th July 2007. 3.38ppb +/- 0.181ppb	258
Figure 6.22. Time series from BBCEAS data recorded 24 th July 2007.	258
Figure 6.23. LAMP campaign time series for NO ₂ and ozone concentrations from 24 th July 2007 to 3 rd August 2007	261
Figure 6.24. LAMP campaign time series for NO ₂ and ozone concentrations from 3 rd August 2007 to 14 th August 2007.	262
Figure 6.25 Subsection of the BBCEAS NO ₂ time series on Monday 30 th July 2007	263
Figure 6.26 BBCEAS NO ₂ concentration according to day of the week	265
Figure 6.27 LAMP measurements of BBCEAS and NO _{xy} where strong agreement is observed	268
Figure 6.28 BBCEAS data and NO _{xy} data 24 th July to 25 th July	270
Figure 6.29 Time series of NO ₂ measurements from NO _{xy} and BBCEAS	273
Figure 6.30 Time series of “interference” and ambient ozone concentration	273

Figure 6.31 Correlation plot of “Interference” and ambient ozone concentration	274
Figure 6.32 Fifteen minute averaged data sets: BBCEAS, NO _{xy} and chemiluminescence detector and Ozone data	276
Figure 6.33. The correlation plots of NO ₂ measurements made by the BBCEAS, NO _{xy} instrument and the chemiluminescence monitor.	278
Figure 6.34. BBCEAS spectrum fitted for water vapour (residual spectrum remaining after subtraction of the fitted NO ₂ absorption). 15 min averaged data. Mixing ratio of water vapour = 0.0144 +/- 1.539x10 ⁻³ from 24 th July evening running period.	281

LIST OF TABLES

Table 1.1. Standard levels and objectives of air pollutant concentration	31
Table 2.1. Type of transition and energy required to induce transition.	61
Table 2.2 Atmospheric measurement using cavity techniques	74
Table 3.1 The Chromex 250is grating parameters, groves per mm and the bandwidth of the measurements	104
Table 3.2 Parameters of the Ocean Optics Spectrometers	109
Table 3.3 Survey of molecular absorbers at green wavelength using BBCEAS measurements	133
Table 4.1. Instrumentation deployed on RSS Discovery cruise D319	146
Table 4.2 BBCEAS instrument components and cavity parameters	149
Table 5.1 Previous RHS measurements at Mace Head	175
Table 5.2 Instrumentation at Mace Head during BIOFLUX II	176
Table 5.3 BBCEAS hours of operation during BIOFLUXII	178
Table 5.4 BBCEAS instrument components and cavity parameters	184
Table 5.5. Absorption cross section source and treatment used in BBCEAS data analysis routine	190
Table 5.6 The statistical and systematic contribution to total error for iodine	193

Table 5.7. Nightly iodine concentration from 10 minute analysis, with corresponding tide height	203
Table 5.8 Correlation coefficients and offset values for the total overlapping data period and individual overnight periods.	214
Table 6.1 LAMP instrumentation	240
Table 6.2. BBCEAS main instrumental components for operation during the LAMP campaign	248
Table 6.3. BBCEAS operating coverage during LAMP	251

Chapter 1

Introduction

The Earth's atmosphere is the gaseous layer surrounding planet. Its main components are nitrogen (78.1%) and oxygen (20.9%), while the remaining 1% is argon, carbon dioxide, water and trace gas species. Anthropogenic activity on Earth has impacted the atmosphere's composition over the last century, particularly the quantities of trace gas species emitted into the troposphere. Naturally occurring trace gas species enable the chemical and physical cycles in the atmosphere to maintain an environment which supports life processes on Earth. The atmosphere protects the Earth's surface by filtering harmful radiation from space and maintains the temperature at the Earth's surface by the green house effect. The increase of pollutant trace gas species emission to the atmosphere adapts the balance of the natural chemical and physical processes altering the composition on the local and global scale, influencing climate change.

Monitoring and quantifying the rates and reaction pathways of chemical and physical process occurring in the clean and urban atmosphere is important to understand the changes occurring due to anthropological activity. Research to accurately measure trace gas species in the atmosphere has been ongoing, increasing knowledge and understanding of atmospheric processes. Although much advancement has been made in recent years, the observed levels of some trace gas species concentrations are not fully explained by current understanding, leading to additional investigation of particular areas of atmospheric chemistry and physics. The accurate measurement of trace gas species in the atmosphere has driven development of state of the art, high

sensitivity scientific instruments. The work in this thesis presents the technique of Broad Band Cavity Enhanced Absorption Spectroscopy (BBCEAS) and its application for measurements of trace gas species in the ambient atmosphere; field measurements were made in the urban atmosphere (LAMP, chapter 6) and the marine boundary layer (RHaMBLe, chapter 4 and BIOFLUX II, chapter 5).

This chapter describes the structure of the atmosphere and gives a brief description of the chemical cycling processes driven by OH and NO₃. The effects of air pollution are described and the protocols introduced to limit pollutant levels presented. The later sections describe the atmospheric chemistry of NO_x, a pollutant species, and reactive halogen species (RHS) in the marine environment. Previous field measurements for NO₂ and RHS are presented providing context for the BBCEAS measurements presented.

Many studies in the urban troposphere have included the measurement of NO_x as it is an important air pollutant with roles in formation of O₃ at low altitudes leading to photochemical smog. NO_x (NO and NO₂) in the atmosphere are rapidly converted to NO₂ (on the minute timescale) and NO₂ is removed from atmosphere by conversion to HNO₃ followed by wet and dry deposition.

1.1 The Earth's atmosphere

1.1.1 Regions and characteristics of the atmosphere.

The Earth's atmosphere is divided into different regions, each region boundary being defined by changes in the temperature profile observed as altitude increases. The four

regions are, the troposphere, the stratosphere, the mesosphere and the thermosphere, which are shown, along with the temperature profile in figure 1.1. Transition points between regions are known as the tropopause, stratopause and mesopause, the altitude of these are not fixed; the “pauses” vary with latitude and season.

The region from the Earth’s surface to approximately 10-15 km is the troposphere; in this region temperature falls with increasing altitude. The absorption of solar radiation by the Earth’s surface results in strong heating of air close to the surface. The heated air rises and strong vertical mixing occurs in the lower troposphere (or boundary layer) due to convection. This mixing process causes chemical species and aerosol emitted at the surface to be raised into the troposphere. The majority of water vapour (rain and clouds) in the atmosphere is within the troposphere and water has important roles in the scavenging of pollutants from the atmosphere.

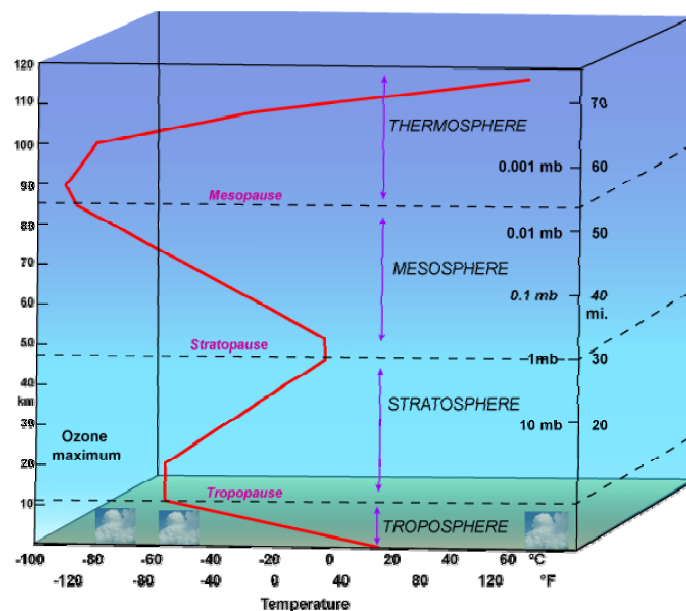


Figure 1.1 The structure of the Earth’s atmosphere, showing temperature and altitude.

http://www2.sunysuffolk.edu/mandias/global_warming/greenhouse_gases.html.

At the tropopause, the upper limit of the troposphere, the temperature profile changes. The temperature increases with altitude through the stratosphere. The stratosphere is the distance from the tropopause to approximately 50 km altitude. The increasing temperature with altitude in the stratosphere is caused by photochemistry of ozone and oxygen.

Ozone and oxygen in the stratosphere undergo chemical processing represented by the Chapman cycle, shown in figure 1.2. The photo dissociation of ozone and subsequent cycling reactions in the Chapman cycle maintain the steady state ozone concentration observed in the stratosphere. The cycle contains both sources and a sinks for ozone. The increase in temperature with altitude is due to excess energy following absorption being released as heat. Energy is also released by the reaction of oxygen atoms combining with oxygen molecules. Stratospheric ozone reaction cycles act as a filter of harmful shortwave radiation, resulting in only radiation of wavelength longer than 290 nm reaching the Earth's surface. This radiation filtering effect limits the photochemical processes that can be initiated in the troposphere to those initiated by radiation with wavelengths above 290 nm.

Pollutant species persist for long time periods in the stratosphere, vertical mixing by conduction does not occur and there is no rain to scavenge pollutants.

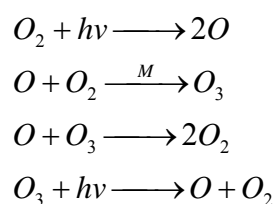
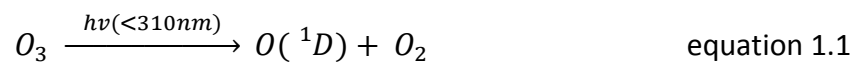


Figure 1.2 The Chapman cycle, Sir Sydney Chapman 1930s, the first two reactions are sources of ozone, while the later two equations are sinks.

The region beyond the stratosphere is the mesosphere, spanning between 50 and 85 km altitude. In this region the temperature decreases with altitude, and thus vertical mixing occurs. The ozone concentration decreases with altitude, reducing the heat release by photochemical reactions. Beyond 85 km from the Earth's surface is the thermosphere. There the temperature profile changes and an increase in temperature with altitude is observed, due to the absorption of short wavelength solar radiation by oxygen, nitrogen and atomic species.

1.2 Chemistry in the troposphere: OH and NO₃

The daytime chemistry in the troposphere is primarily driven by the OH radical. Hydroxyl radicals (OH) are produced in the troposphere via reactions of excited state oxygen (O(¹D)) with water (equations 1.1 and 1.2), the photo dissociation product of ozone. Ozone in the troposphere is approximately 10% of the total ozone budget, and originates from the stratosphere or is formed in the presence of NO₂ by equations 1.3 and 1.4.



The excited state oxygen atom, formed from O₃ photolysis, reacts to form OH, O₃ or ground state O, as shown in equations 1.5 to 1.7. The major fate of O(¹D) is to form oxygen, as water is a small component of the atmosphere. The dominant reaction for oxygen atoms is to regenerate ozone via equation 1.8.



Hydroxyl radicals react with many species in the troposphere. Radical chain reactions of OH oxidise hydrogen, methane, hydrocarbons, CO, forming CO₂ and water, and in effect the atmospheric system is a low temperature combustion system. A schematic of the atmospheric oxidation processes of OH and HO₂ is shown in figure 1.3, which highlights the chemical reactions producing, and destroying OH and HO₂. The presence of NO_x and sulphur compounds and other trace gas species modifies this combustion system.

OH radicals scavenge trace gas constituents from the troposphere, influencing the composition of the troposphere. The scavenging reactions also has an affect on stratospheric behaviour, as reactive species that survive chemical reaction and physical loss processes in the troposphere can be transported to the stratosphere (for example N₂O, methane and CH₃Cl). Once in the stratosphere these radicals can act to destroy ozone.

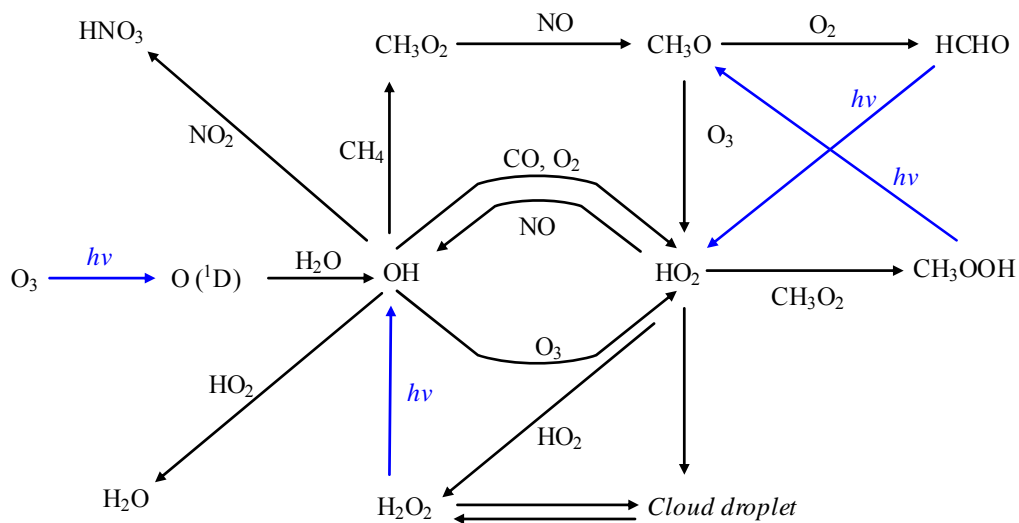


Figure 1.3 Schematic of the atmospheric oxidation processes of OH and HO₂

At night tropospheric chemistry is controlled by NO₃ reactions. NO₃ is formed by the reaction of NO₂ with ozone (equation 1.9) and by the decomposition of dinitrogen pentoxide (N₂O₅)(equation 1.10). The NO₃ concentration in the atmosphere depends upon reaction 1.9, as N₂O₅ is formed and decomposes by the reversible equation 1.10.



During the day NO₃ is rapidly photolysed thus it persists only at night when its dissociation ceases, where it becomes the dominant oxidising species. The photolysis of NO₃ is wavelength dependent, producing NO and O₂ or NO₂ and oxygen atoms as per equation 1.11 and 1.12.



The initiation reactions involving NO_3 are hydrogen abstraction and addition to double bonds, producing nitric acid (HNO_3) and radical species shown in equations 1.13 and 1.14.



The products of reaction 1.13 combine with molecular oxygen, forming peroxy radicals (RO_2). If RH is formaldehyde ($HCHO$) then subsequent reactions form HO_2 . By these reaction sequences NO_3 in the troposphere oxidises and removes organic species at night, forms nitric acid and radical processes produce HO_2 , thus initiating the oxidation chain mechanisms shown in figure 1.3 to provide a pathway for OH formation at night.

1.3 Air pollution and air quality control

Air quality is a global concern, with poor air quality affecting the health of people in both developed and developing nations. Indeed air pollution is estimated to cause two million premature deaths a year worldwide. A variety of cardiovascular and respiratory diseases are linked to air pollution exposure including lung cancers, asthma and bronchitis [*World Health Organisation, 2010*]. Particulate matter (PM) and ozone (O_3) pollution occurrences have quantitative links to increased mortality and morbidity [*Gwynn et al., 2000*]. In order to combat the adverse health effects of air quality

degradation, protocols have been implemented to improve air quality both within the EU (with individual national objectives and directives, driven by the European Commission, Gothenburg Protocol) and globally (World Health Organisation (WHO) guidelines).

The Gothenburg Protocol in 1999 set maximum exposure limits for four main pollutant species: sulphur, NO_x, VOCs and ammonia, which were to be achieved by 2010 [DEFRA, 2010]. The full implementation of this protocol across Europe aimed to cut 63% of sulphur emissions, 41% of NO_x emissions, 40% of VOC emissions and 17% of ammonia emissions compared to the 1990 levels [DEFRA, 2010]. The aim was to reduce the number of regions with excessive acidification by 84% and eutrophication by 35% of 1990 values [DEFRA, 2010]. Excessive ozone levels were to be halved. Within the regional limits, specific pollution sources have their own individual limits driving industry and technology to employ the least polluting or greenest techniques available [World Health Organisation, 2010][European Commission Environment, 2010]. The pollutant limits are set for different time periods, reflecting the degree of impact upon health for short-, medium- and long-term exposure to the various pollutants. These limits and exposure times are shown in table 1.1[European Commission Environment, 2010].

The 2005 version of the World Health Organisation's air quality guidelines recommended reduced limits on key pollutants globally [World Health Organisation, 2010]. The guideline on the ozone upper limit was reduced to 100 µg/m³ for an 8-hour mean, due to correlations between ozone levels and daily mortality with ozone found below the previous limit of 120 µg/m³ (8-hour mean). The sulphur dioxide (SO₂)

guideline levels were lowered considerably to 20 $\mu\text{g}/\text{m}^3$ rather than 125 $\mu\text{g}/\text{m}^3$ as adverse health effects were linked with even modest levels of SO_2 .

The UK strategies for achieving air quality improvements in line with the Gothenburg protocol were first proposed in 2000 and the latest national review of the strategy was completed in 2007 [DEFRA, 2010]. Local authorities (regional, county and city councils) review the current and future predictions of air quality in their area, based on locally recorded measurements. In circumstances where air quality standards are not met, Air Quality Management Areas (AQMA) are declared [DEFRA, 2010]. Authorities within AQMAs are then required to develop and implement action plans and local policy changes to meet the objectives of the Gothenburg protocol. Two hundred AQMAs were declared across the UK in 2007, and the majority of these were due to excess levels of nitrogen dioxide (NO_2) and particulate matter (PM) [DEFRA, 2010].

Pollutant	Concentration	Averaging period	Legal requirement	Permitted exceedences each year
Fine articles (PM2.5)	25 $\mu\text{g}/\text{m}^3$	1 year	Target value enters into force 1.1.2010 Limit value enters into force 1.1.2015	n/a
Sulphur dioxide (SO_2)	350 $\mu\text{g}/\text{m}^3$	1 hour	Limit value enters into force 1.1.2005	24
	125 $\mu\text{g}/\text{m}^3$	24 hours	Limit value enters into force 1.1.2005	3
Nitrogen dioxide (NO_2)	200 $\mu\text{g}/\text{m}^3$	1 hour	Limit value enters into force 1.1.2010	18
	40 $\mu\text{g}/\text{m}^3$	1 year	Limit value enters into force 1.1.2010	n/a
PM10	50 $\mu\text{g}/\text{m}^3$	24 hours	Limit value enters into force 1.1.2005	35
	40 $\mu\text{g}/\text{m}^3$	1 year	Limit value enters into force 1.1.2005	n/a
Lead (Pb)	0.5 $\mu\text{g}/\text{m}^3$	1 year	Limit value enters into force 1.1.2005	n/a
	40 $\mu\text{g}/\text{m}^3$	1 year	Limit value enters into force 1.1.2005	n/a
Carbon monoxide (CO)	10 mg/m^3	Max daily 8 hour mean	Limit value enters into force 1.1.2005	n/a
Benzene	5 $\mu\text{g}/\text{m}^3$	1 year	Limit value enters into force 1.1.2010	n/a
Ozone	120 $\mu\text{g}/\text{m}^3$	Max daily 8 hour mean	Target value enters into force 1.1.2010	25 days averaged over 3 years
Arsenic (As)	6 ng/m^3	1 year	Target value enters into force 1.1.2012	n/a
Cadmium (Cd)	5 ng/m^3	1 year	Target value enters into force 1.1.2012	n/a
Nickel (Ni)	20 ng/m^3	1 year	Target value enters into force 1.1.2012	n/a
Polycyclic Aromatic Hydrocarbons	1 ng/m^3	1 year	Target value enters into force 1.1.2012	n/a

Table 1.1. Standard levels and objectives of air pollutant concentration for given time period, the number of occurrences this limit can be exceeded is also specified [European Commission Environment, 2010].

1.3.1 Controlled atmospheric pollutants: PM, O₃ and NO₂

PM (particulate matter) is classified by its aerodynamic diameter, usually as PM₁₀ (smaller than 10 µm) and PM_{2.5} (smaller than 2.5 µm). PM are solid or liquid aerosol particles suspended in ambient air and made up from sulphate, nitrates, ammonia, sodium chloride, carbon, dust and water. The smaller sized PM_{2.5} particulate is more harmful as it reaches the peripheral parts of the lungs if inhaled, causing detrimental effect to the respiratory systems. However the full extent is still under investigation [DEFRA, 2010].

Ozone (O₃) at ground level is a major component of photochemical smog and its health effects are observed in the respiratory system. Ozone is a trigger for asthma and is strongly linked to decreased lung function and lung diseases [DEFRA, 2010].

Nitrogen dioxide (NO₂), the primary focus of the LAMP campaign, chapter 6, has toxic effects at concentrations over 200 µg/m³, causing inflammation of the airways [DEFRA, 2010]. However, greater concern arises from reactions of NO₂ in the lower atmosphere than from other pollutant species. NO₂ is a major source of nitrate aerosol, forming a large proportion of PM_{2.5}. NO₂ also plays a pivotal role in the formation of tropospheric ozone, the most harmful component of photochemical smog. Thus the methods used to monitor NO₂ must be reliable.

1.3.2. Current NO₂ measurement across the UK to monitor compliance with protocols

The current monitoring system used for NO₂ in the UK is called the Automatic Urban and Rural Network (AURN). AURN comprises 97 measurement sites, shown in figure 1.4, producing hourly averaged data [AURN DEFRA, 2009]. The earliest AURN sites have operated since February 1973. The sites cover 9 different environment types: rural, urban, kerb and roadside, remote, suburban, urban background, urban centre, urban industrial, intermediate and airport [AURN DEFRA, 2009]. Leicester has an urban centre monitoring station (sited at the Leicester council offices), which has operated since 1994.

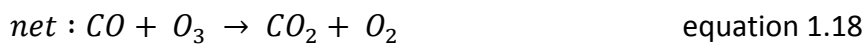


Figure 1.4 Measurement sites comprising the AURN atmospheric monitoring system [AURN DEFRA, 2009].

1.4 Nitrogen oxide chemistry in the troposphere

Nitrogen oxides (NO_x) are the sum of NO and NO_2 . The sources of NO_x are natural, from forest fires and lightning, and anthropogenic, from power generation and combustion engine emissions. The ambient levels of NO_x are higher in urban regions in comparison to remote regions; NO_x are pollutant gas species. The reactions of NO_2 in the troposphere can form ozone by reaction 1.2, or NO reacts with ozone forming NO_2 . If NO_x species are not physically removed or chemically converted, they can be transported into the stratosphere resulting in ozone destruction.

The reaction of OH and CO (equation 1.15 to 1.18) is important as the net reaction produces CO_2 and ozone. NO_x reactions can destroy ozone in the troposphere or be converted to NO_2 , depending upon NO_x concentration. In non-polluted atmosphere (high NO_x) the destruction of ozone occurs via equations 1.19 to 1.21.



In high NO_x conditions NO reacts with HO_2 from equation 1.16 above, producing HO radicals. NO also reacts with any pre-existing O_3 and is converted to NO_2 (equation 1.21). NO_2 is photolysed to O and NO which form ozone in equations 1.3 and 1.4.



Like OH and NO₃, NO_x species also exhibit diurnal trends. NO₂ concentrations increase after sunrise as NO and HO₂ react. This NO₂ concentration generally peaks when local rush hour occurs; this coincides with an NO concentration decrease which continues until evening rush hour. NO₂ photochemically reacts, producing ozone, which peaks during daylight, as the NO₂ concentration decreases. In the evening NO₂ again increases as its photochemistry ceases whilst NO and ozone forms NO₂. NO₂ loss is by the formation of nitric acid which is removed from the atmosphere by wet and dry deposition.

1.5 Iodine chemistry in the troposphere

The section outlines the known and suggested chemistry of reactive halogen species in the marine environment in order to put the Broad Band Cavity Enhanced Absorption Spectroscopy (BBCEAS) measurements into context. The roles of reactive halogen species in tropospheric ozone destruction is a subject of debate and investigation within atmospheric research. The main focus of this section is the chemistry of IO and the sources and sinks of iodine species in the troposphere, to establish why Reactive Halogen Species (RHS), particularly iodine species, have been a topic of atmospheric importance in the last decade.

Reactive halogen species (RHS) in the atmosphere have become an increasingly relevant area of study in the last decade. The chemistry of reactive halogen species has direct impact upon radiative budgets, climate and air quality levels. However the roles of RHS in atmospheric oxidation chemistry are not fully understood.

Measurement of RHS in the coastal marine environment has shown that major sources of reactive halogen precursors are present and elevated concentrations of RHS species, compared to the global background levels, are high enough in places to impact the atmospheric chemistry occurring. The most notable chemical impacts of RHS upon marine environment tropospheric chemistry are the effects on the destruction of tropospheric ozone and the roles in new particle formation. These processes are becoming more widely understood in the coastal marine environment; whilst investigations in the remote and non coastal marine environment have been recently conducted (e.g the RHaMBLe studies [Lee *et al.*, 2009]).

Iodine chemistry in the marine atmosphere has been a subject of interest due to the sources of RHS being concentrated at coastal regions. It is thought that RHS chemistry in coastal regions has a larger impact on chemical processing in the marine environment than elsewhere globally, as seaweeds are restricted to coastal regions thus present in only 0.5% of ocean.

In the troposphere iodine is present in halogen compounds and as molecular iodine, the sources for these compounds is discussed in sections 1.5.1-1.5.3. The reactive forms of iodine in the atmosphere are IO and I atoms. Iodine atoms in the troposphere are generated through the photodissociation of molecular iodine and alkyl iodine compounds by near-UV and visible wavelength radiation. Iodine monoxide is formed

1.5.1 Atmospheric iodine sources: *Iodine from seawater and terrestrial sources*

Seawater contains iodine in the form of iodate (IO_3^-), iodide (I^-) and non volatile dissolved organic iodine: the total concentration of iodine (IO_3^- and I^-) in seawater is $0.45\mu\text{M}$ ([*Carpenter, 2003*]). Several mechanisms for the release of iodine from seawater to the gas phase have been suggested; the main release methods are degassing of iodine in its insoluble organic form and the reaction of iodide with ozone at the sea surface.

The reaction of iodide with ozone at the seawater surface was studied in the laboratory under a variety of conditions by Garland. The contribution of iodine to the atmosphere was calculated to be between 6×10^{11} and 12×10^{11} g of molecular iodine (I_2) each year ([*Garland and Curtis, 1981*]).

Sea air fluxes of trace gas species are calculated using the Liss and Salter two layer model for transfer of slightly soluble gases across the sea air interface ([*Carpenter, 2003*]). Several estimates using this model have been made for methyl iodide (CH_3I), with the reported estimations being in reasonable agreement with each other at $< 3.3 \times 10^9 \text{ mol yr}^{-1}$ (ref 75 of reference [*Carpenter, 2003*]) and between $0.9\text{-}2.5 \times 10^9 \text{ mol yr}^{-1}$ (ref 57 of reference [*Carpenter, 2003*]).

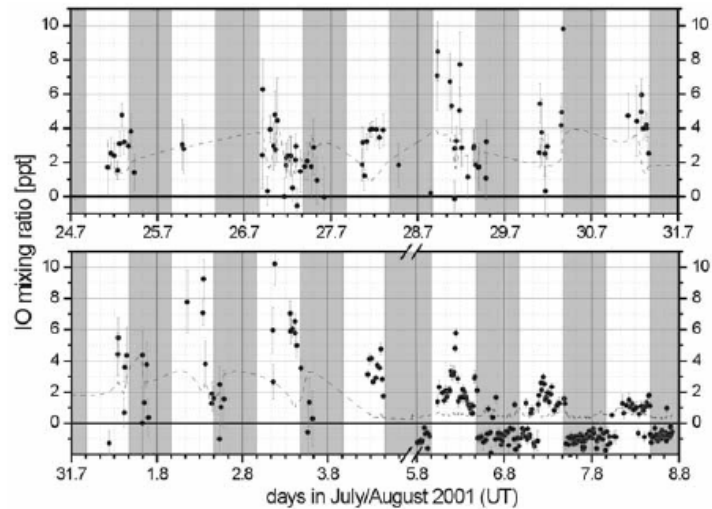


Figure 1.6. Time series of IO at Ein Bokek during 2 weeks of measurement. Dots represent the measured mixing ratio of IO, and the dashed line shows the detection limit. The timescale is universal time (UT) (local summer time (LST) equals UT plus 3 hours). ([Zingler, 2005])

Ocean sources of reactive halogen species (RHS) of a non biological nature have been investigated at the Dead Sea, Israel. In this location algae and plant growth (known iodine sources discussed in section 1.5.2) are limited due to the uniquely high salinity of the environment, providing the ideal site to explore inorganic sources of RHS into the atmosphere. Differential optical absorption spectroscopy (DOAS) measurements for IO at the Dead Sea by Zingler showed an IO presence during daylight on virtually every day of the measurement campaign during 2001, as shown in figure 1.8, with a maximum concentration of 10.2 ppt ([Zingler, 2005]).

The possible sources of IO at the Dead Sea are thought to be iodine escaping from seawater surfaces via reaction sequences involving photochemical irradiance, and reactions with dissolved ozone. Iodide is oxidised to form free molecular iodine (I_2) in the aqueous phase which leaches into the gas phase. Iodine species may also be

released from the gas phase reservoir species HOI, INO₂, INO₃ or I₂ or through liberation by heterogeneous reaction of HX species on sea salt surfaces.

Terrestrial sources of iodine are linked back to atmospheric input. The major route of iodine into soil is through the decomposition of organic tissue which has previously absorbed atmospheric iodine [Carpenter, 2003].

1.5.2 Atmospheric iodine sources: *Iodine from biological, organic sources*

Algae plants accumulate iodine within their structure from seawater, up to a 3000 times concentration. *Laminaria digitata* accumulates iodine to levels between 0.4 and 4.7% dry weight, while the iodide concentration in seawater is approximately 0.45 μM ([Küpper *et al.*, 1998] and [Gall *et al.*, 2004]). When algae experiences oxidative stress (e.g. the exposure to elevated temperatures or ozone, UV light, grazing, etc), the response is to form and release volatile iodocarbons and molecular iodine into the surrounding environment.

The accumulation and release mechanisms of iodine from *Laminaria* are shown in figure 1.7 [Küpper *et al.*, 2008]. The left section shows kelp submerged and unstressed, and accumulation of iodide from seawater is catalysed by vanadium haloperoxidase (turquoise reaction), while oxidative stress at high tide causes iodide to be released into the surrounding seawater. The right section shows the reactions occurring during oxidative stress (red) when iodide is released to detoxify reactive oxygenated species (e.g. aqueous H₂O₂ and gaseous O₃) on the surface of the plant, outside of the cell

membrane. On the plant surface iodide reacts with ozone forming molecular iodine, which is released directly into the coastal atmosphere at low tides.

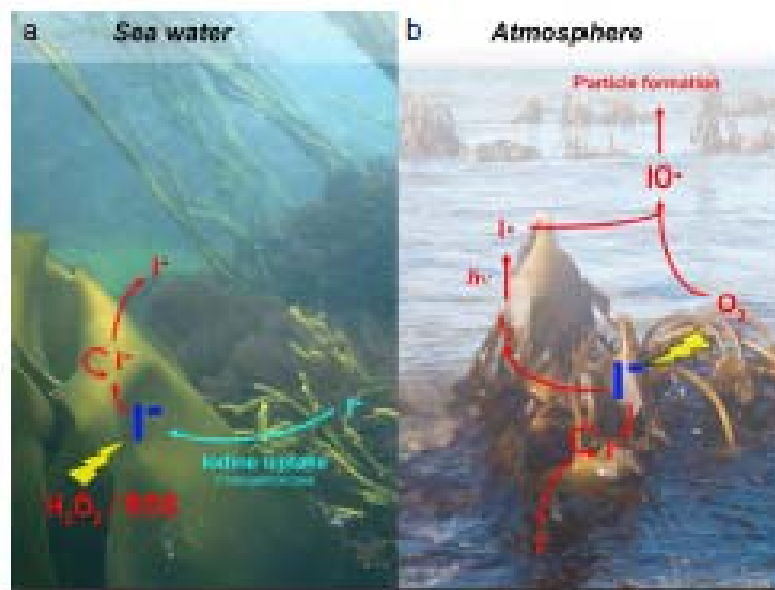


Figure 1.7 Accumulation and release of iodous species in Laminarias [Küpper *et al.*, 2008]

The identification of macro algae as a source for RHS in the marine atmosphere is supported by RHS measurements by Peters *et al.* ([Peters *et al.*, 2005]) using Long Path DOAS and GC/ECD ICPMS at Dagebull in North Germany, Lilia in France and Mace Head in Ireland. At each measurement site elevated VHOCS (volatile halogenated organic compounds) were observed alongside the presence of exposed seaweed plants. The high biological activity in France resulted in extremely high levels of CH₃I (up to 1830 ppt) and CH₃Br (up to 875 ppt), along with CH₂I₂ and IO exhibiting an anti correlation ([Peters *et al.*, 2005]). There was no presence (above instrument detection limits) of BrO, OIO and I₂ in North Germany or France ([Peters *et al.*, 2005]). The Mace Head data showed evidence of OIO, and I₂ concentrations up to 61 ppt, leading to the conclusion that the lack of I₂ observation in France was due to the type of seaweed growing in the

different regions ([*Peters et al.*, 2005]). The dependence of iodine presence with seaweed type has been supported by Ball et al [*Ball et al.*, 2010]. Seaweed species were monitored for iodine emission in the laboratory by spectroscopy of molecular iodine. These experiments showed *Laminarias* to be strong iodine emitters along with *Saccharina latissima* and *Ascophyllum nodosum* as less strong emitters, while *Fucus* species and *Dictyopteris membranacea* did not emit any detectable iodine [*Ball et al.*, 2010].

Molecular iodine was identified as the dominant source of coastal reactive iodine by DOAS measurements at Mace Head during August 2002 ([*Saiz-lopez and Plane*, 2004]). I_2 was observed at concentrations ranging from the detection limit of 3ppt up to a night time maximum of 93 ppt and 25 ppt during the day ([*Saiz-lopez and Plane*, 2004]). The iodine peaks correlated with low tides and were seen on 16 nights and 3 days of measurements, the largest concentrations were observed during darkness. Figure 1.8 from Saiz Lopez et al ([*Saiz-lopez and Plane*, 2004]) shows the iodine concentration and tidal height, a correlation between elevated iodine and low tide is observed. At night time the peak is more pronounced, because iodine has a longer atmospheric lifetime at night when photolysis ceases. Night time measurements of OIO show a similar trend to observed iodine; OIO concentrations peak after the iodine peak, supporting the theory that formation of OIO is by iodine reacting to form iodine atoms which then react to form OIO.

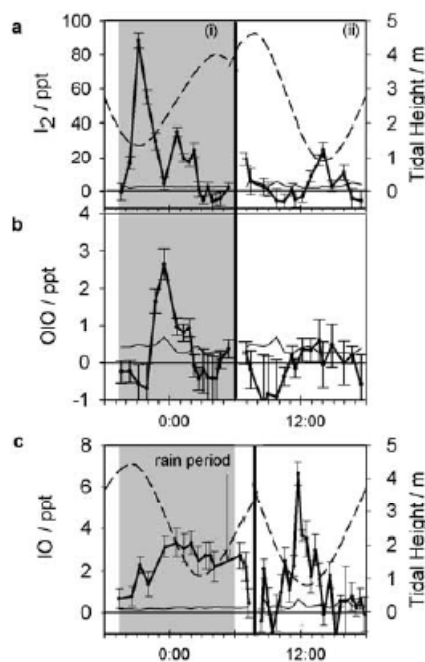


Figure 1.8. Mixing ratio profiles of I_2 , OIO and IO, measured by DOAS at Mace Head, Ireland, during August 2002. The mixing ratios, together with 2σ uncertainties, are shown in black. The detection limit of the instrument, and the tidal height, are plotted as thin black and thick broken lines, respectively. (a) I_2 , (i) August 20/21 night time, (ii) August 26. (b) OIO, measured simultaneously with the I_2 in (a). (c) IO, (i) August 28/29 night time, (ii) August 24. The abscissa shows Greenwich Mean Time. ([Saiz-lopez and Plane, 2004])

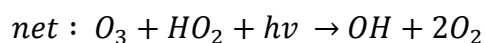
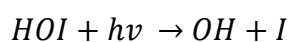
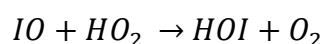
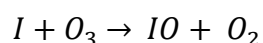
1.5.3 Iodine sinks in the troposphere

Measurements by Baker et al ([Baker et al., 2001]) determined the concentration and speciation of iodine by wet and dry deposition at a coastal site on the south east coast of the UK (Weybourne). The main removal routes for iodine are deposition into rain at a rate of $2.7 \mu\text{mol m}^{-2} \text{yr}^{-1}$, and deposition into aerosol at a rate of $3.6\text{-}6.5 \mu\text{mol m}^{-2} \text{yr}^{-1}$ ([Baker et al., 2001]). The main iodous species in rain and aerosol were found to be iodate (IO_3^-) and iodide (I^-) ([Baker et al., 2001]), which indicates that iodate formation

and iodide volatilisation are slow occurring. Baker et al propose that non volatile iodous organics may also contribute to removal of iodine from the atmosphere through deposition.

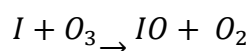
1.5.4 Iodine and ozone destruction

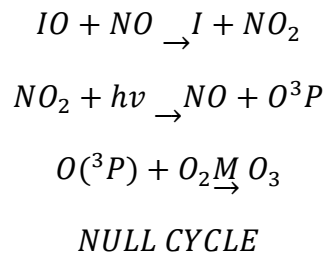
Atmospheric iodine atoms (formed by photodissociation of photo labile iodine compounds) react with ozone to form the reactive IO species. The reactions of atmospheric IO are wide-ranging and many regenerate the reactive iodine atom, which results in net ozone destruction. Other IO reactions produce oxy halogen species. The reaction of IO with HO₂ under low NO_x (<500 ppt) forms hypo iodous acid (HIO) (see equations 1.22), and ozone is destroyed. The net reaction shows that ozone is lost through this cycle and the HO₂/OH ratio is shifted in favour of OH, thus influencing the oxidising capacity of the atmosphere.



Equation set 1.22

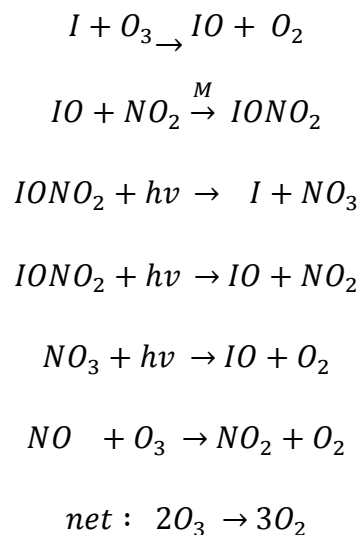
In regions of high NO_x (above 500 ppt), iodine is regenerated and the subsequent reactions of NO and NO₂ results in ozone production and a null cycle.





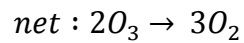
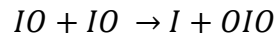
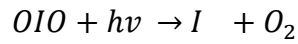
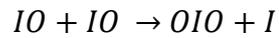
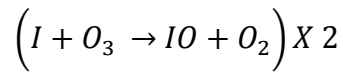
Equation set 1.23

Another pathway for ozone destruction involving NO_x is shown below, with IO reacting with NO_2 forming $IONO_2$. This becomes an effective loss route for ozone only if the photolysis of $IONO_2$ to form I and NO_3 dominates over photolysis to form IO and NO_2 .



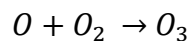
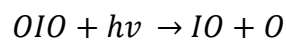
Equation set 1.24.

The self reaction of iodine monoxide with other halogen oxides also results in the destruction of ozone in the troposphere, with two ozone molecules being destroyed per cycle shown in equation set 1.25.



Equation set 1.25.

If iodine dioxide is photolysed in preference to reaction with other gas phase species, the net ozone destruction is reduced as the products go on to react with oxygen to form ozone.



Equation set 1.26.

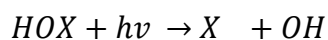
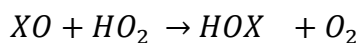
The rate of ozone loss due to the reaction with HO₂ at atmospherically measured values was determined by Alike [Alicke *et al.*, 1999], using 6 pptv of HO₂ loss of ozone was calculated as 0.27 ppbv per hour via the HOI cycle (reaction cycle 1.25). The [NO₂]/[NO] ratio increases in the presence of IO, as NO reacts with IO to form NO₂, and ozone forming reactions are decreased ([Alicke *et al.*, 1999]). Modelling using the measured levels of RHS in the atmosphere showed the levels of IO observed by Allen

([Allan *et al.*, 2000]) (4 pptv max and 1 pptv average) were enough to cause significant additional O₃ depletion ([Allan *et al.*, 2000]) via the IO pathways above.

1.5.5 Iodine and HO₂ / OH chemistry

The [HO_x]/[OH] ratio is disturbed by the presence of reactive halogen species in the marine boundary layer. The OH species is one of the major oxidising agents for trace gas species in the atmosphere and having a life time of 0.1-1 second during the day, its concentration is driven by local chemistry rather than transport processes. The main reaction of OH occurs with CO and other hydrocarbon species, forming peroxy radicals which react further, eventually regenerating OH species. The rates of this are dependent upon NO_x levels (as shown in figure 1.9).

Current chemical modelling methodologies are yet to effectively account and include reactions of HO₂ with halogen monoxides (XO where X = Br, Cl or I) which form HOX. Halogen monoxide and HO₂ reaction acts as a sink for HO₂ and the photolysis of HOX is a pathway for HO₂ to be converted to OH. An alternative sink mechanism is HOX loss by uptake into aerosol.



Equation set 1.27.

Previous chemical modelling to predict the iodine/HO₂ chemistry generally over estimates the HO₂ concentration when model predictions are compared to field

measurements of HO₂. Recent measurements of OH, HO₂ IO and BrO by Bloss have enabled the impact of iodine to HO₂ chemistry to be quantified, indicating that the halogen oxide /HO₂ reactions can account for the discrepancies between modelled and measured values ([Bloss *et al.*, 2005]). Measurements of IO in clean air (low NO_x) conditions observed peaks of IO daily up to 4 ppt ([Bloss *et al.*, 2005]). The impact of the IO/ HO₂ reaction on HO₂ concentration was carried out by comparing the rates of the principal HO₂ radical loss reactions with HO₂, CH₃O₂, NO, O₃, and IO along with loss by uptake onto aerosol ([Bloss *et al.*, 2005]). In some atmospheric circumstances the IO loss pathway dominates, accounting for 40% of the total HO₂ loss measured during NAMBLEX, which coincides with the highest IO observation at 4 ppt ([Bloss *et al.*, 2005]). The photolysis of HOI (formed by the reaction of IO and HO₂) also adds to the production of OH up to 15%. The fractional importance of each reaction to the loss of HO₂ and formation of OH in the marine environment are represented in the pie charts in figure 1.6 below.

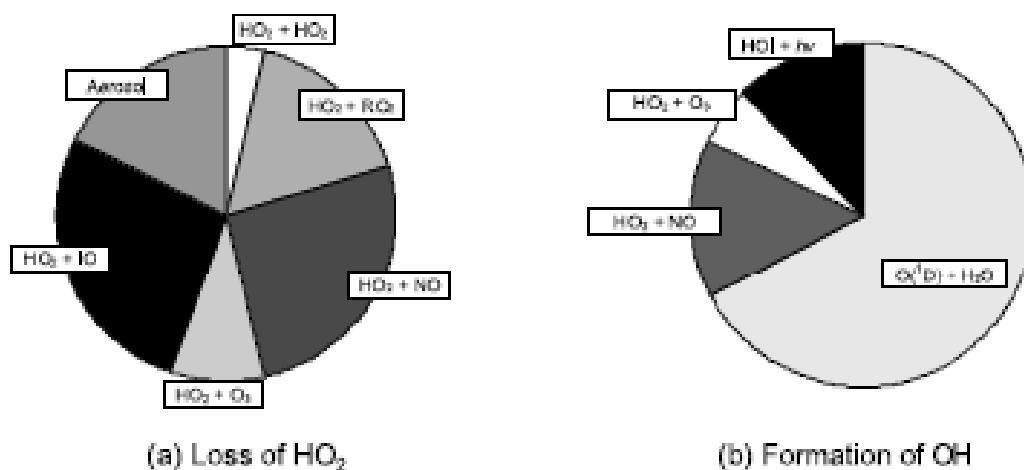
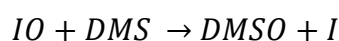


Figure 1.9 The fractional importance of HO₂ loss and OH formation reactions in the Coastal marine environment ([Bloss *et al.*, 2005]). Loss of HO₂ by reaction with IO is comparable to loss via NO reaction.

1.5.6 Iodine and di methyl sulphide chemistry

Iodine monoxide has been associated with the oxidation process of dimethyl sulfide (DMS), which has roles as a precursor to particle formation. DMS is an abundant sulphurous atmospheric species with its main source at the coast being micro algae and phytoplankton. DMS oxidation produces soluble and low vapour pressure products which condense to form new particle nuclei, the building blocks for aerosol production.



Equation 1.28.

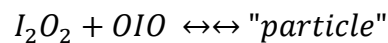
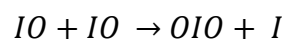
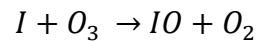
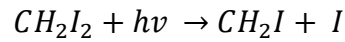
The reaction of IO with DMS has been studied extensively under a variety of laboratory conditions and a spectroscopic study by Nakano showed that under simulated marine environment conditions this reaction can occur at comparable rates to the oxidation of DMS by the hydroxyl radical (OH) and NO₃ ([Nakano *et al.*, 2003]). The Iodine oxide and DMS reaction is of significance in atmospheric modelling. Nakano *et al* report a rate coefficient at 298 K of $2.5 \times 10^{-14} \text{ cm}^3 \text{ molecule}^{-1} \text{ s}^{-1}$ ([Nakano *et al.*, 2003]) which is in close agreement with the rate constant determined by Gravestock of $2.0 \times 10^{-14} \text{ cm}^3 \text{ molecule}^{-1} \text{ s}^{-1}$ ([Gravestock *et al.*, 2005]) and Daykin and Wine of $3.5 \times 10^{-14} \text{ cm}^3 \text{ molecule}^{-1} \text{ s}^{-1}$ ([Daykin and Wine, 1990]). The experimentally determined rate constants of this reaction are in reasonable agreement and enable this reaction to be factored into modelling of the chemistry.

1.5.7 Iodine and particle formation

Iodine and iodine-containing species have been found to be major components of marine aerosol. Laboratory studies into new particle formation from iodine-containing species conducted by Hoffmann ([*Hoffmann et al.*, 2001]), O'Dowd ([*O'Dowd et al.*, 2002]) and Burkholder ([*Burkholder et al.*, 2004]), show that iodous-compounds under marine atmospheric conditions can undergo reaction to form new particles. Hoffmann proposed a mechanism for the particle formation of iodine oxides by homogeneous nucleation, initiated by the photolysis of iodine containing precursors [*Hoffmann et al.*, 2001]. This mechanism is shown by equation set 1.29, with CH_2I_2 photolysis initiating the reaction. The precursor for particle formation can be any photo labile iodine containing gaseous species which undergoes photolysis to generate iodine atoms, leading to nucleation. Iodine atoms in the marine atmosphere react with ozone forming IO, IO self reacts to make OIO. OIO will also self react to produce I_2O_2 . The products of OIO self reactions react in sequences of OIO addition steps, ultimately forming a stable iodine oxide cluster.

Smog chamber experiments conducted by O'Dowd ([*O'Dowd et al.*, 2002]) under coastal atmospheric conditions supported the proposed mechanism for the particle formation put forward by Hoffmann. The simultaneous presence of iodous precursor molecules (e.g. CH_2I_2 or photo labile iodous species) with ozone and UV was necessary for particle production in the experiments; rapid homogeneous nucleation occurred followed by condensation and coagulation growth of the clusters. O'Dowd et al suggested a secondary pathway where I_2O_2 is directly involved in aerosol growth stages and the reaction between IO and HO_2 produces HOI which condenses. The

iodine oxide condensation pathway is the dominant new particle production pathway unless the CH₂I₂ concentration was less than 200 ppt, then the pathway involving HOI to particle formation will dominate ([O'Dowd *et al.*, 2002]).



Equation set 1.29.

Burkholder 2004 ([Burkholder *et al.*, 2004]) induced the nucleation of iodine oxides by UV photolysis of CF₃I and CH₂I₂ in excess O₃. Newly formed particles were detected by an ultra fine condensable particle counter. Modelling of the chemistry observed in Burkholder's experiments showed that IO and OIO concentrations reported from field campaigns were not sufficient to explain the elevated new particle production bursts observed in the coastal region of Mace Head by the mechanism presented by Hoffmann, unless the sources of iodine oxides and their precursors were inhomogeneously located or HOT SPOTS of elevated iodine concentrations were present ([Burkholder *et al.*, 2004]).

The MISTRA modelling study explored the roles of iodine oxides in particle formation for a wide range of atmospheric conditions and scenarios ([Pechtl *et al.*, 2006]). Gas

and aerosol phase chemistry, and aerosol micro physics were included in model. The noteworthy results from this modelling study are summarised in the following points:

1. Clean marine atmospheric scenarios showed that elevated levels of OIO significantly contributed to nucleation and growth of particles. ([*Pechtl et al., 2006*])
2. Hot spots of reactive iodine precursor emission rather than continuous emission sources would enable the new particle bursts already observed in field measurements. The emission rate of RHS is higher in hot spot emission scenarios and the number density of particles increases in a shorter time compared to continuous emission scenarios. ([*Pechtl et al., 2006*])
3. The different clean marine scenarios showed that although alkyl iodide emissions are sufficient to nucleate and form new particles, emissions of molecular iodine significantly enhance the particle burst strength. ([*Pechtl et al., 2006*])
4. In polluted air mass scenarios, OIO concentrations are significantly lower than clean air scenarios; OIO reacts with NO_x , and nucleation rates are lowered. In these situations the nucleation of new particles due to H_2SO_4 becomes the more dominant route, with OIO being involved in the growth stages to form aerosol. ([*Pechtl et al., 2006*])

Macro algae has been identified as a strong source of the iodine species which initiate particle production reactions (see Iodine sources, section 1.5.1 and 1.5.2), this prompting investigation of particle formation from macro algae emissions of condensable iodine vapours ([*Mcfiggans, Coe, Burgess, Allan, et al., 2004*]). The

experimental set up employed by McFiggans is shown in figure 1.10, where a two reactor system enabled the residence time to be prolonged, enabling more reactions before the particles were analysed. Ozonised air was passed through the primary reactor containing the *Laminaria* (macro algae), then into the secondary reactor, increasing the residence time in reactor, before being guided to the monitoring instruments. A SMPS (scanning mobility particle sizer), a particle counter and an AMS (aerosol mass spectrometer) were used to investigate the transit time effects in the growth and composition of formed particles.

Under each of the different experimental conditions, (variable light, variable flow route and ozone concentrations) large particle number concentrations were observed ([*McFiggans, Coe, Burgess, Allan, et al., 2004*]). The transit time through the reactor is important for growth of particles, increased transit time was necessary for particles to grow to a detectable size. Both ozone and light were required for particles to form, while the release of iodine species from the algae did not depend upon ozone.

A non biological molecular iodine source was monitored in the same manner as the *Laminaria* source, with extremely high and repeatable particle number concentrations observed ([*McFiggans, Coe, Burgess, Allan, et al., 2004*]). The particle compositions from non biological iodine were very similar to the seaweed exposure experiments ([*McFiggans, Coe, Burgess, Allan, et al., 2004*]).

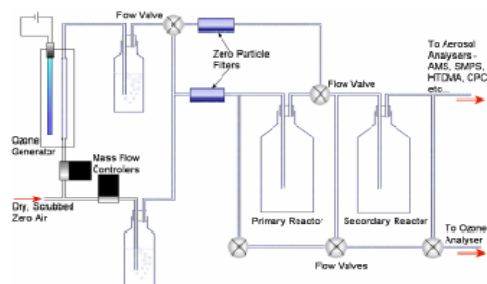


Figure 1.10 Experimental set up from the study linking seaweed emissions to new particle formation [Mcfiggans, Coe, Burgess, J., et al., 2004].

The atmospheric measurements, laboratory experiments and modelling work discussed here show iodine species are responsible for nucleation and particle growth in coastal regions, particularly in regions or scenarios where macro algae is present, confirming a new route to particle formation in the atmosphere.

1.5.8 Field measurements of RHS and their implications

The study of RHS presence and chemical activity in the environment has included field measurements of RHS, alongside calculations and chemical modelling to understand the observations from the field. Many of these studies have been described earlier when presenting the sources, sinks and chemical activity of RHS in sections 1.5.1-1.5.7. Here a chronological summary of early field observations and subsequent laboratory studies and conclusions are given to highlight the impact of RHS chemistry in the atmosphere.

Iodine species in the environment were first observed by GC instruments monitoring iodocarbons over the open ocean. The next development in iodine chemistry followed the first measurement of IO in the atmosphere at Mace Head, Ireland in 1999 using Long Path Differential Optical Absorption Spectroscopy (LP DOAS). A strong diurnal trend in IO was observed with a maximum concentration of 6 ppt being observed which followed solar radiation ([Alicke *et al.*, 1999]). Allen also measured IO using LP DOAS at Mace Head in Ireland. The IO concentrations observed followed a diurnal pattern peaking between 1 and 3.5 ppt, which correlated with solar actinic flux in the near-UV ([Allan *et al.*, 2000]), in agreement with the levels observed by Alicke. In order to account for the concentration of IO observed an additional source for IO alongside the measured iodocarbon levels is required [Allan *et al.*, 2000]. Elevated levels of reactive iodine species at coastal sites have coincided with observations of particle nucleation events. O'Dowd reviewed studies of coastal new particle formation events. The dependence of nucleation events with biogenic iodine emissions was reported and a particle formation mechanism via iodine oxide nucleation processes was described [O'Dowd and Hoffmann, 2005]. Laboratory investigations into self nucleation of iodine oxides to form particles found them to be an efficient source to account for the observed nucleation bursts observed in coastal environments [Hoffmann *et al.*, 2001]. The first spectroscopic observations of molecular iodine at the coastal site of Mace Head were made by Saiz-Lopez during the NAMBEX campaign using LP DOAS. The maximum I₂ concentrations observed were 93 ppt at night and 25 ppt during the day [Saiz-lopez and Plane, 2004]. These measurements enabled sources of iodine to be located as the strong emissions of I₂ from exposed macro-algae at low tide. This suggested source of molecular iodine and links to new particle formation

were investigated by Mcfiggins, who found that iodine within new particles was "1000 times" more likely to have originated in molecular iodine, rather than di-iodomethane and thus hypothesised I₂ release from macro algae [Mcfiggins, Coe, Burgess, Allan, et al., 2004]. The observed particle nucleation events leading to secondary aerosol formation at coastal regions suggests an additional route for atmospheric particles to form.

Researchers studying marine aerosol for both its constituent species and its formation mechanisms have found iodine and iodine-containing species are the major components of marine aerosol. Laboratory studies into new particle formation from iodine containing species have been conducted by Hoffmann ([Hoffmann et al., 2001]), O'Dowd ([O'Dowd et al., 2002]) and Burkholder ([Burkholder et al., 2004]) and show that iodous compounds under marine atmospheric conditions can undergo reaction to form new particles.

The measurements are important as they help to quantify the impact iodous RHS have in the marine boundary layer chemistry. Field measurements of RHS along with laboratory studies of the reaction kinetics have led to more accurate modelling of the chemistry under different conditions. Modelling of atmospheric chemical processes utilising findings from these measurements has led to a better understanding of the chemical and physical processes observed in the marine environment. Davis investigated the impact of iodine on tropospheric ozone and other oxidant species; using chemical modelling, including the then recently updated kinetic parameters for these iodine reactions ([Davis et al., 1996]). The results of the modelling showed that under certain atmospheric conditions the chemistry of iodine species can indeed

enhance the rate of ozone destruction along with influencing the $[\text{HO}_2]/[\text{OH}]$ radical ratio. Different source scenarios for iodine species were investigated and only iodine sources providing concentrations above 1.5 ppt caused an enhancement to the ozone destruction process ([Davis *et al.*, 1996]).

The progress in understanding the RHS chemistry in the atmosphere has advanced hugely in the last decade. However the need for additional RHS measurements in the atmosphere to fully understand the suggested chemistry remains.

1.6 Motivation for this work

This chapter introduces some of the chemistry of NO_x and reactive halogen species chemistry occurring in the troposphere. Many of the chemical reactions in the troposphere produce ozone, a pollutant species, which has adverse effects on the environment and human health. Monitoring trace gas species enables a better understanding of atmospheric processing reaction pathways, and allows the long term effects of reactions to be determined. The inclusion of atmospheric trace gas species measurements in modelling of the atmosphere is vital to accurately predict and account for changes in the atmospheric composition. The current theories of the roles of halogen species on the oxidation chemistry of the marine environment have been discussed, and the research to date highlights the need for additional investigations and measurements of RHS in the marine environment to gain full understanding. The methods for measuring trace gas species in the atmosphere are now numerous: those used to monitor NO_2 are described in chapter 6, LAMP, and presents atmospheric

measurements made using a Broad Band Cavity enhanced Absorption Spectroscopy (BBCEAS) instrument.

The highly sensitive BBCEAS technique has been recently developed ([*Ball et al.*, 2004]); this work involves the development and deployment of BBCEAS instrumentation capable of quantifying trace gas species over extended operation periods. The BBCEAS measurements provide direct quantification of molecular absorbers present at very high dilution. The BBCEAS instrument was configured to operate at different wavelengths and used to monitor the pollutant species NO₂ in the urban atmosphere, and molecular iodine in the marine atmosphere. Iodine is a key species thought to be involved in new particle formation in coastal regions, and the incorporation of BBCEAS observations in modelling may increase the understanding of the RHS processing. The marine measurements also enable the identification of RHS sources to the atmosphere, as BBCEAS is a point source measurement offering advantages over LP DOAS, which is a path integrated measurement. The urban measurements enabled a comparison of the newly developed NO₂ monitoring BBCEAS instrument to well established techniques.

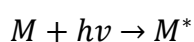
Chapter 2

Introduction to spectroscopy and cavity based spectroscopic techniques

2.1 Introduction to spectroscopy

Spectroscopy is a largely experimental based subject involving the study of the energy changes within atoms or molecules following their interaction with electromagnetic radiation. A photon of light can interact with matter through one of three mechanisms: absorption, spontaneous emission and stimulated emission. These processes are illustrated in figure 2.1 for an idealised system consisting of two energy levels. In each case, the absorption or emission of a photon by a molecule causes a change in the energy state of the molecule, with absorption resulting in the molecule being promoted to a higher energy state and emission resulting in the molecule losing energy and thus occupying a lower energy state. Absorption and emission processes occur only when the photon energy exactly matches the separation between the molecular energy levels; $\Delta E = E_1 - E_0 = h\nu$ where ν is the radiation's frequency and h is Planck's constant.

Absorption occurs when the incident photon has exactly the right energy to excite the molecule from a lower state (E_0) to a higher state (E_1) as shown in the left part of figure 2.1.



Spontaneous emission occurs when an atom or molecule in an excited state (M^*) emits a photon of energy, $E = h\nu$, and the molecule returns to a lower energy state without any external influence.



Induced emission occurs when an atom or molecule resonantly interacts with a photon resulting in the emission of radiation, a second identical photon and the atom or molecule reverts to its lower energy state.



Indeed the need to account for experimental observations of spectroscopic transitions in atoms and molecules at well-defined discrete frequencies specific to a given atom or molecule (e.g. the Balmer series in atomic hydrogen) was one of the driving forces behind the development of quantum theory in the early 20th Century.

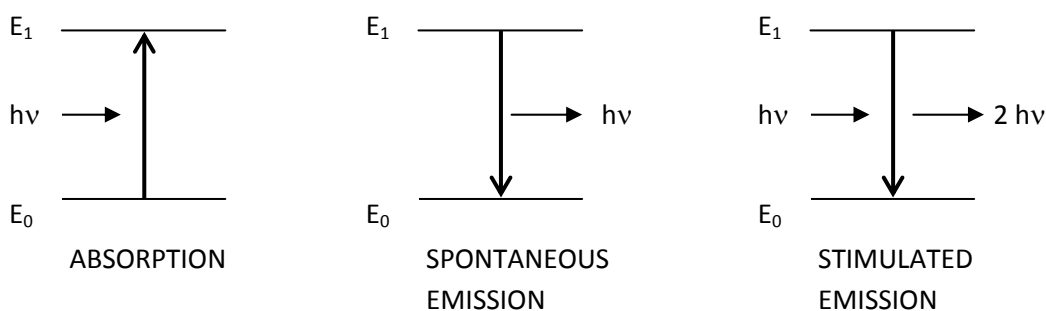


Figure 2.1 Absorption (left) and emission processes (spontaneous (centre) and stimulated (right)) between two energy levels (E_0 , lower, and E_1 higher energy) in a molecule.

2.1.1 Energy levels in atoms and molecules

Rather than just the two levels of the idealised system in Figure 2.1 above, real atoms and molecules possess many energy levels and thus the capacity to absorb or emit light at many different discrete wavelengths. Atoms have electronic energy levels and

molecules have electronic, vibrational and rotational energy levels. Different magnitude energy requirements exist for each type of transition between energy levels; these are shown in table 2.1. Electronic transitions arise from the promotion of an electron from a filled atomic or molecular orbital (two electrons aligned, one spin up and one spin down, in an orbital) to an unfilled orbital. Vibrational transitions arise from quanta of energy causing atoms within molecules to oscillate within the potential energy curve holding the molecule together. The vibrations and bends within simple molecules (e.g. CO₂ or H₂O) require less energy to distort than to rearrange electrons, thus vibrational transitions occur at lower energy, as shown in table 2.1. Rotation of molecules depends upon the moments of inertia of the molecule. Rotation of molecules requires less energy than that required to distort bonds in vibrations, thus smaller quanta are required for rotational transitions. The different energy photons fall into regions within the electromagnetic spectrum: as shown in figure 2.2, the higher energy photons required for electronic transitions fall in the UV and visible regions whilst vibration transitions are induced by infrared photons and rotational transitions by microwave radiation.

Type of state/transition	Region of electromagnetic spectrum	Typical photon energy
Electronic	UV and Visible	20,000 – 100,000 cm ⁻¹
Vibrational	Infrared	1000 cm ⁻¹
Rotational	Microwave	1 cm ⁻¹

Table 2.1. Type of transition and corresponding energy required to induce transition.

electromagnetic spectrum

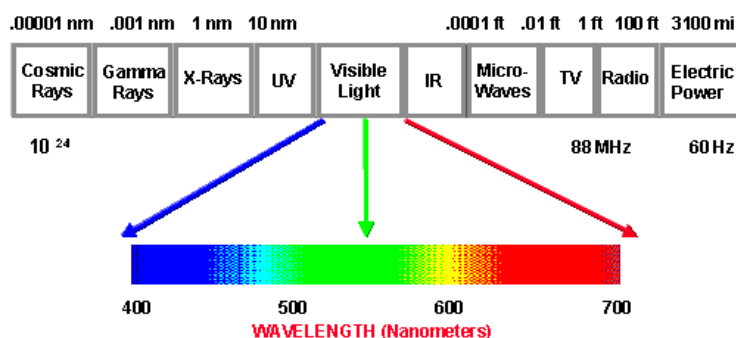


Figure 2.2. The electromagnetic spectrum with the wavelength (nm) for the regions shown above and energy in Hertz (Hz) below. The visible region is expanded with corresponding wavelengths below the expansion.

Each electronic state within a molecule also has its own set of vibrational energy levels, which in turn have their own rotational energy levels. The Born-Oppenheimer approximation stipulates that due to the large differences in frequency or energy for each type of motion the different types of transition can be treated independently. Electronic transitions may be accompanied by a change in vibrational state and electronic state and due to the large number of vibrational and rotational states molecules absorb photons at many different frequencies, which give rise to an absorption spectrum. A representation of a two electronic state system with the associated vibrational and rotational energy levels is shown in figure 2.3.

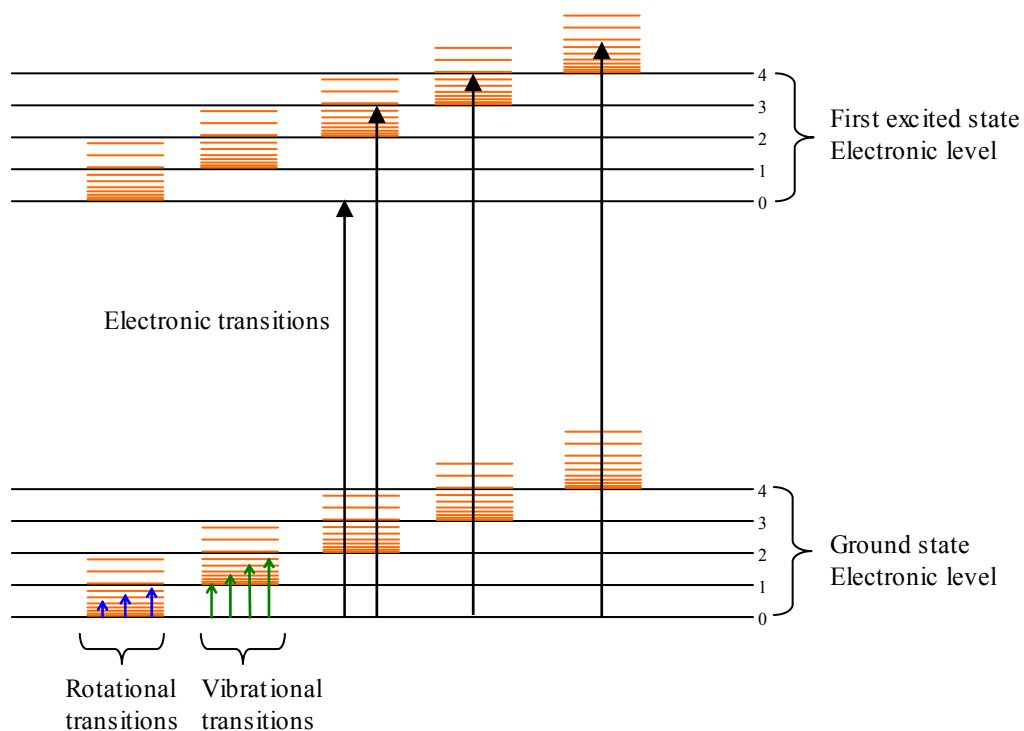


Figure 2.3. An illustration of a two electronic state system: showing the associated vibrational (black lines) and rotational (red lines) energy levels for each electronic level. The different types of transitions between the energy levels are also illustrated.

The diagram in figure 2.3 show absorption processes between energy levels, for any states linked by absorption. Emission can also occur. Whether a particular transition is allowed or forbidden is governed by selection rules, and the form of the rule depends upon the type of transition. For vibrational transitions in harmonic oscillators the selection rule $\Delta v = \pm 1$ applies, where v is the electric dipole moment of a molecule. The molecule need not have a permanent dipole for vibrational transitions to occur, as long as its oscillation results in an oscillating dipole which interacts with the electromagnetic field. For rotational transition in a diatomic the molecule must have

zero point energy (the lowest possible energy greater than zero) and must be polar; transitions are allowed only when $\Delta J = \pm 1$, where J is the rotational quantum number.

The majority of transitions utilised in the BBCEAS work presented here are electronic transitions following absorption of visible radiation (NO_2 , HONO, I_2). The absorption of water is observed for the high vibrational overtones ($\Delta v = 6$ in the stretching modes for the green H_2O band).

2.2 Spectroscopic methods

Spectroscopic methods fall into two basic categories: absorption or emission spectroscopy, with a variety of different methodologies now routinely employed for each category. Absorption spectroscopy utilises the molecule-radiation interactions which involve photon absorption. The molecule undergoes a transition from a low energy state to an excited state, with the absorbed energy being monitored and quantified. Emission spectroscopy utilises the excited state of a molecule; monitoring and quantifying the photons emitted by the molecule as it returns to a lower energy state.

Absorption spectroscopic methods can be a preferable method over emission spectroscopy, as rapid quenching of excited states formed by photon absorption leads to a reduction in emission quantum yield, i.e. it's harder to get emission to occur over quenching processes in many circumstances. Absorption spectroscopy can be a less viable method if the species of interest are in low concentration or if the path length of the sample is short. This stems from the Beer Lambert law discussed in section 2.2.1. A

branch of absorption spectroscopy which employs high finesse cavities (a cavity formed between two highly reflective mirrors) surmounts the issues associated with the need for a long path length for high sensitivity, by enabling long path lengths (several kilometres) by reflection of light within the cavity in compact instrumentation. To date many variants of cavity based absorption spectroscopy for trace quantity detection have been developed. The cavity techniques are described in more detail in sections 2.3 and 2.4.

2.2.1 Absorption spectroscopy

In an absorption experiment radiation incident upon a gas sample interacts with the sample through scattering and absorption. The absorption process depends upon the wavelength of the incident radiation and is defined by the Beer Lambert law. The Beer Lambert law (equation 2.1) relates sample concentration of the absorber, $[x]$, to the absorption given the sample path length, (l) , and absorption cross section $(\sigma(\lambda))$ of the sample species and the incident radiation intensity, $I_0(\lambda)$. An absorption cross section is a measure of the probability of photon absorption at a particular wavelength.

$$I(\lambda) = I_0(\lambda) \exp(-\sigma(\lambda) \cdot [x] \cdot l) \quad \text{Equation 2.1}$$

The illustration of a basic absorption experiment with a single absorbing species in the sample is shown in figure 2.4: all the parameters except the concentration of the sample are measurable. The Beer Lambert law can be used to determine the concentration of the sample species. The product of absorber cross section, absorber concentration and path length $(\sigma \cdot [x] \cdot l)$ must be of sufficient magnitude that

differences between I and I_0 are measurable. For very small concentrations, long path lengths are required in order for the differences between I and I_0 to be detectable. For the very small atmospheric trace gas concentrations in the atmosphere, path lengths of several kilometres are required. The path lengths of LP-DOAS, CRDS and CEAS absorption spectroscopy instruments used for monitoring atmospheric trace gas species encompass path lengths of several kilometres in order to effectively detect such low concentrations. The cavity-based methods are useful because they provide access to long paths in a compact cavity.

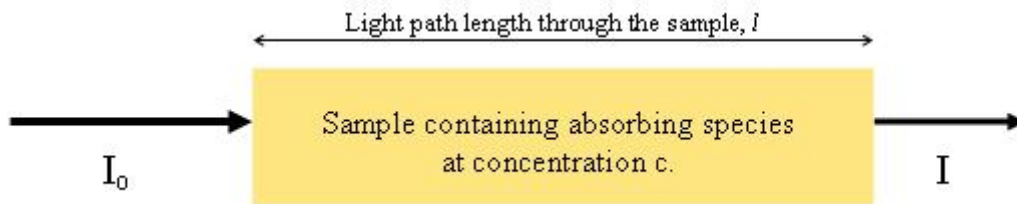


Figure 2.4 Basic absorption of radiation incident onto a single absorber species gas sample with concentration, c .

The spectroscopic analysis of atmospheric samples is more complex than for a single species, as atmospheric samples contain a mixture of gas species, aerosol and particulate matter. The Beer Lambert law is adapted to include more complex terms for the presence of multiple absorbing species and scattering contributions of atmospheric samples, as shown by equation 2.2.

$$I(\lambda) = I_0(\lambda) \exp \left(-l \left(\sum_i^n \sigma_i(\lambda, P, T) x_i + \varepsilon_R(\lambda) + \varepsilon_M(\lambda) \right) \right) \quad \text{Equation 2.2}$$

The additional terms account for multiple absorber species presence; x_i is the concentration of the gas species i of which there may be n different gas species, σ_i is the wavelength, temperature and pressure-dependant cross section of the gas species i . The remaining additional terms ϵ_R and ϵ_M are scattering terms, corresponding to Rayleigh and Mie scattering respectively.

Light Scattering

Electromagnetic radiation can experience scattering. The extent of scattering depends upon size of molecule or atom relative to the wavelength of the radiation. Scattering is a product of electrons within the molecule oscillating and re emitting radiation. If the re-emitted radiation interferes destructively in all but the initial direction of the incident radiation, it appears to have no effect, i.e. is cancelled out. The main forms of scattering are Rayleigh and Mie scattering, named after those who first worked to understand the processes and defined the terms.

Rayleigh scattering.

Rayleigh scattering occurs when a molecules' radius is smaller than the incident radiation wavelength. The scattering can be express as a ratio of particle dimension and radiation wavelength; the dimensionless size parameter α is determined using the particle radius, r , and wavelength of radiation, λ :

$$\alpha = \frac{2\pi r}{\lambda} \quad \text{equation 2.3}$$

Rayleigh scattering occurs when the size parameter is less than 1. The intensity of Rayleigh scattering from un-polarised light depends upon the particle size and wavelength and was first expressed by Rayleigh in 1899. The polarization of the incident radiation has an effect on the scattering; if the incident radiation is polarized perpendicular (at a right angle) to the incident direction, the scattering is isotropic (in the same direction), whilst plane polarized radiation scatters over all directions. The Rayleigh scattering cross section, σ_R is a wavelength-dependent parameter; with shorter wavelengths being scattered more effectively than longer wavelengths, i.e. it is proportional to λ^{-4} .

Mie scattering.

Mie scattering occurs when spherical particles or molecules are of either a comparable size, or larger than the wavelength of incident radiation. Mie scattering has a weaker wavelength dependence compared to Rayleigh scattering and a larger dependence upon size. The size parameter α is determined using the diameter of the particle, d , and wavelength of radiation:

$$\alpha = \frac{d\pi}{\lambda} \quad \text{equation 2.4}$$

Smoke, dust, pollen and water vapour are common causes of Mie scattering.

2.3 Cavity based spectroscopy techniques

The earliest cavity technique cavity attenuated phase shift (CAPS) introduced in 1980 to determine mirror reflectivity. The method was improved upon by the Anderson reflectometer in 1982 and the subsequent conceptualisation of Cavity Ring Down Spectroscopy (CRDS) in 1988 by O'Keefe revolutionised high sensitivity spectroscopy. To date CRDS and the related cavity techniques remain forerunners in high sensitivity measurement techniques. The high sensitivity of cavity techniques makes them an ideal option for use in atmospheric science where the molecules of interest are often present at high dilution.

Cavity based spectroscopy techniques provide high sensitivities by accessing very long path lengths within the cavity; multiple reflections of radiation within the cavity can create path lengths of several kilometres within relatively small instruments. The long path length enables a measureable difference between the incident radiation, I_0 , and I the radiation transmitted through the sample, thus providing a method for absorber quantification using the Beer Lambert law.

Here a brief history of cavity techniques is given, followed by a description of cavity ring down spectroscopy; the first spectroscopic technique to utilise optical cavities, which led to developments of related cavity spectroscopy techniques. Finally the technique of Cavity Enhanced Absorption Spectroscopy is described.

2.3.1 A brief history of cavity techniques

The entirety of the current cavity-based spectroscopic techniques used today stem from work by Herbelin et al 1980. Herbelin developed the cavity attenuated phase shift (CAPS) method to determine mirror reflectivity, which is described well in the review by Scherer et al [Scherer et al., 1997]. Photon lifetime within a cavity is related to the phase shift of the modulated light entering and exiting the cavity. If the photon lifetime and the cavity mirror spacing are known, the reflectivity of the mirror can be ascertained provided the reflectivity of one mirror is already known. Mirror reflectivity was measured using this method with precisions of between 50 and 5000 ppb [Scherer et al., 1997]. The sensitivity of the CAPS method is governed by the uncertainties in phase shift measurement, modulation frequency and cavity length.

The next major advancement in cavity techniques was made by Anderson et al in 1983. Anderson measured the photon lifetime in the cavity by directly monitoring the light intensity decay from light exiting the cavity with a fast detector. When the light intensity within the cavity reached the threshold value (determined by the comparator), the laser light is blocked by the Pockels cell and the light intensity exiting the cavity then decays exponentially according to equation 2.5. The ring down time (τ) is related to the mirror reflectivity (R) according to equation 2.6.

$$I(t) = I_0 e^{-t/\tau} \quad \text{equation 2.5 [Scherer et al., 1997]}$$

$$\tau = \frac{L}{c} \left(\frac{\sqrt{R}}{1-\sqrt{R}} \right) \quad \text{equation 2.6 [Scherer et al., 1997]}$$

This approach to mirror reflectivity determination gave significant improvements over the CAPS method due to the relaxed time constraints of the measurement of decay time and the ease of the decay time measurement in comparison to CAPS.

Cavity Ring Down Spectroscopy (CRDS), developed by O'Keefe and Deacon in 1988 overcame the technical difficulties of CAPS and the Anderson methods which were associated with mode matching between the light source laser and the cavity modes. CRDS employed a pulsed laser light source, which simplified the experimental set up by removing the necessity of complex fast switching and threshold triggering aspects.

2.3.2 Cavity Ring Down Spectroscopy

Cavity ring down spectroscopy is conducted with a typical spectrometer setup, requiring a light source, a sample vessel and a detector to monitor radiation intensity. The sample region of a CRDS instruments is a high finesse optical cavity (a cavity formed between two highly reflective mirrors). A representation of a high finesse cavity is shown in figure 2.4. Two highly reflective, concave mirrors are positioned such that light introduced to the cavity by a pulsed laser, reflects back and forth, and with each pass a small amount of intensity is lost via transmission through the mirrors. The intensity leaking from the optical cavity is measured by way of a suitable detector as a function of time. The peak intensities of the series of output pulses fits to a first order decay, which is used to determine the cavity loss as a function of time (Ring Down Time).

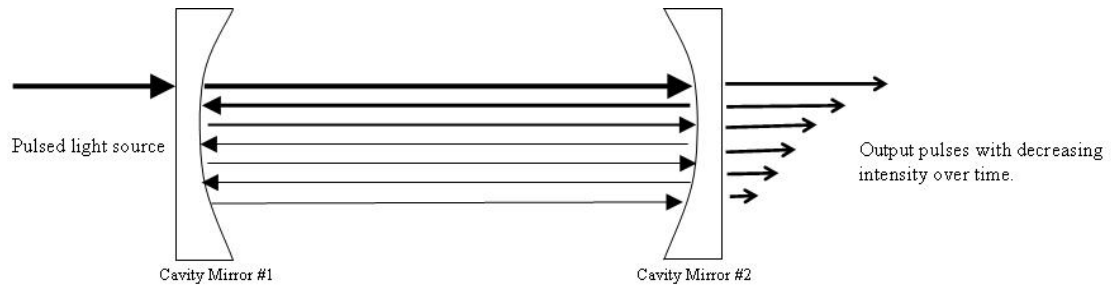


Figure 2.5. Light behaviour from a pulsed source inside an optical cavity showing cavity losses via transmission through the cavity mirror.

The light intensity within an optical cavity for a cavity with no absorbing species present (blue trace) and for the same cavity with an absorbing sample present (red trace) is shown in figure 2.6. In each circumstance light intensity follows a set behaviour pattern. Following light injection into the cavity, light intensity builds to a steady state between 0-150 μs , the intensity remains at the steady state between 150-700 μs , at which point the light source is switched off or blocked, and the light intensity decays exponentially as shown in the region between 700 and 1000 μs .

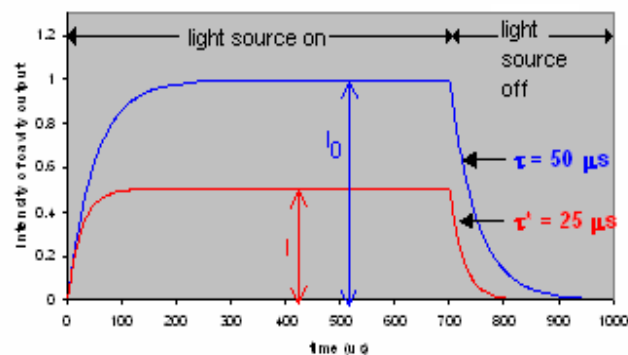


Figure 2.6. Light intensity within an optical cavity over time. I_0 represents the cavity being purged with a non absorbing gas, the background measurement. The sampling measurement I is when the cavity is filled with a sample containing an absorbing species.

The decay of light intensity from the cavity is exponential, decreasing at a rate proportional to the initial intensity as the same fraction of light intensity is lost on each pass of the cavity due to the mirror reflectivity.

For a cavity with no absorber present the loss of light intensity is due only to the cavity mirror surface reflectivity and transmission through the mirror, for a cavity with a sample the loss of light intensity is due to the cavity mirror, transmittance and any absorption and scattering of the sample. Hence the decay of light intensity for a cavity with a sample present is faster than for an empty cavity, as it has additional loss processes.

The ring down time for an empty cavity (τ) (a cavity with no absorbing molecules present), is related to the distance between the cavity mirrors (d), the speed of light (c) and the mirror reflectivity $R(\lambda)$ according to equation 2.8. The loss of light intensity for an empty cavity is due only to imperfect reflections of the mirror.

$$\tau(\lambda) = \frac{d}{c} (\ln R(\lambda)) \quad \text{equation 2.8.}$$

During CRDS operation two ring down times are measured, the ring down time $\tau(\lambda)$ with the cavity filled with non absorbing gas species and the ring down time with the cavity filled with an absorbing or sample species $\tau^*(\lambda)$. The two ring down time measurements enable the sample absorbance per path length to be calculated and thus concentrations of absorber species determined.

The decay times for the empty cavity and cavity with sample present are linked to the absorption processes per unit path length (α) as shown by equation 2.9. The absorption of the sample contains contributions from all absorbing species i , the

concentration x of species i and the absorption path length l . If all parameters but the concentration of the absorbing species i are known equation 2.9, can be used to determine the absolute concentration.

$$\frac{1}{\tau^*(\lambda)} = \frac{1}{\tau(\lambda)} + c\alpha(\lambda) = \frac{1}{\tau(\lambda)} c \sum_i \sigma_i(\lambda) x_i l \quad \text{equation 2.9}$$

Since Cavity Ring down Spectroscopy's (CRDS) first application to study the doubly forbidden visible bands of oxygen by O'Keefe, the technique has been employed in many applications. CRDS and the related cavity techniques are now widely employed techniques for sensitive spectroscopic measurements as they are highly sensitive techniques which can detect the very small concentrations of trace gas species present in atmospheric samples. Table 2.2 summarises some of the atmospheric measurements reported employing cavity techniques.

Cavity technique	Atmospheric absorber	References
Pulsed CRDS	NO ₂ , NO ₃	References 12, 85 and 97 of [Brown, 2003]
CW CRDS	CH ₄ CO ₂ N ₂ O ₅	References 53,61 and 95 of [Brown, 2003]
Broad band BCRDS	NO ₃ , I ₂ , OIO	[Ball and Jones, 2003]
Cavity attenuated phase shift spectroscopy	NO ₂ , Rayleigh scattering	[Kebabian et al., 2005]
BBCEAS (LED)	NO ₃ , I ₂ , NO ₂ , O ₄ , N ₂ O ₅ , HONO	[Ball et al., 2004], (Langridge 2006) and (Langridge 2008)
Incoherent BBCEAS (arc lamp)	NO ₃ , NO ₂ , aerosol Extinction	

Table 2.2 Atmospheric measurement using cavity techniques

2.3.3 Cavity enhanced absorption spectroscopy (CEAS)

Cavity enhanced absorption spectroscopy is a spectroscopic technique related to CRDS. Like CRDS it also utilises a high finesse cavity in order to make highly sensitive spectroscopic measurements. In CEAS light from a continuous wave source is injected into the cavity, rather than a pulsed source as in CRDS. The behaviour of light inside an optical cavity during a CEAS experiment is illustrated in the earlier time section (0 μ s to 700 μ s) of figure 2.6. The measurements performed during BBCEAS operation are time integrated measurements of the steady state light intensity of the cavity with no absorber present (I_0), and the same time integrated measurement with a sample present (I) as shown by the blue and red traces respectively in figure 2.6. This steady state light intensity is proportional to the ring down time, thus inversely proportional to the absorption coefficient. Provided the mirror reflectivity of the cavity mirrors and cavity length are known the absorbance of the sample can be calculated using equation 2.10. During CEAS measurements the laser light source is scanned in frequency, thus building up the spectrum over a range of wavelengths.

$$\alpha(\lambda) = \left[\frac{I_0(\lambda)}{I(\lambda)} - 1 \right] \cdot \left[\frac{1-R(\lambda)}{l} \right] \quad \text{equation 2.10}$$

The calculated absorbance can be used to determine the concentration of the absorber or absorbers in the sample using the Beer Lambert law; for a single absorber the form shown in equation 2.1 or for samples with multiple absorber species equation 2.2.

The first reported CEAS measurements were by Engelen et al in 1998 who recorded the spectra for oxygen, water vapour and ammonia [Engeln et al., 1998]. The most

notable implication of the “new” cavity based spectroscopic technique was that it enabled a relatively simple experimental set up which achieved sensitivities comparable to the more laborious CRDS technique. Following its first laboratory applications CEAS rapidly became a valuable technique in atmospheric research: the simple setup and robustness of the instrumentation and high sensitivity measurements made CEAS and similar techniques forerunners in methods to quantify atmospheric trace gases.

The wide range of atmospheric trace gas molecules under study using cavity techniques just a few years after the development of CEAS and within a decade or so of CRDS is demonstrated in Brown’s review of absorption spectroscopy using cavity based instrumentation for atmospheric studies in 2003 [*Brown, 2003*].

2.4 Broad Band Cavity Enhanced Absorption Spectroscopy (BBCEAS)

The broad band variant of CEAS is used throughout the work presented in this thesis to make quantitative measurements of trace gas species in the atmosphere. This section describes the theory of BBCEAS while specifics for the instrumentation employed during measurements are described in chapter 3 and the results chapters 4, 5, and 6.

Broad band CEAS has further advantages over the original CEAS technique as it employs a broad band continuous wave light source which enables the spectra of entire absorption bands (over the light source band width) to be captured in a single measurement, rather than having to scan laser frequency to produce the spectrum.

The first research scientists to implement a broadband continuous wave light source (a short arc Xe lamp) in a CEAS setup were Fielder et al [Fiedler, 2003] who measured absorption bands of oxygen and azulene. Since this first implementation of broadband light sources the broadband variant of CEAS has been employed by many research groups in both laboratory and field (atmospheric) studies. The principles of operating a BBCEAS instrument and the analysis methods to derive absolute concentrations are described here.

As with CRDS and CEAS, BBCEAS uses an optical cavity formed between two highly reflective ($R > 0.999$) mirrors. Following the injection of broad band continuous wave light into the cavity through the back of one cavity mirror, the light intensity within the optical cavity builds to a steady state. In BBCEAS each wavelength component of the broad band light source has its own steady state intensity within the cavity. This wavelength dependent steady state light intensity, as in CEAS, is directly proportional to the ring down time for a particular wavelength of light within the cavity. The steady state light intensity leaking from the cavity is dispersed in wavelength by a spectrometer and imaged on a suitable detector (typically a CCD) over a specified time period.

For BBCEAS measurements to yield sample species concentrations several types of measurement are required to calculate the absorption (see equation 2.10). $I_0(\lambda)$ and $I(\lambda)$ are time integrated cavity output measurements for the cavity across the wavelength span of the light source. $I_0(\lambda)$ is the time integrated output of the cavity filled with a non absorbing gas: this is the background measurement for the cavity. $I_0(\lambda)$ is a measure of the cavity losses due to the instrumental components, e.g. the

cavity mirrors being imperfect reflectors. $I(\lambda)$ is the time integrated cavity output measurement recorded with a sample present in the cavity, where losses of intensity are due to the instrumental components plus any absorption or scattering processes due to the sample molecules present in the cavity. The cavity mirror reflectivity across the wavelength range of the measurements, $R(\lambda)$, must also be known, along with the length of the cavity, L , the distance between the cavity mirrors.

2.4.1 BBCEAS for atmospheric samples

Samples from the atmosphere contain multiple absorbing chemical species with overlapping absorption cross sections in the bandwidth of the time integrated light intensities of the cavity measurements. This results in the calculated absorbance containing contributions from multiple species which are present at varying concentrations, along with the more broadly spread in wavelength contributions due to Rayleigh and Mie scattering from molecules and aerosol. These different contributions must be separated and quantified to obtain the desired information from the experiments. The analytical method favoured for this task is to adopt the approach of Differential Optical Absorption Spectroscopy (DOAS). DOAS fitting enables different absorber molecules, which have overlapping structured absorption cross sections in the region of interest, to be unambiguously identified and quantified, provided that the mirror reflectivity over the wavelengths of the measurement and the absorption cross sections of the absorbers are known. The methods for determining cavity mirror reflectivity are described in section 2.4.2 while the DOAS method to retrieve absorber concentration from mixed samples is described in section 2.4.3.

2.4.2 Mirror reflectivity determination: theory

The reflectivity, R , of the cavity mirrors changes across the wavelength bandwidth recorded in BBCEAS measurements. A detailed knowledge of the wavelength dependent reflectivity, $R(\lambda)$, is essential to quantify the absorption as any absorption has a direct dependence on $R(\lambda)$, shown by equation 2.10.

$$\alpha(\lambda) = \left[\frac{I_0(\lambda)}{I(\lambda)} - 1 \right] \cdot \left[\frac{1-R(\lambda)}{l} \right] \quad \text{equation 2.10}$$

Mirror reflectivity can be measured directly using cavity ring down spectroscopy. However in the field operation of a BBCEAS instrument, having the additional components necessary to carry out CRDS measurements would add unnecessary complexity to the instrument. Other methods for determining mirror reflectivity exist which require less instrumentation.

Mirror reflectivity can be determined by measuring the absorption of a sample with known concentration. Measurements of a calibration standard can be utilised, where a sample of known concentration of the absorber of interest is monitored. This may not be straightforward if calibration standards of the target absorber are not easily available. Alternatively the absorption of a sample of known concentration, which is not the target absorber, can be measured, as long as it has absorption structure in the same bandwidth measurements. The measurement of water vapour bands have been successfully utilised by Ball [Ball *et al.*, 2004] to determine mirror curves, which were subsequently used for quantitative detection of I_2 and NO_2 across green wavelengths. Langridge utilised the short lived O_2 - O_2 collision complex absorption bands along with the highly structured NO_2 bands across the blue wavelengths to determine the mirror

reflectivity curve in situ to measure NO₂ in ambient laboratory air [Langridge *et al.*, 2006].

The mirror reflectivity varies with the optical alignment of the cavity, and thus for quantitative BBCEAS the mirror reflectivity must be determined with the same alignment as the measurements are recorded. The methods for mirror curve determination used throughout this work are similar to that used by Langridge *et al.*, using a combination of absorber measurements to define the shape and relative position of $R(\lambda)$. The details are described further in chapter 3, section 3.8.

2.4.3 Differential Optical Absorption Spectroscopy

The absorption spectrum (or optical depth) obtained by the BBCEAS formula (equation 2.10) contains components from all of the absorbing gas species present in the sample. The absorption has two components: contributions due to absorption by molecular species and a component due to scattering. Using the DOAS technique the absorption of multiple species with structured absorption in the bandwidth of the measurement can be distinguished from one another and from the underlying smoothly varying contributions due to scattering. DOAS spectroscopy was pioneered by Noxon in the 1970s and has since been a forerunner in sensitive and quantitative atmospheric measurements. Artificial light sources were first employed in DOAS by Platt (1979 JGR 84 (c10)6329-6335) to retrieve gas concentrations of CH₂O, O₃ and NO₂. The first real time DOAS measurements of several species simultaneously were by Platt and Perner in 1983.

The process used to distinguish multiple absorber contributions is illustrated by considering the absorption signals of a single absorbing species A shown in figure 2.7 and for two absorbing species, A and B in figure 2.8. The first measurement is the light intensity as a function of wavelength with no sample present, $I_o(\lambda)$, (reference spectrum in figure 2.7). The light intensity after attenuation by a sample is measured, $I(\lambda)$ (measured signal in figure 2.7). The absorption shown for A has a slowly varying broadband extinction, $\alpha_{BB}(\lambda)$, and an absorption feature at the wavelength marked λ_2 , thus $I(\lambda)$ can be defined by these in a form of the Beer Lambert law, as shown in equation 2.11, where l is the path length and x_A is the concentration of species A. The contribution to the spectrum of only broadband scattering can be represented by equation 2.12, and this is shown in figure 2.7 by the light grey trace labelled $I'_o(\lambda)$. The broadband scattering, $I'_o(\lambda)$ can be constructed by polynomial interpolation to the measured light intensity through a sample ($I(\lambda)$).

$$I(\lambda) = I_o(\lambda) \exp(-\sigma_A(\lambda)x_A l - \alpha_{BB}(\lambda)l) \quad \text{equation 2.11}$$

$$I'_o(\lambda) = I_o(\lambda) \exp(-\alpha_{BB}(\lambda)l) \quad \text{equation 2.12}$$

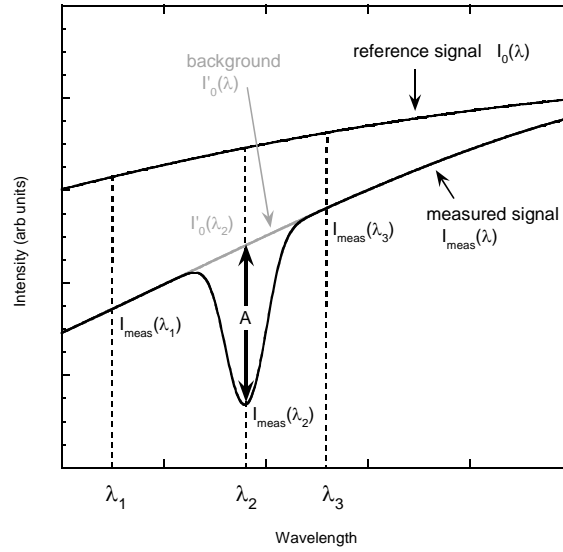


Figure 2.7 Differential optical absorption spectroscopy for one structured absorber, A in the presence of a smoothly varying background extinction.

The optical depth (OD) due to absorbing species A can be determined using the measured intensity ($I(\lambda)$) and the interpolated broadband scattering ($I'_o(\lambda)$) from rearrangement of the Beer Lambert law, shown in equation 2.13.

$$OD_A = -\ln \left[\frac{I(\lambda_2)}{I'_o(\lambda_2)} \right] = \sigma_A(\lambda_2) x_A l \quad \text{equation 2.13}$$

The concentration of A can then be deduced if the absorption cross section of A is known across the bandwidth of the measurement and the path length l .

$$x_A = \frac{1}{\sigma_A(\lambda_2) l} \ln \left[\frac{I'_o(\lambda_2)}{I(\lambda_2)} \right] \quad \text{equation 2.14}$$

This method can also be used to measure the concentration of target species in the presence of other absorbing species. The measured signal due to species A and absorber species B is shown in figure 2.8.

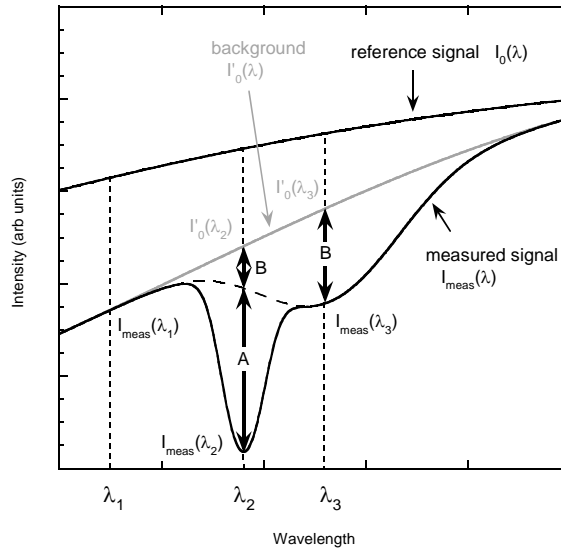


Figure 2.8 Differential optical absorption spectroscopy for two structured absorbers, A and B in the presence of a smoothly varying background extinction.

The same approach used for determining the concentration of A can be applied and the concentration of B determined at wavelength λ_3 , using equation 2.15.

$$x_B = \frac{1}{\sigma_B(\lambda_3)l} \ln \left[\frac{I'_0(\lambda_3)}{I(\lambda_3)} \right] \quad \text{equation 2.15}$$

The optical depth in the presence of multiple absorbers is defined by equation 2.16; measurements at a minimum of N different wavelengths are required to distinguish N different absorbers.

$$OD_{\text{absorbers}} = -\ln \left[\frac{I(\lambda)}{I'_0(\lambda)} \right] = \sum_{\text{absorbers}} (\sigma_i(\lambda)x_i) \times l \quad \text{equation 2.16}$$

The BBCEAS spectra are recorded at several hundred wavelengths simultaneously across the wavelength band width, and thus the DOAS methodology is readily applied for the analysis of BBCEAS spectra. The concentration of absorber species (x_i) is obtained by DOAS fitting of the differential absorption structure of the BBCEAS spectra, as the absorbance contains components from all the absorbing species and the broad band extinction due to scattering, equation 2.17.

$$\alpha(\lambda) = \left[\frac{I_0(\lambda)}{I(\lambda)} - 1 \right] \cdot \left[\frac{1-R(\lambda)}{l} \right] = \sigma_1(\lambda)x_1 + \sigma_2(\lambda)x_2 + \sigma_3(\lambda)x_3 \dots \dots + \alpha_{BB}(\lambda)$$

equation 2.17

2.4.4. Molecular absorber cross sections

A requirement for quantitative BBCEAS is knowledge of the absorber cross section across the wavelength bandwidth of the measurements. A range of chemically active absorbers in the atmosphere are shown in figure 2.9 for the visible and near UV region. These examples highlight the versatility of the BBCEAS technique to monitor different gas species depending upon the wavelengths monitored.

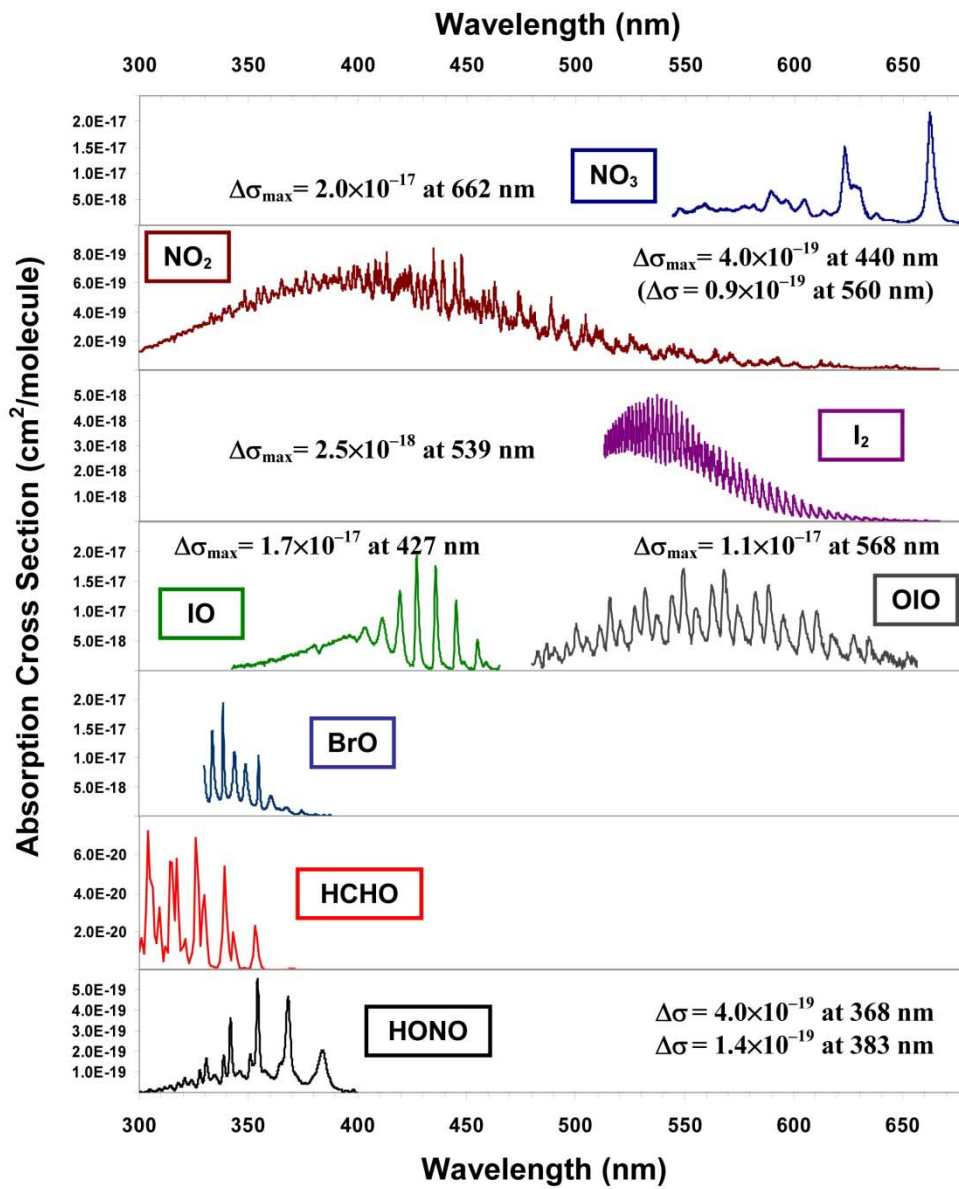


Figure 2.9 Molecular absorber cross sections as a function of wavelength.

2.5 Summary

This chapter provides a basic introduction to the theory of absorption spectroscopy. Absorption spectroscopy possesses a number of useful properties that can be applied to both identify and quantify molecules in the presence of others, such as for example the complex mixture of gases that comprises our atmosphere. Cavity-based absorption methods are reviewed because such methods provide access to the very long absorption paths lengths needed to measure trace gases at the high dilutions that they occur in the atmosphere. The theory of BBCEAS has been presented along with the theory of the DOAS method of analysis to retrieve quantitative information of absorbers present in mixed absorber samples.

Chapter 3

LED BBCEAS instrument: development and operation

3.1. Introduction

The measurements presented in this thesis were conducted using the University of Leicester's Broad Band Cavity Enhanced Absorption Spectroscopy (BBCEAS) instrument. As already introduced in chapter 2, BBCEAS is a highly sensitive technique capable of quantifying the concentrations of trace gases at high dilutions (e.g. the parts per billion or parts per trillion mixing ratios that reactive trace gases occur in the ambient atmosphere). The key requirement is that the target molecules absorb light within the spectrometer's bandwidth. The structured contributions to the measured absorption spectrum are used to identify and quantify the absorbing molecules present in the sample. Since the absorption cross sections of a given absorber are unique to that absorber, the spectral structure enables the different species present in mixed samples to be unambiguously distinguished from one another, and for the concentration of a target absorber to be determined in the presence of other absorbing or light-scattering species.

The high sensitivity, variability of operation bandwidth and unambiguous identification of molecular absorbers gives BBCEAS diverse applications in both laboratory and field studies. BBCEAS can be carried out at a range of time resolutions, thus enabling changes of concentrations to be monitored on rapid time scales. An additional advantage of BBCEAS over other spectroscopic techniques used to sample atmospheric air masses is that, in favourable cases, several species with structured absorptions

within the instrument's band width can be measured at the same time. It is also possible to have the cavity open to the ambient atmosphere (to run the measurements "open-path") and hence conduct measurements in the absence of inlet and wall losses, which is important when monitoring particularly reactive trace species such as radicals. The BBCEAS instrument also combines a long light path with a compact instrument, enabling in situ measurements to be conducted at a precisely defined location and thus pinpointing the sources of reactive trace gas species. In comparison, the complementary technique of long-path DOAS retrieves concentrations averaged over light paths of several kilometres, making locating sources more difficult.

The specific configuration of the BBCEAS instrument depends upon the trace gas absorber species of interest during a particular study. Different wavelength regions have been employed in this thesis to enable a variety of absorber molecules to be quantitatively monitored in both lab and field work applications. This flexibility of BBCEAS is achieved by relatively simple instrumentation modifications, specifically exchanging the LED light source and the cavity mirrors for ones appropriate to a new bandwidth, and adjusting the spectrometer to operate with these new wavelengths. This chapter provides a description of the BBCEAS instrument, from its early laboratory development through to the building of a field capable instrument.

3.2. The BBCEAS instrument: general overview.

The principal components of a BBCEAS instrument are a light source, a high finesse optical cavity and a wavelength-resolved detector. The BBCEAS instrument is shown schematically in figure 3.1, and pictorially in figure 3.2. Each of the principal

components are discussed in detail in dedicated sections which follow. The Leicester BBCEAS instrument is based on the proof-of-principle LED-BBCEAS study of Ball [Ball *et al.*, 2004] and the subsequent NO₂ BBCEAS instrument of Langridge [Langridge *et al.*, 2004].

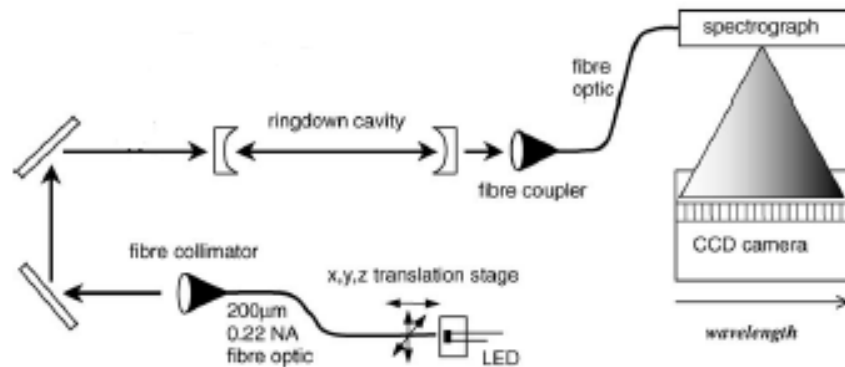


Figure 3.1. Schematic diagram of the optical layout of the LED BBCEAS instrument set up, adapted from Ball [Ball *et al.*, 2004].

The BBCEAS light source, a light emitting diode (LED), provides continuous wave broad band radiation over a bandwidth of typically 50 nm. The LED's emission is coupled into a fibre optic cable and re-collimated at the far end of the fibre using a collimating lens. The input end of the fibre optic cable is held immediately in front of the LED's active area by a mount supported on a finely adjustable x, y, z translation stage. The collimating lens at the output end of the fibre produces a collimated light beam of approx 5mm diameter which is directed, via two turning mirrors, into the cavity through the back of a cavity mirror. These components are shown in figure 3.2, by the left and centre picture in the top panel.

The cavity mirrors, are dielectric mirrors with a high reflectivity (>99%) across a particular wavelength range. Two identical cavity mirrors are used to create a resonant optical cavity. Light coupled into the cavity propagates back and forth in multiple reflections between the cavity's mirrors creating a long absorbance path length. The steady state light intensity leaking from the cavity's output mirror is collected by a ×5 microscope objective lens and focused into a fibre optic cable (shown in figure 3.2, top panel, right picture). This second fibre optic conveys the cavity output to the detector. The detector combines a grating spectrometer to disperse the cavity output according to wavelength and a charge coupled device (CCD) camera or linear diode array positioned at the spectrometer's focal plane to record an image of the wavelength resolved light.

Much of the hardware was common to all BBCEAS applications discussed in this thesis. But the versatility of the BBCEAS technique arises because the instrument can be configured with different LED light sources and cavity mirrors to operate in a particular wavelength range where the targets species has structured absorption features. By exchanging these components, the BBCEAS instrument can be re-configured to quantify a different absorber in another wavelength region. A large part of the development work presented in this chapter concerns the rigorous testing of LEDs for their performance in BBCEAS, e.g. the intensity and long-term stability of the LEDs' emission, and whether the emission spectrum is optimised to the wavelength-dependences of (i) the absorption cross sections of the target molecule and (ii) the reflection characteristics of the cavity mirrors. As LED and dielectric mirror manufacturers introduced new products, which could be potential candidates for use

in BBCEAS, they were investigated in the laboratory. They are incorporated into the field instrument if they perform better than the existing components.

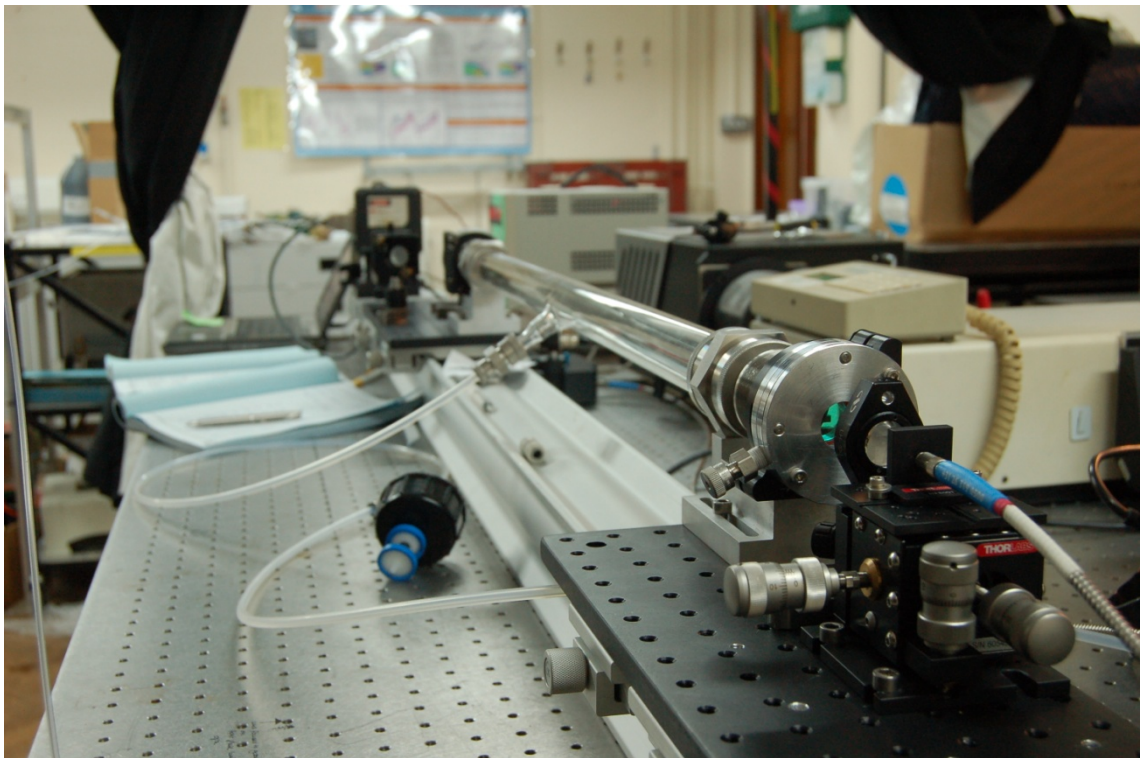
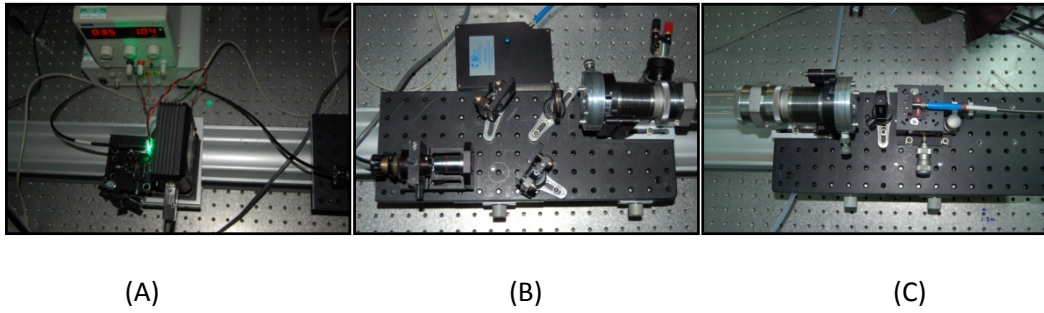


Figure 3.2 The BBCEAS instrument in the laboratory. The top panel of pictures shows, the LED light source (A), the collimating lens, cavity mirror mounting and spectrometer (B), and the cavity mirror and coupling lens (C). Optical fibres guide light from the LED to the collimating lens and from the cavity to the spectrometer. The lower picture shows the complete setup in the laboratory.

3.3 BBCEAS light source: Light emitting diode (LED)

Light emitting diodes now have sufficiently intense emission spectra to make them suitable light sources for broad band spectroscopy. LEDs are efficient, compact and robust light sources, and are thus an ideal option for use in field BBCEAS instrumentation. LEDs possess properties which make them the preferred choice for BBCEAS light sources: they have continuous wave broad band emission, long lifetimes and lower power consumption in comparison to laser sources used in narrow band CRDS. The BBCEAS work presented in this thesis has employed LEDs with emission spectra at near-UV and visible wavelengths to monitor trace gas species which have structured absorption bands at these wavelengths.

A light emitting diode light is constructed from p-n type semiconductor junction, which emits light when a DC voltage is applied across the junction. Manipulation of the interface between the n-type material and the p-type material allows electrons to flow in only one direction. The p-type material accepts electrons from the donor n-type material. The n-type material is pre-treated to increase the amount of negative charge carriers within it. When biased by a voltage, holes within the p-type material and electrons in the n-type are pushed towards the junction resulting in the nonconductive layer becoming thinner. At a sufficiently large voltage, the nonconductive layer becomes thin enough for charge to tunnel across the junction, resulting in the emission of photons when electrons recombine with holes.

The wavelength of the light emitted by an LED is determined by the band gap energy of the materials forming the p-n junction. The earliest LEDs made during the 1950s were made with gallium arsenide (GaAs), which emits infrared wavelengths. The

packing material around the p-n junction of an LED impacts its performance. If the refractive index of the packing material is not a close match to the semiconductor material, back reflection in the packing material can lead to additional heating in the LED. The effects of surrounding temperature changes to LED emission are discussed further in section 3.2.2.

The suitability of commercially available LEDs for use as BBCEAS light sources was investigated in the laboratory. The LED emission was investigated to ensure that there was sufficient light intensity at desired wavelengths. The effect of the surrounding temperature on the LED emission spectra was also investigated.

Potential new light sources were initially identified by viewing the data sheets provided by the LED manufacturers. The data sheets usually include information on the peak wavelength, emission bandwidth and emission intensity at the manufacturer's recommended operating current. However experience showed considerable variability in the peak emission wavelength (± 10 nm was not uncommon) and intensity ($\pm 50\%$), even within LEDs from the same batch purchased at the same time. Thus several LEDs (typically half a dozen) were sourced together and laboratory investigation carried out on each to determine those which were suitable candidates (had sufficient intensity at the desired wavelengths) for use in the BCEAS instrument.

3.3.1 Light source investigations: LED emission spectrum

The optimum position of the fibre optic cable with respect to the LED's emitter is achieved by connecting the output end of the fibre to a fibre-coupled silicon

photodiode and adjusting the x, y, z stage until the maximum photodiode signal is obtained. Once the LED-fibre optic alignment was optimised the light was guided to into the spectrometer and the LED emission spectrum was recorded.

The set up for each of these stages of LED investigation are shown schematically in figure 3.3. To enable absolute comparisons to be made between the intensity of different LEDs, their measured emission spectra were normalised to the voltage recorded by the photodiode during the alignment stage. The fibre optic cable enables the LED output to be guided to either a photo diode, spectrometer or to the collimating lens and cavity.

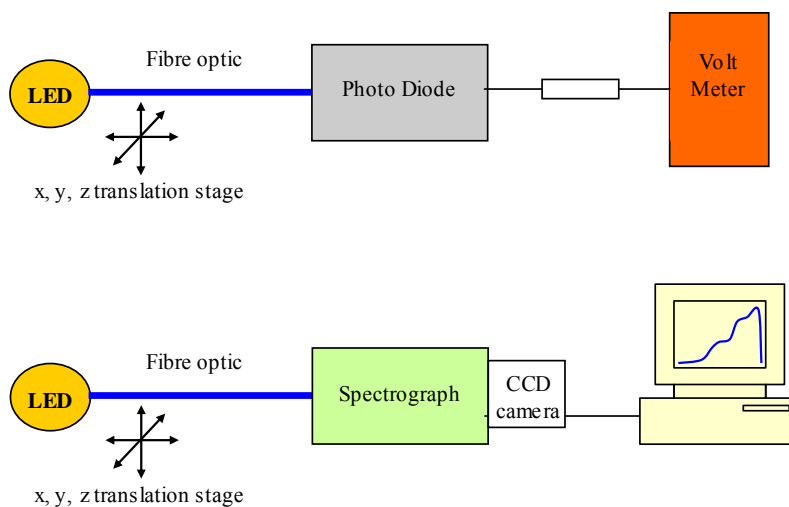


Figure 3.3 LED investigation experiments. Top: positioning of fibre close to the emitter is optimised using the voltage produced by the photodiode terminated through a resistor (wavelength-integrated intensity measurement). Lower: The wavelength resolved LED output is recorded by the spectrometer CCD.

The choice of optimum LED for use in the BBCEAS system depends on a combination of the intensity, peak wavelength and shape of the emission spectrum produced by the LED running at the manufacturer's recommended operating current. The LEDs that

have the highest intensity emission over the desired wavelength ranges are most suited for use in BBCEAS. Even where different LEDs have emissions peaking at the same wavelength, the shape of their emission spectra can vary. For example, the spectra are often asymmetric with the emission tailing to longer wavelength. The typical wavelength bandwidths for the LEDs used in this work ranged from 40 nm to over 60 nm. Also LEDs with smooth Gaussian-like emission spectra are preferred over those with more structured spectra because the former tend to produce smaller baseline undulations in the BBCEAS spectra where there are slight temperature-dependent shifts in LED emission spectra. However this was only a secondary consideration for the green and blue bandwidths because here the brightest LEDs always had structured emissions.

The emission spectra from the commercially available LEDs emitting in the UV-visible bandwidths were investigated for potential use in the proof of principle BBCEAS measurements of nitrous acid: the emission spectra are shown in figures 3.4. The absorption cross section for HONO (nitrous acid) is shown by the black trace in figure 3.4 and the best choice for LED is one whose emission spectrum covers the bandwidth of the absorption structures. HONO has stronger absorption bands to even shorter wavelengths than those shown here but none of the LEDs available at the time of this work could access the shorter wavelengths. The better suited LEDs for HONO detection are the H11A1-HU-30 (dark blue trace, figure 3.4) and C20A1-H390-30 (green trace, figure 3.4) which have strong emission at lower wavelengths.

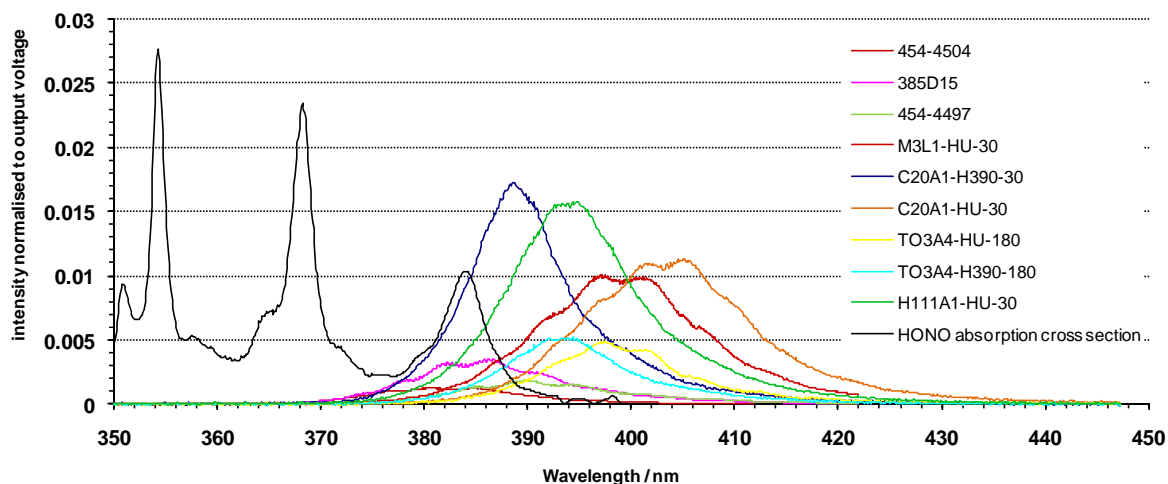


Figure 3.4 LED output from UV LEDs and the HONO absorption cross sections, output has been normalised to the voltage intensity of the LED

The selection of commercially available LEDs with green and blue wavelength emission spectra provided LED's which were sufficiently bright to enable the absorption bands of a variety of atmospheric absorbers to be monitored: the O_2-O_2 and NO_2 absorption bands were used for determining the mirror reflectivity in both the blue and green bandwidths, while the atmospheric species monitored were I_2 and NO_2 .

3.3.2 LED investigations: Temperature effects on LED emission spectra

The emission spectrum of an LED is affected by temperature changes. The LED emission is affected by its environment, e.g. the room temperature and due to current flowing through the LED, which results in heating. The intensity (brightness) and peak wavelength of the LED emission are affected, and thus the temperature surrounding the LED and the drive current used to operate the LED must be controlled in the instrument. The effects of temperature are controlled in the BBCEAS instrument by

mounting the LED on a temperature controlled mount and supplying the LED from a regulated power supply.

Laboratory investigations into the effect of temperature change on LEDs' output typically showed that light intensities were higher and the peak was shifted to a shorter wavelength when the LED was operated at lower temperatures. These effects can be observed in the UV LED emission spectra shown in figure 3.5. The LED was mounted on a temperature controlled mount and operated for a period of several minutes to allow stabilisation at each temperature prior to the emission spectra being recorded. An interesting feature observed in figure 3.5 is the differences between the two traces recorded with the LED stabilised at 10°C. One trace was recorded after the LED had been operated at a unusually high temperatures, and the emission spectrum changed following this heating. The original 10°C trace shown in orange has higher intensity compared to the second 10°C trace shown in purple, which is close to the emission at 20°C in the bright blue trace. This observation shows that the operating conditions of an LED can have long term effect on the emission spectrum. As such LEDs should not be operated outside the manufacturers recommendations. LEDs emission spectrum changes over its lifetime, thus the LED should be operated for extended periods, checking for changes in the emission spectrum, and only utilised in BBCEAS when the emission spectrum is stable.

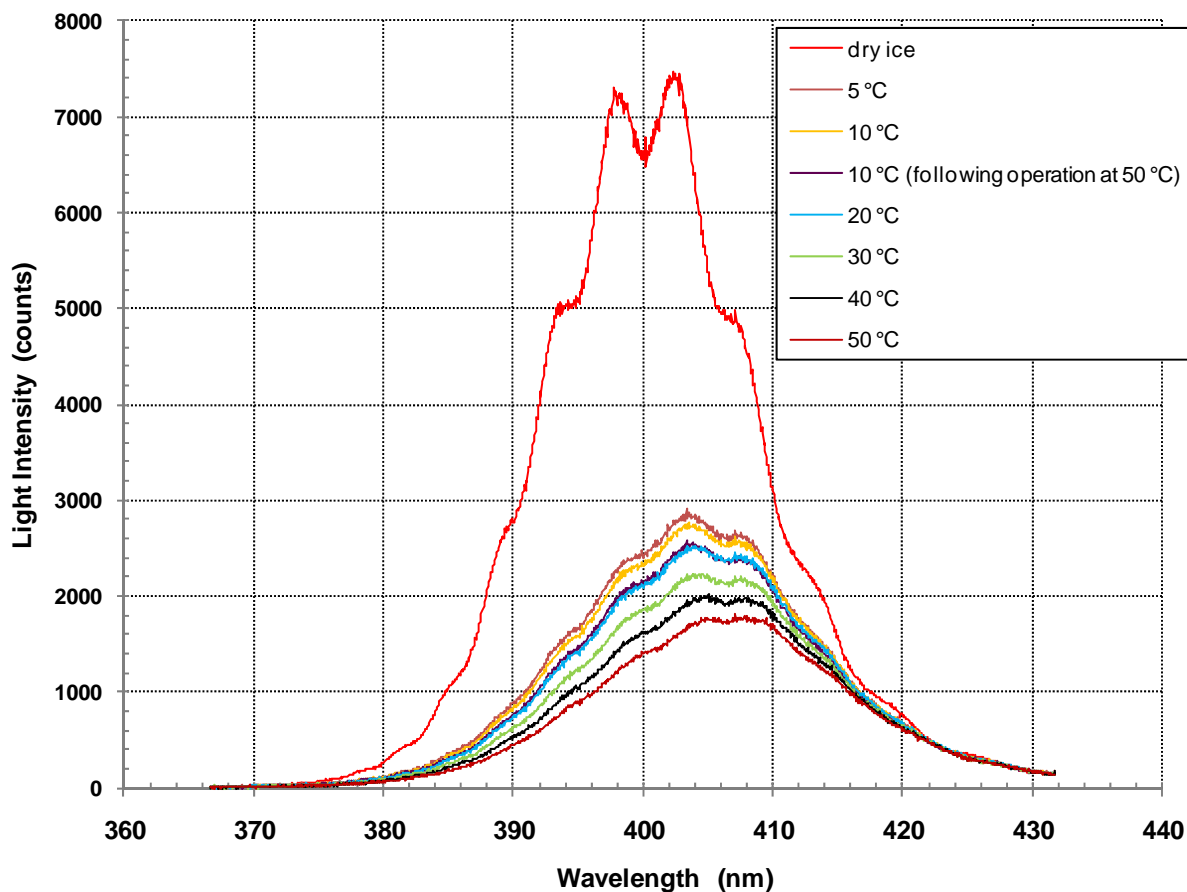


Figure 3.5 The emission spectra of a near-UV LED (M3L1-HU-30) recorded as a function of TEC mount's temperature set point.

The LED emission must be stable over the course of several hours to days for use in long running monitoring instrumentation. If the emission spectra of the LED changes over time, the calculated absorption from sample and flush measurements may include spurious absorbance signals due to the change in LED emission spectrum rather than due to the presence of an absorber.

The investigations into the effect of temperature on LED emission spectra illustrates that maximum light intensity from an LED is achieved by cooling. Thus cooling of the LED is desirable in BBCEAS operation. Cooling with the temperature controlled mount

used in this work below 10°C led to condensation of water from the surrounding air in the laboratory onto the LED. To overcome the issues of condensation whilst maintaining a stable LED emission, a temperature set point (typically 19°C for lab work) close to that of the surroundings was employed. This enabled the Peltier to effectively dissipate the heat. To operate at lower temperatures a larger Peltier cooled mount would be required.

The temperature stabilisation was sufficient for laboratory work when the ambient temperature typically varied over just a few degrees. However temperature stabilisation became an issue during some field deployments, notably the D319 ship cruise (see Chapter 5) where variable and often rather high ambient temperatures resulted in the less than optimal performance of the BBCEAS and difficulty in data analysis.

An alternative solution to maintaining a steady emission spectrum would be to house the LED and fibre coupling mount in a purpose built enclosure. Purging the housing with an inert gas removes the problems associated with water condensation. The housing also thermally insulates the cold side of the LED mount from (warmer) ambient air currents. This type of enclosed LED system is now routinely employed within the Leicester BBCEAS system, but was not developed during the time of the field work presented in this thesis.

3.4 The BBCEAS optical cavity

The BBCEAS optical cavity was formed by two highly reflective ($R > 99.99\%$), concave dielectric mirrors. (The behaviour of light within an optical cavity was described above in chapter 2.) Several manufacturers offer mirrors for cavity-based spectroscopy with reflectivity of $R > 99.9\%$ for visible, near-UV and near-infrared wavelengths. The high reflectivity mirror surface is built up from layers of alternating, high and low refractive index dielectric materials. Light incident upon the mirror surface is reflected at each interface between the different dielectric layers. The reflections are coherent (in phase) and constructively interfere with one another, maximising reflection and minimising transmission of light through the mirror coating. The constructive interference at each interface in a 7 layer mirror surface coating is illustrated in figure 3.6.

The cavity mirrors used in the work presented in this thesis were pairs of identical mirrors supplied by VLOC for the near-UV wavelengths targeting HONO and by Layertec GmbH for blue (12.7mm diameter, high reflectivity X-Y nm, part number 100859) and green wavelengths (25.4mm diameter, high reflectivity X-Y nm, #101851). In order for BBCEAS to yield quantitative measurements, it is vital to know how the reflectivity of the mirrors changes as a function of wavelength, $R(\lambda)$, across the BBCEAS bandwidth. Considerable effort was expended in this work to characterise the mirror reflectivity by performing BBCEAS measurements on known absorbers, particularly O_4 and NO_2 (this is discussed in more detail in Section 3.8).

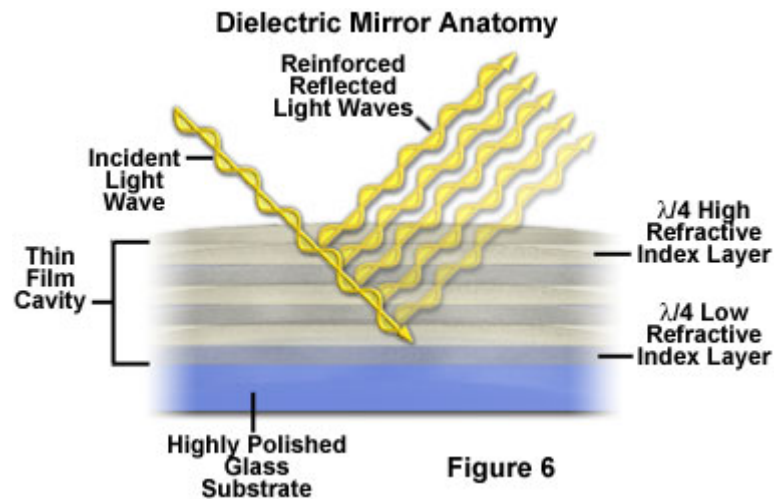


Figure 3.6 Cavity mirror surface structure, showing light reflection and constructive interference at each interface between the layers of different dielectric material.

(<http://micro.magnet.fsu.edu/primer/lightandcolor/mirrorsintro.html>).

The creation and alignment of the cavity is carried out in a series of stages. The first cavity mirror to be positioned is the output mirror. The beam from the collimating lens is reflected by the cavity mirror back towards the lens. An iris positioned close to the lens is used to view the back reflection and the cavity mirror position is finely adjusted (x and y direction) such that the reflected light beam travels the exact same path as the original beam. The second cavity mirror is inserted and an optical cavity is formed. The second cavity mirror sends a reflected light beam back towards the output cavity mirror. The second mirror is finely adjusted in the x and y direction such that this reflection also lies exactly on top of original light path. The light intensity throughput of the cavity is viewed externally and numerically and the cavity mirror position is verified by very small adjustments to the mirror position to maximise the output intensity. When using the UVISEN system (section 3.5.1) a photomultiplier is used to optimise the cavity alignment. When using the Ocean Optics spectrometers the cavity output

was imaged in wavelength continuously by the SpectraSuite software and the best possible alignment being when the maximum intensity at all wavelengths is achieved. Further adjustment decreases the intensity.

3.5. Detectors: spectrometers and CCD imaging

The BBCEAS instrument utilises a grating spectrometer and multi-channel detector to record the wavelength-resolved light intensity exiting the optical cavity. The spectrometer separates light into its wavelength components using a diffraction grating and images the separated light onto a detector (CCD camera or linear diode array) located at the exit focal plane. A schematic showing the components of a spectrometer are shown in figure 3.7.

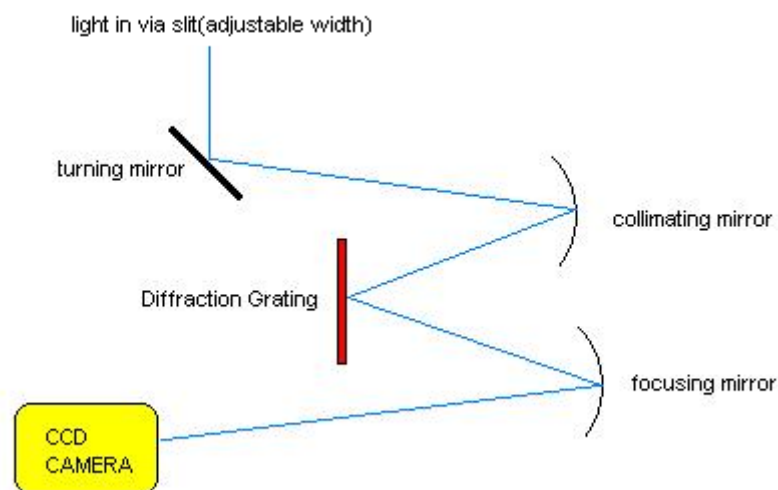


Figure 3.7 Optical layout of an imaging spectrograph, Chromex 250is.

Three different spectrometer/detector combinations were used during the work presented in this thesis. The UVIZEN system comprised a Chromex 250is imaging

spectrograph interfaced to a Wright Instrument's CCD camera (see section 3.5.1). Although rather old (20 years), this system was the most versatile having three rotatable diffraction gratings offering different spectral resolutions and a variable entrance slit. The UVIZEN system was thus used for bench testing prototype BBCEAS systems in new wavelength regions. Two newer HR 2000 and HR 4000 miniature USB spectrometers from Ocean Optics were used for the field instrument and these are described in more detail in sections 3.5.1 and 3.5.2. The Ocean Optics spectrometers are more compact, energy efficient and easily interface to a laptop computer through a USB connection. However they are sealed units that have fixed wavelength ranges and fixed entrance slits, and thus are specific to a single application.

The cavity output spectra are recorded using different software packages for the different spectrometers. The UVIZEN system uses a bespoke software program called UVIZEN which runs in DOS mode (Mr Ray Freshwater, Cambridge University), whereas the Ocean Optics spectrometers operate with the Spectra Suite package supplied by the manufacturer.

3.5.1 Chromex 250is & Wright Instruments CCD camera

The Chromex 250is spectrograph has three diffraction gratings mounted on a rotating turret: 1800 grooves per mm grating for visible wavelengths, 1200 grooves per mm grating blazed at 500 nm and a 600 grooves per mm grating blazed at 500 nm. Table 1 summarises the typical wavelength ranges achievable with each grating and the Wright's Instruments CCD camera used in this work: the 1200 groove per mm grating was used for the majority of BBCEAS experiments because its 65 nm range most

closely matched the width of the LED emission spectra and HR bandwidth of the cavity mirrors. The grating is selected and the central wavelength specified via a key pad on the spectrometer's hand-held controller. Light entered the spectrometer via a microscope object lens ($\times 10$) that focuses the output from a 400 μm diameter fibre optic onto the spectrometer's entrance slit (the slit width was usually 50 μm).

Grating (grooves per mm)	Wavelength range covered with a 26 mm wide focal plane.
1800	43
1200	65
600	130

Table 3.1 The Chromex 250is grating parameters, grooves per mm and the bandwidth of the measurements

The Chromex 250is spectrograph imaged the wavelength-dispersed light leaving its diffraction grating onto a CCD camera positioned at the spectrometer's focal plane. The Wright Instruments camera contains a CCD array of 1152 (horizontal; wavelength dispersed axis) by 298 (vertical) active pixels and was temperature stabilised to -30°C by a Peltier cooled mount. The image for each acquisition was saved as a text file consisting of a number of counts representing the light intensity for each pixel in the CCD array. Since in this application the vertical dispersion of the CCD image carries little information, the image was binned by 4 pixels in the vertical axis before being saved to a computer in order to reduce the file sizes. The pixels are converted to wavelength using Mercury lamp emission lines; the grating is centred such that at least three absorption lines are observed in the scan. The mercury emission lines are well

defined in wavelength, and thus the pixels with the absorption structure can be assigned a wavelength. An example plot of these known wavelength-pixel points is shown in figure 3.8 and the linear fit between the known values obtains the equation for conversion of any pixel to wavelength.

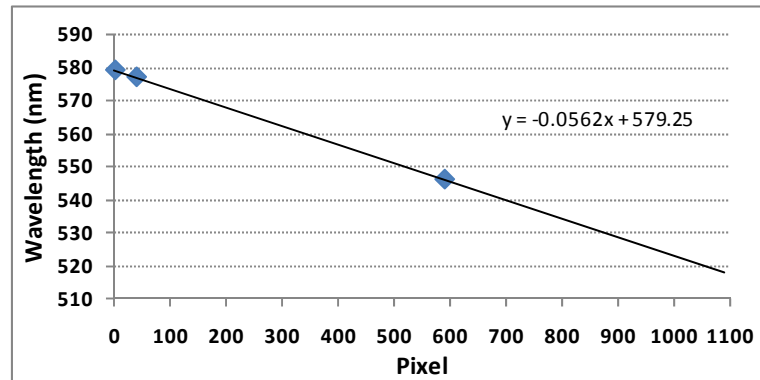


Figure 3.8 Mercury lamp line position and wavelength assignment plot, the equation for the linear fit between the points enables the pixel number to be converted to wavelength.

A representation of a section of the saved file from the UVIZEN system is shown in Figure 3.9, the image represented is for illumination by an atomic mercury emission lamp. The wavelength-dispersed light from the spectrograph illuminates only a small section of pixels across the centre of the camera (pixel columns “A” in figure 3.9), whilst the pixels in the columns either side remain dark. The counts in the latter, non-illuminated pixels (e.g. columns labelled “B” in figure 3.9) were used as a measure of the detector’s dark current.

The light intensity measurement is taken as the average of the counts for all rows in region “A”, the dark current for each pixel is taken by averaging the counts in region “B” of figure 3.9. The pixels at the boundaries of regions “A” and “B” were identified by examining horizontal view through the CCD image file at the pixel of a strong mercury emission line.

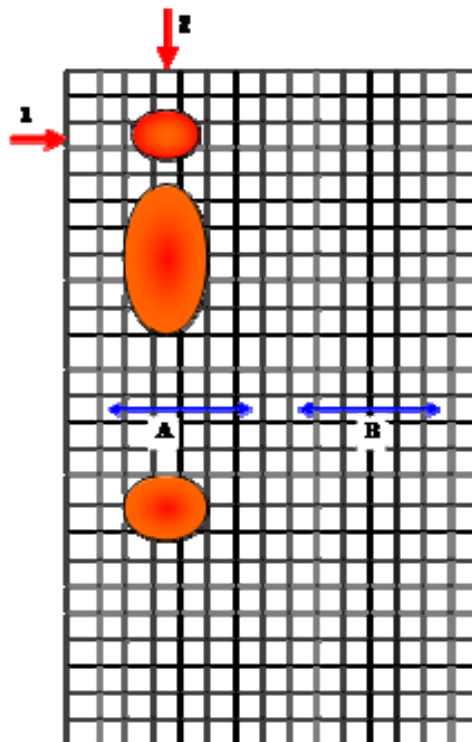


Figure 3.9 Schematic of part the CCD array with spots of light from a mercury lamp source. The actual pixel grid size is 1025 x302pixels.

Example plots for the views shown by the red arrows in figure 3.9 are shown in figure 3.10. The top panel of figure 3.10 is the resulting plot in the direction of arrow 1, which enables the user to define the columns for use in averaging prior to further analysis. The lower panel of figure 3.10 shows the plot in the direction of arrow 2 of figure 3.9: this represents the light intensity measurement dispersed into wavelength

components. For spectral analysis the spectra have the dark current level subtracted. This is done by taking averages of columns 9 to 21 (the illuminated section “A” of the scan) and of columns 26 to 38 (the dark section “B” of the scan), the dark section average is subtracted from the illuminated section average, removing the spectra’s dark current. This subtraction of dark current minimises noise in the fitted spectra produced by DOAS fitting of calculated absorbance.

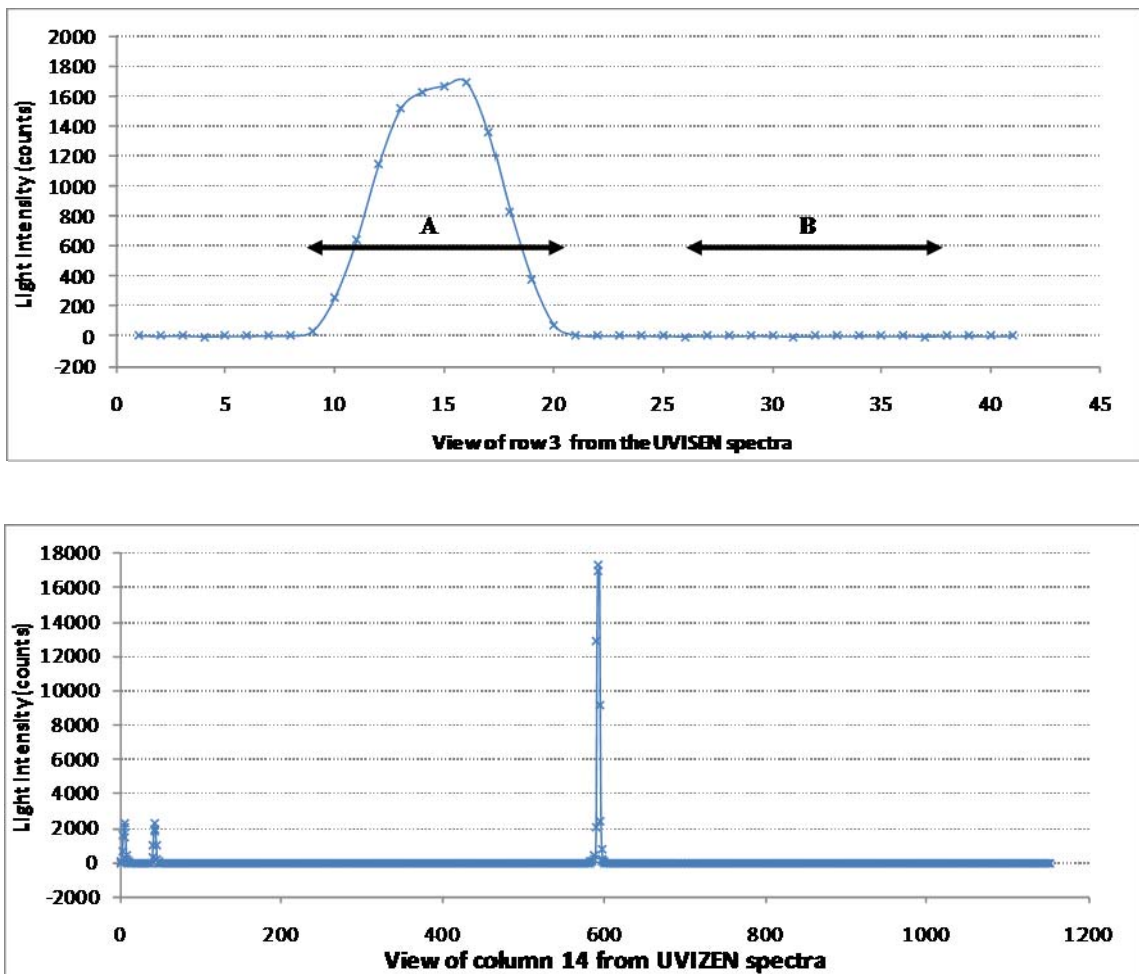


Figure 3.10 View across UVIZEN data file to assign limits used for averaging for illuminated and dark sections CCD array. A and B denote the regions of “A” and “B” across the row highlighted by red arrow 1 in figure 3.9.

3.5.2 Ocean Optics high resolution spectrometer

The Ocean Optics spectrometers HR2000 and HR4000 are compact spectrometers with linear CCD array detectors. The spectrometers had fixed width entrance slits and fixed gratings, specified when the units were ordered from the manufacturer. Thus the Ocean optics spectrometers have fixed spectral resolution and fixed wavelength ranges. The HR2000 covers the wavelength bandwidth 407.0-491.2 nm and the HR 4000 between 504.8-581.9 nm. The devices used in this work were fitted with an SMA fibre coupling to the inlet. The specifications for the two Ocean Optic spectrometers are shown in table 3.2. These compact spectrometers have a single strip linear diode array (one row of pixels) and fixed operating wavelengths. The HR2000 and HR4000 were used in the field instruments for BBCEAS measurements made during the field campaigns: RHAMBLE (discovery cruise D319; chapter 4), BIOFLUX II (chapter 5) and LAMP (chapter 6). The data files from the Ocean Optics spectrometers take the format of two columns; first column has a wavelength designation for each of the pixels in the detector, the second column contains the number of counts representing the light intensity for each pixel in the CCD strip. The SpectraSuite wavelength designation for the pixels was calibrated by measurement of mercury lamp emission lines, creating a calibration file that was used in the analysis routine to correct for the slight variation between the actual and designated wavelength. The method to account correctly for the dark current in the Ocean Optics spectrometers is less simple and discussed further in section 3.6.2.

Property	HR2000	HR4000
Size	148.6 mm x 104.8 mm x 45.1 mm	148.6 mm x 104.8 mm x 45.1 mm
Wavelength range	407.0-491.2nm	504.8-581.9 nm
Detector	Sony ILX511 linear CCD array	Toshiba TCD1304AP linear CCD array
Pixel size	14 um x 200 um	8 um x 200 um
Pixel number	2048	3636
Entrance aperture	SMA 905 to single-strand optical fibre 0.22 NA	SMA 905 to single-strand optical fibre 0.22 NA
Focal length	101.6 mm	101.6 mm
Power consumption	95 mA @ 5 VDC	450 mA @ 5 VDC
Field deployments	LAMP	D319 and BIOFLUX II
Molecular absorbers accessible	NO ₂	I ₂ , H ₂ O, NO ₂

Table 3.2 Parameters of the Ocean Optics Spectrometers utilised during this work.

3.6 BBCEAS instrument stability

The BBCEAS instrument is operated in the field and laboratory for extended time periods, between several hours to several days continuously. The stability of the instrument performance over such time periods must be consistent. The two areas of concern for instrument stability with BBCEAS are vibrational and thermal stability.

3.6.1 Vibrational stability

BBCEAS is an optical technique and thus the optical alignment can be altered by external vibrations. Those of sufficient strength can cause misalignment of the instrument. If the optical alignment is altered during the operation of the BBCEAS instrument, analysis of the data becomes more difficult, as changes in the optical alignment can lead to false positive absorption or undulation in the calculated absorption which is difficult to analyse for trace gas species presence. If the measurements of $I_0(\lambda)$ and $I(\lambda)$ used in the absorption calculation are from differently aligned cavities false positive values or high noise problems occur. To prevent

vibrations changing the optical alignment, the optical components of the BBCEAS instrument were vibrationally isolated from the surrounding environment.

Vibrational isolation in the laboratory work is achieved by mounting all optical components on an optical table (Newport Corporation). The pneumatic supports (legs) of the table provide vibrational isolation in both vertical and horizontal direction. The optical table has a flat surface with an interior honeycomb design for maximum stiffness and internal damping that minimizes the effects of any vibrations created on the optical table surface.

In field applications the BBCEAS is mounted upon a purpose built scaffold (shown in figure 3.11) constructed from Newport X95 optical rails, incorporating anti-vibration mountings in its design (the positions are shown in orange figure 3.11). The optical components mounted above the top scaffold are held rigid to one other; however they remain isolated from external vibrations. The top section was large enough to support two cavity instruments monitoring different trace gas species, as shown in figure 4.5, chapter 4 and figure 5.6, chapter 5.

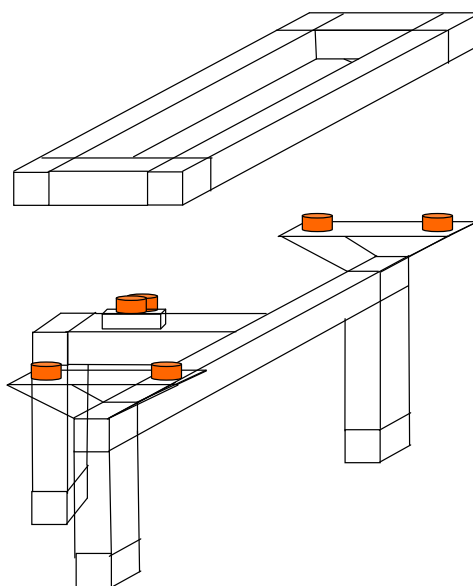


Figure 3.11 Scaffold mounting for field BBCEAS. The top section of the scaffold is shown above its mounting position and the anti-vibration blocks are shown in red.

3.6.2 Thermal stability

The temperature effects on the LED emission spectrum have been discussed in section 3.2.2, thus the LED was mounted upon a temperature controlled mount and driven by a stable power supply in order to maintain a stable emission throughout the work presented here. This was an effective method for the majority of measurements presented in this thesis, with the exception of one field campaign; D319, chapter 4. During the RHaMBLe D319 cruise the temperature fluctuations inside the mobile shipping container laboratory where the BBCEAS electronics were housed ranged between approximately 10 and 25°C. Thus the heat sink mounting block was not always able to maintain the stability of the LED emission spectra. Following the BIOFLUX II field campaign 2007 the LED stability is now maintained by housing the LED in a purpose built enclosure which maintains the stability over wider temperature variations.

Temperature also has an effect upon the detector: the dark current inherent in CCDs and diode arrays increases with increasing temperature. Detector dark current results from thermal energy (not photons) promoting electrons across the band gap of a pixel's semiconductor material. The presence of dark current adds noise to the BBCEAS measurements, and hence it is determined (by measurement or calculated) then subtracted from the BBCEAS measurement during analysis. The accurate removal of the dark current can be vital when analysing BBCEAS measurements for trace gas absorption, as often the absorption signals are small. Along with the dark current levels observed on the CCD, spikes on top of this dark current can occur due to stray light and photons reflecting from components inside the detector. Although not temperature dependent these spikes also add noise to the spectra, and thus are determined and subtracted from the BBCEAS measurements in the analysis.

The UVISEN system has minimised dark current due to the internal cooling of the CCD and the recorded data contain regions with the dark current value. This enables the dark current for each measurement to be subtracted from the data prior to any spectral analysis (see section 3.5.1). The full cooling to -30°C of the CCD in the UVISEN system takes some time after being switched on. The dark current following powering up was monitored and the dark current plots are shown in figure 3.12. The red trace dark current was recorded immediately upon switching the CCD on, with the dark current between 700 and 1000 counts. As the CCD cools, the dark current reduces to less than 50 counts at the CCD's optimum operating temperature, as shown in the yellow trace. [The sharp spike observed at pixel 15 in the 15:32, 15:35, 15:39 and 15:41 pm dark current scans is a mercury emission line from the laboratory's fluorescent

tube lighting. The lights were switched off during the remaining dark current measurements.]

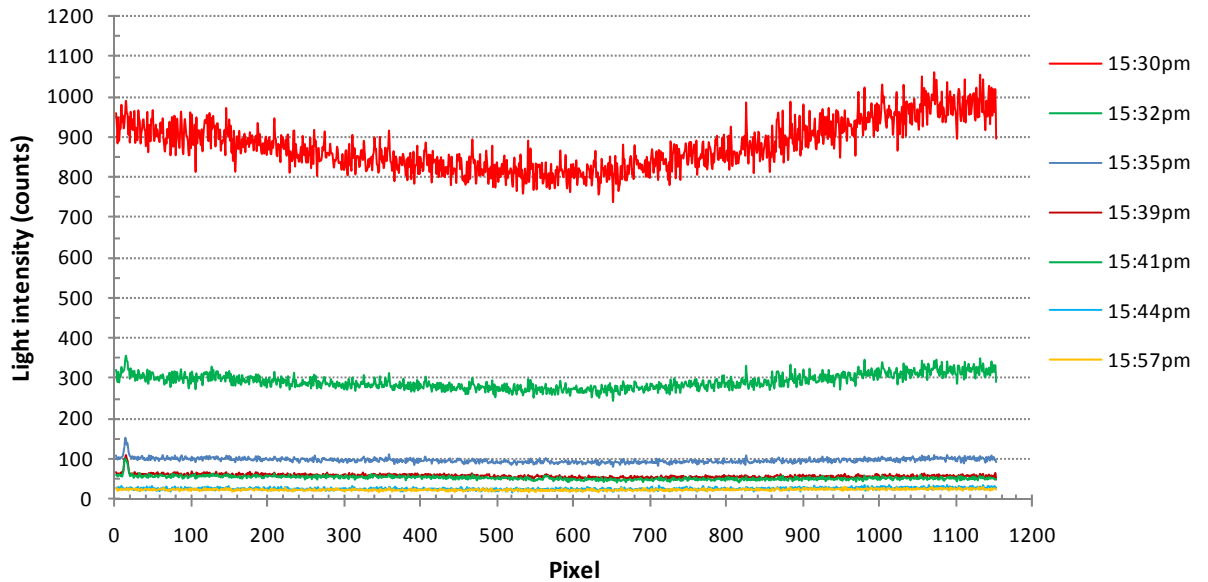


Figure 3.12 Measured dark current on CCD with Chromex spectrometer following power up.

The linear diode array detectors used in the Ocean Optics spectrometers do not have an integral cooling system, and thus their dark current is more strongly influenced by the external environmental temperature. When the Ocean Optics spectrometers were used in air conditioned laboratories, the dark current throughout the course of the measurements remained reasonably constant and could be subtracted for the measured spectra before further analysis. Figure 3.13 shows spectra recorded by the HR2000 under illumination by light from the cavity (red trace) for one spectrum obtained during the LAMP campaign (chapter 6). The black trace shows the dark current measured by blocking the light from the cavity with a piece of card. Most of the spikes on the measured spectrum are also present in the dark current spectrum, and so subtraction of the dark current spectrum produces a much smoother spectrum (blue) which greater reduces the noise in the calculated BBCEAS spectrum.

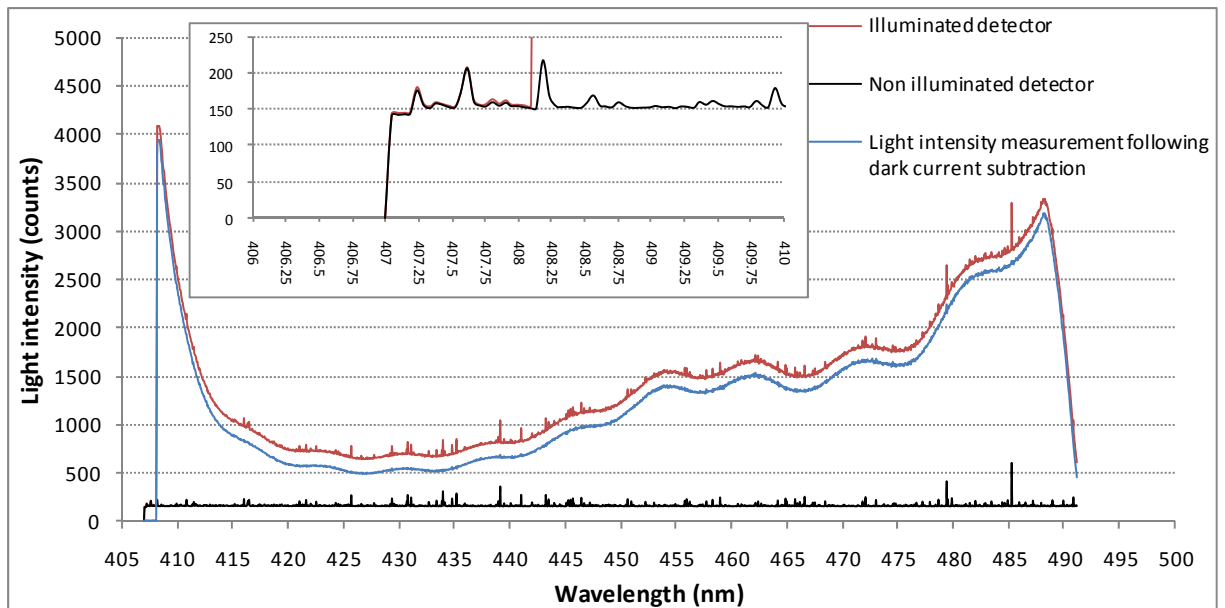


Figure 3.13 Ocean optics HR2000 measured scans for illuminated (red trace) and non-illuminated (black trace) detector. The blue trace shows the red trace after subtraction of the dark current spectrum. The inset shows the short wavelength section of the detector where the pixels between 407 nm to 408 nm are never illuminated (i.e. the red trace overlies the black trace).

The method of subtracting a measured dark current spectrum from a sample spectrum is sufficient if the temperature at which all BBCEAS measurements were acquired remains relatively stable (or if the dark current spectrum is obtained immediately before or after the other measurement). However during field deployments, the electronic components and spectrometer of the BBCEAS instrument were often located in less stable temperature environments. The variation in the external temperature results in the dark current varying over the course of measurements. Thus the periodic measurement of the dark current and its subtraction from the data does not sufficiently account for the true dark current at the time the measurement was made, contributing noise to the BBCEAS spectra.

As such a different approach was used to estimate variable dark current spectra appropriate to the variable conditions the spectrometer was operating under during

field work. A facet of the Ocean Optics spectrometer's design means that the first few pixels of the detector are not illuminated by the wavelength-dispersed light diffracted off the grating (presumably these pixels are hidden behind one of the spectrometer's internal components). These dark pixels are shown in the inset of figure 3.13, the traces for both the illuminated and non-illuminated detector lie exactly on top of each other for the pixels between 407 nm and 408 nm for the HR2000.

Measurements of the dark current across the whole detector at two different temperatures for the HR4000 are shown in figure 3.14, highlighting that the first few hidden pixels are affected by the temperature in the same manner as the usually illuminated pixels; the higher the temperature the more dark current. The lower temperature recorded dark current has lower intensity across the whole measurement in comparison to a dark current measurement at a slightly higher temperature. The number of counts in these first few hidden pixels can thus be used as a proxy for the Ocean Optics detector's temperature and the dark current across the detector was related to this temperature.

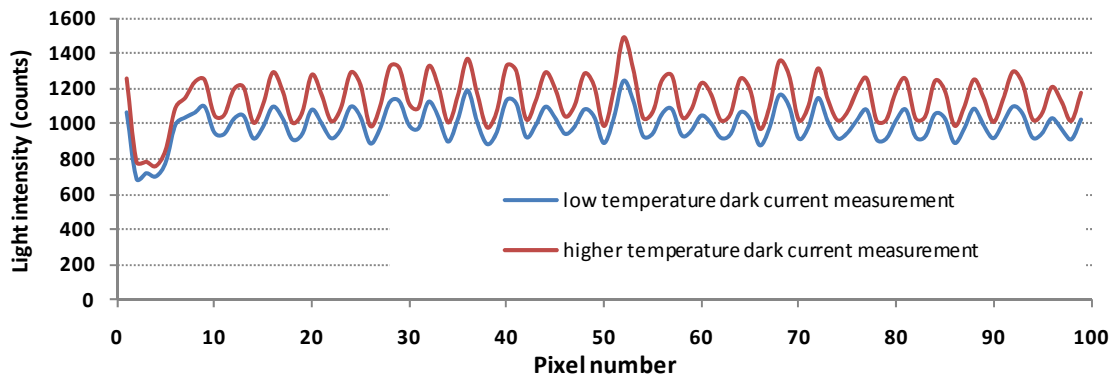


Figure 3.14 Dark current measurements made at different temperatures for the HR4000 Ocean Optics spectrometer. Only the first 100 pixels of the measurement are shown.

The relationship between the dark current in the non-illuminated pixels and the rest of the CCD was investigated by Dr S Ball. The mean value and the standard deviation of the dark current in the non-illuminated pixels of the Ocean Optics detectors were found to vary predictably with temperature. Each pixel in the detector was found to have its own dependence on temperature; measurements of dark current at many temperatures were used to relate this individual dark current dependence to the early non-illuminated pixels. This relationship was used to calculate the dark current for the whole detector for measured dark currents. The calculation efficiently reproduced the measured dark spectra, and thus provided a method to accurately infer the dark current for existing BBCEAS acquisitions.

The calculation of the dark current across the whole CCD from each individual scan's non-illuminated pixels was implemented within the Mathcad analysis procedures which was employed to analysed BBCEAS scans recorded in the field, where the detector experienced a range of temperatures.

3.7 Analysis of BBCEAS data to obtain absorber concentration

The analysis and spectral fittings presented in this thesis were performed with specially written programs written in Mathcad, a mathematical software package. Analysis routines were adapted to suit each particular data set. Laboratory investigative work was analysed on a file by file basis, importing BBCEAS SpectraSuite or UVIZEN files individually as specified by the user. BBCEAS spectra recorded in the field required automated analysis routines that could analyse several hundred files in one run.

The general principles of all analysis routines are the same; the sample absorbance is calculated from the background light intensity measurement $I_0(\lambda)$, the sample light intensity measurement, $I(\lambda)$, and cavity mirror reflectivity, $R(\lambda)$, and cavity length, d , using the standard absorption equation (equation 3.1).

$$\alpha(\lambda) = R_L \left(\frac{I_0(\lambda)}{I(\lambda)} - 1 \right) \left(\frac{1-R(\lambda)}{d} \right) \quad \text{equation 3.1}$$

The calculated absorbance was analysed for the presence of absorber species by differential optical absorption spectroscopy fitting methods. The general processes in the mathcad analysis routines are represented by the main sections in figure 3.15. The methodology of DOAS fitting has been described previously (Chapter 2), so is not discussed here.

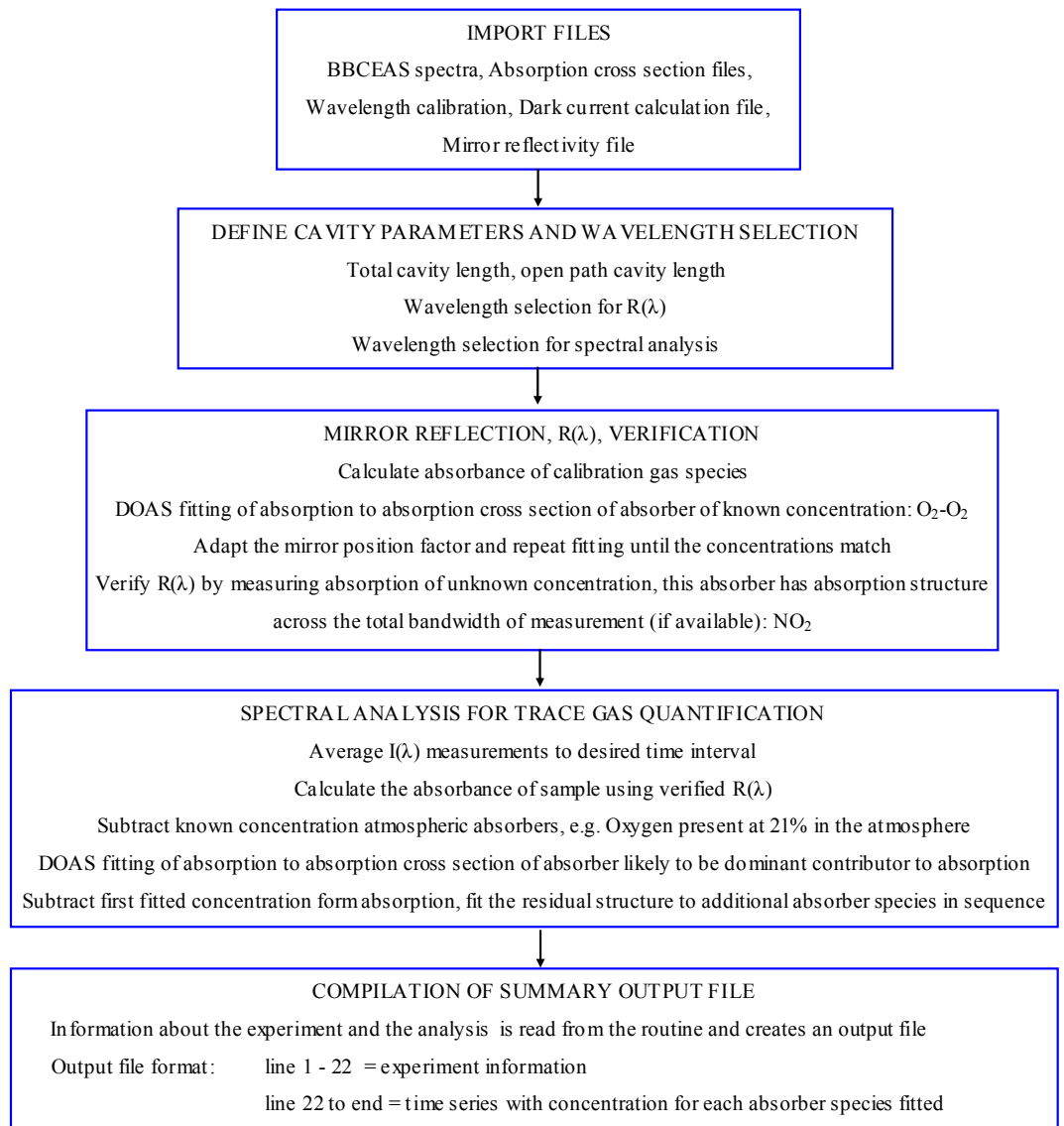


Figure 3.15 Outline of mathcad analysis routine used to for quantitative analysis of BBCEAS spectra

3.7.1 File import to analysis routine

In order to perform analysis the mathcad file reads information for the data file for use in calculations, the BBCEAS spectra, the absorption cross sections of molecular absorbers, wavelength calibration file, dark current calculation file for the detector (Ocean Optics spectrometers only) and mirror reflectivity file.

The light intensity measurements from BBCEAS are imported at the start of the routine. For single file analysis, typically used for laboratory investigations, all files are imported individually and manually by the user. For multi file analysis, typically used for field measurements, files are imported to the routine using programming loop functions. The user specifies the location of the files, using the file naming convention and also selects the exact number of files to be imported.

The absorption cross sections for molecular absorbers which have absorption features in the measurement bandwidth are imported into the analysis routine for use in the DOAS fitting. If the absorption cross section is measured at a higher resolution than the resolution of the detector (spectrometer) it is degraded to the resolution of the detector. The water vapour absorption bands are calculated from the HITRAN database at the detectors resolution.

The wavelength calibration files for the Ocean Optics spectrometers assign the true wavelength to each pixel. The wavelength calibration files were created by using the emission lines from a mercury lamp and consist of the Ocean Optics default wavelength vs. Hg lines wavelength.

The cavity mirror curve text file consists of the mirror reflectivity at a number of wavelengths which have been determined through laboratory investigations (see section 3.8). The mirror curve text file is imported into the Mathcad analysis routine and a curve fitting function (cubic spline) within the programme used to define the reflectivity at each of the pixels used in the analysis.

The BBCEAS measurements are treated to remove the dark current value from each file; this process is different for single file and multi file analysis routines. The single file

analysis uses measured dark currents, an average is calculated and this average dark current subtracted from each of the BBCEAS measurements. The multi file analysis uses programming loops and the dark current calculation method, using dark pixels from each individual measurement to calculate and subtract the specific dark current during that measurement. The dark current correction text file specific to the detector and is imported by the user for use in calculating the dark current for each individual BBCEAS file read into the analysis routine.

3.7.2 Definition of cavity parameters and selection of subsection of BBCEAS spectra

Prior to any spectral analysis specific parameters of the instrument set up are imported into the analysis routine. The total detector size is specified, in pixels (0-3647 for the HR400 and 0-2050 for the HR2000) and enables the analysis to be made using a pixel by pixel scaling in the calculations.

The user inspects the BBCEAS spectra and defines the subsection of the data to be used in the analysis. The whole wavelength span of the detector is not selected due to low light intensities and or saturation of the detector at some pixels. The subsection selected is dependent on the LED emission spectrum, the cavity mirrors and integration time of the BBCEAS measurements.

The cavity parameters specific to the BBCEAS measurements are entered by the user. The total cavity length, the distance between the cavity mirror surfaces, and the open cavity length, (the section of the cavity exposed to sample) are used to define the cavity length factor. The cavity length factor accounts for any sections of the cavity

which are not filled with sample during a measurement. The cavity length factor is the total cavity length divided by the open cavity length.

3.7.3 Mirror reflectivity determination

The cavity mirror curve text file consists of the mirror reflectivity at a number of wavelengths which have been determined through laboratory investigations (see section 3.8). The mirror curve text file is imported into the Mathcad analysis routine and a curve fitting function (cubic spline) within the programme is used to define the reflectivity at each of the pixels used in the analysis. This highly defined mirror reflectivity curve is used in the absorbance calculations for the measurements of known concentration absorber. No length factor is included in the absorbance calculation as the total cavity length is filled with sample species.

A mirror shift factor is defined by the operator. If this is set to 1 the mirror reflectivity takes the form from the text file. Changing the mirror shift factor acts to reposition the whole mirror curve. Making it smaller increases the reflectivity uniformly and increasing the position factor uniformly decreases the reflectivity. The calibration sample absorbance is differentially fitted to its absorption cross section across the bandwidth selected by the operator. This single spectrum fitting produces a fitted BBCEAS absorption spectrum, the concentration of the absorption species, the error in the fitting process and the standard deviation of the residual spectrum (the spectrum following removal of the fitted amount of absorber species).

The absorber is present at known concentration and thus if the fitting does not retrieve the correct concentration the mirror position factor is altered, and the absorption refitted. This process is repeated until the retrieved concentration matches the known concentration of the absorber. The mirror reflectivity across the wavelength bandwidth of the measurements is now verified. The calibrated mirror reflectivity is used in the analysis of BBCEAS spectra of unknown concentration absorber species recorded with the same optical alignment.

3.7.4 Spectral analysis for trace gas quantification

The BBCEAS spectra for the sample, $I(\lambda)$, are analysed either as a single calculated absorption, for laboratory work, or within programming loops to analyse multiple files in one run. Field measured BBCEAS spectra are averaged to the desired time frame within the mathcad analysis routine, the minimum time being the averaged integration time used whilst the spectra were originally recorded.

The absorbance due to the sample is calculated using equation 3.2; the length factor is included to account for the sections of the cavity which are not filled with ambient sample gas. This is the sections of the cavity within the purpose built mirror mounts; within the mirror mounts flush gas is utilised to maintain clean mirror surface during long term operation. The details of the mirror mountings are described and illustrated in section 3.10 below.

$$absorbance = \left(\frac{background\ average}{sample} - 1 \right) \cdot \frac{1 - mirror\ reflectivity}{total\ cavity\ length} \cdot length\ factor \quad \text{equation 3.2}$$

The calculated absorbance of ambient sample is differentially fitted to absorption cross sections of molecular absorbers in sequence. The first absorber species fitted is one which is likely to have the highest contribution to any absorbance. For measurements at coastal sites water vapour is a dominant absorber, so its contribution usually dominates the absorbance and thus is fitted first. The amount of fitted absorber is subtracted from the absorbance and the remaining spectrum, the residual, is fitted for the presence of other trace gas species. This process of sequential fitting produces a series of fitted BBCEAS spectra, each with an associated concentration, error in fitting and standard deviation of the remaining residual spectrum.

3.8. Mirror reflectivity determination measurements

The mirror reflectivity, $R(\lambda)$, determines the enhancement factor of the cavity, and thus the average path length that photons of different wavelength take through the sample gas inside the cavity – see also chapter 2 section 2.4.2. A detailed knowledge of how the mirror reflectivity varies with wavelength is vital for making BBCEAS measurements quantitative. Inaccuracies in the shape of the mirror reflectivity curve act to distort the spectral structure in the sample's absorption co-efficient calculated via equation 3.1, and so the differential fitting of the molecular absorption cross sections to the sample's spectrum is of poorer quality.

The shape of the mirror reflectivity curve for each set of cavity mirrors is extensively investigated in the laboratory prior to use in field BBCEAS instrumentation. Mirror manufacturers tend only to provide an estimate of the peak reflectivity at the mirror's most efficiently reflected wavelength. Instead, the cavity mirrors are often supplied

with data sheets showing a measurement of the mirrors' transmission versus wavelength, $T(\lambda)$. A useful first estimate of the mirror reflectivity curve is provided by the relationship $R(\lambda) = 1 - T(\lambda)$, which assumes that any photon not transmitted through the mirror is reflected. This relationship necessarily overestimates the mirror reflectivity because it neglects absorption of photons by the mirror substrate, but it usually gives a reasonable representation of the shape of the mirror curve. Data points were taken every 2 to 5 nm across the full range of the mirror transmission curve, the corresponding reflectivity was calculated and the reflectivity data points saved as a text file. This mirror reflectivity is used in the Mathcad analysis, where the reflectivity at intermediate wavelengths is interpolated using a cubic spline function.

The interpolated mirror curve is used in for the differential fitting of absorption calculated from measurements of background, $I_0(\lambda)$, and known concentration absorber samples, $I(\lambda)$, to verify and refine the wavelength dependence of the mirror curve file. The cavity mirrors used in the field campaigns presented in chapters 4, 5 and 6 were investigated in the laboratory using measurements of NO_2 and $\text{O}_2\text{-O}_2$, such that the wavelength dependence of reflectivity is well defined, using methods similar to Langridge [Langridge *et al.*, 2006].

Langridge utilised the short lived $\text{O}_2\text{-O}_2$ collision complex absorption bands along with the highly structured NO_2 bands across the blue wavelengths to determine the mirror reflectivity curve in situ to measuring NO_2 in ambient laboratory air [Langridge *et al.*, 2006]. The $\text{O}_2\text{-O}_2$ absorption cross section has regions with little or no band structure in the blue region so a two step method was employed to deduce $R(\lambda)$. Firstly NO_2 measurements were used to derive the shape of the mirror curve by optimising the fit

of the structured NO₂ absorption cross section to the BBCEAS spectrum across the whole wavelength window of the measurement. Then the O₂-O₂ absorption used to place the mirror reflectivity on an absolute scale.

For this work the structure of NO₂ absorption bands was used to refine the wavelength dependence of the curve, as the structure enabled many comparison points between the fitted spectrum and the absorption cross section. The NO₂ gas source used was the headspace of a nitric acid bottle: a syringe was used to sample the headspace and inject the gas into the cavity which had been recently flushed with non absorbing gas (N₂). The NO₂ absorption was not used to determine the absolute mirror reflectivity because the NO₂ “headspace” sample could not be independently calibrated. The mirror curve text file was altered at wavelengths where the differential fitting produced mismatched fitted spectra to the absorption cross section. The fitting process was repeated with iterations of the mirror curve file until the fit was optimised.

The concentration of O₂-O₂ in pure oxygen has no uncertainty. Consequently the mirror reflectivity determined from NO₂ measurements was placed onto an absolute scale by measuring the light intensity of the cavity filled with pure oxygen. The differential fitting and uniform movement of the mirror reflectivity across the bandwidth of the measurements to higher or lower values until the known concentration is retrieved.

During the field measurements presented here the BBCEAS cavity is exposed to the atmosphere. In order to derive the cavity mirror reflectivity for the particular optical alignment, background measurements with the cavity enclosed and filled with non

absorber gas, and calibration sample measurements of pure oxygen within the cavity are performed and the absorbance used to position the reflectivity taken from the lab derived reflectivity text file. The “calibrated” mirror reflectivity was then used in the analysis of ambient samples to retrieve the concentrations of real atmospheric absorber species.

An example of mirror reflectivity calibration measurements during the set up period of the LAMP campaign (Chapter 6), and the resulting fitted O₂-O₂ spectrum is shown in figure 3.16. For this campaign compressed air was used to record background measurements, $I_o(\lambda)$. The air flush contains 21% oxygen, and thus the background measurements contain absorption due to O₂-O₂ and this must be subtracted from the “known concentration” for pure oxygen and the fitting of the sample absorbance to this lower concentration by repositioning the mirror reflectivity. The measurements of $I_o(\lambda)$ and $I(\lambda)$ are an average of three data files for the background and also for the oxygen sample, each being a 2 second integration, with 5 scans per spectrum, and 10 spectra per file. The target concentration is $1^2 - 0.207^2 = 0.9572$, 1^2 being the target for a pure oxygen sample and 0.207^2 being subtracted due to the absorption of oxygen present in the air (background) measurement.

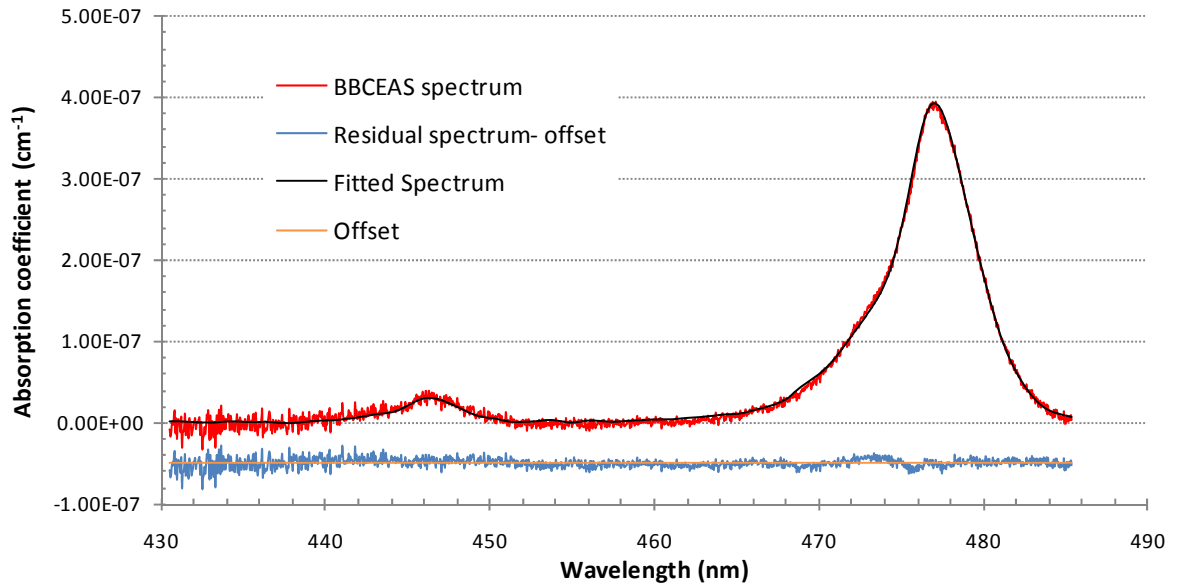


Figure 3.16 Calibration of cavity mirrors using oxygen absorption. The spectrum shows the fitting of O_2O_2 bands ([*Hermans, 2008*] absorption cross sections) to measurements in pure oxygen made on 23rd July 2007. The fitted amount of oxygen is 0.9572 ± 0.00186 and the standard deviation of the residual spectrum is $5.67 \times 10^{-9} \text{ cm}^{-1}$, shown with an offset of $-5 \times 10^{-8} \text{ cm}^{-1}$.

Following this calibration measurement using oxygen absorption the cavity was open to free airflow in the laboratory, spectra were recorded in the same manner as the oxygen sample and the spectra were analysed for the presence of NO_2 . This fitting verified the shape of the reflectivity curve, and the resulting fitted spectrum is shown in figure 3.17. The fitted NO_2 spectrum shows NO_2 present in the laboratory air at 1.47 ± 0.078 ppbv, and the standard deviation of the residual spectrum is $4.06 \times 10^{-9} \text{ cm}^{-1}$.

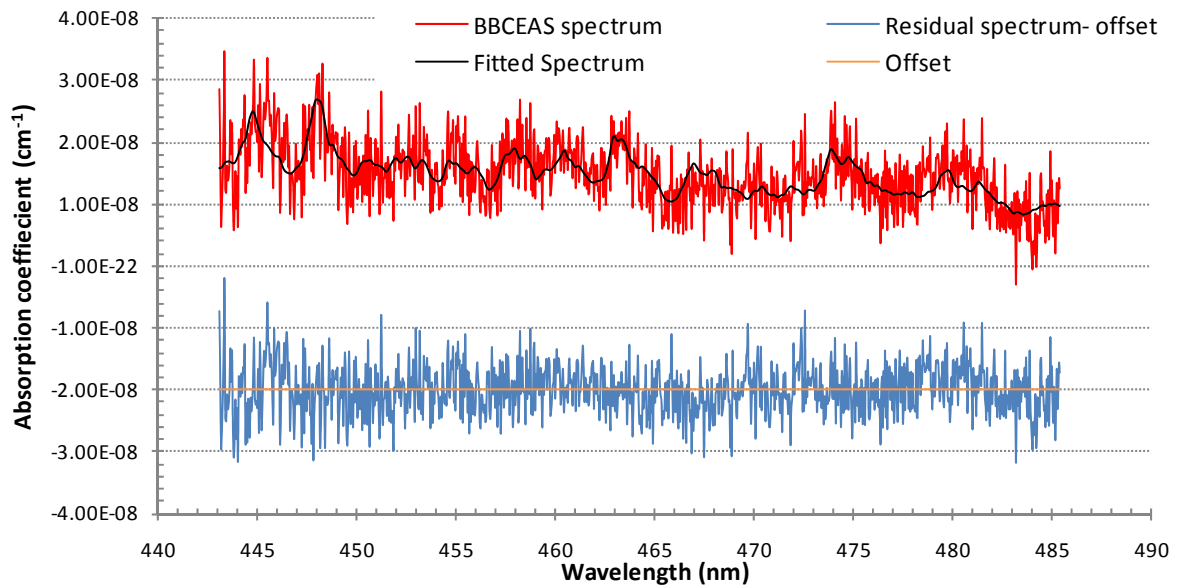


Figure 3.17 Verification of cavity mirror reflectivity using NO₂ absorption in laboratory air. The spectrum shows the fitting of NO₂ bands ([Vandaele et al., 1998]) absorption cross sections) to measurements of lab air made on 23rd July 2007. The fitted amount of NO₂ is 1.47 +/- 0.78 and the standard deviation of the residual spectrum is 4.06x10⁻⁹ cm⁻¹, shown with an offset of -5x10⁻⁸cm⁻¹.

The BBCEAS spectrum (red trace) is determined by differential fitting of the absorbance calculated from measurements of $I_o(\lambda)$, where the cavity was purged with air, and $I(\lambda)$ where the cavity was filled with either pure oxygen or open to the ambient laboratory air. The residual spectrum (blue trace) is the calculated absorbance minus the fitted amount of absorber species (O₂-O₂ or NO₂) and shows there is little structure remaining in the absorption. For the NO₂ measurements this confirms the mirror reflectivity at each wavelength is now the correct and can be utilised in analysis.

3.9. Lab measured spectra

During developmental work in the laboratory various components to be used in field BBCEAS instrument were investigated and the best available options employed. This includes LED choices and operation, as described in section 3.3 above, as well as which fibre optic cables to use in the various positions and the cavity mirror selection.

Laboratory development of a BBCEAS to monitor nitrous acid (HONO) in the atmosphere was begun, and proof of principle measurements of HONO absorption in the laboratory were made. The work on the HONO measurement BBCEAS instrument was stopped due to the LEDs available at the time not having sufficient intensity at the favourable UV wavelengths. LEDs in the visible region offered more potential as light sources for use in BBCEAS instruments. The cavity mirrors available during the HONO investigations had relatively modest reflectivity, $R_{\text{peak}} = 99.90\%$, compared to our usual requirement of $R = 99.95\%$, and their reflectivity falls off rapidly at wavelengths around the more intense HONO band at 368 nm. The investigations for HONO measurements were conducted using the UVISEN system. Although this is a functional system its operation required a user to begin each measurement manually, and thus would be too laborious for field operation over extended time periods. The laboratory measured HONO absorption recorded is presented in section 3.9.1.

Following the successful LED BBCEAS measurements of HONO, investigations into the capability of BBCEAS operating at visible wavelengths to measure molecular iodine were carried out. LEDs were of sufficiently brightness and cavity mirrors with very high reflectivity across visible wavelengths were more readily available, guiding the work in this thesis to the detection of molecular iodine (I_2) and NO_2 in the atmosphere.

3.9.1 Nitrous acid detection by BBCEAS

The HONO spectrum presented in figure 3.18 was measured in the laboratory using HONO diluted in nitrogen introduced to the cavity. HONO was generated upstream of the cavity from $\text{NaNO}_2(\text{s}) + \text{HCl}(\text{g})$ reacting to form $\text{NaCl}(\text{s}) + \text{HONO}(\text{g})$ [Febo *et al.*, 1995]. The BBCEAS instrument comprised the C20A1-H390-30 LED, the VLOC cavity mirrors and the UVIZEN system set to operate with the 1200/500 nm grating centred at 385 nm. The integration time for each measurement was 15 s and an average of 3 measurements were used in the calculation of sample absorbance. HONO is present at a mixing ratio of 782 \pm 4.9 ppbv and the residual spectrum has a standard deviation of $2.25 \times 10^{-7} \text{ cm}^{-1}$.

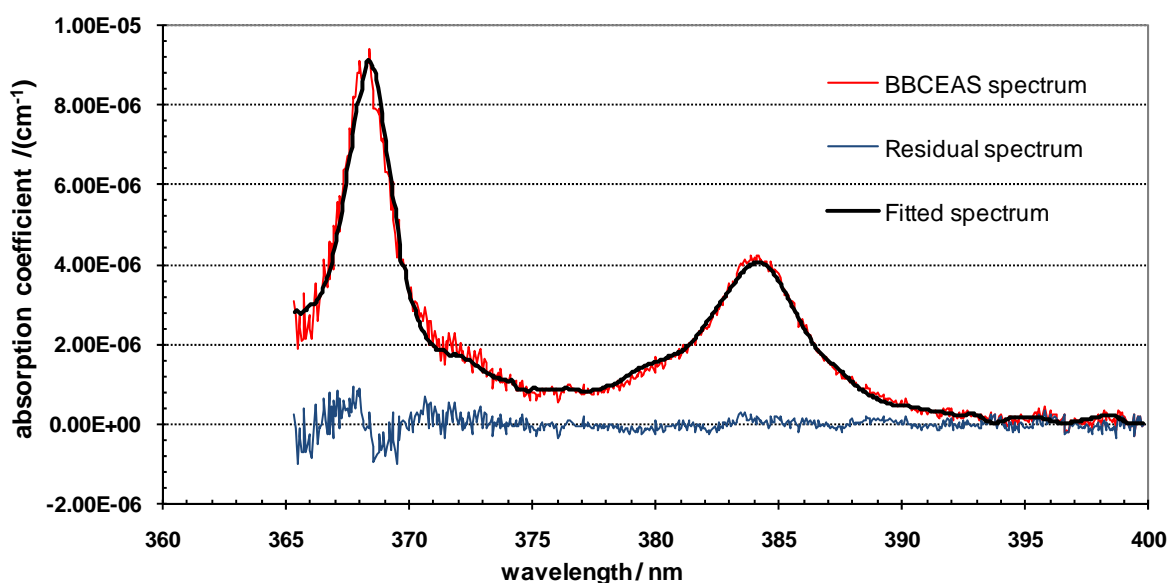


Figure 3.18 Fitted BBCEAS spectrum of HONO measurements made on 29th November 2006. The fitted amount of HONO is $7.83 \times 10^{-2} \pm 4.86 \times 10^{-9}$ and the standard deviation of the residual spectrum is $2.25 \times 10^{-7} \text{ cm}^{-1}$.

Since this HONO spectrum was recorded, other research groups have successfully employed cavity based techniques for the measurement of HONO. IBBCEAS using a xenon arc lamp was employed by Gherman [*Gherman et al.*, n.d.]. Langridge et al were able to construct an LED BBCEAS instrument using a brighter near-UV LED, better mirrors and a better detector (a more modern PI Acton spectrometer & CCD camera, [*Langridge et al.*, 2009]) than were available for this study. These better suited components gave the Langridge study a detection limit of 0.3 ppbv [*Langridge et al.*, 2009], compared to ~4ppbv for the example UVIZEN-BBCEAS spectrum shown in this thesis. The Ball group recently (May 2010) took part in an inter-comparison of HONO instruments at the EUPHORE chamber in Valencia: they achieved good agreement with other HONO instruments and a similar 0.3 ppbv sensitivity using the same cavity mirrors & LED borrowed from the Cambridge University group, who produced the Langridge study, but used an Ocean Optics QE65000 miniature spectrometer with integral cooled CCD detector. 0.3 ppbv is now sufficient sensitivity to make viable LED-BBCEAS measurements of HONO in the ambient atmosphere.

3.9.2 Survey of absorbers species in the visible region: green wavelength BBCEAS measurements

The availability of bright LEDs at visible wavelengths guided this work to the development of BBCEAS operating at green wavelengths. Some atmospherically important molecules have structured absorptions in this bandwidth and the potential for a field BBCEAS instrument to monitor molecular iodine was investigated using the UVIZEN system. Layertech (#101851) cavity mirrors and luxeon green (LXHL-ML3C) LED were implemented into the instrument, the cavity mirror reflectivity investigated using measurements of O₂-O₂ and NO₂. The BBCEAS instrument was then tested for the capability of monitoring particular trace gases at concentrations similar to those likely to be found in the atmosphere. A range of molecular absorbers were introduced into the cavity and the absorbance monitored and quantified using DOAS fitting. The UVZEN system was operated using grating 2 set to a central wavelength 553 nm and the optical alignment optimised using a photomultiplier tube. The cavity mirror position was adjusted and the maximum achieved voltage used to infer alignment was optimised.

The results from the spectral fitting of laboratory BBCEAS measurements of O₂-O₂, NO₂, I₂, water vapour and Br₂ recorded on 7th November 2006 are shown in figures 3.19 to 3.23. The oxygen and NO₂ measurements were used to verify the cavity mirror reflectivity before other absorbing species were introduced into the cavity. Each recorded spectrum was made with 15 s integration and averages of these scans were used to calculate the sample absorbance. The number of scans averaged depended upon how many measurements were recorded. Table 3.3 summarises the number of

scans averaged in the absorbance, the amount of each absorber retrieved by the differential fitting of each absorber and the absorption cross section used in the fitting. The concentrations observed by this series of measurements are higher than would be expected for atmospheric measurements due to pure samples being introduced to the cavity in flows of nitrogen gas.

Molecular absorber species	Number of 15s scans averaged for calculation of sample absorbance	Amount of absorber present in sample	Standard deviation of residual spectrum (cm^{-1})	Absorption cross section reference
Oxygen	4	1.0 +/- 0.035	1.38×10^{-8}	[<i>Hermans, 2008</i>]
NO ₂	8	18.52 +/- 0.73 ppbv	1.07×10^{-8}	[<i>Vandaele et al., 1998</i>]
I ₂	8	378.9 +/- 17.9 pptv	5.74×10^{-9}	[<i>Saiz-lopez et al., 2004</i>]
H ₂ O	5	0.012 +/- 0.0019	1.38×10^{-8}	HITRAN 2004 spectral database
Br ₂	8	417 +/- 10.11 ppbv	2.38×10^{-8}	

Table 3.3 Survey of molecular absorbers at green wavelength BBCEAs measurements

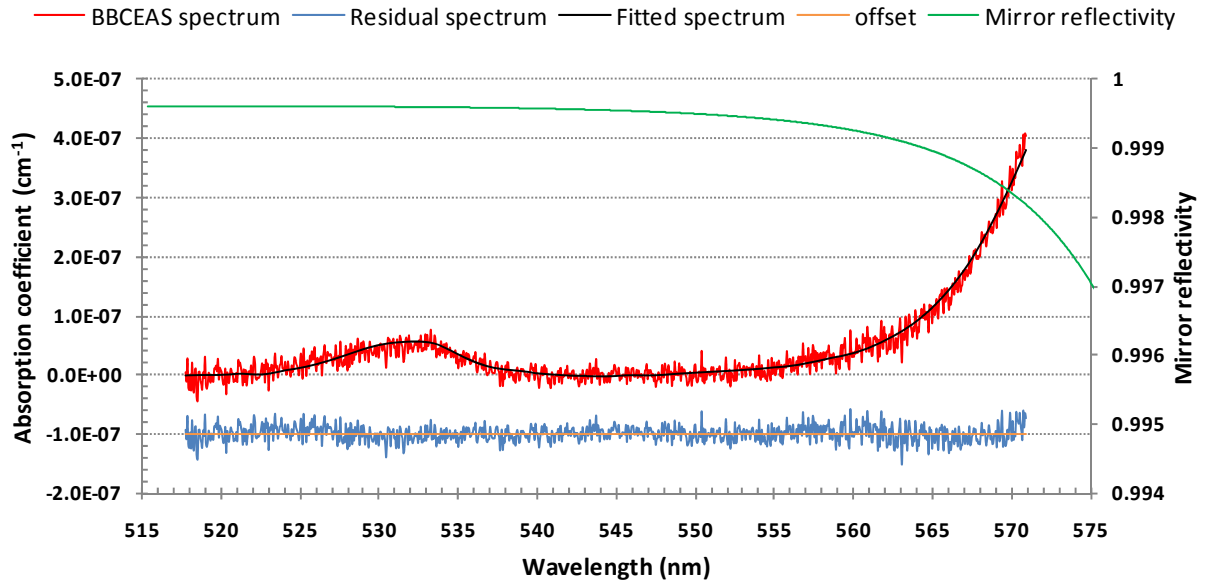


Figure 3.19 Calibration of cavity mirrors by fitting the O₂-O₂ absorption bands (Hermans 2008 absorption cross sections) to measurements in pure O₂ made on 7th November 2006. The fitted amount of oxygen from the inferred O₄ band is 1.00+/- 0.035 and the standard deviation of the residual spectrum is 1.38X10⁻⁸ cm⁻¹. The residual spectrum is shown with an offset of -1x10⁻⁷ cm⁻¹.

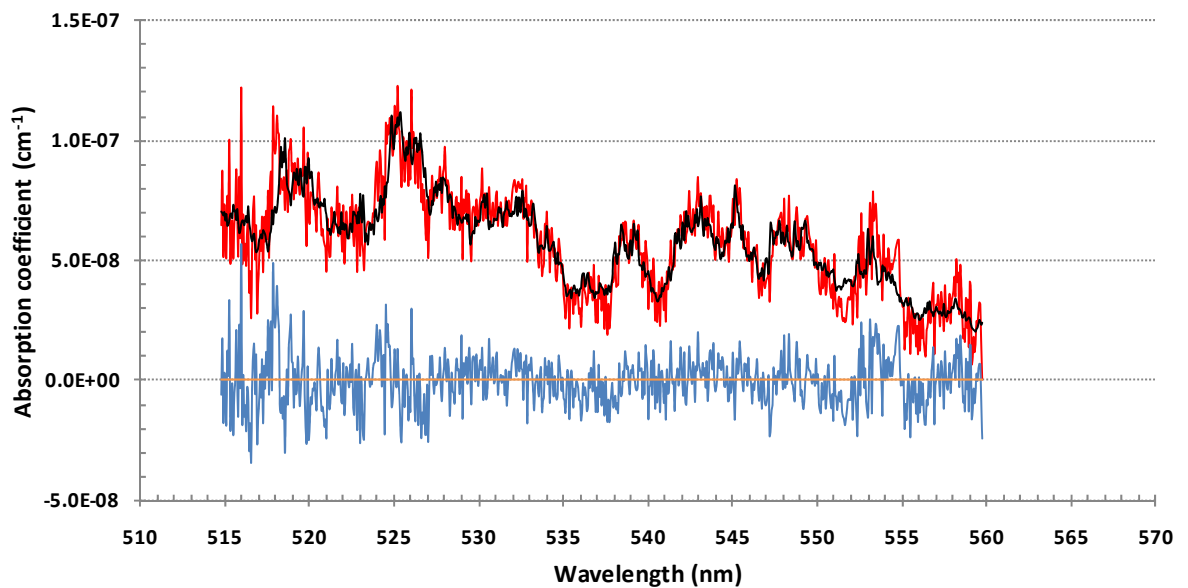


Figure 3.20 Calibration of cavity mirrors by fitting the NO₂ absorption bands [Vandaele et al., 1998] absorption cross sections) to measurements of NO₂ made on 7th November 2006. The fitted amount of NO₂ is 18.52+/- 0.73 ppbv and the standard deviation of the residual spectrum is 1.07X10⁻⁸ cm⁻¹.

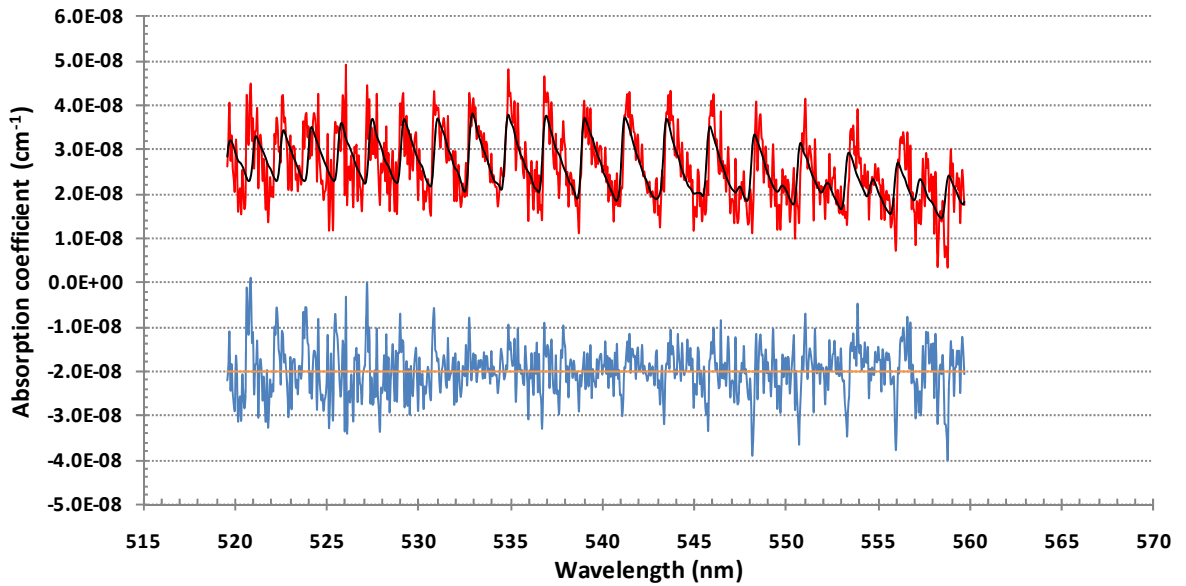


Figure 3.21 Fitted BBCEAS spectrum produce by fitting the I_2 absorption bands ([Saiz-lopez *et al.*, 2004] absorption cross sections) to measurements of I_2 made on 7th November 2006. The fitted amount of iodine is 378.9 ± 17.89 pptv and the standard deviation of the residual spectrum is $5.74 \times 10^{-8} \text{ cm}^{-1}$. The residual spectrum is shown with an offset of $-2 \times 10^{-8} \text{ cm}^{-1}$.

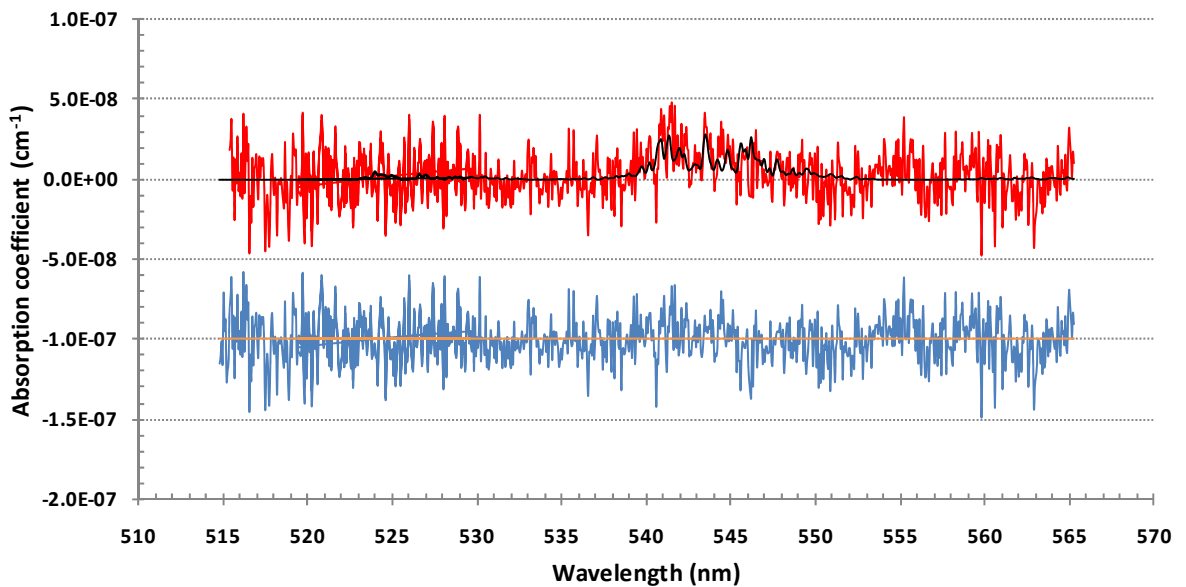


Figure 3.22 Fitted BBCEAS spectrum produced by fitting the water absorption bands (HITRAN determined water vapour absorption bands) to measurements made on 7th November 2006. The fitted amount of water 0.0129 ± 0.0019 and the standard deviation of the residual spectrum is $5.74 \times 10^{-8} \text{ cm}^{-1}$. The residual spectrum is shown with an offset of $-1 \times 10^{-7} \text{ cm}^{-1}$.

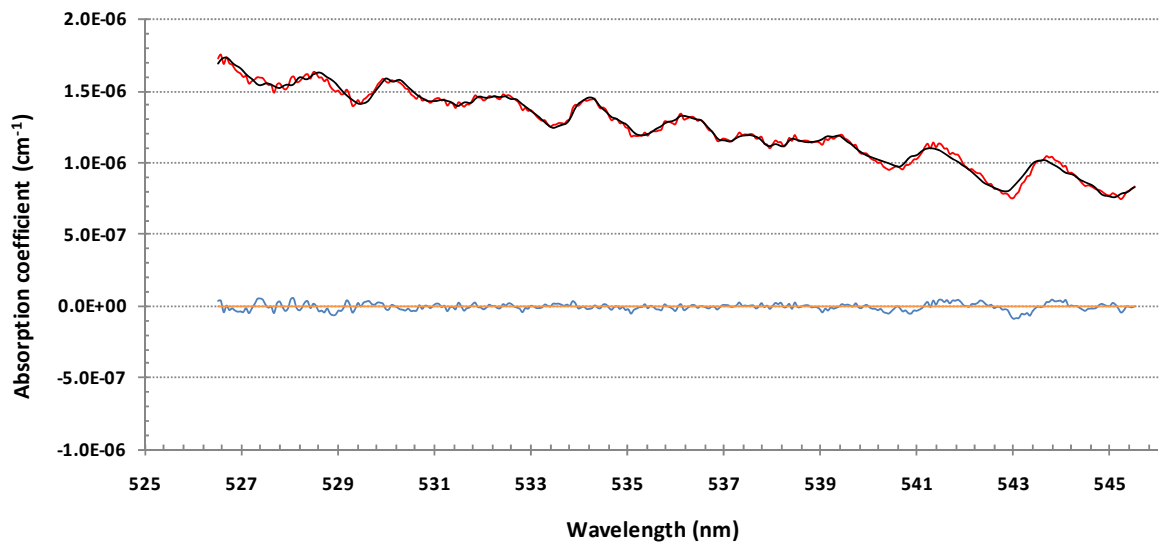


Figure 3.23 Fitted BBCEAS spectrum produce by fitting the Br₂ absorption to the Br₂ cross sections, measurements made on 7th November 2006. The fitted amount of bromine is 417 +/- 10.11ppbv and the standard deviation of the residual spectrum is $2.389 \times 10^{-8} \text{ cm}^{-1}$.

The spectra presented here recorded using the UVISEN system highlight the absorber species likely to be present in atmospheric samples across this bandwidth in the marine environment. The quality of these spectra is less than optimal for atmospheric monitoring, but improvements to the BBCEAS instrument following these measurements and increased operator experience resulted in a very capable field BBCEAS instrument operating at green wavelengths. The utilisation of the Ocean Optics HR4000 spectrometer not only provided a compact detector for the instrument, but also enabled the process of cavity alignment to be optimised more efficiently compared to using the photomultiplier tube as per the results here.

The Ocean Optics spectrometer software visualises the light coupled into it continuously enabling adjustments to the cavity alignment to be monitored across all the wavelengths of the detector. The optimised cavity alignment was taken to be when

the light intensity through the cavity was maximised and further adjustment to the mirror position reduced the observed intensity throughput.

3.10. Instrument adaptations for field deployment

The BBCEAS instrument is an optical instrument of high sensitivity. In order to maintain the high sensitivity the optics must remain clean and optimally aligned during operation. The operation of BBCEAS in the field (non lab situations) required the design and build of specialised enclosures which house the optical components of the instrument. The electronic components of the BBCEAS, namely the LED, spectrometer and user interface are housed within a 19" rack. This rack is situated within a laboratory space at a distance up to 10 m from the BCEAS cavity during field operation. The housing of the components being housing in the 19" rack enables transportation to many locations with minimal disruption to the setup. The rack is shown in figure 3.24 in the portside laboratory container onboard RSS Discovery during the D319 measurement campaign.



Figure 3.24 The 19" rack housing the electronic components of the BBCEAS instrument: in situ onboard RSS discovery during D319.

The mirrors used to create the cavity in the field BBCEAS instrument are housed in specialised mounts (Figure 3.25) designed to protect the mirror surfaces from contamination e.g. by ambient aerosol, yet still enable fine movements (x and y direction) for alignment purposes. The mounts are designed to introduce a small flow of non absorbing gas across the cavity mirrors' reflective surface. This flow helps to minimise any deposits of small particles or dust onto the surface. The cavity mirrors within their mountings and the remaining optical components of the BBCEAS are housed inside larger weather-proof enclosures mounted to the gantry.

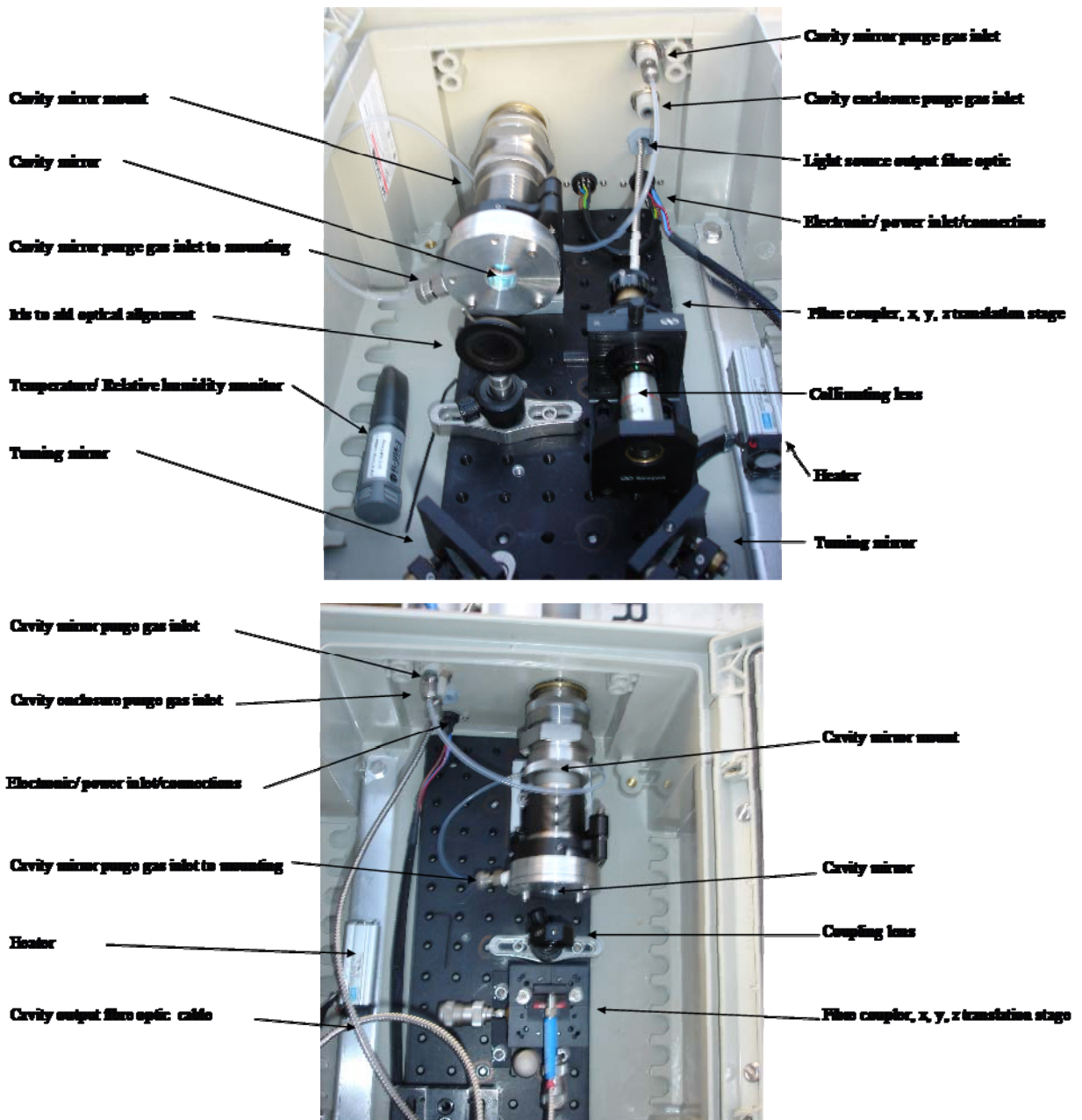


Figure 3.25 BBCEAS cavity enclosures, top panel shows the input enclosure and the lower panel shows the cavity output enclosure.

The weather-proof enclosures were constructed to maintain the optimum configuration of the BBCEAS over extended periods of operation. The insides of the two enclosures are shown in figure 3.25, whilst external views are shown in results

chapters, figures 4.5 and 5.6. The optical components can be accessed and adjusted from the top opening of the enclosure, with relative ease depending upon the site of the cavity. The enclosures have the facility to be purged with non-absorbing, non-condensable gas, to prevent any condensation onto the optics. Small heating devices are also situated in each enclosure to regulate the temperature within the enclosure one or two degrees above ambient temperature, which also helps to minimise the likelihood of any condensation. The top of the enclosures has a secondary surface, an aluminium plate spaced approximately 5cm above the plastic enclosure top. Reflection from this plate acts to reduce heating within the enclosure due to sunlight absorption; heat is dissipated from the metal plate by the air flow through the space below.

Chapter 4

Iodine measurements during D319: part of the Reactive Halogens in the Marine Boundary Layer (RHaMBLe) project.

4.1. Introduction to RHaMBLe

The RHaMBLe field study aimed to better understand reactive halogen cycling processes in the marine boundary layer, particularly the involvement of RHS (Reactive Halogen Species) in catalytic ozone destruction and new aerosol formation. Two open ocean studies of the remote boundary layer were conducted within RHaMBLe to characterise both organic and inorganic reactive halogen species in the mid latitude Atlantic Ocean. The Cape Verde Atmospheric Observatory on Sao Vicente off the west coast of Africa provided long term continuous measurements of RHS together with an intensive measurement period in May and June 2007, which was timed to coincide with the D319 cruise of the RSS Discovery research vessel. The RSS Discovery ship transacted the biologically active upwelling region west of Mauritania to investigate the regional contribution and spatial variability of biogenic RHS sources. Measurements recorded during flights of the Dornier aircraft from the Cape Verde Islands added a vertical component to the studies. The route travelled during D319 aimed to pass varying biologically active regions which would enable the study of the remote open ocean boundary layer chemistry to attempt to address the following questions.

1. Is iodine released at sufficient levels in the open ocean to initiate aerosol nucleation, as has been observed at coastal sites?

2. What effects do RHS in the remote open ocean have on the ozone budget and other radical species?

This chapter presents the BBCEAS measurements made on the Discovery Cruise D319 in what was the first non laboratory field deployment of the BBCEAS instrument.

4.2. D319 cruise track and air mass origin

The D319 cruise of RSS Discovery mobilised from Lisbon, Portugal on 19th May 2007. The route is shown in figure 4.1. The ship travelled southward from Lisbon passing the Canary Islands and docked at Sao Vicente, Cape Verde on 15th May 2007. The next day the ship headed east into the upwelling region off the Mauritanian coast. The ship tracked back and forth from day 146 to day 152, passing through different gradients of biological activity in the upwelling region before heading north to reach the UK on the 11th June 2007. The northward leg of the cruise (from day 153 onwards) followed a zig zag route, with the ship headed at an angle of approximately 315 degrees into the prevailing winds, such that background air blew onto the portside of the ship where the atmospheric sampling instrumentation was located. This enabled the instruments to sample the remote atmosphere rather than sampling air influenced by the ship's own emissions.

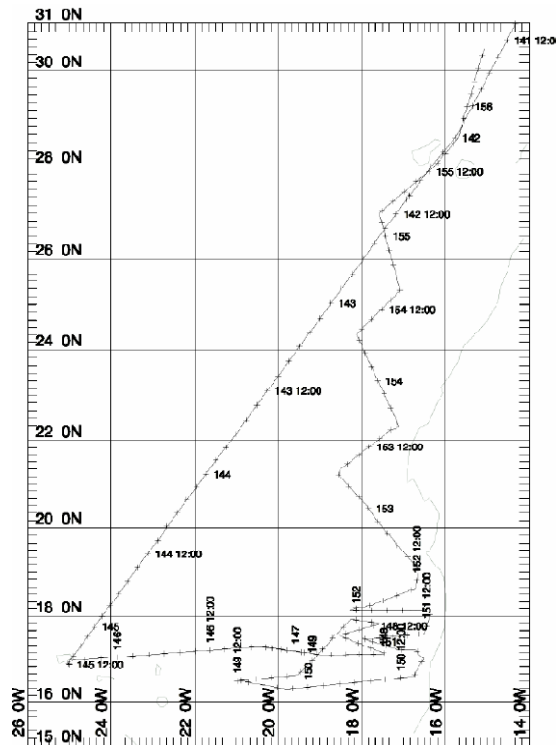


Figure 4.1 RSS Discovery ship track during D319 cruise 2007. Markings denote two hour time periods, x axis denotes longitude and y axis latitude.

The route travelled during the D319 cruise is also illustrated by the blue trace in figure 4.2 and was chosen to reach Cape Verde in order that ship board measurements coincided with the intensive deployment at the UK SOLAS Observatory on Soa Vicente. During the simultaneous measurement period close to Cape Verde the RSS Discovery provided a latitudinal characterisation of trace gases and aerosol in the marine atmosphere. Following this period the Mauritanian upwelling region was transected multiple times to assess the contributions of highly and less biologically productive waters to reactive halogen species in the remote marine atmosphere. The monthly averaged chlorophyll satellite data from MODIS for May 2007 is shown alongside the

ship's track in figure 4.3 below; this illustrates the different regions of biological activity which were encountered.

The air masses reaching the Discovery during the campaign are shown in figure 4.2 and originated from a variety sources. Lee et al [Lee et al., 2009] have classified these into three different types using 5 day back trajectories. Clean marine air was sampled around the Cape Verde Islands and is shown by purple back trajectories. While travelling from Cape Verde towards Africa, air masses reaching the ship originated from Europe and had experienced long range transport; they are shown by the green back trajectories. Air masses from the African continent were encountered during the time RSS discovery transacted the Mauritanian upwelling region close to the African coast, these are shown by the red back trajectories. Air masses sampled with air from the clean air sector occurred as the Discovery was on its UK bound return leg and past the Canary Islands.

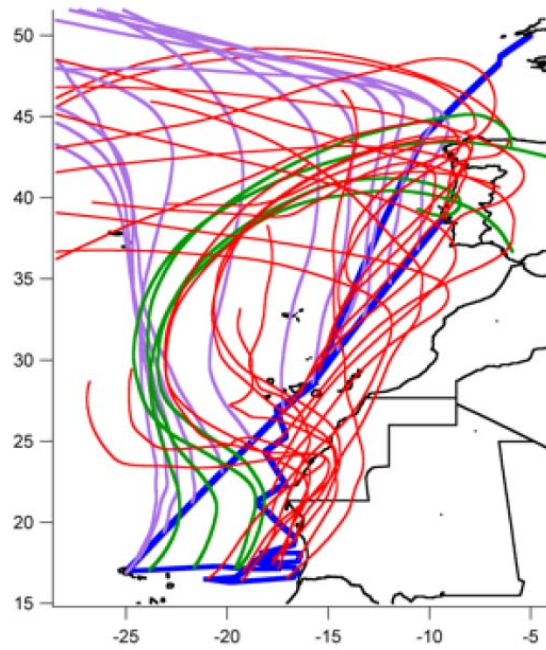


Figure 4.2. The 5 day back trajectories of air masses reaching RSS Discovery, the purple are clean air sector origin air masses, the green are long range transport from Europe and the red have experienced more recent African continental influence. Lee et al 2010 [Lee et al., 2009]

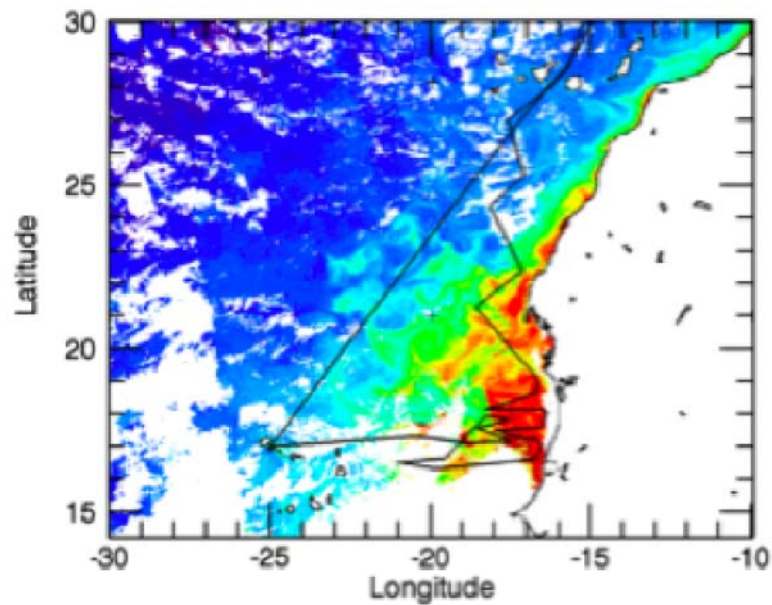


Figure 4.3. Track of RHaMBLe Discovery Cruise D319 in the working area south of 30°N with an overlay showing the MODIS retrieved chlorophyll a averaged for the month of May 2007. Lee et al 2010 [Lee et al., 2009]

4.3. D319 measurement instrumentation

A variety of state of the art scientific instrumentation was deployed during D319 to measure halocarbons, gaseous iodine species, NO, NO₂, ozone, solar actinic flux, and the number concentration, size and hygroscopicity of aerosol particles. The range of instruments deployed on D319 are summarised in table 4.1 and further details are reported in an overview paper by Lee et al [Lee et al., 2009].

Target species	Instrument	Technique	DL (integration time)	Reference
IO	FAGE LIF (U. Leeds)	Laser Induced Fluorescence at 445 nm	0.23 pptv (30 min)	Whalley et al. (2007)
IO, I ₂	BBCEAS (U. Leicester & Cambridge)	LED Cavity Enhanced Absorption Spectroscopy	20, 200 pptv, 0.9/3 ppbv (10 min)	Langridge et al. (2008)
NO ₂ , blue/green λ s	GC/MS (U. York)	Gas chromatography Mass Spectrometry	0.05 pptv (70 min)	Carpenter et al. (2009)
Halocarbons, (air)	GC/MS (U. York)	Gas chromatography Mass Spectrometry	0.05 pptv (2 hr)	Carpenter et al. (2009)
Halocarbons, (water)	SMPS, CPC, OPC (U. Manchester)	Electrical mobility sizing & optical counting	$x \text{ nm}^{-1} \text{ cm}^{-3}$ (6 min)	Allan et al. (2009)
Aerosol	Andersen & CCI (U. Manchester & UEA)	Hi-Vol & lo-vol cascade impactors	$x \text{ nm}^{-1} \text{ cm}^{-3}$ (6 min)	Allan et al. (2009)
Aerosol	HTDMA, CCNc (U. Manchester)	Sub- & supersaturated water uptake	$\text{GF}_{\text{D},90\%} \pm 0.05$ (10 min) $S_{\text{crit}} \pm 0.02\%$	Allan et al. (2009)
O ₃	2B Technologies (U. York)	uv absorption	2 ppbv (1 min)	Lee et al. (2009)
NO	EcoPhysics CLD780 (U. York)	Chemiluminescence	1.5pptv (1 min)	Lee et al. (2009)
NO ₂	EcoPhysics CLD780 (U. York)	Photolytic conversion & Chemiluminescence	5pptv (1 min)	Lee et al. (2009)
Actinic flux & photolysis rates	Spectral radiometers (U. Leicester)	λ -resolved photon flux	1 min	Edwards and Monks (2003)
Photosynthetic pigments	HPLC (U. York)	Liquid chromatography of seawater samples		
Wind speed, direction, T, RH, PAR, TIR	Foremast Met. Station (UKORS core)			

Table 4.1. Instrumentation deployed on RSS Discovery cruise D319. Lee et al 2010 [Lee et al., 2009]

4.3.1 Location of the BBCEAS instrument during D319.

The BBCEAS cavity (sensor) was located on a purpose built gantry fixed to the railings and deck on the port side of Discovery in front of the ship's smoke stack, as shown schematically in figure 4.4. Additionally figure 4.5 shows a photograph of the BBCEAS

cavity in situ. The LED light source, spectrometer and other electronics were housed in the port side laboratory container and linked to the cavity via fibre optics, protected from the elements inside plastic tubing.

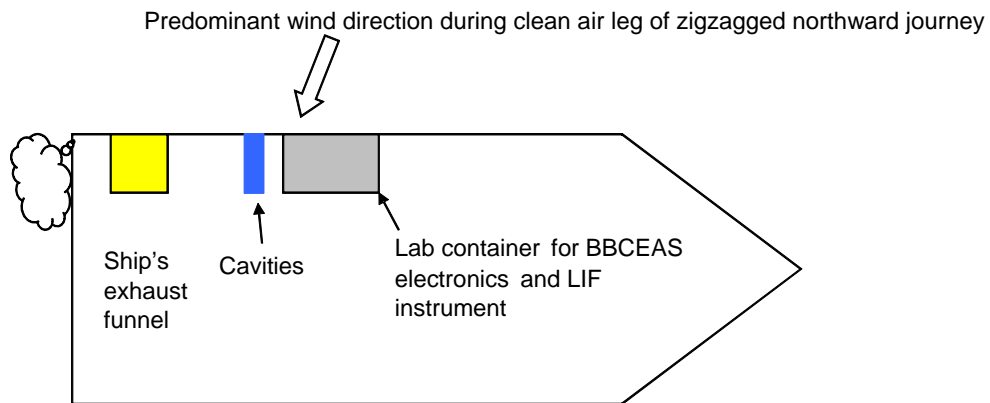


Figure 4.4 Diagram to illustrate positioning of BBCEAS cavity sensors on RSS Discovery.



Figure 4.5. BBCEAS instrument cavity mounted on the gantry on the deck of RSS Discovery. Two BBCEAS cavities are shown in tandem; Leicester I₂ detector and Cambridge IO detector. The BBCEAS is shown in a background ($I_0(\lambda)$) measurement mode in which a length of plastic tubing is inserted to enclose the light path and a flow of nitrogen gas passed into the enclosure to expel ambient air.

4.3.2 Operating parameters BBCEAS during D319

For the I₂ measurements onboard Discovery, the BBCEAS instrument was operated at green wavelengths and used a HR4000 ocean optics miniature USB connected spectrometer. Table 4.2 summarises the BBCEAS hardware and main operating parameters. Spectra of the cavity's transmission, $I(\lambda)$, for ambient samples were acquired with 1 second integration time using the Spectra suite software supplied with the HR4000 spectrometer. Ten such spectra were averaged within the spectra suite program to provide an averaged scan, which was saved to the computer for spectral analysis later.

The spectrometer RH4000 has a fixed wavelength range of 504.8-581.9nm within which the absorption cross sections of I₂ are highly structured. This enables the atmospheric monitoring of I₂ with this configuration of BBCEAS. The O₂-O₂ bands at 447 nm and 478 nm and NO₂ absorption features (shown in chapter , figure 5.6) were used to calibrate the mirror reflectivity, $R(\lambda)$, regularly during the course of the D319 cruise. Details on the methodology can be found in chapter 3, section 3.8.

BBCEAS setup during D319			
Light source	Green LED	LUXEON III (3 watt)	Temperature stabilised at 18° C Drive Current = 1 Amp
Cavity mirrors	Layertech	101851	25 mm diameter
Light input fibre	QP-400-2-uv/vis-BX	Ocean optics	400um diameter, 0.22NA, 10m length
Cavity output fibre	QP-400-2-uv/vis-BX	Ocean Optics	400um diameter, 0.22NA, 15m length
Cavity length	117cm 84cm and 48cm		total length between cavity mirrors section of cavity open to free airflow
Spectrometer	HR4000	Ocean Optics	504.8-581.9nm, 3648 pixels, 50um slit Resolution 0.12nm FWHM

Table 4.2 BBCEAS instrument components and cavity parameters.

Hour	00:00	01:00	02:00	03:00	04:00	05:00	06:00	07:00	08:00	09:00	10:00	11:00	12:00	13:00	14:00	15:00	16:00	17:00	18:00	19:00	20:00	21:00	22:00	23:00	
Date																									
21/06/2007																									
22/06/2007																									
23/06/2007														o								o			
24/06/2007										o															
25/05/2007								o												o					
26/05/2007										o							f,o				o				
27/05/2007									o																
28/05/2007						o							f							o					
29/05/2007							o																o,f		
30/05/2007						f, x							f					x		f	x				
31/05/2007								f		x,f							f,x								
01/06/2007						f,o,x	f					f			f	x,o									
02/06/2007							f													f,o,x					
03/06/2007									f,x										f,x						
04/06/2007							f	f,x					f						f,x						
05/06/2007							f	f	x			f				f					x				
06/06/2007												f,x													
07/06/2007								f	x,o									f,x							
08/06/2007									f,x						f	x									
09/06/2007								f,x	rain																
f	nitrogen flush																								
	running for all or part of hour open path																								
x	NO2 calibration																								
o	Oxygen dimer calibration																								

Figure 4.6 Chart showing operation hours of BBCEAS I₂ instrument during D319 cruise. The green shaded areas indicate instrument sampling ambient air, while the letters denote background and calibration BBCEAS measurements.

The data coverage achieved during the D319 cruise is illustrated by the hours of operation of the green BBCEAS instrument shown in figure 4.6. Following the initial set up whilst in dock in Lisbon the BBCEAS instrument virtually continuously sampled ambient air from 23rd May to 9th June 2007. The extended time periods (>1hour) where the BBCEAS was not sampling ambient air flow on 25th and 27th May and 1st, 2nd and 5th June 2007 were due to disassembling the cavity to clean the cavity mirrors, complete realignment of the optical train and for acquisition of the N₂ background spectra and O₂-O₂ and/or NO₂ calibration spectra. Mirror reflectivity was determined in situ using the O₂-O₂ absorption bands throughout the measurement campaign, as indicated in figure 4.6, and NO₂ absorption features towards the latter part of the campaign, from 30th May 2007.

4.3.3 BBCEAS measurements on RSS Discovery

The different types of measurements required for quantitative BBCEAS during D319 operations are described here. All BBCEAS measurements were made using the spectra suite software supplied by ocean optics. Data acquisition was performed in two modes which either saved continuously until stopped manually by the operator (used for ambient sampling, $I(\lambda)$) or recorded data for a specified number of files (used for background, $I_o(\lambda)$ and calibration spectra).

Background N₂ flush measurements, $I_o(\lambda)$, and mirror reflectivity, $R(\lambda)$, determination measurements were recorded regularly throughout the D319 cruise as indicated in figure 4.6. The background N₂ flushes are required firstly to calculate the sample's absorption spectrum. Secondly the background N₂ flush also serves as a guide to the

instruments optical alignment and any possible degradation of the cavity mirrors. Background N₂ flush spectra recorded on day one of the D319 measurements were significantly different to those BBCEAS spectra recorded on day two of D319. Investigation of the cavity showed that cleaning of the cavity mirrors and cavity re aligned was required. Comparison of the background N₂ flushes from day to day were then used throughout the D319 BBCEAS measurements to indicate when alignment had degraded and/ or mirror surfaces had dirtied, enabling necessary adjustments in order to record data with the best possible sensitivity.

Background spectra of the light intensity transmitted by the cavity in the absence of any absorbers, $I_0(\lambda)$, were obtained by placing a section of rigid plastic tubing between the mirror mount enclosures to enclose the light path of the instrument. The enclosed cavity was purged with dry nitrogen (from a liquid nitrogen boil off source onboard) at 2 s.l.p.m supplied into the centre of the enclosed cavity to expel atmospheric air. The measurement of light intensity within the cavity was recorded on 1 second integration and averages of 10 scans were saved to file.

Spectra of the light intensity transmitted by the cavity containing the atmospheric sample were obtained in an open path mode by removing the tubing enclosure to allow air to pass freely between the cavity mirrors. The spectra suite software running parameters were set to those of the background measurement, (1 second integration and averages of 10 scans saved to file). The instrument was then set running, continuously saving scans until stopped manually at a later time. In the open path mode the cavity mirror mounts use a flow of nitrogen (approx 1.2 s.l.p.m split to two mounts) passed across the cavity mirror surface to minimise particle deposits on the

surface. This nitrogen flow fills the region from the mirrors surface to the open end of the mounting, thereby reducing the fraction of the cavity length occupied by the sample. For D319 operation the open section of the BBCEAS cavity was 84 cm, while the geometric cavity length was 117 cm. This yields a length factor of R_L of $117/84=1.39$ which was used to correct the measured absorption coefficient and for the effects of excluding ambient sample from the full length of the cavity (see equation 4.1). Here the geometric length has been used to determine the length factor used in the analysis, as the spectroscopically determined fraction of cavity open to the ambient sample was found to be close to the geometric value.

4.3.4. Cavity Mirror reflectivity measurement ($R(\lambda)$)

The cavity mirror reflectivity varies with wavelength, and needs to be characterised carefully for the BBCEAS measurements to be quantitative. The shape of the cavity mirror reflectivity curve was measured in laboratory investigations prior to D319. However the path length achieved inside the cavity under field conditions is not always as great as those achieved under laboratory conditions due to, e.g. imperfect cavity alignment and/ or degradation of mirror surface cleanliness. Therefore the laboratory defined $R(\lambda)$ was used as a basis and verified in the field by measuring BBCEAS spectra of a known absorber; during D319 this was O_4 in pure oxygen. Towards the later part of the campaign NO_2 bands were used to verify the reflectivity curve shape.

The cavity was filled with pure oxygen introduced to the centre of the enclosed cavity at 2 s.l.p.m from gas cylinders (BOC). The measurement of light intensity was carried out over the same integration time and averaging as the background, $I_o(\lambda)$,

measurement, with a minimum of 50 files saved. Each oxygen file was fitted individually; this provided a short time series of O_2-O_2 concentration to verify that all the ambient air had been expelled from the cavity. This enabled the relevant files to be averaged for the mirror curve determining analysis. An example of a fitted BBCEAS O_2-O_2 absorption spectrum in pure oxygen is shown in figure 4.7. In the analysis that produced figure 4.7 the mirror reflectivity curve from prior lab characterisation was adjusted (by multiplying $1-R(\lambda)$ by a wavelength independent scaling factor) such that the O_2-O_2 band intensity was consistent with that of pure oxygen. This scaled $R(\lambda)$ curve was then used in the analysis of ambient BBCEAS spectra. The O_2-O_2 band, although useful for scaling a known mirror reflectivity curve, does not provide as much detail on the shape of the curve as a calibration absorber with highly structured absorption cross sections, like NO_2 for example, which has structured bands across the full measurement bandwidth. The NO_2 source was only available during the latter days of the campaign, but the NO_2 concentration was not known exactly due to parts of the dynamic gas calibration system being broken during shipping from the UK to Lisbon prior to the D319 cruise. Flow from the NO_2 permeation tube source to the cavity was controlled by the dynamic gas flow calibration system. An example of the fitted BBCEAS NO_2 spectrum from these measurements is shown in figure 4.8. In the absence of separate NO_2 concentration, the NO_2 calibration spectrum in figure 4.8 was used for additional verification of the mirror curve shape, while the O_2-O_2 measurements provided positioning onto an absolute scale.

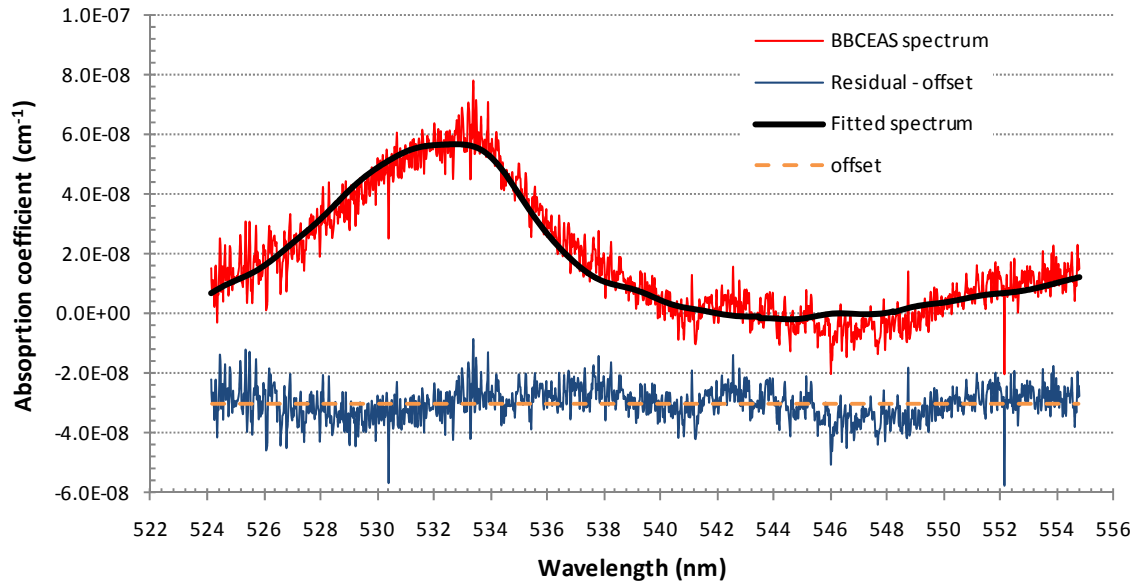


Figure 4.7. Calibration of cavity mirrors by fitting the O₂-O₂ absorption bands (Hermans 2008 absorption cross sections) to measurements in pure O₂ made on 1st June 2007. The fitted amount of oxygen from the inferred O₄ band is 1.00+/- 0.00958 and the standard deviation of the residual spectrum is 5.40X10⁻⁹ cm⁻¹. The residual spectrum is shown with an offset of -3x10⁻⁸. To retrieve the correct O₄ signal, the R(λ) curve from lab characterisation was scaled by a factor of 1.7.

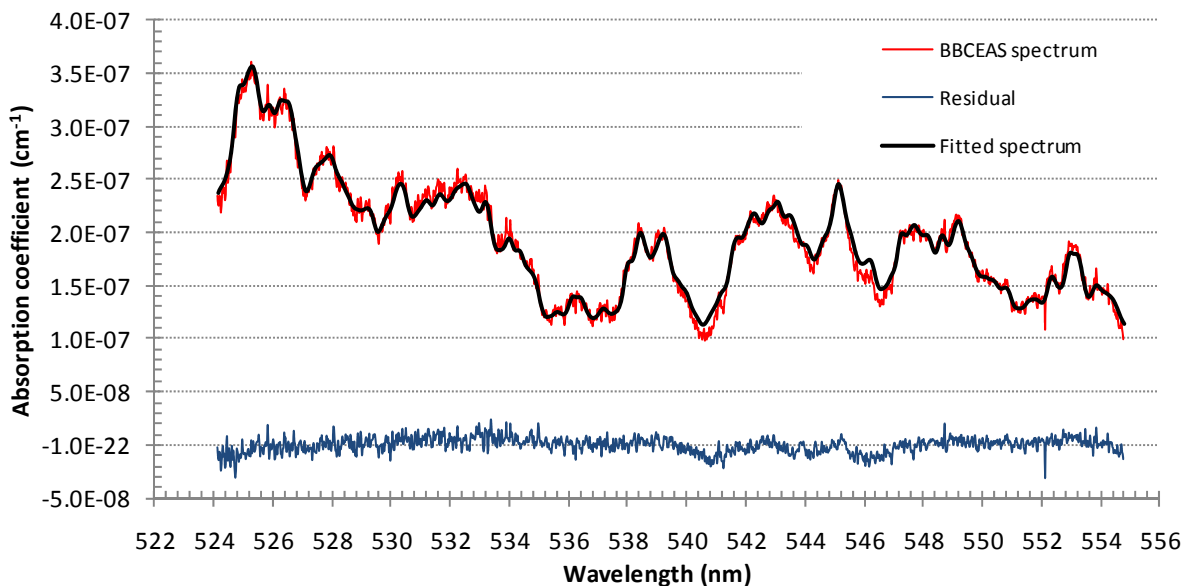


Figure 4.8. NO₂ Calibration spectrum fitted with the Vandaele [Vandaele et al., 1998] NO₂ absorption cross sections. The fitted amount of NO₂ is 61ppbv +/- 0.0327ppbv and the standard deviation of the residual spectrum is 7.17X10⁻⁹ cm⁻¹.

4.4. BBCEAS trace gas measurements during D319.

The BBCEAS spectra recorded during D319 were analysed using “in house” analysis routines created in MathCAD. The Mathcad analysis calculates the BBCEAS spectra from $I(\lambda)$ and $I_0(\lambda)$ measurements, checks that the $R(\lambda)$ mirror curve, produces the correct retrievals of unity O_4 features in pure oxygen calibration spectra, and performs a DOAS fit of the ambient spectra’s differential structure to yield time series of each molecular absorbers’ concentration. The analysis routine is the same as that used for other campaigns and details of the analysis are described in chapter 3.

4.4.1 BBCEAS of ambient water vapour during D319

The D319 BBCEAS data were recorded over the ocean with ambient air temperatures ranging between 18-23^oC and humidity between 70-90%. Thus water vapour was present in the ambient samples at around 1.5% mixing ratio and the water vapour absorption band around 540 nm is a strong contributor to the BBCEAS spectrum. This water vapour is the first molecular absorber to be fitted to the BBCEAS spectra in the Mathcad analysis routine. Moreover the quantification of water vapour concentration in the BBCEAS spectra and comparison of these to meteorological data for D319 serves to verify the BBCEAS instrument is retrieving real atmospheric concentrations. When the spectral fitting for water vapour absorption bands retrieves concentrations that agree with meteorological data, any subsequent fitting for other trace gas species in the spectrum can be taken to be reliable. The retrieval of well matched water vapour concentration between different instruments shows the mirror reflectivity curve calibrations are correct, and the correct length factor is being utilised during the

analysis. If spectral fitting gives water vapour concentrations that do not agree with meteorological data or water vapour bands are not observed, the BBCEAS is functioning less than optimally. Thus there is little to be gained in attempting to fit for smaller absorption signals, such as I₂.

Examples of BBCEAS measurements during D319 when water vapour bands were observed and fitted occurred during 26th and 28th May 2007, and are presented below. The retrieved water vapour concentrations were found to be in reasonable agreement with meteorological data values. Attempts were then made to fit other trace gas species (NO₂ and I₂) in the residual spectrum remaining after the fitted water vapour contribution was subtracted from the absorption. Figure 4.9 shows an example of a BBCEAS spectrum of ambient air, clearly showing the H₂O band at around 540 nm (fitted here with the Hitran database - black trace).

The water vapour spectrum shown in figure 4.9 corresponds to the first data point of the BBCEAS data (blue points) shown in the time series in figure 4.10. The BBCEAS data is in close agreement with the meteorological data (red points) during this measurement. The standard deviation of the residual spectrum following the fitting of water is $1.18 \times 10^{-8} \text{ cm}^{-1}$, much greater than that of the calibration spectra; O₄ $5.4 \times 10^{-9} \text{ cm}^{-1}$ and for NO₂ $7.17 \times 10^{-9} \text{ cm}^{-1}$. The differences between the open path recorded spectra and the calibration spectra are due to reduction in path length inside the cavity, due to ambient aerosol, or poor alignment of the cavity, or dirty mirror surfaces.

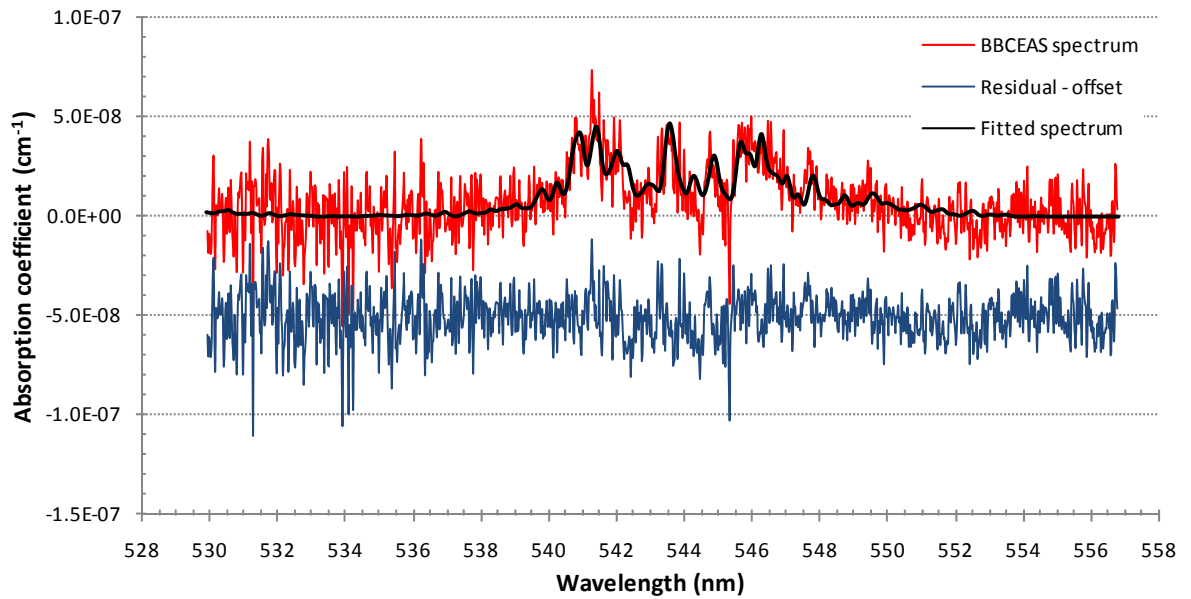


Figure 4.9 Absorption of ambient air fitted for water vapour absorption bands of the HITRAN 2004 spectral database, degraded to the spectrometer resolution to measurements made on 26th May 2007. The fitted amount of water is 0.023 +/- 0.00138 % and the standard deviation of the residual spectrum is 1.186×10^{-8} . The residual spectrum is shown with an offset of 5×10^{-8} .

Analysis of BBCEAS data recorded on the night of 26th May 2007 showed that the water vapour concentrations retrieved from fitting the BBCEAS spectra agreed well with meteorological data for the first part of the time series (section A of figure 4.10). The fitted BBCEAS spectrum shown in figure 4.9 corresponds to the first blue point measurement shown in the time series of figure 4.10. However after 146.98 (section B, figure 4.10) the fitted water concentration in BBCEAS substantially overestimates compared to the meteorological H₂O amount and became substantially less certain (larger error bars on the blue points). This degradation in instrument performance coincided with an increase in wind speed which could have lead to seawater/spray deposits on the cavity mirror surface. Around the same time the average continuum absorbance (calculated between 529.9 and 556.8 nm) remaining in the BBCEAS spectrum after fitting H₂O increases rapidly during the measurements (green points in

figure 4.10). This indicates a substantial reduction in the path length inside the cavity, caused by either a rapid increase in ambient aerosol extinction or more likely a degradation of the cavity mirror reflectivity. Indeed this degradation of instrument performance coincided with wind speed change which may increase sea spray deposits and thus decrease mirror reflectivity.

The subsequent fitting for other trace gas species after the water vapour is subtracted from the absorption yielded no detectable iodine absorption signals, on only a few occasions was NO₂ detected.

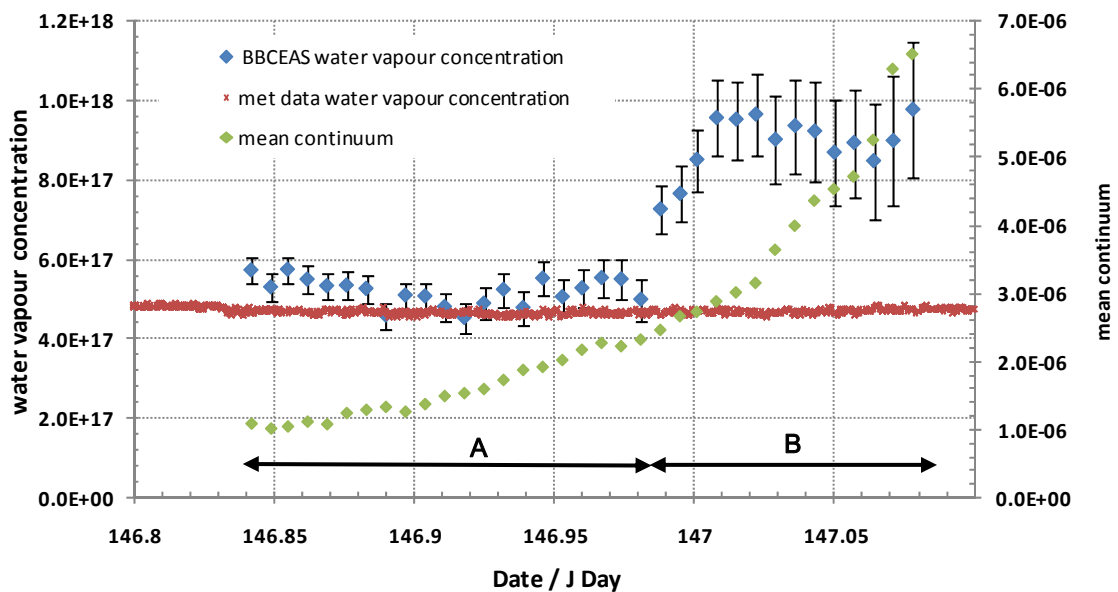


Figure 4.10. Time series from BBCEAS fitting of water vapour shown in blue points, also shown is the meteorologically determined concentration (red points).

4.4.2 BBCEAS of ambient NO₂ and I₂ during D319

During the 28th May 2007 the BBCEAS measurement analysis and fitting of water vapour bands provided concentrations that agreed reasonably with meteorologically determined concentrations. The subsequent fitting for NO₂ and iodine showed a positive NO₂ signature in some of the data, but no detectable iodine above an approximate detection limit of 200 pptv. An example of a BBCEAS spectrum fitted for NO₂ is shown in figure 4.11. The two BBCEAS instruments were operated in tandem to monitor two RHS species: I₂ by the Leicester BBCEAS at green wavelengths and IO by the Cambridge University BBCEAS at blue wavelengths.

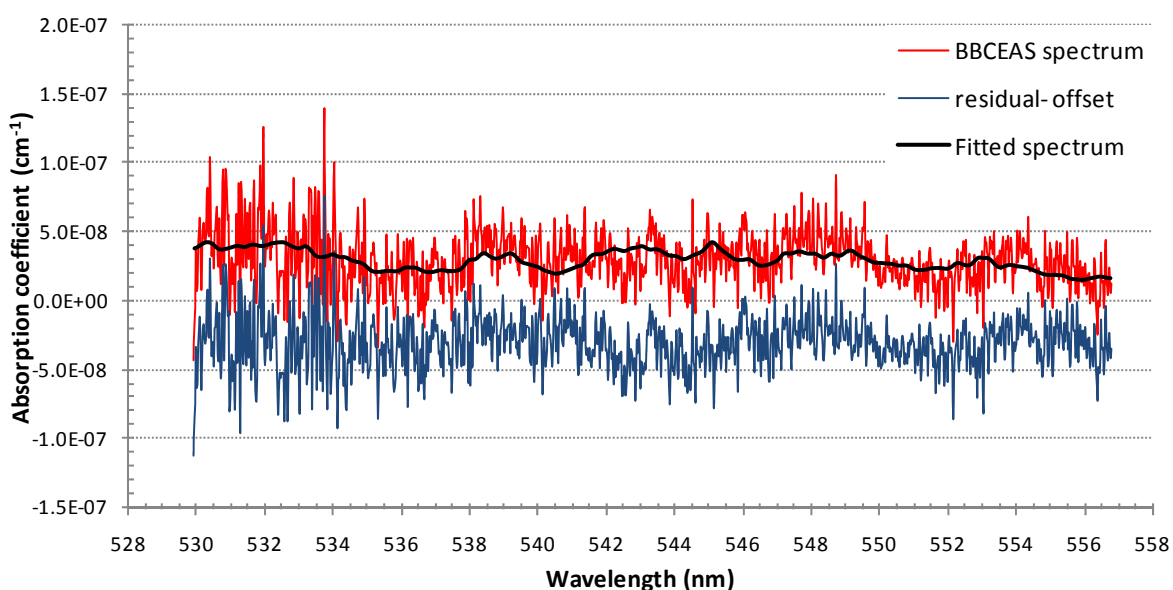


Figure 4.11. Resulting NO₂ fitted spectrum from analysis of ambient air measurements made on 28th May 2007. Fitted water vapour concentrations are the subtraction from the absorption and the remaining absorption features are fitted to NO₂ absorption cross sections. The fitted amount of NO₂ is 10.68 +/- 1.5 ppbv and the standard deviation of the residual spectrum is 1.89X10⁻⁸. The residual spectrum is shown with an offset of 3x10⁻⁸ cm⁻¹.

The time series of the retrieved NO_2 concentrations on the 28th May 2007 from the both BBCEAS instruments operating at green and blue wavelengths is shown alongside NO_{xy} data in figure 4.12. The two BBCEAS instruments (operating over different wavelength ranges) retrieved similar quantities of NO_2 , but both BBCEAS instruments found substantially less NO_2 than the NO_{xy} instrument from 16:48 hrs onwards. The good agreement between the cavity instruments but not with the NO_{xy} instrument suggests that the BBCEAS instruments were monitoring open ocean air, whilst the NO_{xy} instrument was influenced by the ship's own emissions. The NO_2 concentrations from the NO_{xy} instrument are much greater than one would expect for the open ocean and are highly variable. The NO_{xy} authors state that NO_2 levels reported are not background levels but either instrument error or due to influence from the ship's smoke stack. This shows the importance of firstly making sure all instruments are located sufficiently close together that they all sample the same air, and secondly that perturbing the atmosphere with one's own emissions should be avoided.

The comparison between the two BBCEAS instruments operating across different wavelength regions is possible for NO_2 due to the absorption cross section of NO_2 having rapidly varying structure across green and blue wavelengths. Along with similar NO_2 concentrations being retrieved by both cavity instruments (green and blue traces in figure 4.12) similarities are observed in the standard deviation of the residual spectrum for both cavity instruments: these are shown in figure 4.13. The standard deviation of the residuals increase and decrease at the same time for both green and blue BBCEAS, which suggests both instruments are measuring something "real", such as sea spray aerosol rather than random drifts in the instrument alignment.

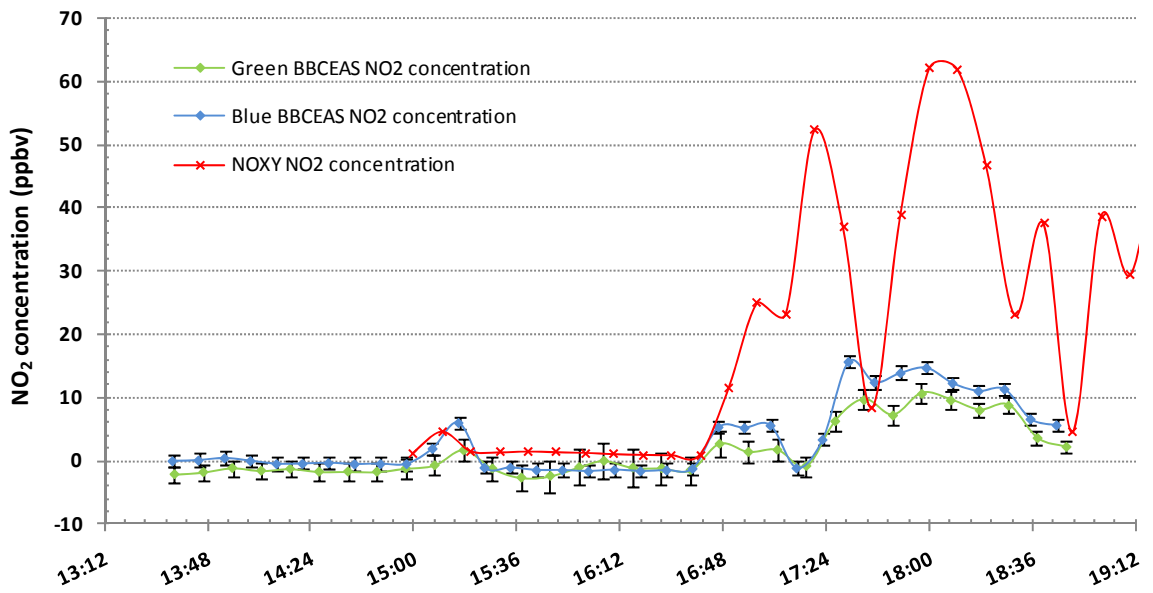


Figure 4.12. Time series of NO₂ concentration from Green and Blue BBCEAS and NO_{xy} instrument sampling on 28th May 2007.

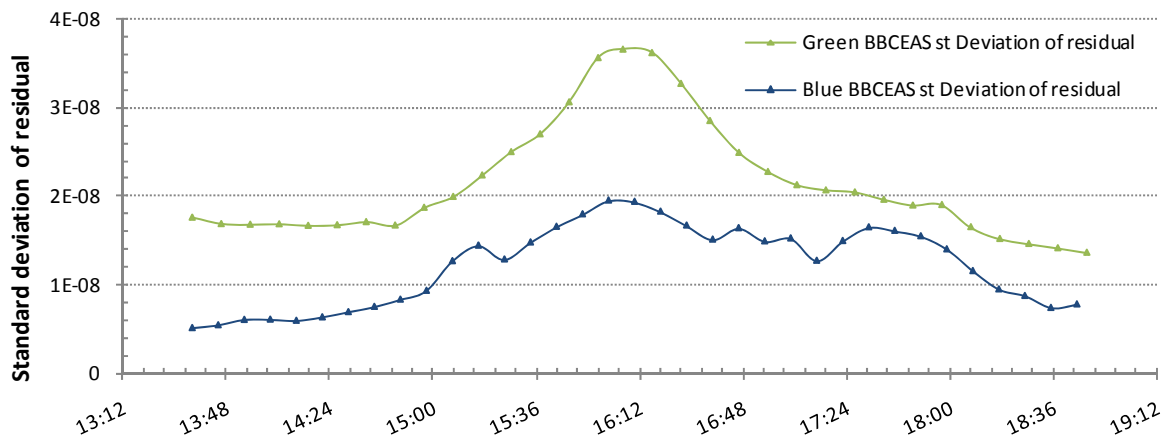


Figure 4.13. Time series of standard deviation of residual spectrum from Green and Blue BBCEAS instrument sampling on 28th May 2007.

4.5 Challenges of operating the BBCEAS instrument during D319 and lesson learnt

D319 was the first (non lab) field deployment of the BBCEAS instrument. Moreover operating conditions during the ship deployment are particularly challenging. Some challenges were foreseen prior to deployment (e.g. the cavity's optics were enclosed in weatherproof housings); some conditions were not anticipated, leading to a non optimal operation of the BBCEAS and occasioning of some ad hoc modifications. Nevertheless the D319 deployment provided a valuable learning experience, both for operating the instrument under adverse field conditions and valuable training experience for the instrument operators. Adaptations made to the hardware post D319 and the benefits of greater operating experience undoubtedly contributed to the success of later BBCEAS deployments to measure I_2 at Mace head (BIOFLUX II, August/September 2007) and NO_2 in the urban atmosphere (LAMP, July 2007). The operational issues during D319 are outlined below along with details of the attempts to resolve them during the campaign.

Mirror mounts which allowed a flow of dry nitrogen to be passed over the cavity mirror surface had been constructed prior to D319, in order to keep the optical surfaces dry and free from contaminants such as sea salt. The wind strength and wave height during D319 were such that sea salt aerosol was still deposited onto the cavity mirror surface. This degraded the mirror reflectivity and reduced the effective path length of the BBCEAS measurement leading to decreased sensitivity of the instrument. Figure 4.14 shows an example of the build up of sea salt particles on a cavity mirror. Regular cleaning of the mirror surfaces and re alignment of the cavity was necessary throughout the D319 cruise to remove salty deposits from the mirror surface. In an

attempt to reduce the ingress of sea salt, additional lengths of tubing were added to the mirror mounts to increase the volume the mirror mount purges with dry N₂. This did help limit the sea salt deposits, but also reduced the amount of the cavity path covered by the ambient sample (RL increased from 1.39 to 2.43) thereby reducing the BBCEAS instruments sensitivity. The shorter open cavity (use of tubular extensions) was used from the 31st May until the end of the measurements. The analysis of spectra recorded during this time produced no observable water vapour bands, and thus was not analysed further, suggesting that shortening the open cavity reduced the instrument sensitivity too much and the instrument was not capable of observing the trace gas concentrations required in the open ocean environment.

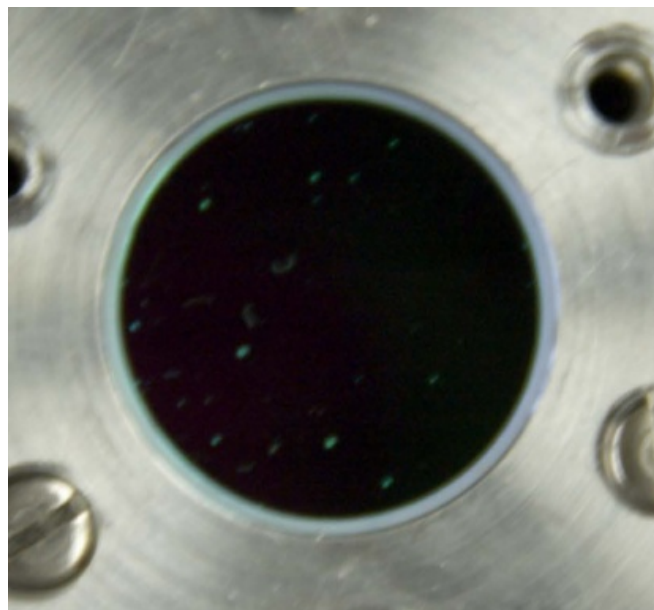


Figure 4.14 Cavity mirror surface with salt deposits, following a period of sampling ambient airflow during D319.

Anti vibration mountings had been built into the BBCEAS mounting gantry prior to deployment. These anti vibration mounts were designed to decouple the BBCEAS cavities from the movement or vibration of the ship, thus preserving the optical alignment. In order for the anti vibration mounts to be effective, the gantry must be firmly fixed to the deck/site. During D319, fabric strapping was used to lash the gantry in place on deck and subsequent wetting and stretching of the strapping led to movement of the gantry, which could have contributed to the cavities going out of alignment and hence increased noise in the BBCEAS spectra.

The maximum distance between the electronic components housed in the container laboratory and the cavities on the portside deck was limited by the fibre optics length of 10 m. A suitable location had been identified for the electronics in the container laboratory during the pre deployment planning stage: however the arrangement of the lab container onboard D319 was somewhat different. The location of the container cable feed through meant the distance between the electronics and the cavities was at its absolute maximum. This added strain to the fibres which caused additional noise in the BBCEAS measurements.

The port side laboratory container housing the BBCEAS electronics was subject to large temperature variations and this compromised the stability of the LED light source and the spectrometer. Previous lab work (chapter 3, section 3.3.2) shows that the emission spectra of LED changes with temperature. For D319 the LED was mounted on a temperature stabilised mount which, in previous operating conditions had been more than capable of keeping the light output stable. Unfortunately under the extreme temperature variations encountered during the D319 cruise the LED output varied

substantially. Changes in the LED emission spectrum can produce large false signals in the BBCEAS spectra, especially where the emission spectrum of the green LED is structured and these structures vary with temperature. This additional LED induced structure in the BBCEAS spectra prevented any useful retrieval of atmospheric trace gas absorber species, including the ubiquitous water vapour bands.

Weather conditions: rain and strong winds made cavity alignment difficult and in some cases dangerous leading to periods where it was not possible to safely operate the BBCEAS optimally. The operator also had to cope with the effects of sea sickness.

4.6 Summary and conclusion

This first field deployment of the BBCEAS instrument experienced many demanding conditions during the D319 cruise, resulting in the usual high sensitivity of the BBCEAS instrument under lab tests not being achieved in the field.

Absorption features of water vapour and NO₂ (likely from the ship's own pollution) were detected on occasions shortly after the cavity mirrors had been cleaned and realigned. Example BBCEAS spectra of H₂O and NO₂ have been presented and comparison of the quality of these fits to other campaigns using the same BBCEAS system highlights the less than optimal operating performance during D319. The calibration measurements of O₂-O₂ during D319 retrieved 1.0 +/- 0.0096 with a standard deviation of the remaining residual spectrum of $5.4 \times 10^{-9} \text{ cm}^{-1}$, while the best quality water vapour spectrum retrieved from ambient air sampling showed 0.023 +/- 0.0013 with a standard deviation of the residual spectrum $1.186 \times 10^{-8} \text{ cm}^{-1}$. Similar

measurements made at Mace Head and reported in chapter 6 retrieve O_2-O_2 with standard deviations of the residual spectrum of $2.7 \times 10^{-9} \text{ cm}^{-1}$ and water vapour in ambient air sampling at 0.0126 ± 0.0002 , with a standard deviation of the residual $1.99 \times 10^{-9} \text{ cm}^{-1}$.

Methods devised pre-D319 to keep the BBCEAS instrument in optimal working conditions were not able to withstand the particularly harsh environment experienced at sea. However the lessons learned from the D319 deployment have enabled the instrument to be further adapted for field applications. This resulted in the improved BBCEAS system recording very high quality data over extended measurement periods. NO_2 was monitored at blue wavelengths during LAMP (chapter 6) one month after D319, and Iodine at green wavelengths during BIOFLUX II (chapter 5), two months later.

Similar operating issues affected the Cambridge BBCEAS instrument, which was able to use NO_2 in the ships smoke stack to test the instrument was operating satisfactorily, in a similar manner to that used by the I_2 BBCEAS with water bands. The Cambridge BBCEAS instrument did not yield much useful data during D319 either, yet the same instrument was deployed measuring NO_3/N_2O_5 at the BT tower providing high quality data.

The BBCEAS technique is capable of measuring ambient trace gas species; however the operating conditions during D319 were very difficult yielding an unusually complex BBCEAS data set.

Chapter 5

Iodine measurements at Mace Head: the BIOFLUX II campaign

This chapter focuses on the deployment of the LED BBCEAS instrument during the BIOFLUX II campaign at Mace Head, on the west coast of County Galway in Ireland, during August and September 2007. Mace Head is a region of active halogen chemistry, (which has been described in chapter 1), and for BIOFLUX II the LED BBCEAS instrument was configured to quantify molecular iodine in the ambient atmosphere using the I_2 molecule's structured absorption bands at green wavelengths. This deployment also enabled the BBCEAS instrument to be robustly assessed for its capabilities as a field instrument, sampling ambient atmospheric air and operating over extended timescales in a variety of atmospheric conditions. The laboratory studies reported previously by Ball et al [Ball et al., 2010] found that that different seaweed species emit iodine at different rates and with different emission time profiles [Ball et al., 2010]. In this chapter, ambient I_2 measurements from BIOFLUX II are reported and then interpreted with relation to tidal height (and other meteorological data) in order to determine if the I_2 amounts in the environment are also dominated by emissions from certain species, and when the largest emissions occur.

5.1 Introduction

The BBCEAS instrument, configured to operate at green wavelengths, has been used successfully to investigate the emission of iodine into the gas phase from different seaweed species during laboratory based studies at Roscoff and at Manchester

University [Chapter 4 and Ball et al., 2010]. These studies showed that the spectroscopic technique of BBCEAS could unambiguously detect and quantify molecular iodine at trace gas concentrations amongst mixtures of other absorbing species. However as discussed in Chapter 4, the first field campaign deploying the BBCEAS instrument “in the real atmosphere” from onboard the RHaMBLe D319 ship cruise experienced particularly demanding conditions. D319 provided valuable field experience for determining the optimal operation of the instrument in the field. The D319 experience informed engineering improvements to the BBCEAS instrument hardware (which were made prior to the Mace Head deployment) and improvements to the practice of operating the instrument under field conditions.

5.1.1 Adaptations to the BBCEAS instrument between D319 and BIOFLUXII

During D319 the mirror mount open aperture was 1.5 inch diameter, during BIOFLUX II this was reduced to 0.75 inch using Teflon inserts. This was large enough for the light beam diameter to pass into the enclosure; but the inserts reduced the target area any salt particles have for getting to the cavity mirror surfaces. Another effect of the Teflon inserts was to confine the N₂ mirror purge inside the mounts.

The D319 experience gave insight into the best practice for BBCEAS operation. The required regularity for recording N₂ flushes (I₀ spectra) and oxygen calibrations, to help monitor cavity alignment, mirror surface cleanliness, and keep the instrument operating in optimally was gained. The frequency of the I₀(λ) spectra and calibration measurements employed during BIOFLUX II is illustrated in table 5.3, showing these measurements were made at a minimum of twice daily if possible. The cavity was aligned at 90 degrees to the prevailing south-westerly wind direction at Mace Head.

This aimed to limit sea salt deposits upon the mirror surfaces, as passing air was not directed into the mirror enclosures. The positioning of the instrument components in the downstairs room in bottom cottage lab, which contained far less other equipment, enabled the required space for the electronic components along with more stable temperature compared to D319. It also enabled us to choose our route for cables to run to the outside cavity. An additional operating improvement was the cooling of the HR4000 spectrometer (see figure 5.6). The benefits of cooling the spectrometer are (i) smaller & less noisy dark current, thus less noise in BBCEAS spectra, also (ii) changes in room temperature cause less changes in detector noise if the detector is cooled and temperature controlled.

Additional challenges in the operation of BBCEAS in the field is in the fitting multiple absorbers in the calculated absorbance. The larger absorbing species must be accurately quantified and subtracted from the absorbance in order to detect and quantify other atmospherically important target trace gas species. There are however, benefits of multiple absorbers because, like D319, the water vapour bands can be used to inform how well the BBCEAS is operating (see section 5.6).

Other challenges in BBCEAS operation are the influence of aerosol and operating for long time periods. Aerosol present at high levels lowers the sensitivity of the BBCEAS as particles in the light path block or limit the path length, decreasing the enhancement of the cavity. The instrument housing was modified to enable more sensitive atmospheric monitoring of trace gas species than had been possible during D319 cruise measurements.

Operating for long time periods (e.g. over the majority of a month long campaign) has demands upon the operator and the quality of the measurements can also depend upon external influences such as weather.

The modifications to the instrument setup following the D319 cruise were tested in the field during a month long deployment of the instrument to monitor Iodine in the coastal environment at Mace Head, Ireland.

5.2 Iodine chemistry and Mace Head

The Mace Head atmospheric observatory was the ideal site for the I₂ BBCEAS instrument to be deployed in the field, as the first spectroscopic measurements of molecular iodine in the atmosphere were recorded here by Saiz Lopez et al, using long path DOAS [Saiz-lopez and Plane, 2004] and iodine has been repeatedly measured here since this first measurement [Peters et al., 2005][Saiz-lopez et al., 2006]. Particle nucleation episodes have been observed alongside the elevated iodine concentration at Mace head ([Coe et al., 2006] [Yoon, Junkerman, et al., 2007]). The particle composition was analysed and found to be mixtures of iodine oxide species [O'Dowd et al., 2002] [Hoffmann et al., 2001]. The pathway of new particle formation in the marine environment has been studied extensively as it provides an additional route to particles alongside the established routes. The proposed pathway of formation of marine aerosol from iodine species is shown in figure 5.1.

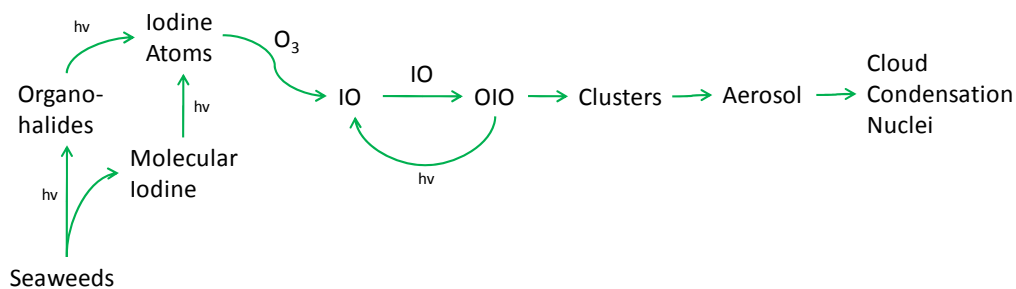


Figure 5.1 Particle formation pathway in the gas phase involving iodine species.

The Mace Head Atmospheric Research Station has a large abundance of seaweeds growing close to the site, many of which are known iodine emitters, e.g. *Laminaria* [Ball *et al.*, 2010].

Iodine is emitted from seaweeds as a response to agitation and oxidative stress [Küpper *et al.*, 2008][Ball *et al.*, 2010]. The iodine emission from stressed seaweed occurs over an extended period and exhibits a fluctuating pattern in concentration. The I_2 concentration rapidly increases after exposure to ambient air then decays over time. The iodine concentration exhibits additional burst and decay cycles occurring at relatively evenly spaced times. However, the peak intensities of these additional and sequential I_2 bursts decreases compared to the initial iodine concentration peak. Dixneuf has also monitored the time dependant iodine emission from *laminarias* in laboratory studies observing a similar pattern of I_2 concentration bursts with a fluctuating time dependence [Dixneuf *et al.*, 2009].

5.2.1 Mace Head Site Information.

The Mace Head atmospheric research station on the west coast of Ireland close to Carna, County Galway is operated by the Physics Department at the National University of Ireland, Galway. It is a site which generally experiences uniquely clean air masses with westerly exposure to the north Atlantic, which provides the opportunity to make observations and measurements in a northern hemisphere background environment. The clean air sector is the air arriving at the site from 180 degrees to 300 degrees is depicted by the shaded area in map 5.1. The closest city to the site is Galway, situated 88 km to the east of Mace Head, the islands in close proximity to the Mace Head measurement site are uninhabited and shipping routes in the Atlantic Ocean are over 150km from the site.

The Mace Head site location is shown in figure 5.2: this shows a map of the site on the right and a picture of the site on the left. The picture is taken from the national coastal survey and shows the coastline and tidal fetch region. Imposed upon the picture is the position of the BBCEAS (red spot) and the distances to the closest Laminaria beds (yellow lines). The atmospheric observatory at Mace Head has several platforms and location sites available for instrument location and sampling: the cottage lab is 300 m from the shore and two shore side laboratories 50 m from the shore and a 22 m scaffold tower.

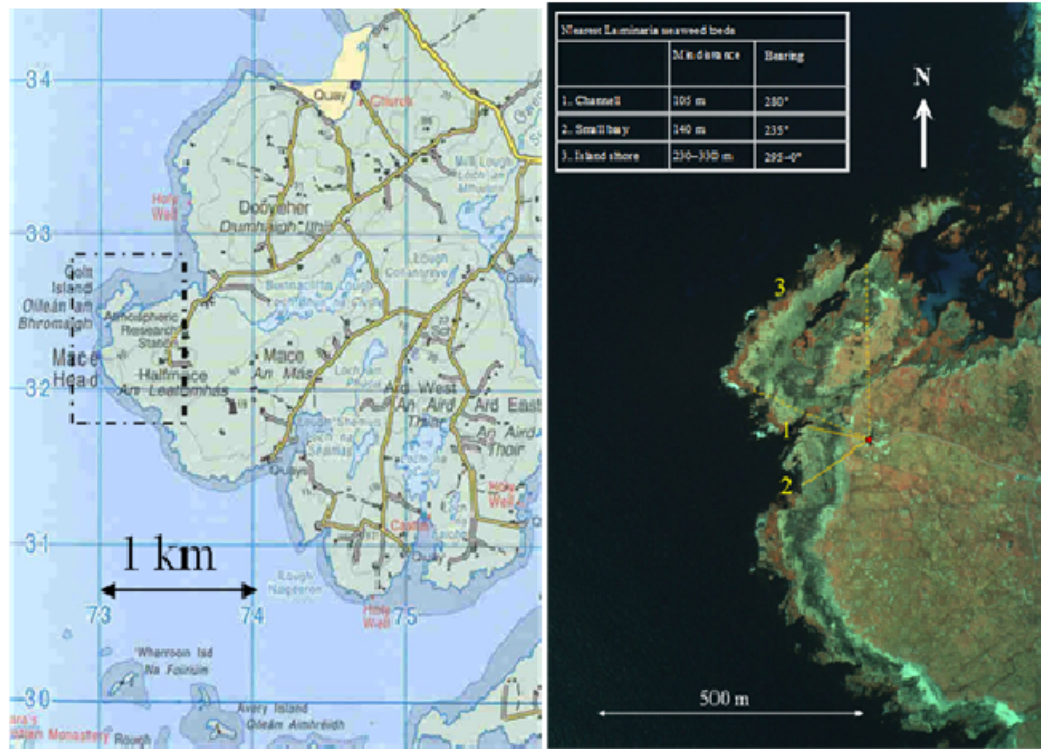


Figure 5.2 Map of the atmospheric research station site at Mace Head. Right hand pane shows larger region near Mace Head and the left hand pane the inset showing the BBCEAS position (red dot) with the closest laminaria bed illustrated by 1, 2 and 3. Picture on right is taken from the national coastline survey by the Marine Institute, Ireland 2000.

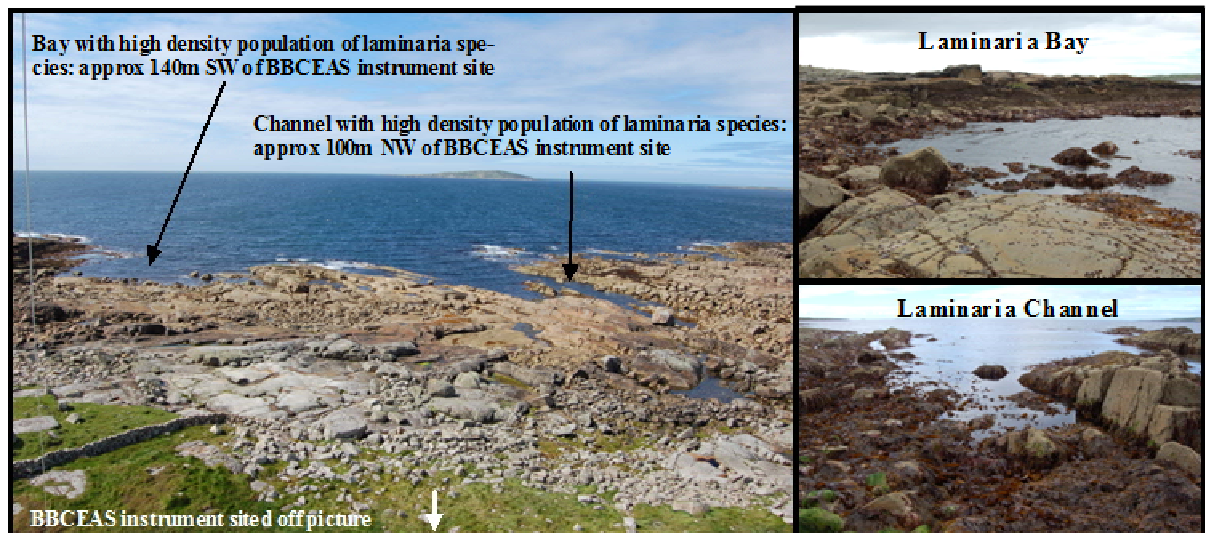


Figure 5.3. The locations of high density Laminaria populations at Mace Head. Pictures taken by A. Hollingsworth from the tower situated between two lower cottage laboratories, above the BBCEAS instrument location.

5.3. Aims & instrumentation for BIOFLUX II

BIOFLUX II was a European Science Foundation (ESF) funded exchange project led by the INTROP (interdisciplinary tropospheric research: from the laboratory to global change) theme “Do we understand the impact of aerosols on global change?” BIOFLUX II focused on using recently developed state of the art instrumentation to quantify the sources of newly-nucleated marine aerosol particles, the iodine oxides, produced via photolysis of organic iodine species and I_2 emitted directly from seaweeds and plankton. The exchange enabled the BBCEAS instrument to be deployed at Mace Head to measure molecular iodine under ambient atmospheric sampling conditions, and, together with the datasets from other co-deployed instrumentation, to further the understanding of the formation processes of marine aerosol and the impact these processes have on the climate.

Reactive Halogen Species measurement methods employed at Mace Head over the last decade show the region has elevated levels of RHS compared to background tropospheric levels. These studies provided valuable insights into the chemical processing of RHS which lead to the formation of marine aerosol, more details of the chemical processes and the measurement methods can be found in chapter 1, Iodine chemistry in the troposphere. The majority of RHS measurements at Mace Head prior to BIOFLUX II have used the Long path DOAS technique. The published measurements of RHS at Mace Head are summarised in table 5.1.

RHS measurement at Mace Head			
Author	target species	Technique	Dates of measurements
Allan et al 2000[<i>Allan et al.</i> , 2000]	IO (DL0.24ppt, max 1.17ppt)	LP DOAS	May 1997
Alicke et al 1999 [<i>Alicke et al.</i> , 1999]	IO (DL 0.9 ppt, max 6.7ppt)	LP DOAS	May 1997
Peters et al 2005[<i>Peters et al.</i> , 2005]	OIO (DL 0. ppt, max ppt) I ₂ (DL 20ppt, max 61ppt)	LP DOAS	June 1998
Carpenter et al 2001[<i>Carpenter et al.</i> , 2001]	IO (DI 0.5 ppt, max 3ppt)	LP DOAS	September 1998
O Dowd 2007[<i>Yoon, Junkerman, et al.</i> , 2007]	Particles size	SMPS and CPC	May 2002
Saiz Lopez et al 2004 [<i>Saiz-lopez and Plane</i> , 2004]	I ₂ (DL 3ppt, max 93ppt), OIO (DL 0.5ppt, max 3ppt) IO (DL 0.5 ppt, max 7ppt)	LP DOAS	August 2002
Saiz Lopez et al 2006 [<i>Saiz-lopez et al.</i> , 2006]	I ₂ (DL 20ppt, max 94 ppt) OIO (DL 4ppt, max 13ppt)	BBCRDS	August 2002
Coe et al 2006[<i>Coe et al.</i> , 2006]	Particle size and composition	DMPS and AMS	August 2002
Yoon 2007[<i>Yoon, Ceburnis, et al.</i> , 2007]	Particle size	SMPS	January 2002- June 2004
Bale et al 2008	Iodine atoms	Resonance fluorescence	August 2007

Table 5.1 Previous RHS measurements at Mace Head. Key to acronyms: LP DOAS = long path Differential optical absorption spectroscopy, BBCRDS = Broad Band Cavity Ring Down Spectroscopy, DMPS =D M particle sizer, AMS = aerosol mass spectrometer, SMPS = S M particle sizer.

The range of instrumentation deployed during the BIOFLUX II exchange in order to monitor atmospheric, chemical, and physical parameters relating to aerosol nucleation from iodine-containing biogenic gases is shown in Table 5.2. Three participants received INTROP exchange awards (shown by * after student/scientist in table 5.2) and substantial added value to this exchange came from the co-ordinated timetables with other research groups whose measurements overlapped in part, with our visit to Mace Head.

After an initial set up period, the INTROP-supported instruments were operated throughout the exchange period for as often as meteorological conditions and personnel presence allowed. The measurement period of the I₂ BBCEAS instrument

overlapped with unusually low tides peaking on 29th August and 13th September during which two nearby seaweed beds containing large populations of laminaria digitata were exposed (105 metres NW and 140 metres SW of the BBCEAS gantry, shown in figure 5.2).

Instrumentation and scientists at BIOFLUX II 2007			
PhD student/ scientist	PI & institution	Species detected	Instrument
Anna Hollingsworth*	Dr S Ball Leicester Univ	I ₂ photolysis rates	Broadband cavity enhanced absorption spectrometer (520-580nm bandwidth); Spectral radiometer
Ailsa Benton*	(Prof R L Jones) Cambridge Univ	IO	Broadband cavity enhanced absorption spectrometer (430-460nm bandwidth)
Karen Homsby Dr Charlotte Jones* Dr Rosie Chance	Dr L Carpenter York Univ	Organohalogen; I ₂	GC-MS on line air sampling; REA (relaxed eddy accumulation); Denuder tubes
Other groups/instruments visiting Mace Head during Bioflux II			
Roisin Commene Dr Trevor Ingham	(Dr D E Heard) Leeds Univ	IO	FA GE (fluorescence assay by gas expansion)
Dr Catherine Bale	Dr W Bloss Birmingham Univ	I atoms	Resonance fluorescence
Dr Katja Seitz	(Prof U Platt) Heidelberg Univ	I ₂ , IO, OIO	Long-path differential optical absorption spectroscopy (LP DOAS)
Continuous measurements at Mace Head Atmospheric Research Station			
Gerry Spain	Dr H Berresheim, (Drs C O'Dowd & G Jennings) NUI Galway	Meteorology, aerosol particle numbers & size distribution.	Core instruments at Mace Head research Station.

Table 5.2 Instrumentation at Mace Head during BIOFLUX II and associated personnel.

5.4. Meteorological data during BIOFLUX II

The temperature and relative humidity data for the duration of the BBCEAS measurements during BIOFLUX II are shown in figures 5.3. These data were provided by the operators of the Mace Head Atmospheric Research Station from their commercial met instruments, which are run continuously as part of a long term monitoring programme [NUI GALWAY, n.d.]. Rainy periods and misty weather conditions were experienced overnight on the 29th and 31st August 2007, overnight on the 1st September, during the day on 2nd September, and throughout the 4th-5th September 2007. During these occasions the relative humidity is close to 100%: see top panel of Figure 5.4. Generally the BBCEAS instrument was not operated during bad weather conditions. Experience showed that if the BBCEAS was operated during unfavourable weather, the data yielded little useful information. One of the criteria used to decide which data should be excluded from analysis is a high continuum absorbance. This indicates aerosol, mist or rain. BBCEAS an optical technique ceases to be reliable in rain or mist (fog), as one droplet of water in the light path of the instrument during a measurement causes signal loss. Another criterion used to exclude less high quality BBCEAS data was the mismatch between water vapour concentrations from BBCEAS and met data.

The hours of operation of the BBCEAS instrument are shown in table 5.3 whilst the meteorological data, tidal height and photolysis rate for I₂ during the BBCEAS measurements is shown in figure 5.4. The BBCEAS measurement period, days 238 to 257 experienced wind coming predominantly from between the South West and North West. This is the clean air sector as defined during NAMBLEX by Heard et al [Heard et

al., 2006], where air reaching the site has not recently been impacted by land based emissions. The BBCEAS measurements also covered periods of spring tides, where the maximum tidal height difference occurs. The photolysis rates for iodine (J_{I_2}) provide guide to the likelihood of observing I_2 and also indicate periods of rain, such as for example on day J247 in the time series, a rainy day during the campaign.

Hour	00:00	01:00	02:00	03:00	04:00	05:00	06:00	07:00	08:00	09:00	10:00	11:00	12:00	13:00	14:00	15:00	16:00	17:00	18:00	19:00	20:00	21:00	22:00	23:00	
Julien day	Date																								
237	25/08/2007																								
238	26/08/2007																								
239	27/08/2007								F,O,D			F,O,D													
240	28/08/2007															F,O,D									
241	29/08/2007											F,O,D										F,O,D			
242	30/08/2007								F,O,D								F,O,D								
243	31/08/2007									F,O,D								F,O,D							
244	01/09/2007								F,O,D	R								F,O,D							
245	02/09/2007								F,O,D								F,O,D								
246	03/09/2007								F,O,D																
247	04/09/2007								F,O																
248	05/09/2007								F,O,D									F,O,D							
249	06/09/2007									F,O,D									F,O,D						
250	07/09/2007											F,O,D	F,O,D												
251	08/09/2007							F,O,D					F,O,D												F,O,D
252	09/09/2007										F,O,D			F		F		F,O,D				F,O,D			
253	10/09/2007	F	F,O,D					F,O,D			F		F,O,D			F,O,D								F	
254	11/09/2007								F,O,D								F,O,D								F,O,D
255	12/09/2007							F,O,D									F,O,D					F,O,D			
256	13/09/2007																								
		F	nitrogen flush measurements for mirror calibration and $I_0(\lambda)$ spectra																						
			running for all or part of hour open path, I_2 detection																						
		D	detector dark current measurement																						
		O	Oxygen dimer measurement for calibration of mirror reflectivity curve $R(\lambda)$																						

Table 5.3 BBCEAS hours of operation during BIOFLUXII.

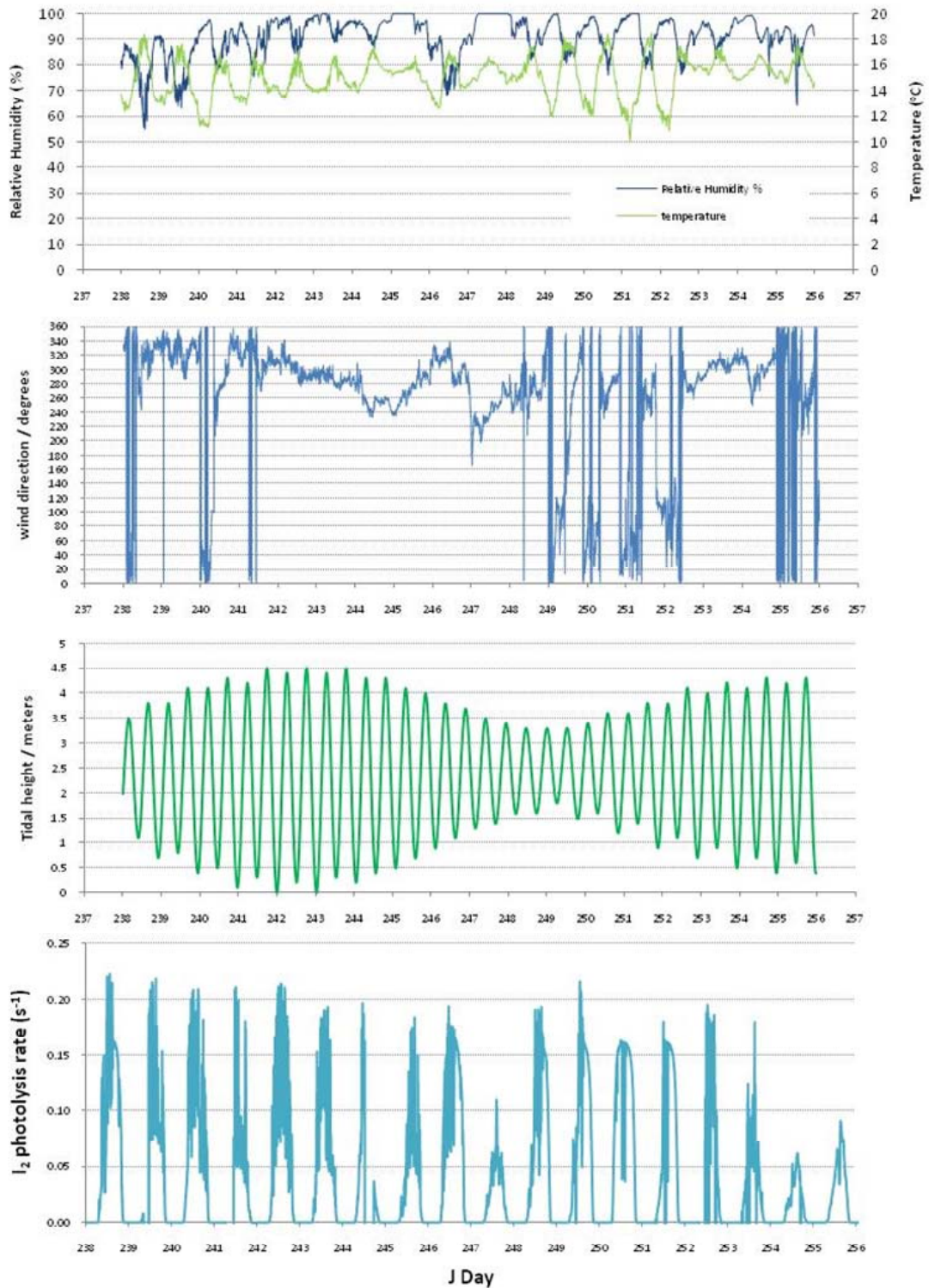


Figure 5.4 Meteorological data for Mace Head during BIOFLUX II BBCEAS measurements. Temperature and Relative Humidity (top panel), wind direction (2nd panel), tide height (3rd panel) and photolysis rate for I₂ (bottom). Data in top and middle panel from Mace Head Atmospheric Research Stations core instrumentation; tide data from admiral tides website, with cubic spline interpolation between high and low tide points.

5.5. The I₂ BBCEAS instrument and measurements during BIOFLUX II

For BIOFLUX II, the BBCEAS instrument was operated using an LED that emitted light at green wavelengths and an ocean optics HR4000 spectrometer (detecting across the wavelength range 504.8 -581.9 nm). This enabled atmospheric I₂ to be detected by this instrument using the iodine molecule's highly structured absorption cross sections at green wavelengths (see Figure 5.5). Figure 5.5 shows that other atmospheric molecules have structured absorption cross sections in this wavelength region, and thus need to be considered in analysis of the data.

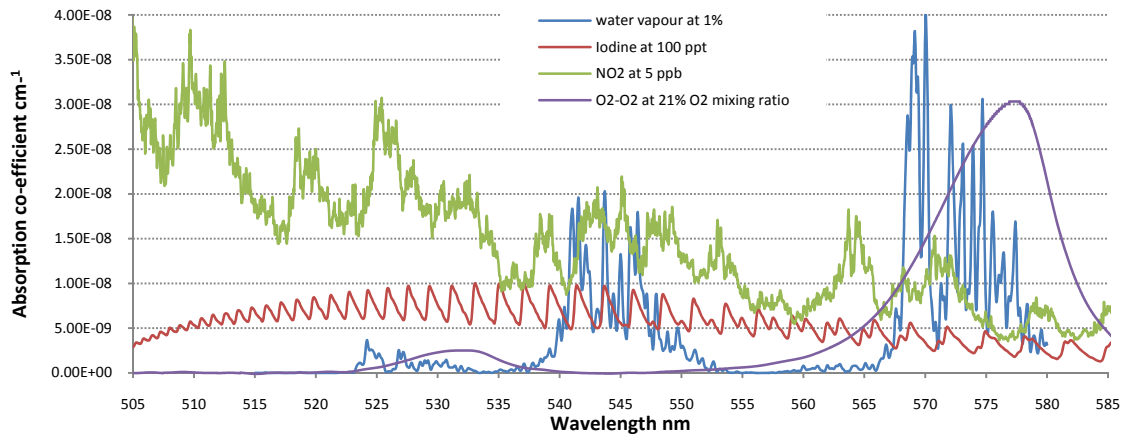


Figure 5.5. Differential spectral structure due to molecular absorbers at green wavelengths, shown at typical atmospheric mixing ratios for O₂-O₂ and H₂O and close to peak observed value of I₂ during measurements and NO₂ at 5 ppbv.

The absorption spectra shown in Figure 5.5 are calculated from the product of the molecules' absorption cross sections and an assumed mixing ratio typical for atmospheric conditions (O₂-O₂ for 21% mixing ratio of oxygen and 1% water vapour). The iodine absorption is shown for 100 pptv (close to the peak concentration of 93

pptv observed at Mace Head around low tide from previous work [Saiz-Lopez & Plane, GRL, 2004; Saiz-Lopez et al, ACP, 2006]) and for NO₂ at 5 ppbv (a value more typical of polluted regions and above what was monitored at Mace Head during the BIOFLUX II campaign, but is used in Figure 5.2 to produce an NO₂ absorbance that illustrates the spectral structure).

The BBCEAS cavity (sensor) was located on a purpose built gantry approximately 10 m in front of the shore-side cottage laboratory, towards the shore line as shown in figure 5.6. The LED light source, spectrometer and other electronics were housed in one of the shore-line cottage laboratories and linked to the cavity via fibre optics, protected from the elements inside plastic tubing.



Figure 5.6 BBCEAS instrument cavity mounted on gantry at Mace Head. Two BBCEAS cavity instruments set up in tandem: the Leicester I₂ detector and Cambridge IO detector. Pictures taken by the author from the tower between and above the shore side cottage laboratories at Mace Head.

5.5.1. Operating parameters BBCEAS during BIOFLUX II

The main hardware components of the BBCEAS I₂ instrument, summarised in table 5.4, were the same as the D319 ship cruise in Chapter 4. BBCEAS spectra of ambient air

were recorded using an HR4000 Ocean Optics USB miniature spectrometer. Two integration times for measurements were used during BIOFLUX II; for each integration time, individual spectra were acquired with the spectrometer manufacturer's Spectra Suite software and averaged for a total acquisition time of one minute before the files were saved to the computer for later off-line analysis. From 26th August to 7th September 2007, individual spectra were acquired with an integration time of 250 micro seconds and 240 individual spectra were averaged to produce a single spectrum with a net integration time of 1 min. From the 7th to the 12th September 2007, individual spectra were acquired with an integration time of 333 μ s and 180 individual spectra were averaged to produce single spectra with net integration time of 1 minute. These acquisitions and averaging was carried out using the ocean optics spectra suite software. The HR4000 spectrometer has 3648 pixels covering a fixed wavelength range of 504.8-581.9 nm. For the 1 minute averaged BBCEAS spectra; the light intensity throughput of the cavity, was recorded over all the pixels, covering the total wavelength span. Two example spectra are shown in figure 5.7. The blue trace shows the 1 minute averaged BBCEAS spectra for the cavity filled with nitrogen, whilst the red trace is the 1 minute averaged spectra for the cavity open to the atmosphere. The red trace of the atmospheric sample spectra lies below the blue trace of pure nitrogen spectra; this is due to additional extinction in the atmospheric sample. Not all the pixels of the detector carry useful information for calculating the BBCEAS absorption spectrum. Only a subsection of these wavelengths was taken and used in the analysis procedure for atmospheric absorbers illustrated by the two green lines in figure 5.7. At short wavelengths the light intensity throughput for the cavity is low, due to the LED emission. The inclusion of the low intensity, low wavelength section of the spectra in

the DOAS fitting process leads to increased noise in the spectra at the lower wavelengths. At longer wavelengths the light intensity is sufficient to saturate the detector, and thus is also excluded from use in the fitting procedure. The saturation wavelength depends upon the cavity extinction, as observed in figure 5.7 the red trace saturates at longer wavelengths than the background nitrogen measurement. This saturation wavelength can vary over the course of a measurement run. Thus the upper limit is chosen to prevent saturated wavelengths being included in the analysis, enabling data from extended operating times to be analysed in the same analysis programme run. For the measurements at Mace Head the subsection of data used in analysis was 535 nm to 561 nm.

The spectrometer was placed in a cooled enclosure. This served two purposes, firstly to reduce the dark current contribution to spectral noise and secondly to attempt to reduce the influence of room temperature variations on the BBCEAS spectra. The traces shown in figure 5.8 are the cavity throughput light intensities at different temperatures experienced during one extended run of the BBCEAS instrument. As the external temperature increases the level of noise on the trace also increases. Much of this noise can be removed from the analysis by subtracting the corresponding dark current at the same temperature as the data was recorded. This process uses the signal in the first few non-illuminated pixels of the detector as a metric for the detector's temperature, and is explained in more detail in chapter 3. This temperature correction is particularly important for the BIOFLUX II data set as the method of cooling the spectrometer was rudimentary, being built ad hoc whilst at the site. The method used ice blocks typically used to keep picnic boxes cooled which were replaced periodically throughout the measurements. Although a rudimentary method, it was

effective as figure 5.8 shows. The BBCEAS was normally operated with the red trace of figure 5.8.

BBCEAS setup during BIOFLUX II			
Light source	Green LED	LUXEON III (3 watt)	Temperature stabilised at 18° C
Cavity mirrors	101851	Layertech GMBH	25 mm diameter
Light input fibre	QP-400-2-uv/vis-BX	Ocean optics	400µm diameter, 0.22NA, 10m length
Cavity output fibre	QP-400-2-uv/vis-BX	Ocean Optics	400µm diameter, 0.22NA, 15m length
Cavity lengths	118cm (total length between the cavity mirrors)	87cm (cavity length exposed to atmosphere)	Length factor used in analysis = 1.35 (118cm/87cm= 1.35: the mirror mounts are flushed with non absorbing N ₂ to limit dirtying of mirror surface)
Spectrometer	HR4000	Ocean Optics	504.8-581.9nm, pixels, 50um slit

Table 5.4 BBCEAS instrument components and cavity parameters.

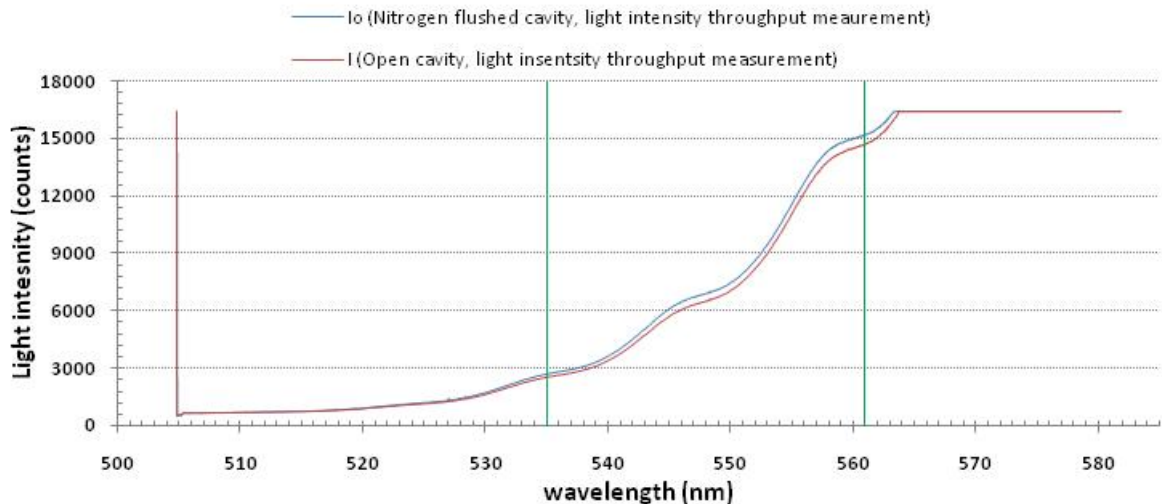


Figure 5.7 Light intensity throughput measured at Mace Head on 26th August 2007. Blue trace shows the nitrogen filled/ background cavity measurement (I_0) and the red trace shows an atmospheric sampled measurement (I). The green vertical lines show the subsection of data used in analysis for trace gas species presence and quantification.

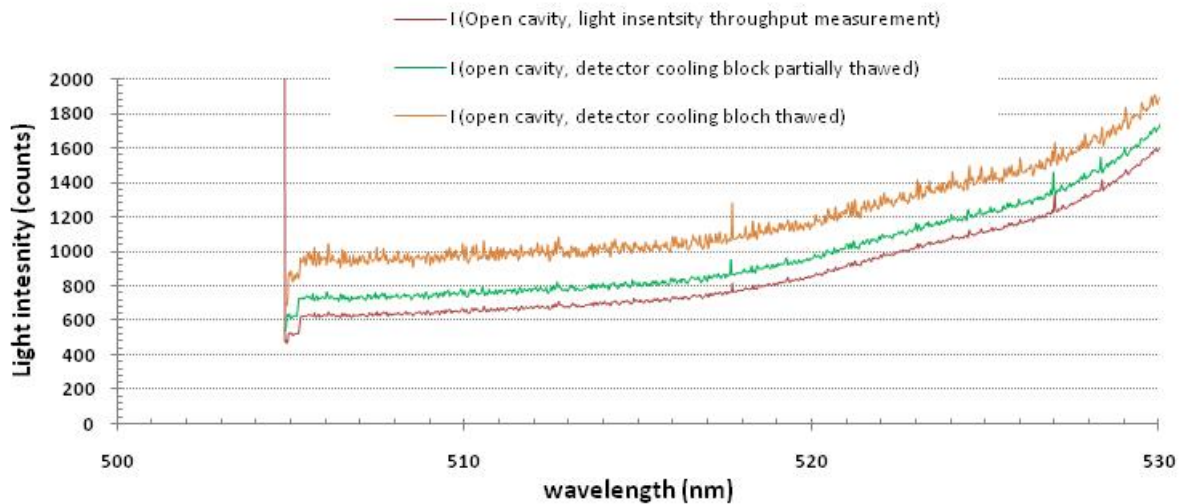


Figure 5.8 Light intensity throughput variation with temperature measured at Mace Head on 26th August 2007

The chart showing hours of operation (table 5.3) illustrates the data coverage achieved during BIOFLUX II. The BBCEAS instrument operated in a virtually continuously sampling mode of ambient air from 26th August to 12th September 2007 following the initial set up and testing. The short time periods missing at several times daily were due the necessary background measurements and mirror reflectivity determination using the O₂-O₂ absorption bands at 547 nm and 578 nm, required for quantitative analysis.

The more extended down times from measurements were due to weather conditions being unfavourable on several occasions during the measurement period. The BBCEAS measurement period covers a sufficiently long time to monitor emissions from seaweeds over the complete tidal cycle, covering two periods where the high/low tide difference is at or close to its maximum.

5.5.2. Acquisition of $I(\lambda)$ sample spectra and $I_0(\lambda)$ nitrogen flush spectra

The general principles of the BBCEAS technique and the fitting of the differential structure in BBCEAS spectra to retrieve quantitative absorber amounts was discussed in chapters 2 and 3. This section details how the BBCEAS instrument was operated during BIOFLUX II to make the required measurements of $I(\lambda)$ and $I_0(\lambda)$. The mirror reflectivity ($R(\lambda)$) measurement required to obtain concentrations of molecular absorbers is described in the next section. The BBCEAS measurements were recorded in a similar fashion to those made during the D319 RHaMBLe cruise campaign, using the Ocean Optics Spectra Suite software package in a semi automated mode.

The cavity mirror mounts used during BIOFLUX II introduce a flow of non absorbing gas across the mirror surface to minimise foreign particle deposits onto the mirror surface enabling longer operating times for the instrument before cleaning and alignment modification is required. During BIOFLUX II this mirror purge flow was set to 1.2 s.l.p.m (standard litres per minute) with N_2 . This leads to a length factor of 1.35 being included in the analysis to account for the sections of the cavity not containing atmospheric sample during the measurements. The length factor is determined from the geometric cavity length; the total cavity length is divided by the exposed cavity length: 118 cm / 87 cm.

The background measurements (I_0) during BIOFLUX II were made while the area between the cavity mirrors along the light path was enclosed but unsealed, using a section of rigid plastic tubing supported between the mirror mount enclosures. The enclosed cavity was then purged with nitrogen (flowed at 3 s.l.p.m) introduced to the centre of the enclosed cavity for several minutes to expel atmospheric air before data

was recorded. The light intensity within the nitrogen filled cavity over a user defined integration time was recorded and an operator specified number of files were saved. Throughout BIOFLUX II a minimum of 10 background or nitrogen flushed files were saved: each file saved was an average of scans to produce one data file per minute. An example of a file name for background measurements at Mace Head is 070828_n2flush_2210_00001.txt. The file names were part user defined, containing information on the date of measurement (070828), the type of measurement (n2flush), and time of start of the series of measurement (2210), whilst the file name endings were sequential numbers, automatically generated by the spectra suite software package.

The tube enclosing the cavity was removed for ambient atmospheric sampling ($I(\lambda)$), i.e. the cavity was operated “open path” with the ambient air flow passing freely between the cavity mirror mounts. The same operating parameters, (integration time for individual spectra, and number of scans to average to yield spectra with a net acquisition time = 1 minute) were used as for the acquisition for the background measurement (I_0). For all the sampling periods the light intensity measurement across the wavelengths of the detector was averaged to 1 minute before being saved as text files. The file naming was similar to that of the background data using “openpath” to define the type of measurement and including the date and start time.

5.5.3 In situ calibration of mirror reflectivity using O_4 absorption

Throughout BIOFLUX II mirror reflectivity determination measurements were recorded several times daily in order to ensure that any changes in the cavity mirror alignment,

and thus sensitivity of the instrument was recorded. This enabled accurate analysis of the data and any cleaning and re-alignment of the cavity to maintain a high sensitivity within the instrument.

The cavity mirrors (Layertech GMBH #101851, 25mm diameter) have undergone extensive measurements in the laboratory and the shape of mirror curve has been well defined prior to the BIOFLUX II campaign. During BIOFLUX II the absolute positioning of the mirror curve was determined by measuring the oxygen absorption bands periodically in a similar method to that used during D319. The calibration sample was introduced to the cavity in a similar manner to the background flushed measurements. The flush over the cavity mirror surface was stopped, thus filling the whole cavity region with oxygen, introduced to the centre of the enclosed cavity at a rate of 3 s.l.p.m, expelling atmospheric air and nitrogen. The measurement of light intensity within the cavity was made using the same parameters as the background (I_0) measurements, saving a minimum of 10 files, which are averaged to 1 minute and named in the same format as the background file names.

The averaged measurements of the oxygen purged cavity and the nitrogen purged cavity and the lab based reflectivity curve were used to calculate and the O_2-O_2 absorbance. This absorbance was then differentially fitted to the O_2-O_2 differential absorption cross section and the mirror curve positioned on the absolute scale such that the retrieved concentration of O_2-O_2 is 1 (unity). An example of the resulting BBCEAS fitted O_2-O_2 absorption spectrum is shown in figure 5.9. This spectrum is of better quality than that obtained during D319.

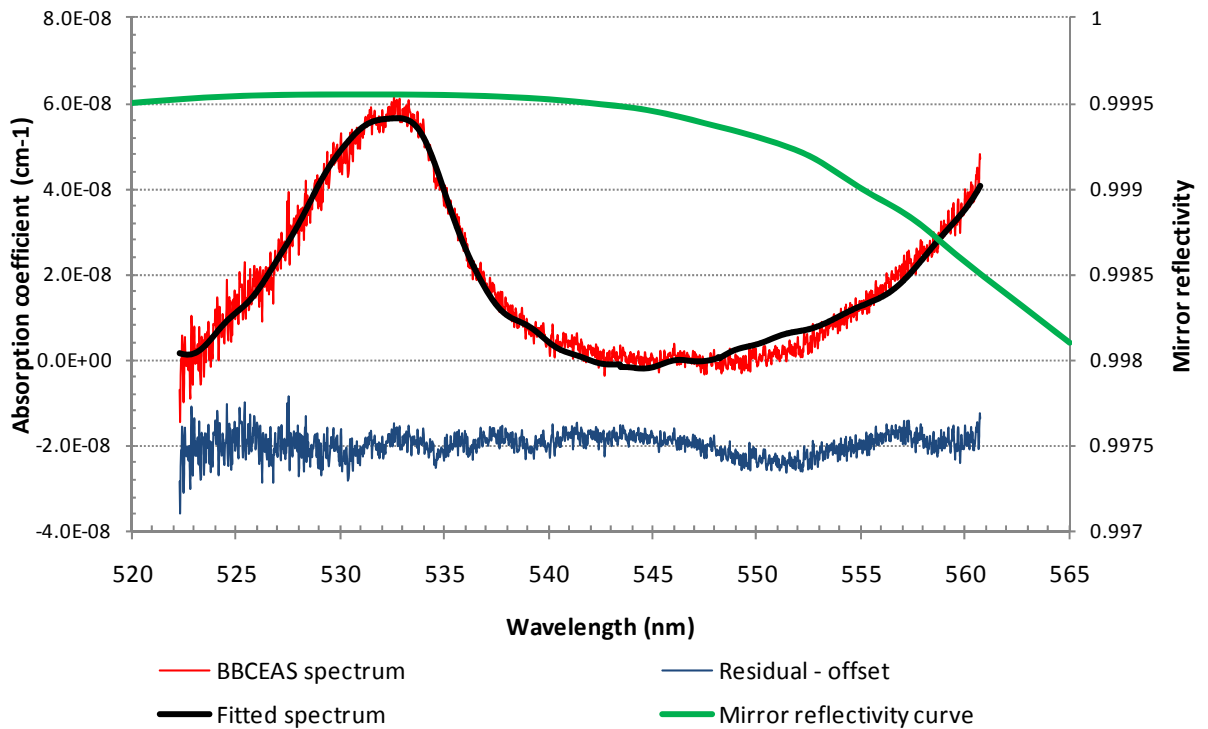


Figure 5.9 Calibration of cavity mirrors inferred by fitting the O₂-O₂ absorption bands to the Hermans [Hermans, 2008] absorption cross sections to measurements made on 26th August 2007. The fitted amount of oxygen is 1.00+/- 0.0038 and the standard deviation of the residual spectrum is 2.72X10⁻⁹. The residual spectrum is shown with an offset of 2x10⁻⁸cm⁻¹.

5.5.4. Mathcad analysis routine details

The “in house” written analysis routine in Mathcad software package imports spectra recorded using the Spectra suite acquisition software (background, sample and calibration measurements for the day) along with literature absorption cross section files for the target absorber species. The cross sections used to analyse the BIOFLUX II measurements are listed in Table 5.5 (these cross sections were also used to generate the molecular absorption spectra shown previously in Figure 5.5).

The programme takes subsections of the BBCEAS data according to the wavelengths defined by the operator. For this campaign the data between 535 and 561 nm was selected. Cavity parameters are defined by the operator for the specific set up at Mace Head Atmospheric Research Station. A length factor of 1.35 was used throughout the campaign.

Absorber species	Authors and treatment of data before use in BBCEAS analysis.	Level of uncertainty
Water vapour	HITRAN 2004 spectral database, degraded to the spectrometer resolution 0.12nm	2 %
Molecular iodine, I ₂	Calculated using PGOPHER spectral simulation package and scaling methods by S Ball [Ball et al., 2010] using Saiz Lopez [Saiz-lopez et al., 2004]	Estimated uncertainty 15%
NO ₂	Vandaele [Vandaele et al., 1998] (MEASUREMENTS OF THE NO ₂ ABSORPTION CROSS-SECTION FROM 42 000 cm ⁻¹ TO 10 000 cm ⁻¹ (238-1000 nm) AT 220 K AND 294 K)	Less than 3% for λ > 250nm
O ₂ -O ₂	Hermans 2008 [Hermans, 2008]	No information provided by author. By comparison to Greenblatt et al 1990 estimate uncertainty of 5% [Ball et al., 2010]

Table 5.5. Absorption cross section source and treatment used in BBCEAS data analysis routine.

The mirror reflectivity for the particular day is determined prior to and immediately following a set of ambient air samples using pure oxygen BBCEAS measurements. The oxygen and nitrogen flush files are used to calculate the BBCEAS spectrum of pure oxygen in an analogous way to sample spectra. The differential fit of O₂-O₂ absorption cross sections to the BBCEAS spectra yields the O₂-O₂ amount for an assumed mirror curve. The assumed mirror curve is shifted, to make the mirrors more or less reflective, until the O₂-O₂ band intensity matched that of pure oxygen. This produced mirror

curves to be used in the analysis of the atmospherically sampled data and enabled any changes in the BBCEAS instrument performance to be monitored.

The next stage of the analysis routine uses the background measurement, $I_0(\lambda)$, and the atmospheric sampled measurements, $I(\lambda)$, to calculate the sample absorbance. The operator could average the 1 minute averaged BBCEAS spectra to any multiple before DOAS fitting. For the analysis of this BBCEAS data, typically 10 files were averaged for analysis giving a 10 minute time resolution.

The sample absorbance is then analysed for the presence of absorbing trace gas species by the differential fitting for each absorbing molecule in sequence. Ambient water vapour is the dominant absorber in the Mace Head BBCEAS spectra, being present at mixing ratios between 1 and 2% in every spectrum. Therefore its absorption structure was fitted first, and, once quantified by the DOAS fit, was subtracted from the absorbance spectrum. The residual spectrum (absorption spectrum minus fitted water spectrum) was then fitted for either molecular iodine or NO_2 in two separate but parallel DOAS fits.

As an extra quality assurance check, the Mathcad analysis routine plots and performs DOAS fits on sequences of individual oxygen calibration BBCEAS spectra (calculated from a single oxygen spectrum and the average $I_0(\lambda)$ N_2 flush spectrum) and individual flush-versus-flush BBCEAS spectra (calculated from a single $I_0(\lambda)$ spectrum and the average $I_0(\lambda)$ N_2 flush spectrum). The operator can then inspect these spectra for consistency. In particular, checks are made for the presence of water vapour absorption features and/or a significant continuum absorbance that might indicate the presence of residual ambient air in the first few spectra in any calibration sequence

caused by yet incomplete purging of the cavity tube by the calibrant gas. Any compromised spectra can thus be excluded from further analysis.

5.5.5. Errors in retrieved concentrations for absorber species

Each of the retrieved concentrations from the BBCEAS analysis routine has an associated error, which is shown by the error bars in the time series. This total error is a combination of statistical and systematic errors. The statistical error is the error in retrieving the absorber concentration from the differential structure in the BBCEAS spectrum. It is the uncertainty in the gradient of a plot of differential absorption coefficient (from the BBCEAS measurements) versus the differential absorption cross section.

The systematic error is also a combination of errors. The systematic error is associated with the uncertainties and errors in the literature absorption cross sections used in the fitting procedure, and the uncertainty in the cavity enhancement factor. The uncertainty in the cavity enhancement factor is the result of the mirror reflectivity determination using the O₂-O₂ absorption cross sections. This sets the level of uncertainty due to the cavity enhancement factor to 5%.

The statistical and systematic error can be combined and give the approximate error for the retrieval of molecular iodine, the main target of BBCEAS measurements during BIOFLUX II. The total error is defined using equation 5.1

$$total\ error = \sqrt{statistical\ error^2 + systematic\ errors^2} \quad \text{equation 5.1}$$

The errors which are combined to determine the total error for the measurements are explained for the retrieval of iodine. The values for each component of error for the retrieval are shown in table 5.6. When measuring concentrations close to the detection limit the statistical error dominates, i.e. the absence of iodine is measured as 0+/- 10 pptv, while the systematic errors begin to dominate the overall error as the observed concentration increases. If, for example, the BBCEAS measurements retrieves 100 pptv then the total error becomes the square root of the statistical error squared plus (18% of 100pptv)². Thus larger errors are observed for the high iodine points observed throughout BIOFLUX II.

Statistical errors		Systematic errors	
Uncertainty in retrieving I ₂ signal from DOAS fitting of BBCEAS differential spectra structure	Approx 10 pptv during BIOFLUX II.	I ₂ absorption cross section	13%
		Cavity enhancement (mirror reflectivity from O4 spectra)	5%
		Length factor: assume geometric length factor measured to nearest mm.	Assumed negligible
		TOTAL	18%

Table 5.6 The statistical and systematic contribution to total error for iodine.

5.6. Spectral analysis: water vapour retrievals and time series

The BBCEAS data recorded during the BIOFLUX II campaign were analysed using home written analysis routines created in the MathCAD programme (described in chapters 3, and above in section 5.5.3). The MathCAD analysis routine calculated a BBCEAS spectrum of the ambient air samples for each cavity transmission spectrum recorded by the Ocean Optics HR4000 spectrometer/Spectra suite software (1 minute acquisition time). Ten sequential spectra were then averaged prior to DOAS fitting to retrieve the structured absorbers' concentrations. This 10 minute time resolution was a compromise between wishing to produce high resolution time series that could capture fast changes in the I₂ emissions reaching the site and the need to keep tractable the analysis of the large BIOFLUX dataset (data processing times; output file sizes etc). The complete data set of BBCEAS measurements during BIOFLUX II averaged to a 10 minute resolution was comfortably sufficient to check the quality of data, provide an overview of the whole campaign and to identify particularly "interesting" periods for re-analysis at high time resolution.

The MathCAD/DOAS analysis routine used in this thesis fits the various structured contributions to BBCEAS spectra sequentially, starting with largest absorber. At Mace Head, a coastal measurement site, water vapour was the largest contributor to the BBCEAS spectra and thus was the first atmospheric absorber to be fitted in the MathCAD analysis routine. The absorption bands of water vapour shown in figure 5.5 (an assumed 1% water mixing ratio typical of a coastal site) are larger than the overlapping with iodine bands for [I₂] = 100 pptv (comparable with the maximum iodine amounts detected at Mace Head in previous work [Saiz-lopez *et al.*, 2006]. In

order to observe and quantify iodine (or other trace gas species) the water vapour absorption signal needs to be accurately quantified and subtracted from the BBCEAS spectra. In the data from the BIOFLUX II campaign, water vapour structure was present in every calculated absorbance and the structured H₂O absorption bands can be seen by eye in many of the spectra prior to differential fitting. Subsequent work in the research group has refined the analysis routine to use singular value decomposition (SVD) to fit BBCEAS spectra simultaneously for the absorption cross sections of multiple absorbers, thereby relieving the operator of the need to make judgement calls about the order for fitting the molecular absorbers. Tests performed fitting representative BBCEAS spectra at blue wavelengths show that the absorber amounts retrieved using the present sequential method are the same within measurement error as for the more sophisticated SVD analysis provided that (i) one makes reasonable choices about the order for fitting the various absorbers and (ii) the cross sections of the different absorbers are not strongly correlated (Fig 5.5 above shows that the molecular absorbers have very distinct absorption signals at the present green wavelengths). Although more cumbersome, the sequential spectral fitting is more than sufficient for analysing the field work data presented in this thesis.

Fitting water vapour absorption bands also acts as an internal quality assurance that the BBCEAS analysis routine is performing well. This is gauged in two ways. Firstly the detailed shape of the water absorption band in the BBCEAS spectra is compared to that of water's absorption cross sections to verify that the shape of the cavity mirrors' reflectivity vs. wavelength curve $R(\lambda)$ used to calculate the sample's absorption coefficient is correct. An example of a fitted water vapour spectrum is given in figure 5.10 which shows an excellent correspondence between the water vapour band's structure

present in the fitted cross sections and in the measurement, thus confirming the appropriate mirror curve was determined from the “calibration” measurements. Secondly if the absolute water vapour concentrations retrieved by BBCEAS measurements agree with meteorological data, one can have confidence that the scaling applied to the mirror reflectivity curve to retrieve the correct O_4 absorption signal in oxygen calibration spectra also holds throughout the run of ambient air measurements. This likewise verifies that the appropriate length factor has been applied to account for the ambient sample being excluded from the nitrogen-purged cavity mirror mounts. Retrieval of the “correct” water vapour concentration from fitting the BBCEAS spectra also gives confidence for the quantitative retrieval of other absorber concentrations from their signals in the BBCEAS spectra. This is because (i) multiple contributions to the measured absorbance add linearly in proportion to their concentration \times cross section [Beer-Lambert law] and (ii) all contributions thus scale in the same way with mirror reflectivity and length factor.

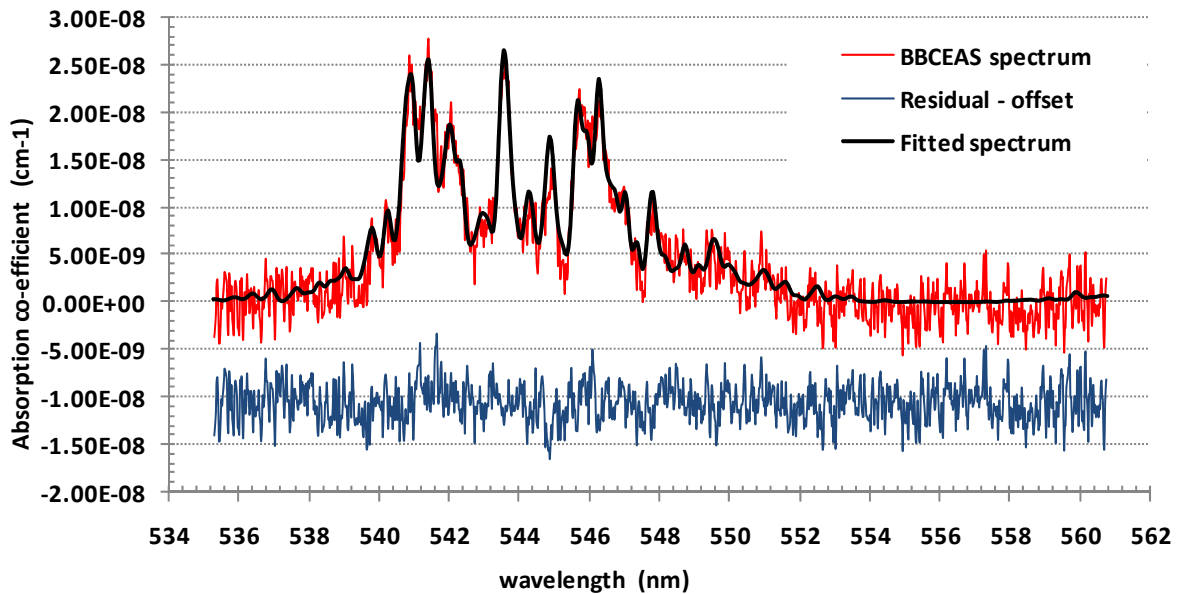


Figure 5.10. The fitted amount of water vapour is 0.0126 ± 0.0002226 and the standard deviation of the residual spectrum is 1.995×10^{-9} . The residual spectrum is shown with an offset of 1×10^{-8} in order to see more clearly any structure remaining in the residual spectrum. The spectrum was recorded on 26th August 2007.

The BBCEAS derived water vapour concentrations measured during BIOFLUX II were generally found to be in good agreement with water vapour concentrations calculated from meteorological measurements of relative humidity. The two data sets are shown in figure 5.11 for the whole campaign, and in figure 5.12 for one particular day (J241 = 28th August 2007). The trend in figure 5.12 is typical of the BIOFLUX data: there is a very close agreement between the two water vapour measurements at the start of a measurement run, i.e. closest to when the nitrogen flush $I_0(\lambda)$ background spectra were obtained and when the O_4 mirror reflectivity calibration was performed. The agreement becomes slightly worse further into the time series (as also evidenced by the larger error bars on the later BBCEAS water data points), but the two measures of

[H₂O] still agree to within about 5%. Possible explanations for the gradual loss of agreement are that the cavity has become partly misaligned and/or the mirror reflectivity has been affected by deposition of aerosol particles, the HR4000 spectrometer's cooled enclosure had warmed up, or the LED emission spectrum has changed slightly. Thus the data acquisition was stopped, the cavity mirrors were cleaned and the cavity was realigned, the cooling block inside the spectrometer's enclosure was replaced, and a sequence of new $I_0(\lambda)$ background spectra were recorded. Periods of significant, prolonged disagreement between BBCEAS H₂O and the meteorological data coincide with poor weather, e.g. rain or sea mists which prevented the BBCEAS instrument from operating effectively: data where the two water measurements disagreed by more than 10% or more were discarded. There are also highly select occasions when other molecules (with structured absorption cross sections in this wavelength window) are present at elevated levels in the BBCEAS spectra, and hence the assumption that water vapour's absorption should be fitted first is compromised. The most notable example is the exceptionally high I₂ concentrations observed during the night-time low tide of J242-243, 30th August 2007, which cause the H₂O retrieved from the BBCEAS spectra to depart from the meteorological measurement around J243.0 (figure 5.11).

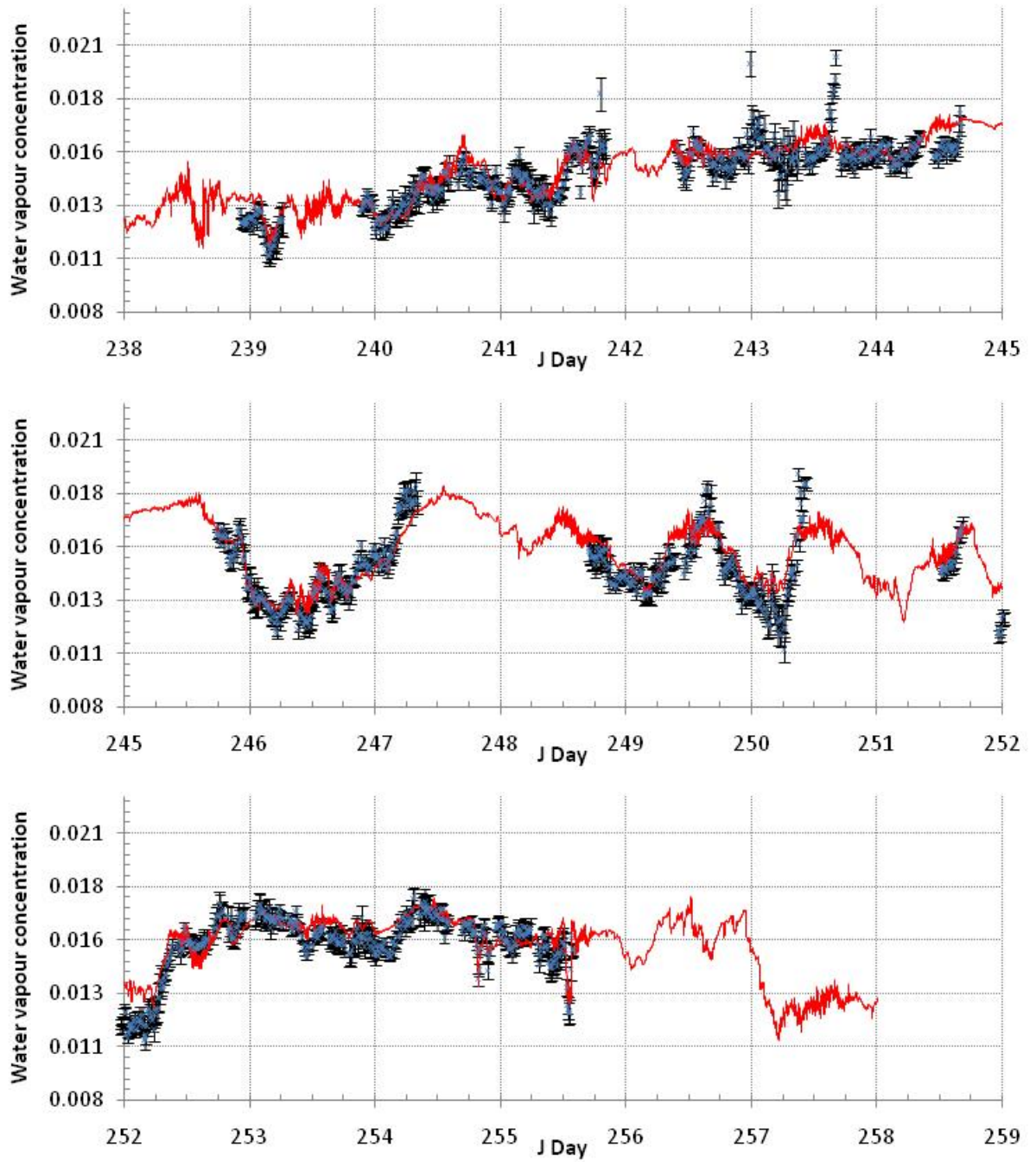


Figure 5.11. BIOFLUX II BBCEAS derived water vapour concentration, averaged to 10 minutes (blue), shown with concentrations determined from relative humidity measurement (red).

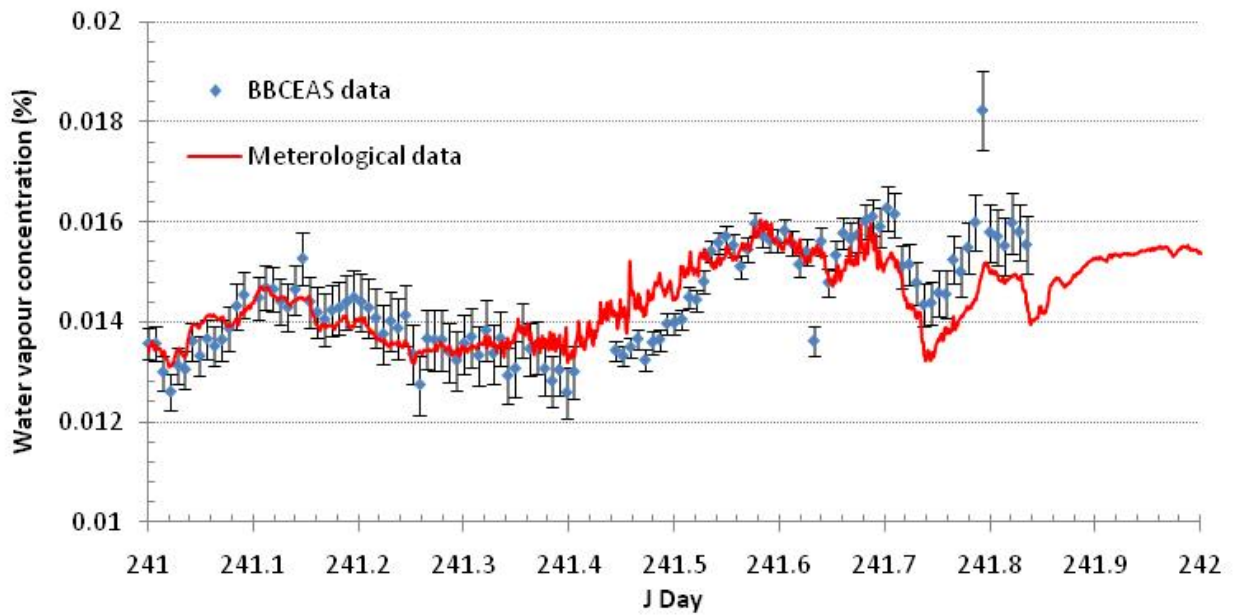


Figure 5.12 One day section of time series shown in figure 5.6.

5.7. Spectral analysis: Molecular Iodine retrievals and time series.

The absorption coefficient of the fitted water signal, $\sigma(\text{H}_2\text{O}) \times [\text{H}_2\text{O}]$, was subtracted from the BBCEAS spectra and the remaining spectrum was analysed for the spectral signature of molecular iodine. The molecular iodine absorption bands between 505-585 nm are shown above in figure 5.5. As stated above, the BBCEAS data for the whole measurement period was analysed by averaging files to 10 minutes enabling any periods of elevated iodine to be observed in the first instance before higher time resolution analysis of 2 minutes was used to look more closely at specific periods during the campaign (see later section 5.7.4).

5.7.1 BBCEAS derived iodine concentrations: 10 minute time series

The full BBCEAS derived time series of I_2 for the BIOFLUX II campaign analysed on 10 minute resolution is shown in figure 5.13. Each period where iodine concentration is elevated occurs during the night (in darkness), with the peak iodine concentrations coinciding with the lowest tides during BIOFLUX II. The first I_2 seems to appear consistently when the tide gets down to 0.6-0.4 m, iodine was not observed on nights when the tide height did not reach these low levels. Iodine was not unambiguously detected during the daytime BBCEAS measurements; iodine presence and JI_2 are in antiphase.

Obvious spectral signature (50 pptv and above) of iodine were observed in the 10 minute averaged data analysis on the nights of the 27th, 28th, 30th and 31st August and the 2nd and 11th September 2007 (J days 240, 241, 243, 244, 245 and 255) for extended periods of 10's of minutes to over an hour. While observations on the nights of the 8th and 9th September 2007 (J days 252 and 253) show less pronounced peak iodine concentrations of 20 ppt and 30 ppt. Details of the iodine concentrations are contained in Table 5.6: the time of the first iodine presence and peak iodine concentration, along with the tide height for each [I_2] are listed.

Spectra for one high concentration and one low concentration of observed iodine from the 10 minute analyses are shown in Figures 5.14 and 5.15: both fitted BBCEAS spectra show the clear structure of the iodine absorption bands. The first spectrum in figure 5.14 shows the highest iodine concentration observed during BIOFLUX II in the 10 minute analysis where the retrieved iodine mixing ratio is 280 ppt.

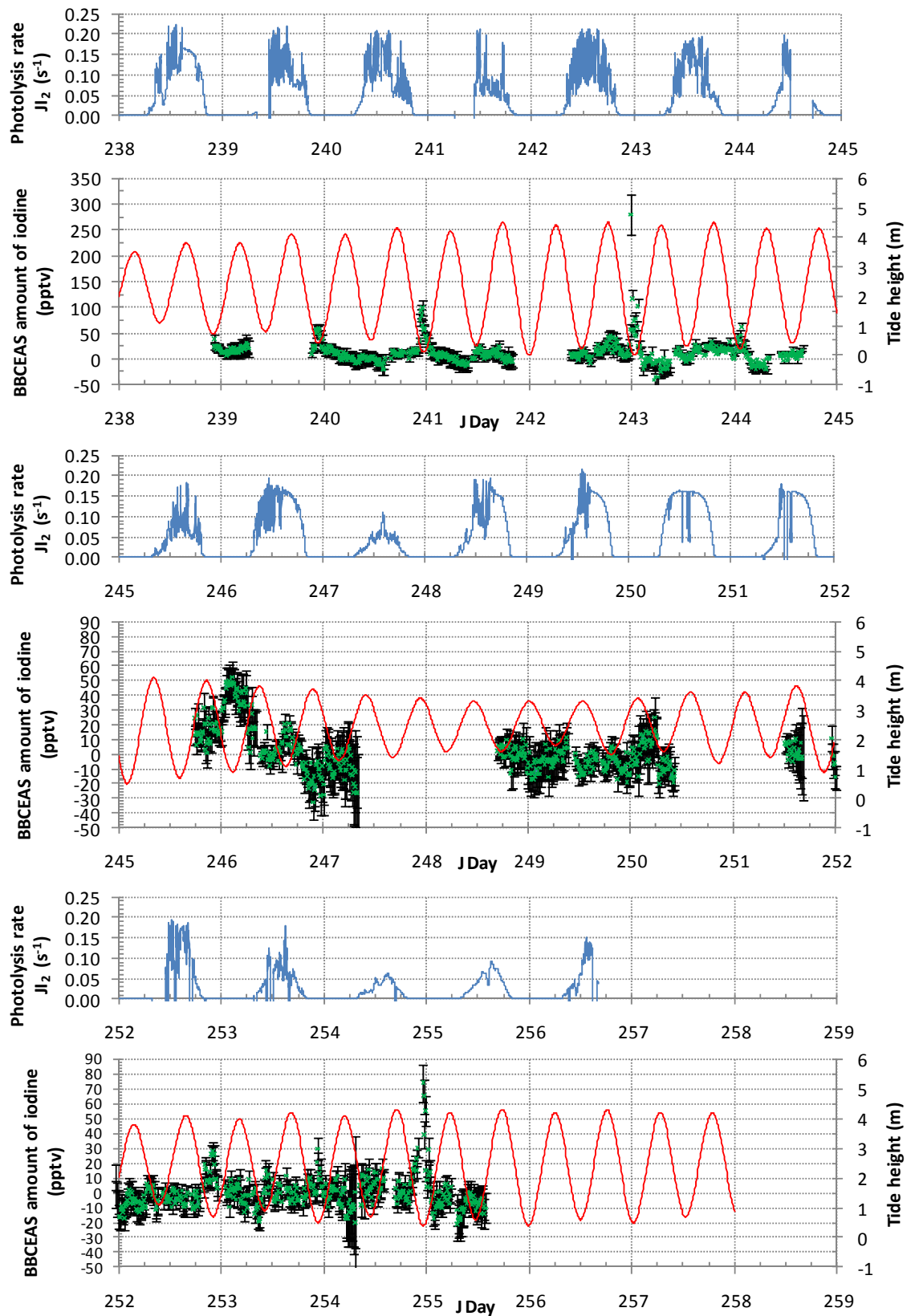


Figure 5.13. BBCEAS determined Iodine concentration (green points) and tide height (red trace) with photolysis rate for iodine (J_{I_2}) (top panels, blue trace).

Night (J Day)	Maximum iodine concentration / pptv			First iodine concentration / pptv		
	Time (hh:mm)	Peak[I ₂]	Tide Height (m)	Time (hh:mm)	First [I ₂]	Tide Height (m)
239-240	22:33	59.3	0.4	21:59	24	0.53
240-241	22:59	98.8	0.14	21:50	19.3	0.61
242-243	23:39	280	0.28	23:29	28.68	0.38
243-244	01:36	61.1	0.21	02:11	22.83	0.46
245-246	02:34	52.2	0.91	00:14	29.3	1.9
252-253	22:04	28.1	0.71	20:03	19	1.54
253-254	22:33	29.6	0.49	22:23	20.7	0.52
254-255	23:09	74.1	0.4	21:07	19.8	1.27

Table 5.7. Nightly iodine concentration from 10 minute analysis, with corresponding tide height. The maximum for night shown on left hand side and the first detectable iodine shown on the left hand side.

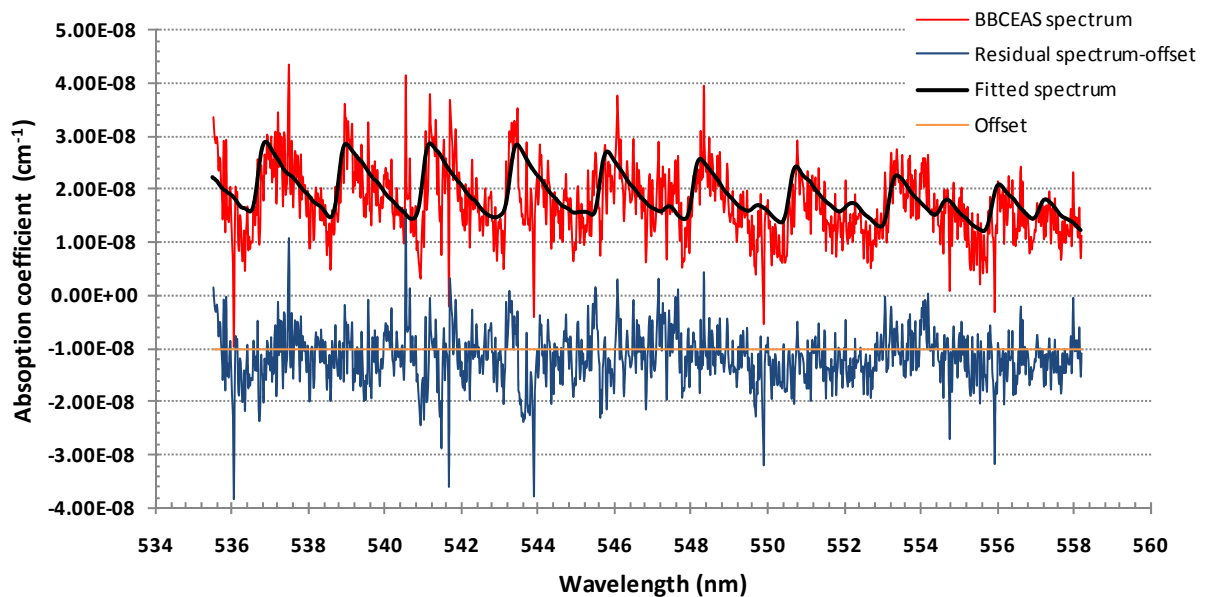


Figure 5.14 The fitted amount of iodine is 280.6 ± 11.3 pptv and the standard deviation of the residual spectrum is $5.17 \times 10^{-9} \text{ cm}^{-1}$. The residual spectrum is shown with an offset of $1 \times 10^{-8} \text{ cm}^{-1}$ in order to see more clearly any structure remaining in the residual spectrum. The spectrum was recorded on 30th August 2007 between 23:34 to 23:44hrs.

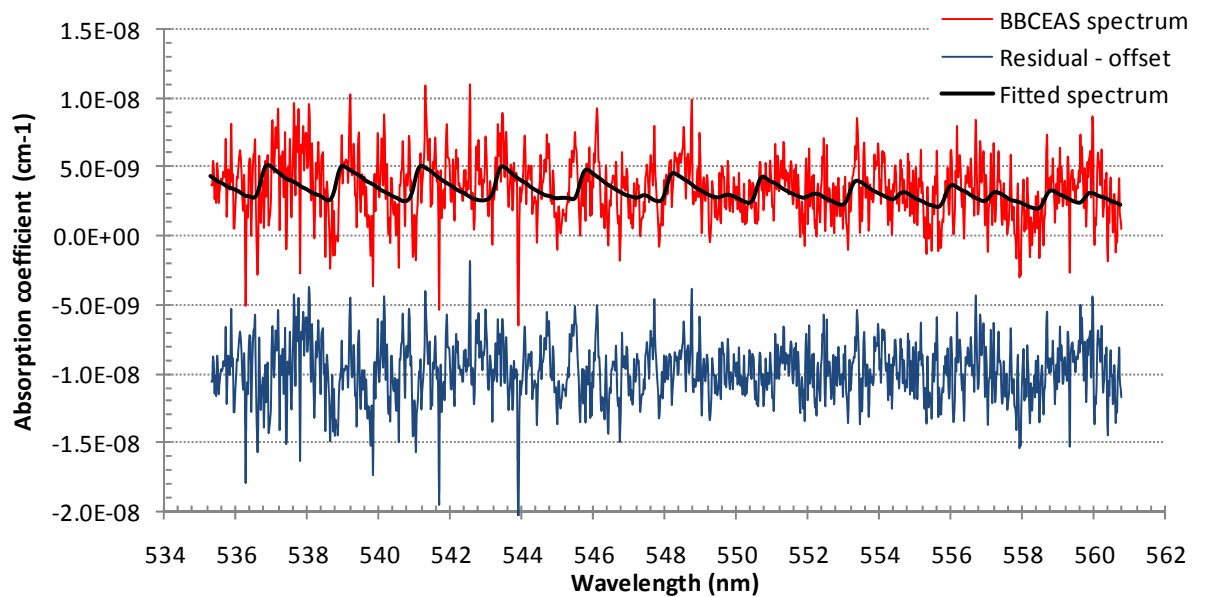


Figure 5.15 The fitted amount of iodine is 50ppt +/- 4.86 ppt and the standard deviation of the residual spectrum is 2.11×10^{-9} . The residual spectrum is shown with an offset of 1×10^{-8} in order to see more clearly any structure remaining in the residual spectrum. The spectrum was recorded on 27th August 2007 between at 21:08 to 22:08hrs.

5.7.2 Iodine correlation with tide, wind directions and reasons for observed patterns

The occasions when iodine is detected by BBCEAS in the 10 minute analysis are shown in greater detail in figure 5.16, alongside the tide height and wind direction. Correlation plots between BBCEAS iodine concentrations and tide height, wind direction and time of day are shown in figure 5.17. Interpreting the BBCEAS data alongside tide heights and wind direction provides a method to accurately locate the iodine source. The strongest iodine signals (in the 10 minute averaged data) were observed on 28th August, 30th August and 11th September 2007 peaking at 99, 280 and 74 ppt, respectively. These BBCEAS measurements yielding higher I₂ concentrations were recorded during the night of and nights either side of the spring tides of the 30th-31st August 2007, when the inter tidal region exposed is at its monthly maximum.

The dependence of iodine concentration peaks occurring alongside tidal height minimum in the monthly tidal cycle strongly suggests the likely source of iodine at Mace Head to be seaweeds plants growing in abundance in the deeper coastal waters around Mace Head: those growing in the shallower waters are not known iodine emitting seaweeds [Ball *et al.*, 2010]. Seaweeds tend to grow in species bands following the bathymetry (water depth), and thus the tide needs to fall below a particular level, for iodine emission to be triggered. This indicates the source of iodine is deeper water seaweed species exposed or more exposed when tide height is lowest. The correlation plot shown in figure 5.17 and the top panel corroborates this; iodine mixing ratios above 40 pptv are observed only when the tide height is below 0.5 m. As the tide height becomes lower than 0.5 m the laminarias are exposed to the atmosphere and respond to this exposure by emitting iodine. This is observed as a sharp increase in iodine concentration in the time series followed by the iodine concentration gradually decreasing over time, until the tide height rises to over 0.5 m, submerging the seaweed, ceasing emission of iodine to the atmosphere.

The local region to the north west of the BBCEAS instrument has a deep channel, shown in figure 5.2, which has a large population of laminaria species, known iodine emitters, which are only exposed to the atmosphere during the lowest tides in the monthly cycle. The exposure of larger volumes of the iodine emitting seaweeds during the lowest low tides results in the higher concentrations of iodine being observed during and close to the spring tides.

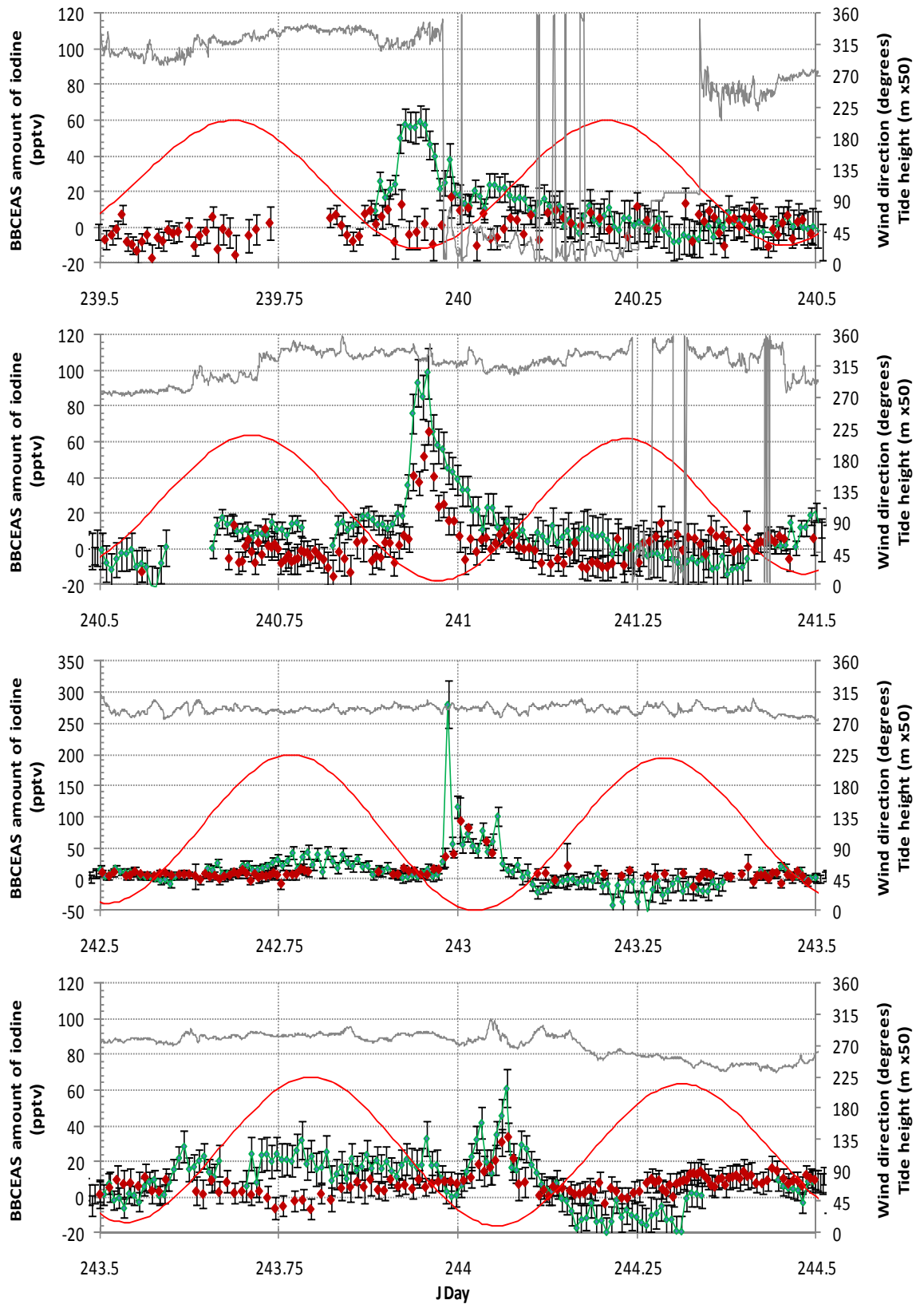


Figure 5.16. continues

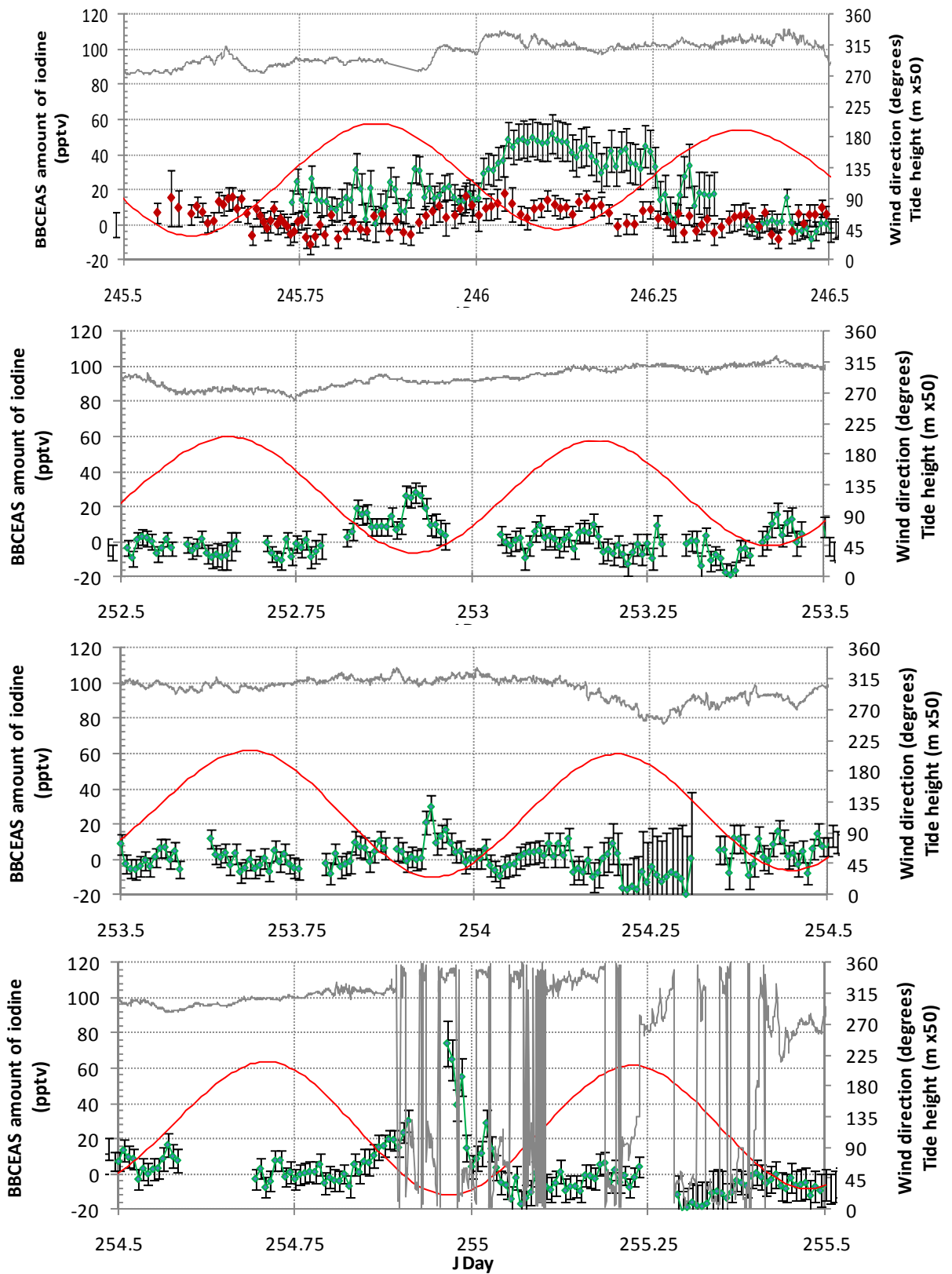


Figure 5.16. Time series showing the BBCEAS retrieved iodine concentrations peaks observed during BIOFLUX II. BBCEAS I₂ shown in green, tidal height shown in red and wind direction shown in grey. Data from a concurrently operated LP DOAS at Mace Head from K Seitz is shown as red diamonds in the first 4 panels.

This is supported by examining the wind direction during episodes of elevated iodine concentrations. Typically the wind direction was generally westerly to north westerly, originating from the clean air sector. During the time periods when iodine was observed the wind direction was between 270 and 360 degrees (see figure 5.17, middle panel), and thus air reaching the instrument had travelled over seaweed beds densely populated with laminarias.

These field observations correlate well with laboratory studies using this BBCEAS instrument in a similar setup to monitor iodine emission from different seaweed species [Ball *et al.*, 2010]. The kelps (*Laminaria*) were shown to be the biggest iodine emitting seaweeds of those under investigation, with emission peak values between 14,300 and 86,900 pptv shortly after exposure to the atmosphere [Ball *et al.*, 2010]. These high mixing ratios compared to atmospheric measurements during BIOFLUX II are likely due to the detector being in very close proximity to the seaweed sample during laboratory study. The emission pattern observed here in the BBCEAS data is similar to that observed by Ball [Ball *et al.*, 2010]. An initial peak iodine concentration was followed by a period of decay over an extended time, and on occasion a second emission peak, due to changes in wind direction bringing plumes from neighbouring seaweed beds and/or the tide uncovering new beds that start emissions later than the first uncovered beds.

During night time BBCEAS measurements where no iodine peak is observed, on the 3rd, 5th, 6th and 8th September 2007 (J days 246, 249, 250 and 252), the tidal difference was at its smallest, not reaching lower than 0.5 m. This reinforces identification of the

iodine source being the seaweeds growing in the deeper waters, which are only exposed to the atmosphere when the tide height was below 0.5 m.

During the daytime BBCEAS measurements, molecular iodine was not unambiguously observed. This day time absence and night time presence of iodine during low tides can be explained by a combination of the high photolysis rate of iodine (I_2) of 0.16 s^{-1} on a clear day during BIOFLUX II and the separation of the location of the iodine source and the detector. The sources of iodine at Mace Head were located 100 m downwind from the BBCEAS instrument location, which is sufficiently long that photolysis converts iodine into other RHS faster than iodine is transported to the instrument for detection.

Leigh modelled the transport of I_2 from seaweed beds to a measurement site at Roscoff [Leigh *et al.*, 2009] for the RHaMBLe Roscoff measurement campaign. This was attempted to explain measurements of I_2 by BBCRDS, particularly the day time measurement of 50 pptv I_2 on 15th September 2006 at Roscoff [Leigh *et al.*, 2009] [Mcfiggans *et al.*, 2010]. The modelling showed that I_2 could be transported over the distance between proposed sources to the measurement site, if the photochemical destruction processes of I_2 were excluded from the calculations [Leigh *et al.*, 2009]. This exclusion is not physically reasonable, and Leigh *et al.* suggest the need to explore alternative explanations, such as localised emissions and or the chemical recycling of I_2 . One explanation for this daytime iodine observation suggests that under semi polluted conditions, when NO_x is approx 2 ppbv (levels similar to those observed at Roscoff during RHaMBLe) iodine atoms converted to IO and react with NO_2 forming $IONO_2$. The iodine reservoir species $IONO_2$ can react with I to re-release I_2 and NO_3

[Mcfiggans *et al.*, 2010] [Mahajan *et al.*, 2009]. This pathway to explain daytime iodine observations at Roscoff also supports the absence of daytime iodine during BIOFLUX II. The NO_x levels during BIOFLUX II were not sufficient to enable the conversion to the reservoir species IONO₂ for transport and recycling processes.

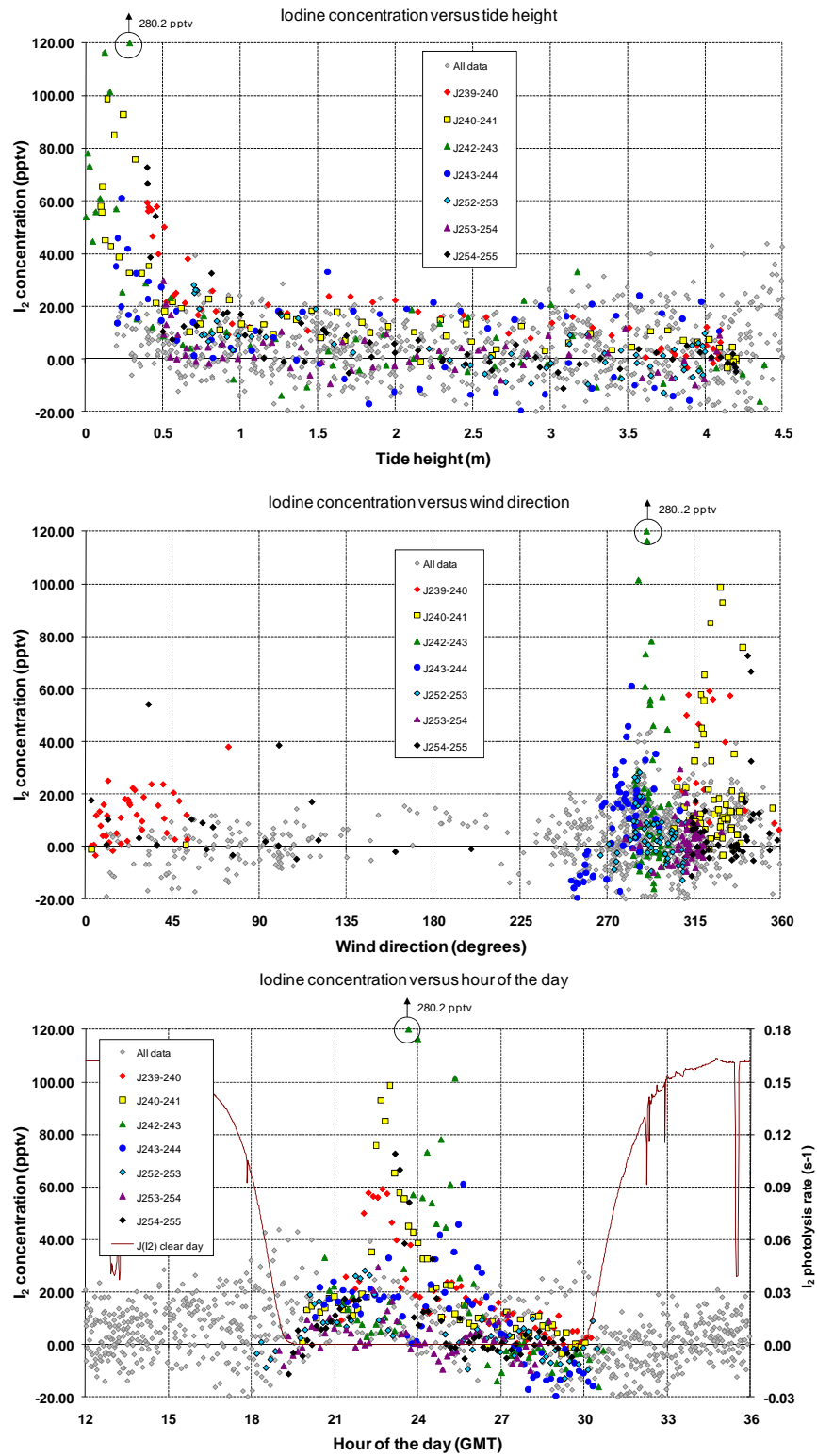


Figure 5.17 Correlation of BBCEAS determined I₂ concentration with tide height (top panel), wind direction (middle panel) and hour of the day (bottom panel).

Comparison of BBCEAS I_2 with IO measurements from a LIF (Laser Induced Fluorescence) instrument (University of Leeds, operated by R Commane) illustrates the anti correlation between I_2 and IO concentrations observed at Mace Head. The IO data from the days where both BBCEAS and LIF operated concurrently during BIOFLUX II is shown in figure 5.18. The IO mixing ratio increases rapidly following the daytime low tide while no IO is observed during or shortly after the night time low tides. This is an expected observation as IO is produced photo chemically during the day via the photolysis of molecular iodine to iodine atoms which react to forming IO. IO can also be formed from I_2 and NO_3 under high NO_x conditions via photolysis and the IO + NO_2 cycle [Mahajan *et al.*, 2009]; however the NO_x levels at Mace head were not sufficiently high for this route to be viable.

The trends in IO concentration elevation observed by LIF supports the absence of identifiable I_2 during the day time low tides in the BBCEAS data recorded close to the spring tides. Photochemical reactions convert molecular iodine into iodine atoms, which react with ozone forming the reactive species IO, IO has roles in particle formation (see chapter 1 section 1.5).

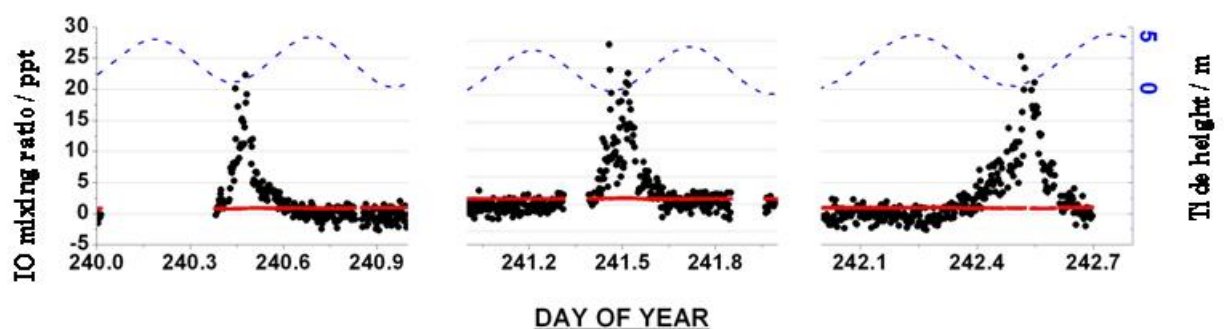


Figure 5.18 LIF IO data, plot from R Commane

5.7.3 Comparison of 10 minute BBCEAS analysis to Long Path DOAS data set

The DOAS instrument operated from the 26th August 2007 through to the 9th September 2007, recording iodine signals on three nights, 28th, 30th and 31st August 2007 (J day 240, 242 and 243). The DOAS instrument does not report data for the night of the 29th August 2007 (J day 241), most likely due to weather conditions which also prevented BBCEAS measurements. The I₂ concentrations from both instruments over these nights are shown in figure 5.16. The iodine peak concentrations observed in both the BBCEAS and DOAS data set show a strong time correlation but the maximum peak values obtained differ. The DOAS data always reporting concentrations lower than BBCEAS by up to an order of magnitude.

The correlation between the BBCEAS and DOAS data for the whole time both measurements were operating and the nights of 27th, 28th, 30th and 31st August 2007 was carried out using only positive data and the resulting plots are shown in figure 5.20. For the total data set a correlation coefficient of 0.32 and an offset of 5.3 pptv is observed, the BBCEAS data retrieving higher concentrations. Analysing the correlation of the individual nights where both BBCEAS and DOAS observed iodine peaks shows the BBCEAS retrieves higher I₂ concentrations (positive offset values) with correlation coefficients ranging between 0.08 and 0.67 as shown in table 5.7.

The wind direction when the data sets show stronger correlations on the 28th and 30th August 2007 originates from the west (270°). The less well correlated data on the night of 27th August 2007 occur with wind direction originating from more northerly directions, and can be seen in figure 5.16.

Date	Coefficient	Offset (pptv)
26 th August-9 th September 2007 (238-255)	0.32	5.3
27 th August 2007 (239.5-240.5)	0.08	5.66
28 th August 2007 (240.5-241.5)	0.83	7.61
30 th August 2007 (242.5-243.5)	0.29	6.31
31 st August 2007 (243.5-244.5)	0.24	5.87

Table 5.8 Correlation coefficients and offset values for the total overlapping data period and individual overnight periods.

The variation between the two data sets can be explained by the different instruments having different spatial resolutions and locations coupled with the varying wind direction. The DOAS instrument operated with a total light path of 13.61 km, which reached from Mace Head across the bay to the town of Roundstone (situated to the north of Mace Head), where the retro reflector array was situated, and back to Mace Head. This path covered two intertidal regions and a substantial region above seawater, which is illustrated in figure 5.19. The BBCEAS, a more compact instrument was located close to the inter-tidal region (approx 105-140 m from closest shoreline) at Mace Head only, and is shown in figure 5.4. There are some days during BIOFLUX II when the BBCEAS instrument sees I_2 , but the DOAS instrument does not, for example on from j 239-240. This is further evidence for the spatial inhomogeneous distribution of I_2 emission sources around Mace Head.

The difference in iodine concentration observed by these instruments supports a theory of “hot spots” of iodine emissions from the different types of seaweed growing on the shore line exposed only during the lowest tides. The strongest I_2 signals

observed by both instruments correspond to the spring tides, when the inter-tidal region exposed is at its monthly maximum.

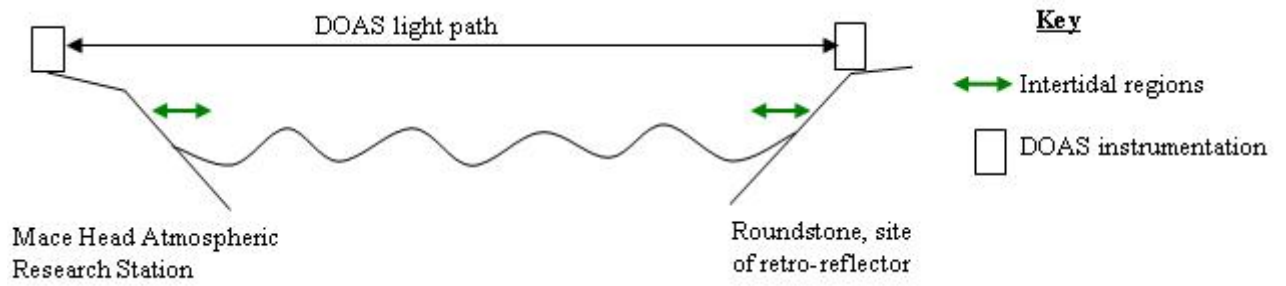


Figure 5.19 Illustration of DOAS light path from Mace Head to the retro reflector sited at Roundstone

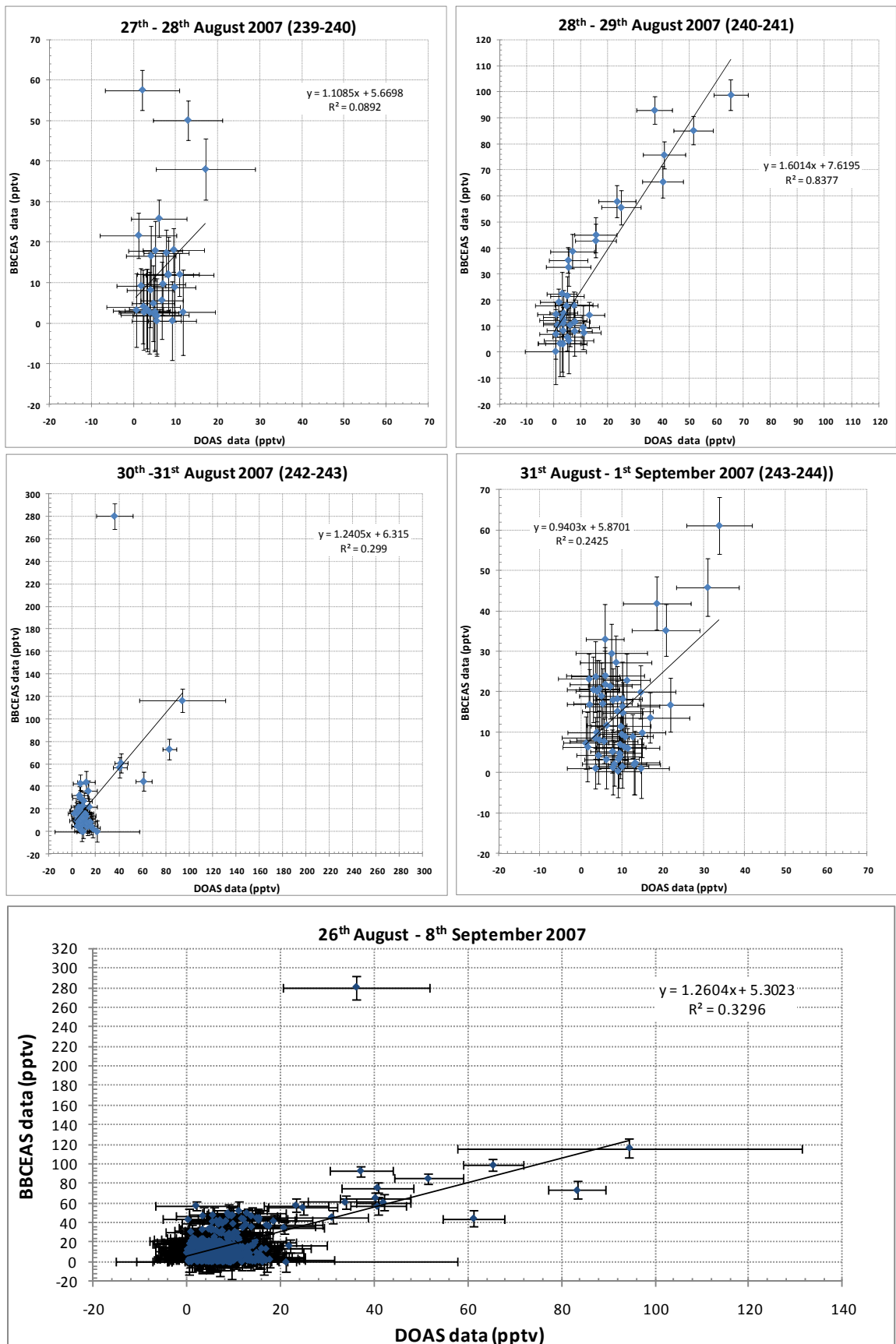


Figure 5.20 Correlation plots between BBCEAS and DOAS data for Iodine concentration during BIOFLUX II, data taken midday to midday. Lower plot is correlation for whole period of overlapping BBCEAS and DOAS data.

5.7.4 Analysis of night of 30th – 31st August 2007 on 2 minute resolution

The night of the highest iodine signal, 30th August 2007 was analysed at a 2 minute resolution and the peak iodine mixing ratio of 608 pptv observed, the short time series for the overnight measurements is shown in figure 5.21 and the resulting fitted BBCEAS spectrum for the peak iodine concentration is shown in figure 5.22. The time series shows iodine concentration varied rapidly over the course of a few minutes at a time with a strong initial peak at low tide, followed by several smaller I₂ peaks during the low tide period.

The short term variability of iodine concentration has impacts upon both the occurrence and rate of particle production. Hoffman observed a non linear dependence of particle production with the initial concentration of iodine precursor species during laboratory studies [*Hoffmann et al.*, 2001]. The iodine concentration observed using BBCEAS over short time scales (of several minutes) at Mace Head can reach several hundred parts per trillion per volume, greater than that observed during previous measurement campaigns. The subsequent photolysis of iodine in the atmosphere during daylight and the subsequent reactions of iodine atoms to form oxides, which in turn may form particles, could be much more enhanced than previously thought.

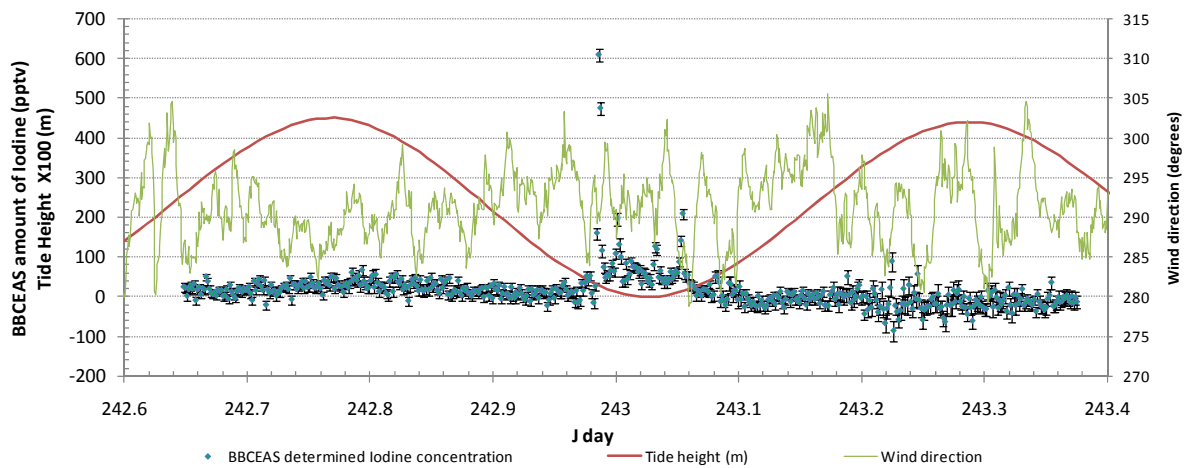


Figure 5.21 BBCEAS determined iodine concentration (blue points) and tide height (red trace) and wind direction (green trace) analysed at 2 minute average for the night of the 30th August 2007.

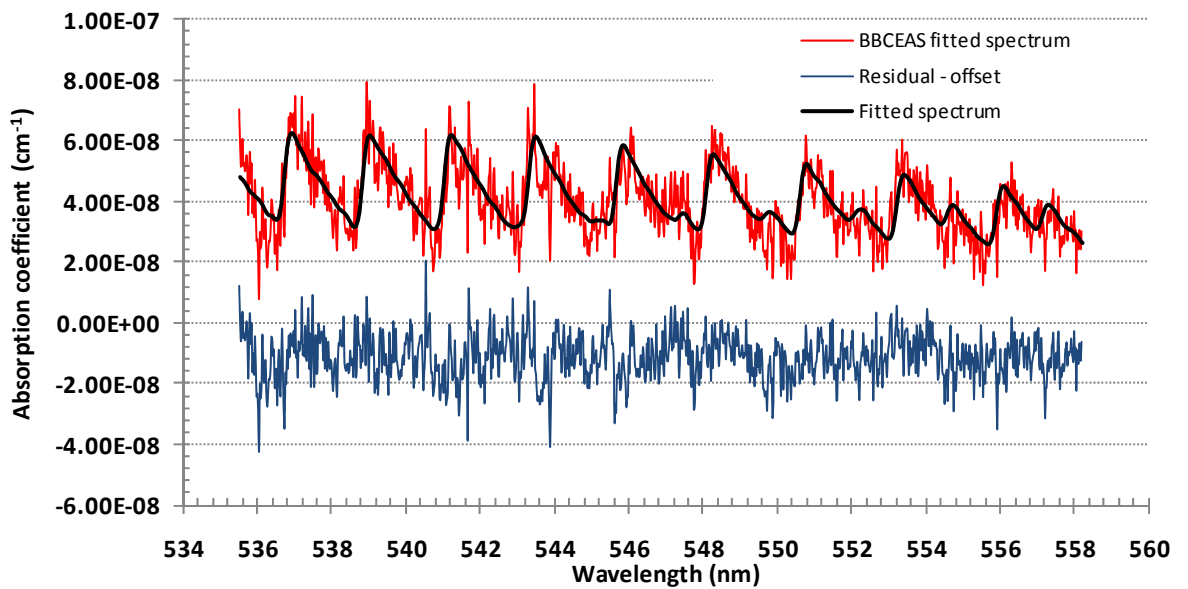


Figure 5.22 The fitted amount of iodine is 608ppt +/- 17ppt and the standard deviation of the residual spectrum is 7.45×10^{-9} from a two minute average analysis. The residual spectrum is shown with an offset of 1×10^{-8} in order to see more clearly any structure remaining in the residual spectrum. The spectrum was recorded on 30th August 2007 (242.98).

5.8 Summary and conclusion.

The results presented in this chapter have shown the BBCEAS instrument is capable of detecting varying concentrations of I_2 (above a typical detection limit of ~ 17 ppt) in the marine atmosphere over an extended measurement period at Mace Head. The excellent agreement between the BBCEAS determined water vapour concentrations and meteorological data for the BIOFLUX II measurement period provided an additional quality assurance for the subsequent retrieval of molecular iodine in the data set. Mixing ratios of I_2 up to 608 pptv for 2 minute analysis and 280 pptv for 10 minute analysis were observed coinciding with night time low tides, while no spectrally identifiable iodine was observed during daylight measurements. The iodine concentration peaks observed by BBCEAS agrees with previous measurements of I_2 at Mace Head using BBRDS measurements by Bitter et al [Bitter et al., 2005][Saiz-lopez et al., 2006] and LP DOAS by Saiz-lopez et al [Saiz-lopez and Plane, 2004] and Peters et al [Peters et al., 2005]. BBRDS recorded I_2 peaks close to low tide [Saiz-lopez et al., 2006] with a maximum peak of 94 ppt [Bitter et al., 2005] at Mace head during NAMBLEX 2002, this value correlates well with the BBCEAS peak values observed on nights of J 240, 242 and 243 in 2007, when the low tides were of similar heights for both campaigns. Both BBRDS and BBCEAS provide a point source measurement, due to the similarities of the techniques and both were situated in close proximity to the shoreline cottages during measurements made at Mace Head. These similarities between the instruments and site explain why the two campaigns produce data of similar magnitudes for observed iodine concentrations.

The LP DOAS authors, Saiz Lopez et al, report an abrupt increase in iodine mixing ratio corresponding with night time low tides, measuring maximum mixing ratios for iodine over spring tides of 94 pptv [Saiz-lopez and Plane, 2004] and 61pptv [Peters et al., 2005]. Saiz Lopez et al [Saiz-lopez and Plane, 2004] also reported daytime iodine peaks of 25 pptv, however daytime iodine peak occurrences are not supported by the BBCEAS measurements presented here.

The complementary behaviour of I_2 and IO seen by BBCEAS and the LIF IO measurements provides an explanation for BBCEAS not detecting I_2 during day time measurements. This fits with the current understanding of iodine chemistry in the marine boundary layer, whereby I_2 emitted into the atmosphere at low tides during daylight hours undergoes rapid photolysis on the timescale of ~ 10 s to produce iodine atoms which react immediately with ozone to form IO. This conversion occurs faster than iodine being transported from its source to the BBCEAS instrument for detection, thus explaining no daytime iodine peaks are observed even during the spring tides. During BIOFLUX II the distance from the proposed source to the BBCEAS cavity was over 100 m, and thus the I_2 concentrations observed are what remains following dilution and photolysis. Mace Head is a clean environment, and it is therefore not expected that iodine will be recycled by the iodine nitrate, as was observed in the polluted marine atmosphere at Roscoff during RHaMBLe [Leigh et al., 2009].

The difference in the magnitude of the nightly occurring peak iodine concentration value seen on nights on and close to the spring tides, along with the lack of detectable iodine on nights where the tidal range is at its smallest during the campaign, is a strong indicator that the iodine source is attributable to certain seaweed species. The

seaweed species that grow in deeper water (Laminarias) around the measurement site are the major source of iodine to the atmosphere at Mace Head. These laminaria beds are exposed only during the largest tidal height changes concurrent with the highly elevated levels of molecular iodine observed by BBCEAS.

No doubt much more can be learnt about iodine's affect on marine boundary layer chemistry from modelling efforts that would incorporate the BBCEAS I_2 time series and data from the other instruments deployed during BIOFLUX II. However, this is beyond the scope of this thesis which is focusses largely on development and deployment of the BBCEAS instrument. An ongoing collaboration with Dr Bloss and his group at Birmingham University aims to model the evolution of reactive iodine species from their tidal source region inland over the Mace Head site; this study will also model the effects of iodine's chemistry on the radical budgets at the Mace Head site.

CHAPTER 6

BBCEAS measurements of NO₂ during the Leicester Air Quality Measurement Project

6.1 Introduction to LAMP

This chapter presents data from atmospheric field measurements conducted in the urban environment as part of the Leicester Atmospheric Monitoring Project (LAMP). Air pollution and air quality issues have been discussed in chapter 1, and outlines of some protocols that have been implemented in order to improve and conserve air quality. Measurement methods used to monitor the pollutant species NO₂ in the atmosphere are described along with previous inter-comparisons between instrumentation. The later sections present the BBCEAS measurements of NO₂ during LAMP and a comparison with concurrently operated chemiluminescence NO_x instruments.

6.1.1 LAMP project aims

The LAMP project aimed to further understand urban air quality and chemical processing in the urban atmosphere. In particular, NO₂ levels in the urban boundary layer were monitored by state-of-the-art research instruments deployed alongside commercial instruments commonly used by local authorities to fulfil their legislative obligation to monitor NO_x. The LAMP campaign thus provided an opportunity to compare and validate recently developed instrumentation with well established in situ

measurement techniques deployed at the same site over a period of several weeks, and this chapter focuses particularly on the inter-comparison of the BBCEAS with other NO₂ detectors. A subsidiary aim of the LAMP project was the study of aerosol formation from VOC oxidation chemistry in the urban environment.

6.2 Review of NO₂ instrumentation

Sections 6.2.1 to 6.2.5 review the many research instruments that have been devised to quantify NO₂ in the atmosphere. The instruments broadly fall into two categories: chemical detectors or spectroscopic instruments. Within the spectroscopic instrumentation, fluorescence and absorption techniques have been the preferred spectroscopy techniques developed for atmospheric monitoring. The absorption spectroscopic techniques utilise infrared and visible wavelengths, and employ a variety of light path types.

6.2.1 Chemiluminescence detectors

Chemiluminescence detectors have the longest history of being used to measure ambient NO₂. Such instruments are capable of long term unattended operation making them an attractive choice for air quality monitoring applications: indeed today they are used as the UK national standard in monitoring NO₂. Early proponents of the method, Kley and McFarland [*Kley et al.*, 1981], used a nitric oxide chemiluminescence instrument to measure NO and NO₂ in a variety of locations, both urban and rural,

ground based and airborne in order to construct NO_x tropospheric profiles. A schematic of their instrument is shown in figure 6.1.

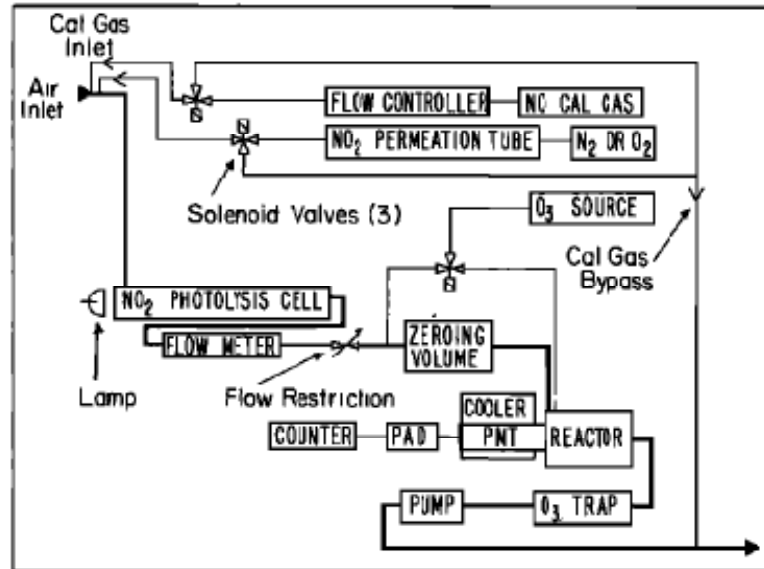
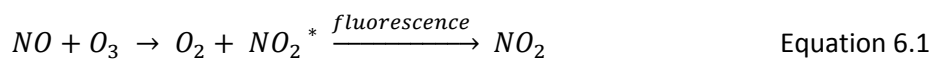


Figure 6.1. Schematic of an early NO and NO₂ detector a chemiluminescence detector [Kley *et al.*, 1981].

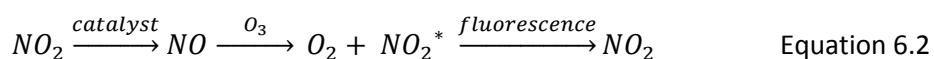
A typical chemiluminescence detector operates with two modes, yielding alternating measurements of NO and NO₂. The NO mode operates by reacting NO in the sampled ambient air with ozone produced inside the instrument. This reaction forms electronically excited NO₂ (NO₂^{*}) – see equation 6.1. The fluorescence of NO₂^{*} back to ground state NO₂ is measured by a photomultiplier tube (or other light detector) and is used to infer the concentration of NO. Calibration is performed by sampling a known concentration of NO from a cylinder of a gas standard.



The NO₂ mode operates by first passing the ambient air sample over a solid catalyst (typically molybdenum oxide) reducing any NO₂ present to NO. The sample is then

passed to the same detection system as the NO mode, where all NO (ambient NO plus the extra NO from reduction of NO₂) is converted to NO₂* by reaction with ozone.

Again the fluorescence from the excited state NO₂* is detected, as shown by equation 6.2. The difference between the two modes is used to infer the NO₂ concentration.



Under certain sampling situations, other gas phase molecules in the atmosphere may be reduced to NO on the catalyst, thus contributing an extra NO₂ signal above the actual ambient NO₂ being measured. In order to limit this interference photolytic converters are now used, which show a better selectivity for converting only NO₂ to NO before detection. The interference produced in molybdenum (or surface) catalyst chemiluminescence instrument has been well documented by, Steinbacher who compared their performance to chemiluminescence instruments with photolytic converters [Steinbacher *et al.*, 2007]. A bias of retrieving higher NO₂ concentration was observed when using molybdenum catalysts: the largest discrepancies were observed during spring and summer, and were attributed to interferences from NO_y species produced by atmospheric photochemistry [Steinbacher *et al.*, 2007]. Elevated (1031 m above sea level), and non elevated (539 m above sea level) measurement sites were compared. 70-83% of measured NO₂ was classified as a “real” measurement (i.e. not due to interferences) at the elevated measurement site, whilst this decreased to 43-76% for the non elevated site [Steinbacher *et al.*, 2007]. PAN and HNO₃ are the dominant interfering species and accounted for the remainder of the total NO₂ signal observed [Steinbacher *et al.*, 2007]. The extent of the interference was highly

influenced by meteorological conditions, varying the degree of overestimation on an hourly timescale [Steinbacher *et al.*, 2007].

Satellite spectroscopic NO₂ measurements and ground based chemiluminescence measurements by were compared over 7 years by Ordenez *et al.* [Ordenez *et al.*, 2006]. High correlations were observed for the near-surface measurements, however a summer bias of ground data showing higher NO₂ than satellite retrieved data was observed. When the chemiluminescence measurements were corrected for known interferences (e.g. PAN and nitric acid), the bias with respect to the satellite data was reduced [Ordenez *et al.*, 2006].

The first field comparison of a research grade instrument, a TLDA, with chemiluminescence detectors for NO_x measurement was performed in Mexico City by Dunlea [Dunlea *et al.*, 2007]. As described in the next section, TLDA is a spectroscopic technique that is highly selective for NO₂ and produces an absolute measure of the NO₂ concentration (relying only on the accuracy of the molecular absorption cross sections). A recurring discrepancy was observed (see figure 6.2), with chemiluminescence detection observing higher concentrations of NO₂ than the TLDA quantities [Dunlea *et al.*, 2007]. Dunlea explored the interferences and determined an interference factor. This was variable and generally peaked in the afternoon when O₃ levels also peaked, causing up to 50% interference [Dunlea *et al.*, 2007]. The sources of interference were identified as ozone and NO_z (NO_z is non-NO_x fraction of reactive nitrogen), with HNO₃ identified as causing 60% of the observed interference [Dunlea *et al.*, 2007]. The correlation between PAN and particulate nitrate was not good, thus the

primary interferences in this case were attributed to photo chemically-produced gas phase nitric acid and alkyl nitrates [Dunlea et al., 2007].

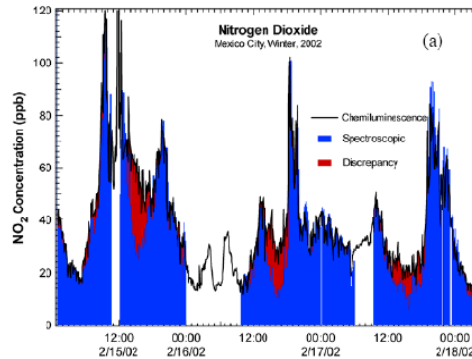


Figure 6.2. Time series of NO_2 measurements from a standard chemiluminescence NO_x monitor (black line) and a TLDAS spectroscopic instrument (blue shading) on board the ARI Mobile Lab at the Pedregal fixed monitoring site during the 2002 [MCMA] campaign. The red shading highlights the additional NO_2 (the interference) measured by the chemiluminescence instrument [Dunlea et al., 2007].

6.2.2. TDLAS: Tuneable diode laser absorption spectroscopy detection of NO_2

An example of a TDLAS system is shown in figure 6.3. Light from an infrared laser source is split into two beams: a signal beam and a reference beam. The signal beam is directed into a Herriott multi-pass absorption cell, consisting of two highly reflective concave mirrors set apart by a distance close to their radius of curvature. The light is injected in an off-axis configuration through the input hole in one mirror and then propagates back and forth, progressing around the mirrors with each reflection, before exiting the coupling hole. On exiting the cell, light is directed to the infrared detectors. The reference beam is directed through the reference cell then onto the reference detector. The reference cells contain a high concentration sample of the target gas. Thus light passing through the reference cell produces a strong absorption signal which

is used to record a reference spectrum for that gas species. The reference spectrum is used to lock the signal peak position for that gas species, acting as an internal wave number calibration. The change in absorption is detected as the laser frequency is swept across the trace gas absorption features. Absolute concentrations of absorbers present in the Herriot cell [Li, 2004] are retrieved by fitting the measured absorption lines with absorption cross sections calculated using standard spectroscopic databases (e.g. HITRAN), the laser line shape measured in the reference cell and temperature and pressure measurements in the main sample cell. The TDLAS instrument enables absolute concentration retrieval with the added benefit of not requiring calibration gas samples in the field [Li, 2004]. The laser sweeping approach enables 100s of “fingerprint” lines to be fitted for each species, with up to 8 species fitted per spectrum, enhancing sensitivity and selectivity [Li, 2004].

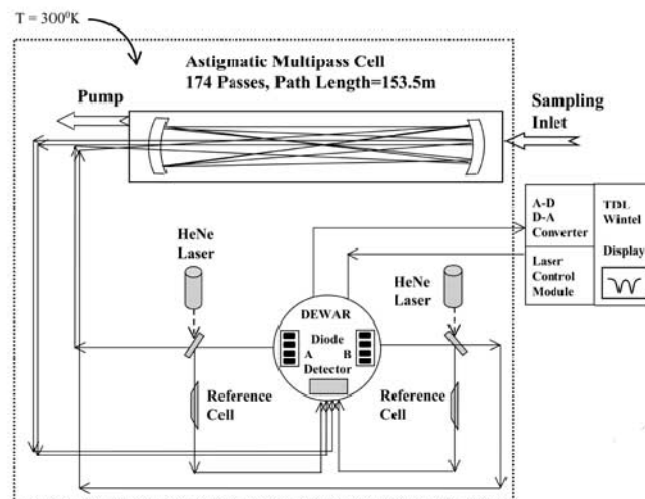


Figure 6.3 Schematic of dual channel TDLAS system used to measure formaldehyde, nitrogen dioxide, and sulfur dioxide in New York during 2002 [Li, 2004].

During the PM_{2.5} Technology Assessment and Characterization Study, New York, (PMTACS-NY 2002), a TDLAS was deployed from 23rd July to 7th August producing absorption spectra at 1s time resolution [Li, 2004] with a 91% coverage over the measurement period. Broad plumes of NO₂ were observed by TDLAS during the day. These plumes were also captured by other instrumentation, and the wind direction data suggested transport from local city regions [Li, 2004]. Additionally, many narrow spikes in NO₂ concentration were observed during night time measurements. These occurrences correlated with meteorological data, indicating the sources were other instrumentation on site rather than the infrequent local vehicular emission sources at the site [Li, 2004][Li, 2004].

6.2.3 Cavity techniques to measure atmospheric NO₂

The following three sections briefly describe different cavity techniques; more details on the instrumentation can be found in the individual references.

6.2.3.1 Cavity Attenuated Phase-shift Spectroscopy (CAPS).

A modulated broadband LED light source is coupled into a resonant cavity, and light transmitted by the cavity is detected by a photomultiplier tube. The presence of absorbing gas species in the cavity results in a phase shift in the light exiting the cavity relative to the modulation signal applied to the light source. The phase shift is proportional to concentration of the absorber. An illustration of a CAPS instrument used to measure NO₂ concentration is shown in figure 6.4. This instrument was used for a two day comparison of CAPS and TDLAS, splitting the airflow to the two

instruments. However first it was necessary to calibrate the CAPS signal against the absolute NO₂ measurements produced by the TDLAS system over a range of different NO₂ concentrations supplied by dilution of a standard sample. Thus, in this application, CAPS on its own does not provide an absolute measurement of the absorber's concentration.

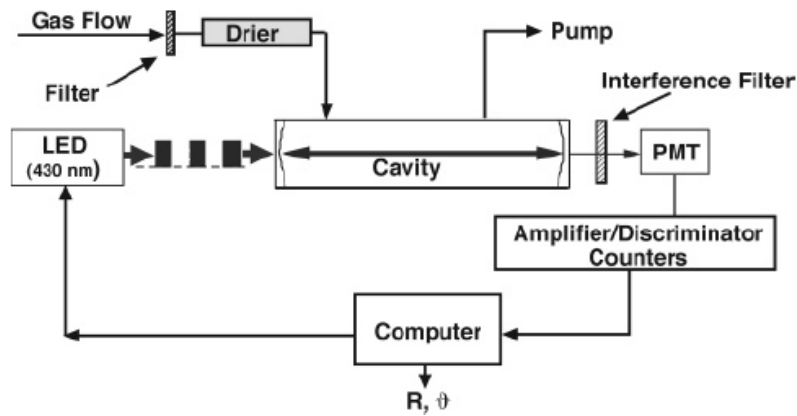


Figure 6.4 Attenuated phase shift spectroscopy; set up for ambient NO₂ measurement [Kebabian *et al.*, 2005]

Comparison of the NO₂ measurements showed the CAPS method effectively measured both large and small variations in NO₂ concentration over the measurement period. A typical diurnal cycle for NO₂ was observed with increases in NO₂ being complementary to local commuting patterns [Kebabian *et al.*, 2005]. The average difference between the two instruments was 14%, which the authors stated was due to the CAPS sensor shifting from its original calibration over the course of the measurements [Kebabian *et al.*, 2005]. This highlighted the need for regular calibrations and adjustment of alignment in this cavity system in order to make reliable measurements [Kebabian *et al.*, 2005].

The CAPS method is a non wavelength specific technique, and so can suffer from interference due to other gas species absorbing within the wavelength range of its light source. This potentially results in the NO₂ concentrations attributed to the CAPS signal being biased higher than the actual levels. In the study by Keabian et al, common interference molecules had little or no absorbance structure across the light source output (a 10 nm bandwidth around 430 nm), but in some atmospheric sampling regions aromatic hydrocarbons and halogen compounds have absorption features comparable to NO₂ in this region and would cause interference problems [Keabian et al., 2005].

6.2.3.2 Incoherent broadband CEAS:

Continuing previous work of proving the principle of BBCEAS using LED light sources [Ball et al., 2004], Langridge [Langridge et al., 2006] developed a compact and low cost LED-based Broadband Cavity Enhanced Absorption Spectrometer for quantifying NO₂ in ambient air, a schematic diagram of which is shown in figure 6.5. The cavity mirror reflectivity was determined in situ by measuring the O₂-O₂ absorption band at 446 nm along with measurement of known concentrations of NO₂, thus ensuring retrieved concentrations were absolute. Laboratory samples of various dilution of NO₂ were recorded with 30 s integration times and examples of the resulting fitted spectra are shown in figure 6.6. These spectra demonstrate unambiguous and quantitative detection of NO₂ using this laboratory BBCEAS instrument.

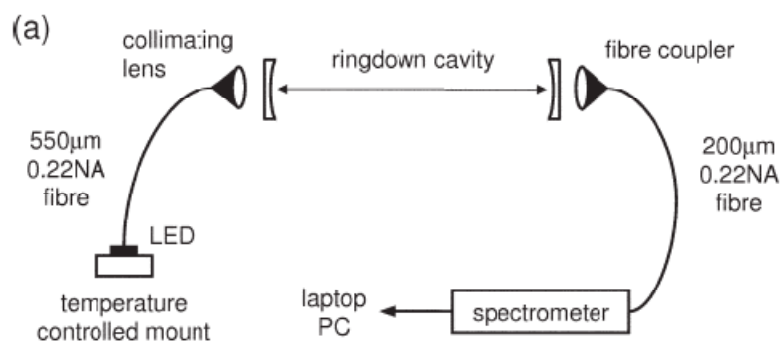


Figure 6.5. Optical layout of the LED based broadband cavity enhanced absorption instrument used for quantifying NO₂ in laboratory trials [Langridge *et al.*, 2006].

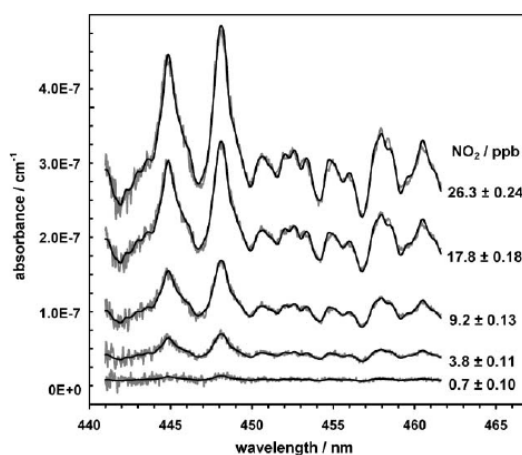


Figure 6.6. Fitted BBCEAS spectra of NO₂ samples prepared from the thermal decomposition of N₂O₄ [Langridge *et al.*, 2006].

The BBCEAS instrument was also used to sample ambient laboratory air alongside a simultaneous measurement of NO₂ using a chemiluminescence detector with a thermal NO₂ converter. The two instruments used identical acquisition times and the comparison extended over a 38 hour period. The instruments showed very good agreement in their measured NO₂ amounts, see for example figure 6.7. The NO₂ concentrations measured ranged from 3 to 34 ppbv during this comparison, and the correlation gave an R² correlation coefficient of 0.998 [Langridge *et al.*, 2006]. The

BBCEAS systematically found lower NO₂ concentrations than the chemiluminescence detector, and these differences (largest difference = 6%) were most pronounced when the highest NO₂ concentrations were observed. The authors suggested the difference could be due to other NO_y compounds contributing to the signal in the chemiluminescence instrument – a demonstration of the benefits of a direct spectroscopic measurement of the target species

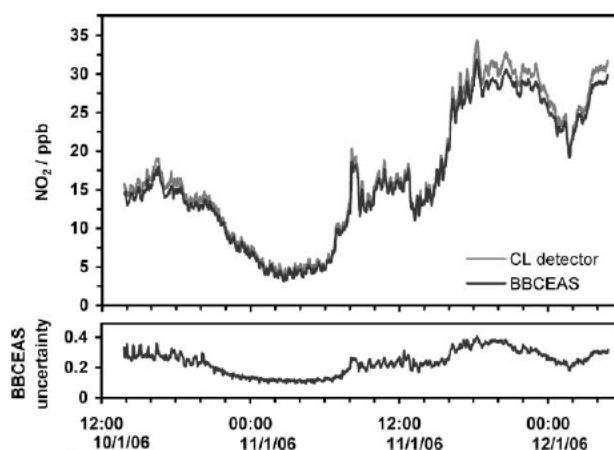


Figure 6.7. The top panel shows a time series of measurements of NO₂ in ambient laboratory air made by the BBCEAS spectrometer and a commercial chemiluminescence detector. The lower panel shows the statistical uncertainty associated with fitting the NO₂ differential structure in the BBCEAS spectra [Langridge *et al.*, 2006].

Wu *et al.* developed a similar BBCEAS instrument using a blue LED light source and measured NO₂ in ambient laboratory air. Wu *et al.* used the same approach to determine the in situ cavity mirror reflectivity by measurement of O₂-O₂ bands and NO₂ standard gas mixtures [Wu *et al.*, 2009]. An Allan variance analysis was used to

determine the instrument's long-term stability and sensitivity and thus to optimise the averaging time to achieve the maximum signal to noise ratio [Wu *et al.*, 2009].

6.2.3.3 Pulsed cavity ring down

A pulsed CRDS instrument for simultaneous NO₂, NO₃ and N₂O₅ was deployed alongside a photolysis-chemiluminescence detector by Osthoff [Osthoff *et al.*, 2006]. The basis of the cavity ring down technique was described above in chapter 2 and the instrument schematic shown in figure 6.8. Absorption at 532 nm was used to monitor NO₂ due to the convenience of 532 nm light being the output from the frequency doubled Nd:YAG laser used to pump a dye laser providing 662 nm light to the instrument's other NO₃ and N₂O₅ ring down cavities [Osthoff *et al.*, 2006]. The measurements were made at two sites: in Boulder Colorado during 2005 and on board the NOAA research vessel Ronald H Brown in 2004. During the Boulder campaign the sampling of the cavity instrument and P-CL detector was located within 1 metre of each other, and an excellent correlation of $R^2 = 99.1\%$ [Osthoff *et al.*, 2006] was observed between the two data sets shown in figure 6.9. The data sets from the Ronald H Brown ship-board measurements were made with a 3.5 m displacement in sampling position, and so on occasion the different instruments were sampling different air masses. A slightly reduced correlation of 98.8% [Osthoff *et al.*, 2006] was observed between the cavity ring down and chemiluminescence detector on board R H Brown.

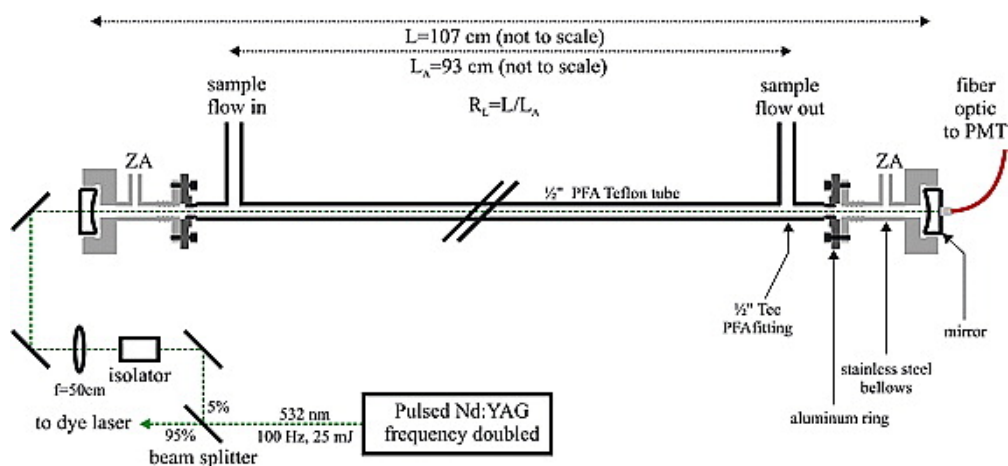


Figure 6.8 Schematic of pulsed Cavity Ring-Down Spectrometer for NO_2 measurements [Osthoff et al., 2006].

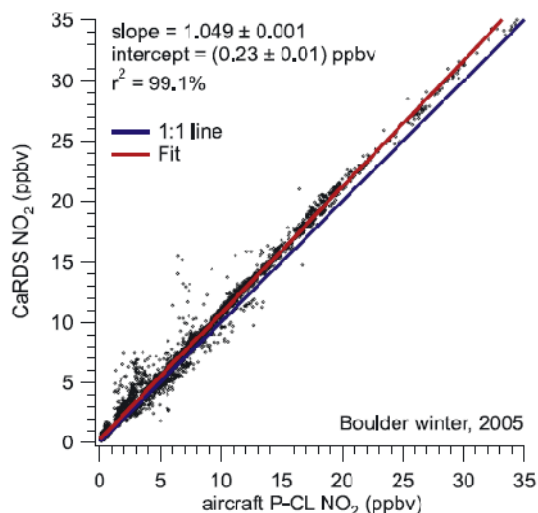


Figure 6.9. Correlation plot of CRDS data with P-CL data averaged to 1 minute and recorded at Boulder [Osthoff et al., 2006].

6.2.4 Laser induced fluorescence (LIF) detection of NO_2

At its simplest, LIF involves the use of laser light which is tuned on and off resonance with an absorption feature specific to the target molecule, in this case NO_2 , and detection of the resultant fluorescence. Thornton improved early examples of this type of instrument, reducing detection limits to 1ppt and increasing the sensitivity to 15

ppt/10 s rather than 40-80 ppt/ 10 s at ambient pressure [Thornton, 2000]. The Berkley NO₂ LIF instrument is comprised of a laser excitation system, a detection cell, gas flow systems and data acquisition and control systems, occupying a 1m³ area [Thornton, 2000]. Two field deployments of the Berkley NO₂ LIF system were carried out to test its performance as a field instrument. The first deployment during 1998 was in Sierra Nevada, US, in a forest/ foothills environment with a detection limit of 85ppt/10s. Following adaptations to decrease laser scatter and increase the signal an the LIF was deployed in Nashville, US, 1999, with a detection limit of 15ppt/10s [Thornton, 2000]. No interference effects due to fluorescence of other atmospheric components were observed during either measurement period. The Nashville NO₂ LIF measurements were coincident with NO₂ measurements by a photolysis-chemiluminescence (P-CL) detector and an active DOAS system, enabling an informal instrument comparison [Thornton, 2003]. The different data sets are shown in figure 6.10 and exhibit excellent agreement with each other. The P-CL and LIF data sets showed average agreement within 5%. The NO₂ levels were above 1 ppbv for the duration of the measurements, and thus this comparison was not a test for the detection limit of the instruments.

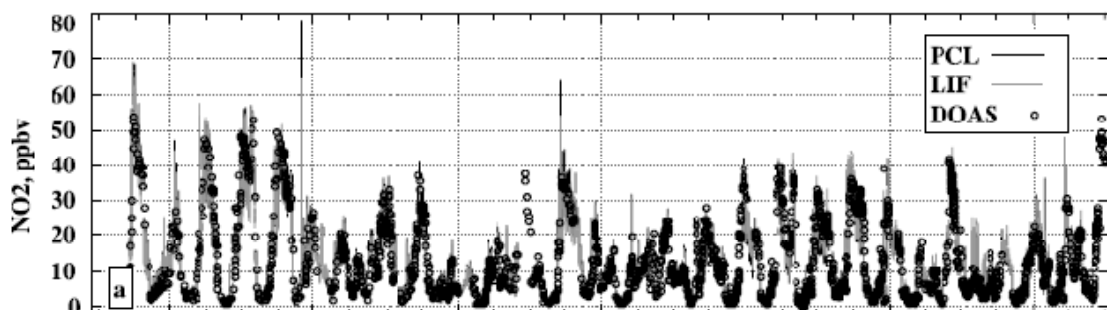


Figure 6.10 One-minute average NO₂ mixing ratios measured by the P-CL (black trace) and LIF (grey trace), and DOAS (open circles) instruments for 18 June–14 July 1999 [Thornton, 2003].

6.2.5 Gas chromatography with luminol chemiluminescence detection (GC/LCD) for NO₂

NO₂ and PAN (peroxyacetyl nitrate) have been simultaneously detected using an instrument utilising fast gas chromatography to separate different chemical species and luminol chemiluminescence for their detection [Marley *et al.*, 2004]. The instrument consists of a 30 feet long capillary column and the luminol chemiluminescence emission at 425 nm occurs by reaction at the gas/liquid interface on the solid support. The instrument operates at detection limits in the parts per trillion with 30 second to 1 minute resolution [Marley *et al.*, 2004]. The luminol detection method achieves a higher sensitivity than ozone chemiluminescence as the 425 nm luminescence of luminol coincides with the maximum sensitivity of commercially available photo multiplier tubes [Marley *et al.*, 2004].

The fast GC/LCD was used for atmospheric NO₂ and PAN measurements during MCMA 2003 an air quality study in Mexico City centre. The campaign provided an opportunity to compare the GC/LCD instrument with DOAS and TDLAS measurements at the same site. The GC/LCD results compare well with the DOAS data. When GC/LCD data was averaged to the same timescale as TDLAS data, the correlation shows an R² value of 0.83 [Marley *et al.*, 2004]. The GC/LCD values were slightly higher than TDLAS values; this can be explained by considering the sample inlet positions for the two instruments. The inlets were not co-located and thus the instruments may have at some time during the campaign sampled different air masses.

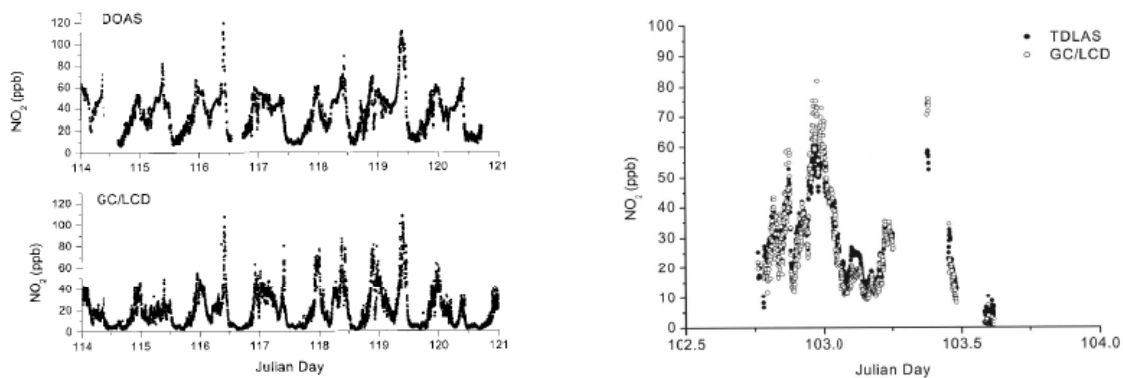


Figure 6.11. *Left*: NO₂ concentrations derived from collocated DOAS (upper) and GC/LCD (lower) during MCMA 2003 [Marley *et al.*, 2004]. *Right*: NO₂ concentrations from GC/LCD and TDLAS over 12-13th April 2003 night during MCMA [Marley *et al.*, 2004].

6.3. Instruments participating in the LAMP campaign

A consortium of scientific instrumentation was co-deployed at the University of Leicester during the summer of 2007: these are listed in table 6.1. The measurement site at the Space Research Centre (SRC) is approximately 1 km south of the city centre within the University of Leicester campus. The LAMP campaign ran from 13th July 2007 until 18th September 2007. The availability of individual instrumentation varied, and not all participants were present for the duration of the campaign due to other commitments. Nonetheless an extended period of overlapping measurements between instruments monitoring key species was possible. The BBCEAS instrument operated in a virtually continuously mode from 24th July to 14th August 2007 to obtain atmospheric NO₂ concentrations. Thereafter the BBCEAS instrument was deployed in Ireland during BIOFLUX II (as already discussed in chapter 5) to measure I₂.

LAMP instrumentation			
Instrument	Species detected	Technique	Institution
Broadband cavity enhanced absorption spectrometer (BBCEAS)	NO ₂	spectroscopy 430-485nm bandwidth	University of Leicester
NO _x	NO and NO ₂	Chemiluminescence detector with diode blue light photolytic converter	NCAS University of York. J Lee
Commercial chemiluminescence detector	NO ₂	Molybdenum oxide catalysts	Leicester city Council
Concurrent Multi-Axis Differential Optical Absorption Spectroscopy (CMAx-DOAS)	O ₄ , NO ₂ and aerosol optical depth (AOD)	Scattered light measurements at various elevation angles	University of Leicester. L Krammer
Mobile LIDAR	AOD and ozone; boundary layer height	Time resolved detection of back-scattered light & wavelength-resolved attenuation of back-scattered light.	University of Manchester
Sun photometer	AOD	Direct solar irradiance at 440, 670, 870 and 1020nm	Aeronet
Chemical ionisation time of flight mass spectrometer (CIR-TOF-MS)	VOC	Time of flight mass spectrometry	University of Leicester. K Wyche
Peroxy radical chemical amplifier PERCA	OH + sum RO ₂	Luminol chemiluminescence detection of NO produced via peroxy radicals' catalytic reaction	University of Leicester.
Spectral Radiometers	Photolysis frequencies	2π upward pointing hemisphere, 0.5 second integration time averaged to 1 minute	University of Leicester
Filter samples	Aerosol speciation	Filter sample once per day	University of York. J Hamilton
Bottled air samples	VOC s	GCFID (Gas chromatography flame ionisation detection)	University of York. J Hopkins
Ozone monitor (commercial instrument)	O ₃	UV absorption	University of Leicester
CO monitor (commercial instrument)	CO	Vacuum UV fluorescence CO analyser	University of Leicester
Meteorological data (commercial instruments)	T, wind speed, wind direction, relative humidity.	Measured at 3m and 10m on site	University of Leicester

Table 6.1 LAMP instrumentation

6.3.1 NO₂ instrumentation and sampling positions during LAMP

During LAMP four techniques were used to quantify NO₂. The BBCEAS was operated at wavelengths of 407.0-491.2 nm enabling the unambiguous identification and quantification of NO₂. The BBCEAS cavity was located on the SRC roof top (approximately 10 m height above ground) for the duration of the BBCEAS measurements and sampled air flow passing “freely” over the building.

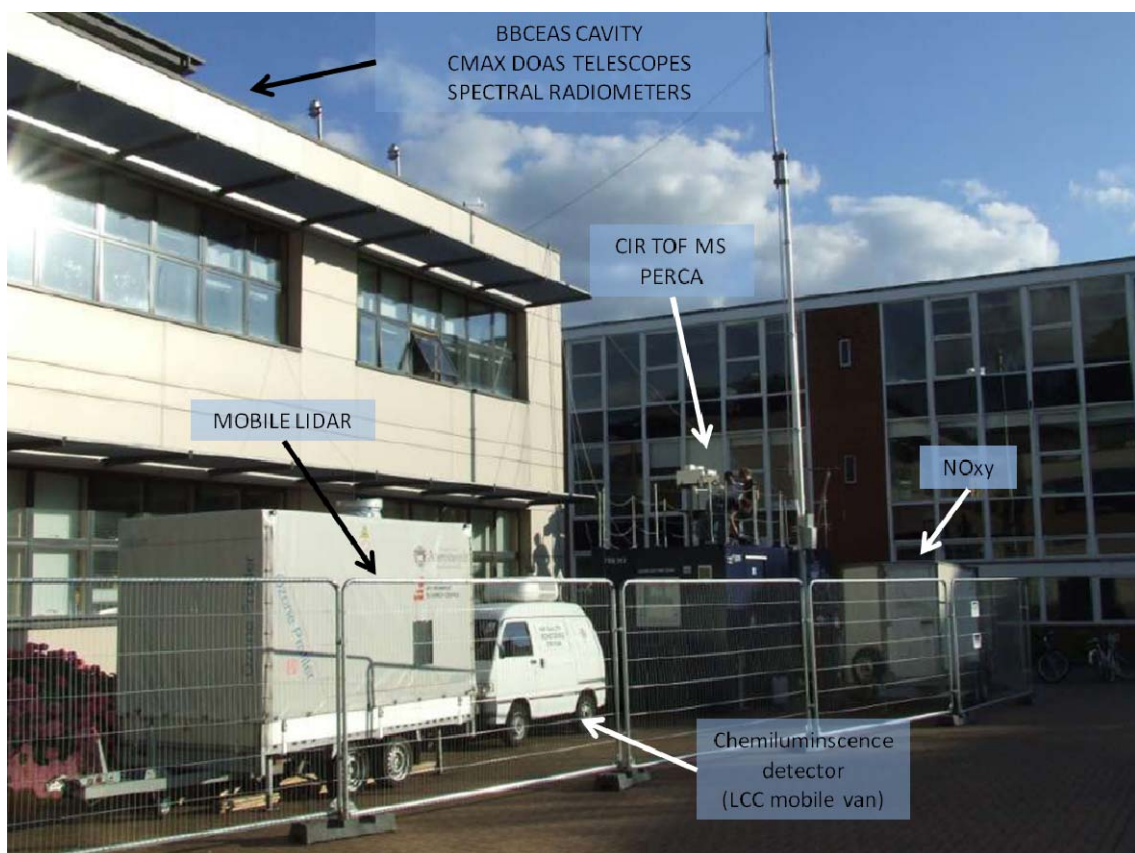


Figure 6.12. Instrument locations at the LAMP measurement site SRC building, University of Leicester.

Chemiluminescence monitors: (API M200a analyser, Enviro Technology) operated by Leicester City Council. This is a molybdenum oxide catalyst chemiluminescence instrument operating as described in section 6.2.1 above. The Leicester City Council

chemiluminescence detector was housed in the council's mobile measurement van, which was parked close to the SRC building for the duration of the LAMP measurement campaign.

NO_{xy} (University of York: Dr J Lee): This was a single channel chemiluminescence NO detector and NO_y converter using a diode-based blue light photolytic converter to limit any interference from other nitrogen containing compounds. The NO_{xy} instrument was housed inside a trailer located in the car park next to the SRC and sampled from two positions: from 20th July 2007 to 30th July 2007 sampling was from the main manifold at 10 m height, thereafter sampling switched to ground level (3m height) until 12th September 2007. Sampling at 10 m height provided an opportunity to compare NO_{xy} data with data from the BBCEAS system also sampling from this height.

CMAX DOAS (University of Leicester, Dr L Krammer): This is a passive DOAS system with 5 angled telescopes each viewing light that has taken a different path through the atmosphere. All viewing angles are imaged simultaneously on an imaging spectrometer. The CMAX DOAS telescopes were situated on the SRC roof top and five angles of view were recorded simultaneously (12, 10, 8 and 6 degrees and zenith), giving excellent spatial coverage.

The instrument positions are illustrated in the figure 6.12 and the positioning enabled the NO₂ monitors to be as co located as possible at the site within the requirements of each instrument.

Ultimately comparisons of these data sets may allow quantification of the interferences, if any, due to other pollutants in the urban environment in Leicester on

NO₂ measured by chemiluminescence detectors. LAMP also provided the opportunity to test newly developed instruments alongside more established methods and commercial NO₂ detectors.

6.4 LAMP site information and meteorological data

6.4.1 LAMP site information

The LAMP site is approx 1 km south of the city centre, within the University of Leicester campus and is illustrated in figure 6.13. The red dot shown on the right-hand maps indicates the measurement site. The areas surrounding the site were toured regularly during the LAMP measurement period and any activities such as landscaping, decorating and building work were noted.



Figure 6.13 LAMP measurement site. Left: site position within the city. Right: site position within the University of Leicester Campus, red dot marks main site, green and red rings annotate the areas surveyed daily.

6.4.2 LAMP meteorological data

The temperature, relative humidity and wind direction data for the duration of the BBCEAS measurements during LAMP are shown in figure 6.14. These data were recorded at the 10 m sampling height, immediately adjacent to where BBCEAS cavity was located. Rain periods are typically when relative humidity was above 90%: in these circumstances any recorded BBCEAS data is taken to be unreliable and is not included in the analysis. As an optical technique, even one droplet of water in the light path of the instrument affects the intensity measurement and the data cannot be accurately analysed for the presence of trace gas species. Wind direction points shown bottom panel of figure 6.14 are very scattered, and show no obvious direction prevalence. The polar histogram of wind direction in figure 6.15 shows some evidence of wind mainly from either the north (i.e. travelling over the city centre) or from the south west.

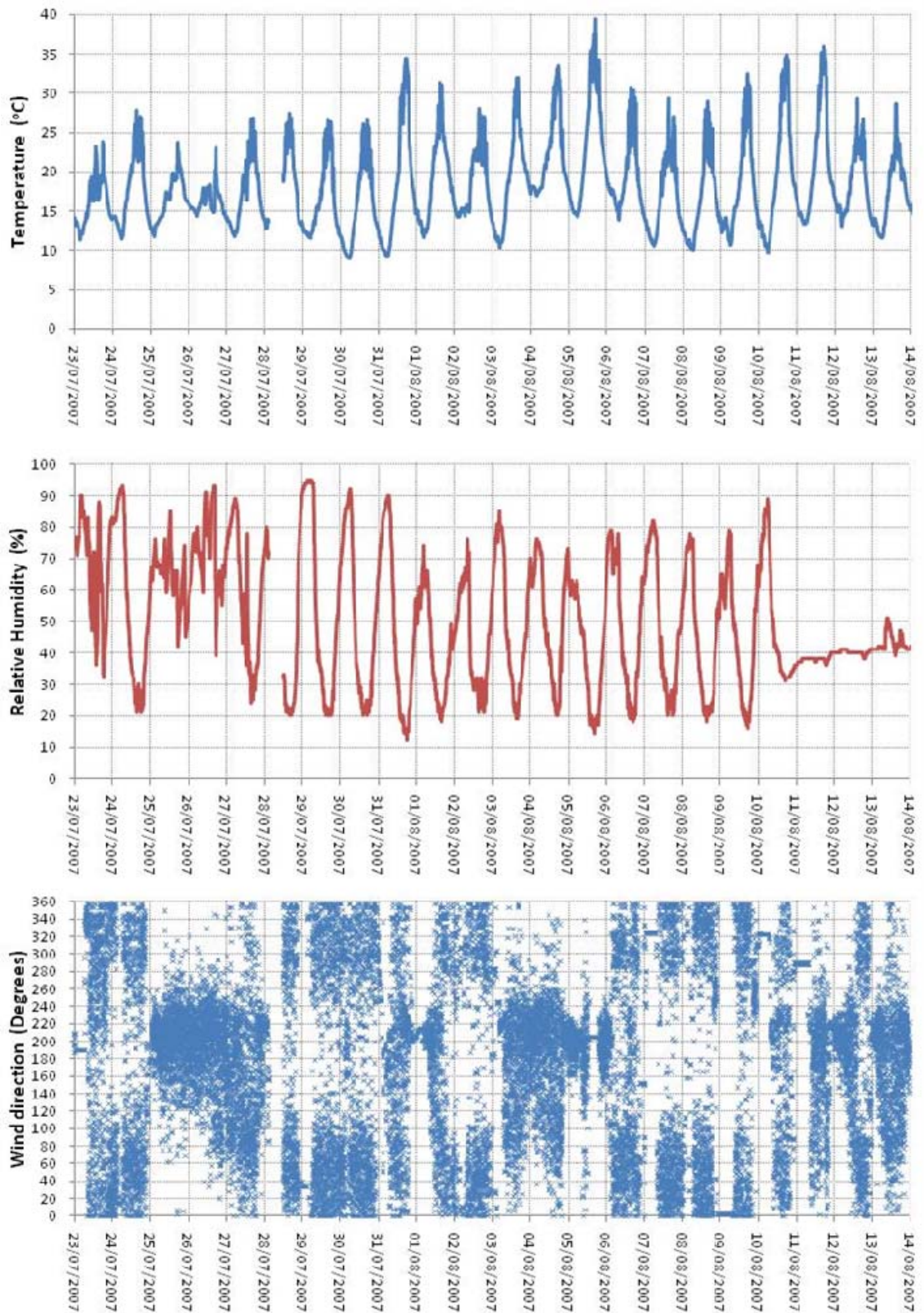


Figure 6.14. Temperature (top panel), relative humidity (middle panel) and wind direction (bottom panel) during LAMP measured at 10m sampling height.

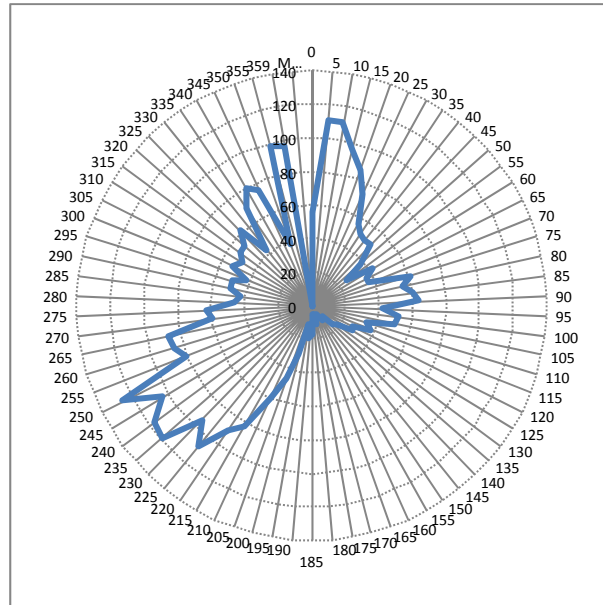


Figure 6.15 Wind direction occurrences in specified directions throughout the LAMP campaign.

6.5 BBCEAS instrument and measurements during LAMP.

The BBCEAS field instrument was configured to operate at blue wavelengths. The BBCEAS cavity (sensor) was located on the Space Research Centre’s roof space, below the CMAX DOAS telescopes as shown in figure 6.16. The light source, spectrometer and other electronics were housed in the optical laboratory on the 2nd floor of the building. The electronics and spectrometer in the lab were connected to the cavity outside by fibre optics and electrical cables passing via the SRC building’s built-in feed-through pipe to the roof space.

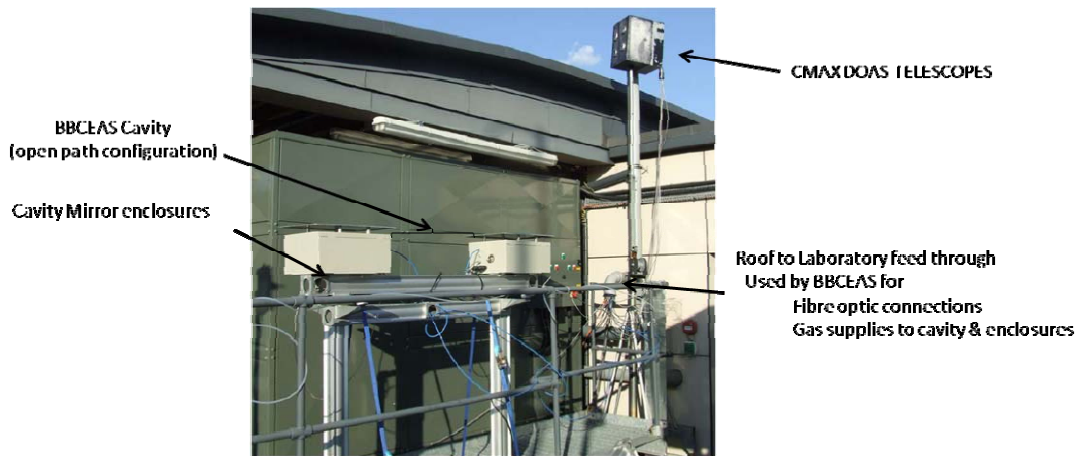


Figure 6.16 BBCEAS cavity location on SRC roof top, the CMAX DOAS telescopes are also shown.

6.5.1 Operating parameters of the BBCEAS instrument during LAMP

The main components of the BBCEAS instrument are summarised in the table 6.3. BBCEAS data were recorded using an Ocean Optics HR2000 spectrometer with an integration time of 2 seconds per spectrum. Thirty of these 2 second spectra were averaged together by the SpectraSuite operating software, and the resultant average spectrum (one minute acquisition time) was saved to the computer for later analysis. The HR2000 spectrometer has a fixed wavelength range of 407-491.2 nm. NO₂ absorption cross sections are highly structured in the blue wavelength region making it a suitable NO₂ monitoring region. Also there are O₂-O₂ bands at 447 nm and 478 nm (shown in figure 6.17) which are suitable for the in situ measurement of the mirror reflectivity during the course of the campaign.

BBCEAS setup during LAMP			
Light source	Royal Blue LED	LUXEON III (3 watt)	Temperature stabilised at 18° C
Cavity mirrors	#100859	Layertec GmbH	12.7 mm diameter
Light input fibre	QP-400-2-uv/vis-BX	Ocean optics	400 um diameter, 0.22NA, 10 m length
Cavity output fibre	QP-400-2-uv/vis-BX	Ocean Optics	400 um diameter, 0.22NA, 15 m length
Cavity length	115cm (total length between cavity mirrors)	91.4cm (cavity length exposed to atmosphere)	Length factor used in analysis = 1.258 (115cm/91.4cm= 1.258: the mirror mounts are flushed with zero air to limit contamination of mirror surface)
Spectrometer	HR2000	Ocean Optics	407.0-491.2 nm, 2048 pixels, 50um slit

Table 6.2. BBCEAS main instrumental components for operation during the LAMP campaign.

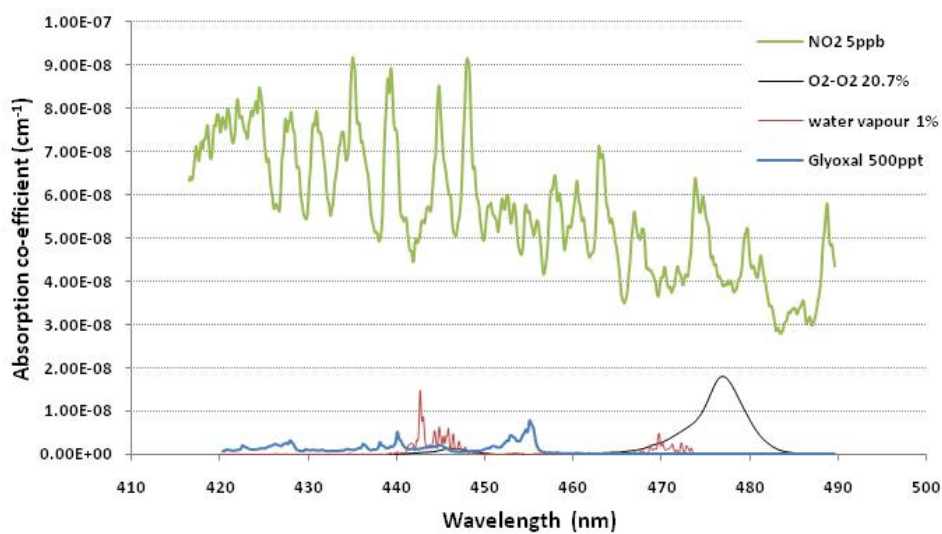


Figure 6.17. Absorption spectra of molecular absorbers in the blue wavelength region for reasonable atmospheric concentrations. These spectra have been calculated from the molecular absorption cross sections degraded for the BBCEAS instrument function.

The HR2000 spectrometer recorded the steady-state light intensity throughput of the cavity across its full wavelength range, and examples of such spectra are shown in figure 6.16 for the cavity filled with Nitrogen (blue trace) and for the cavity open to the atmosphere (red trace). A subsection of the wavelengths between 434 nm to 485 nm (as indicated by the two green lines in figure 6.18) was used in the analysis procedure for quantifying the NO₂ absorption signal. The dark current (shown as the orange trace in figure 6.16) was measured periodically, and was relatively stable during LAMP due to the 19 inch rack containing the LED, electronics and detector being sited in an air conditioned laboratory. The dark current was subtracted from the raw spectra to remove reoccurring spikes in the signal, thus reducing noise in the resulting spectra.

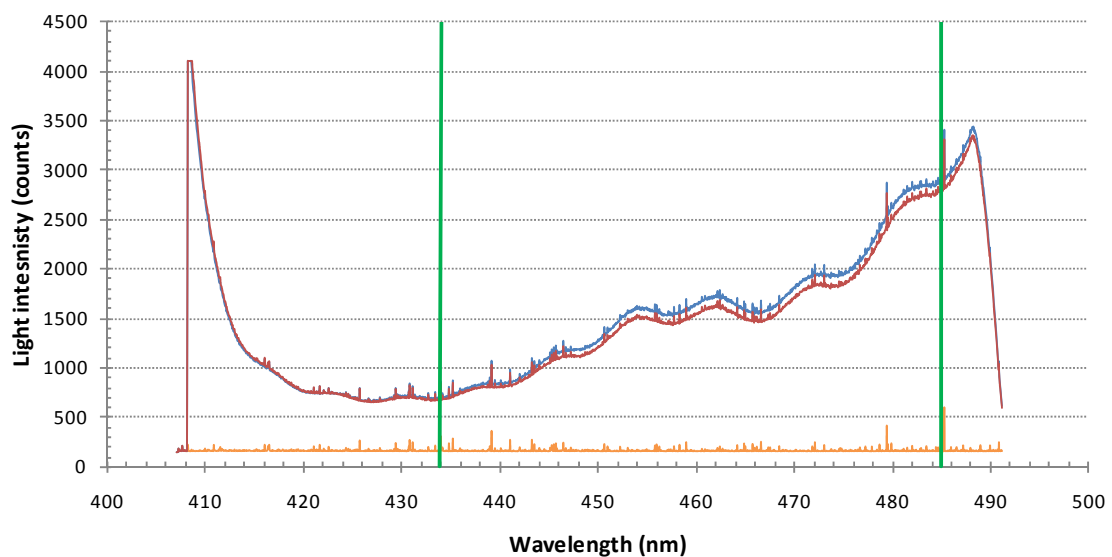


Figure 6.18 Light intensity throughput of the BBCEAS cavity measured at LAMP on 24th July 2007. Blue trace shows the nitrogen filled/ background cavity measurement (I_0) and the red trace shows an atmospheric sampled measurement (I), note the lower counts in the red spectrum indicating absorption and/or aerosol scattering in the ambient air sample. The orange trace is a measure of the dark current on the detector. The green vertical lines show the subsection of data used in analysis for trace gas species presence and quantification.

The hours of BBCEAS operation during LAMP are shown in table 6.3. This figure illustrates the high level of data coverage achieved by the BBCEAS instrument. Measurements were recorded between the 24th July 2007 and 14th August 2007. The instrument typically ran for over 24 hours unattended before an operator was required to again make background measurements and mirror reflectivity determination using the O₂-O₂ absorption bands. Typically background measurements and mirror reflectivity determination measurements took 1-1.5 hours. The sixteen periods of >24 hour continuous BBCEAS data obtained during LAMP enabled weekday/weekend trends to be observed and comparisons to be made between BBCEAS and the other in situ NO₂ monitors over an extended measurement period. Occasional extended downtimes (compared to usual BBCEAS operation) were due to limited site access and the consequent depletion, e.g. the compressed air cylinder used to purge the cavity's mirror mounts of ambient aerosol, for example between July 30th and 2nd August 2007.

	00:00	01:00	02:00	03:00	04:00	05:00	06:00	07:00	08:00	09:00	10:00	11:00	12:00	13:00	14:00	15:00	16:00	17:00	18:00	19:00	20:00	21:00	22:00	23:00	
24/07/2008																		FO							
25/07/2008											FO							FO							
26/07/2008									FO													FO	A	F	O
27/07/2008												FO			FO										
28/07/2008													FO												
29/07/2008																									
30/07/2008																								FO	
31/07/2008																									
01/08/2008																									
02/08/2008					A		FO											FO							
03/08/2008											FO														
04/08/2008																									
05/08/2008																		FO							
06/08/2008																					A		FO		
07/08/2008										FO								FO							
08/08/2008														FO											
09/08/2008																								FO	
10/08/2008																									
11/08/2008					FO	A												FO							
12/08/2008													FO												
13/08/2008												FO	FO												
14/08/2008					FO	A																			

MEASURING OPEN PATH
 MEASURING NOXY CALIBRATION SOURCE
 DATA POSSIBLE CORRUPT, CAVITY MIRROR MOVED DURING RUNNING

Table 6.3. BBCEAS operating coverage during LAMP. Dark blue filled squares illustrates when the instrument was sampling air. The Letters F and O denote when background nitrogen flush and oxygen measurements were made for calibration of the cavity mirror reflectivity.

6.5.2 BBCEAS measurements during LAMP.

This section details how the BBCEAS instrument was operated during LAMP to make the $I(\lambda)$, $I_0(\lambda)$ and mirror reflectivity, $R(\lambda)$, measurements needed to obtain concentrations of molecular absorbers. All BBCEAS measurements during LAMP were made using the Ocean Optics SpectraSuite software supplied by the manufacturer. Throughout the course of LAMP, background measurements and mirror reflectivity measurements were recorded between once and twice per day in order to ensure that any changes in the cavity mirror alignment and/or the LED's emission spectrum were captured, and accurate mirror reflectivity curves were available for use in analysis. Inspection and comparison between sequential background $I_0(\lambda)$ measurements also showed if the cavity mirrors had "dirtied" or moved from optimal alignment, enabling

any necessary cleaning of the mirror surfaces and re-alignments to be made in order to provide data of a continuously high standard.

The different measurements required in BBCEAS for quantitative analysis have slightly different methods for recording spectra. The next section describes how each measurement was made during LAMP.

6.5.2.1 Operating parameters for ambient measurements

To calculate the sample absorbance from BBCEAS data, both a background measurement and a sample measurement are required along with knowledge of the mirror reflectivity, as discussed in chapter 2.

The cavity mirror mounts used during LAMP introduced a light flow of zero air from cylinder source across the cavity mirror surface to minimise foreign particle deposits onto the mirror surface thereby enabling longer operating times for the instrument. During LAMP, the mirror purge flow was set to 1.2 s.l.p.m (standard litres per minute). This purge gas fills the mirror mount region, and thus a length factor of $R_L = 1.258$ is included in the analysis to account for the sample gas being excluded from the sections of the cavity during the ambient air measurements. This calculation uses the geometric measurements for the total cavity length, 115cm, and the section of the cavity open to sample during measurements, 91.4cm; $115 \text{ cm}/91.4 \text{ cm} = 1.258$. Separate measurement of the length factor performed by measuring the increase in the O_2O_2 band's intensity when flushing the mirror purge regions with oxygen

produced a length factor of 1.32, agreeing to within 5% with the geometric length factor.

The background, $I_0(\lambda)$, measurements were made while the section along the light path between the open ends of the cavity mirror mounts was enclosed by a section of rigid plastic tubing supported between the mirror mount enclosures. The enclosed cavity was then purged with zero air (flowed at 3 s.l.p.m), introduced via a gas fitting in the centre of the plastic tube for several minutes to expel atmospheric air before $I_0(\lambda)$ data was recorded. The light intensity exiting the cavity was recorded over an integration time specified by the operator in the spectrometer's SpectraSuite user interface and was saved to a laptop computer. Throughout LAMP a minimum of 10 background files were saved, where each file saved was an average of 30 scans of two seconds integration time each to produce one data file per minute. File names were defined in the same way as during BIOFLUX II –see chapter 5.

For ambient air sampling (i.e. recording the $I(\lambda)$ spectra), the BBCEAS instrument was operated “open-path” with ambient air passing freely between the cavity mirror enclosures, as shown in the photograph in figure 6.15 above. The same operating parameters, (integration time and number of scans averaged) were used for the $I(\lambda)$ spectra as for background $I_0(\lambda)$ spectra, except the software was set to acquire continuously until interrupted by the operator at a later time.

6.5.2.2 Operating parameters for O₄ calibration measurements to determine mirror reflectivity curve

Throughout LAMP, O₂O₂ calibration spectra in pure oxygen samples were recorded at least once every 24 hours to check for any degradation in the cavity mirror reflectivity and to check for any changes in the cavity mirror alignment. The O₂O₂ calibration spectra informed when the cavity mirrors needed cleaning and the cavity re-aligning, and contributed towards keeping the instrument operating at its optimum sensitivity.

The cavity mirrors (Layertec GmbH #100859, 12.5mm diameter) had undergone extensive testing in the laboratory to define the shape of the mirror reflectivity curve shape prior to the LAMP campaign by recording BBCEAS spectra of NO₂ samples diluted to various concentrations in air or nitrogen. Thus in the field measurement, it was sufficient to just record BBCEAS spectra in pure oxygen in order to determine the absolute mirror reflectivity at the O₂-O₂ band wavelengths and then scale the lab-derived mirror curve accordingly.

Pure oxygen from a gas cylinder was flowed continuously through the cavity and the light intensity transmitted by the cavity was measured for the same acquisition time and averaging protocol as the background measurement. The oxygen filled cavity measurement and the background measurements were then used to calculate the absorbance due to O₂-O₂ and wavelength-independent scaling factor applied to multiply $1-R(\lambda)$ such that DOAS fitting of the O₂-O₂ BBCEAS spectrum retrieved the correct concentration of the oxygen dimer (effectively, this process shifts the mirror curve's position up/down on the reflectivity axis). An example of a fitted O₂-O₂ absorption spectrum is shown in figure 6.19. The flush gas used during LAMP was

compressed (zero) air which contains 20.7% oxygen. Thus contrary to previous chapters in which an O₂-O₂ mixing ratio of unity is retrieved for a correctly calibrated mirror curve, here the target for the fitted amount here is $1 - 0.207^2 = 0.957068$ rather than unity, as air used as flush gas contains 20.7 % oxygen, thus representing the relative difference in O₂-O₂ mixing ratio in air and pure oxygen.

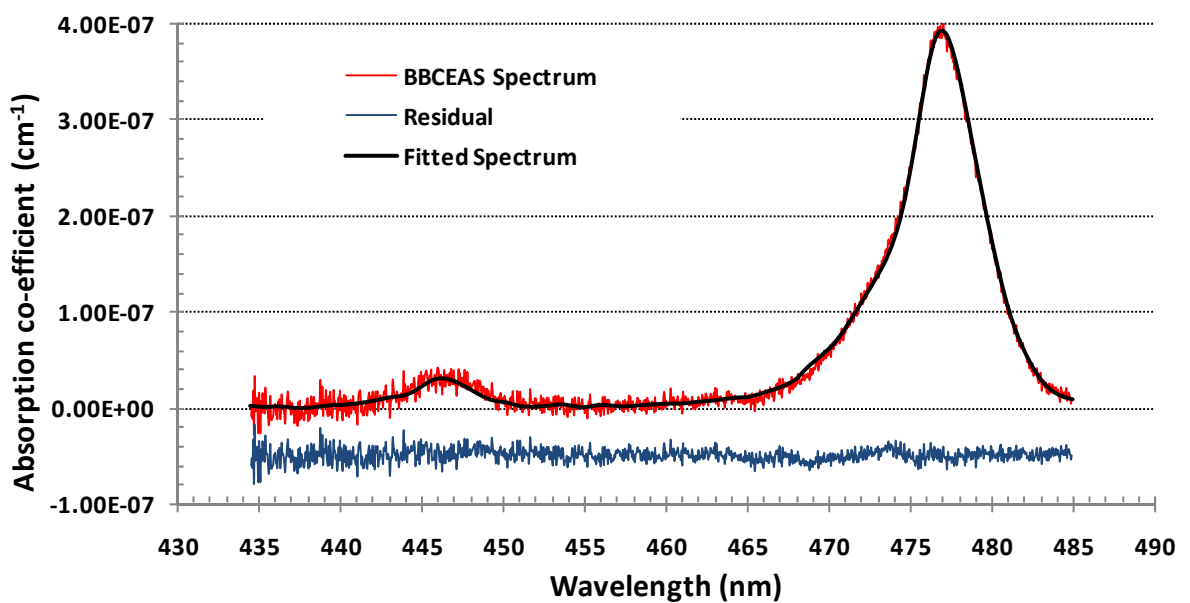


Figure 6.19. Calibration of cavity mirror reflectivity by fitting the O₂-O₂ absorption bands in a BBCEAS spectrum of pure oxygen with the Hermans[Hermans, 2008] absorption cross sections. Calibration measurements made on 24th July 2007. The fitted amount is 0.9719 ± 0.0022 and the standard deviation of the residual spectrum is $6.62 \times 10^{-9} \text{ cm}^{-1}$. The residual spectrum is shown with an offset of $5 \times 10^{-8} \text{ cm}^{-1}$ for clarity.

6.5.3 Mathcad analysis routine details

The home written analysis routine in Mathcad software package imports the BBCEAS recorded data (background, sample and calibration measurements for the day) along

with literature absorption cross section files for the target absorber species, for the LAMP measurements the cross sections used are those used in the analysis of BIOFLUX II data, and are shown in chapter 5.

The Mathcad routine is similar to the description in chapter 5 section 5.5.3, with the parameters of the LAMP spectra implemented within the routine. Data was analysed on a one minute timescale with no further averaging of the BBCEAS $I(\lambda)$ files. The absorbance due to NO_2 was the first species in the fitting routine due to its strong absorption at these wavelengths. The absorption spectrum for $[\text{NO}_2]$ at 5 ppbv was shown in figure 6.20. Other molecules that also have structured absorption bands in this wavelength region are water vapour, which has weak absorption bands in this window, and the oxygen complex $\text{O}_2\text{-O}_2$, present in the atmosphere at 20.7%. $\text{O}_2\text{-O}_2$ is removed automatically in these BBCEAS measurements as a consequence of using synthetic air as the flush gas for background measurements: the $\text{O}_2\text{-O}_2$ absorption signal is present at atmospheric concentrations in both the background and the sample measurement and thus cancels out when calculating the sample's absorption coefficient. The residual spectrum remaining after subtraction of the fitted NO_2 spectrum and the aerosol extinction continuum can then be fitted for other molecules/ absorbing species that may be present in the sample, for example water vapour and glyoxal.

6.6. Spectral analysis: NO₂ retrievals and time series

The MathCAD analysis routine used to analyse the LAMP BBCEAS data provides a time series of concentrations for the molecular species included in the fitting routines. Each data point in the time series has an associated fitted absorption spectrum for each of the gas phase species fitted. The BBCEAS spectra were analysed at their native 1 minute time resolution (single file analysis) for the duration of BBCEAS measurements. Examples of the NO₂ BBCEAS spectra are shown in figures 6.20 and 6.21 and the LAMP time series from which they are taken is shown in section 6.22.

Recorded at high ambient NO₂ concentration, spectrum 6.20 shows the very obvious spectral signature of NO₂. Figure 6.21 shows one of the lowest NO₂ concentrations observed during LAMP, yet the absorption features of NO₂ are still readily apparent. These spectra illustrate the range of NO₂ concentrations observed over the course of LAMP, and the quality of the BBCEAS measurements and the spectral fitting process.

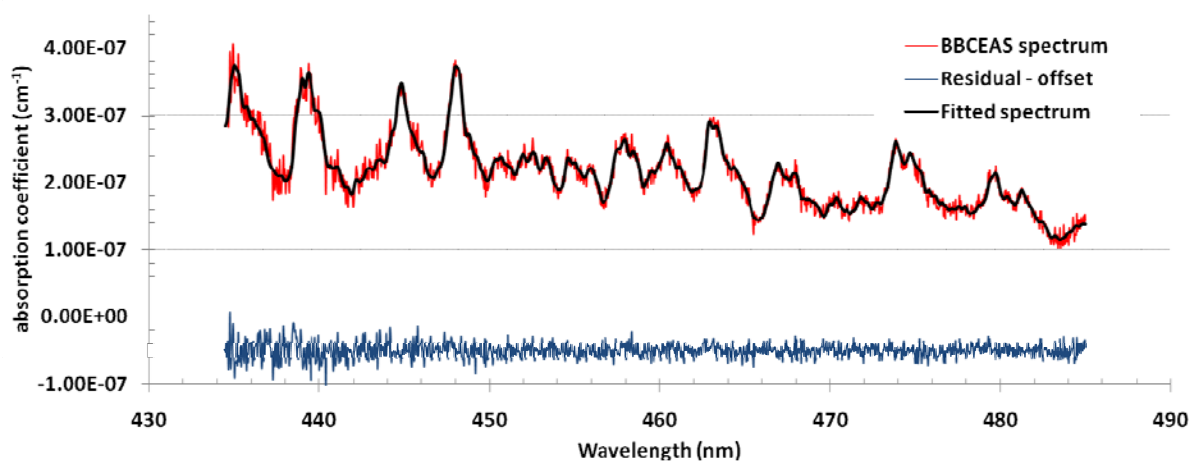


Figure 6.20. BBCEAS spectrum of ambient NO₂ (red) and spectral fit (black) from the evening of 24th July 2007. This spectrum is #160 in the time series corresponding to 20:24hrs (GMT). The fitted NO₂ amount is 20.4ppb +/- 0.182 ppb. The standard deviation of the residual spectrum is 1.003x10⁻⁸ cm⁻¹ and is shown offset from the BBCEAS spectrum by 5x10⁻⁸ cm⁻¹.

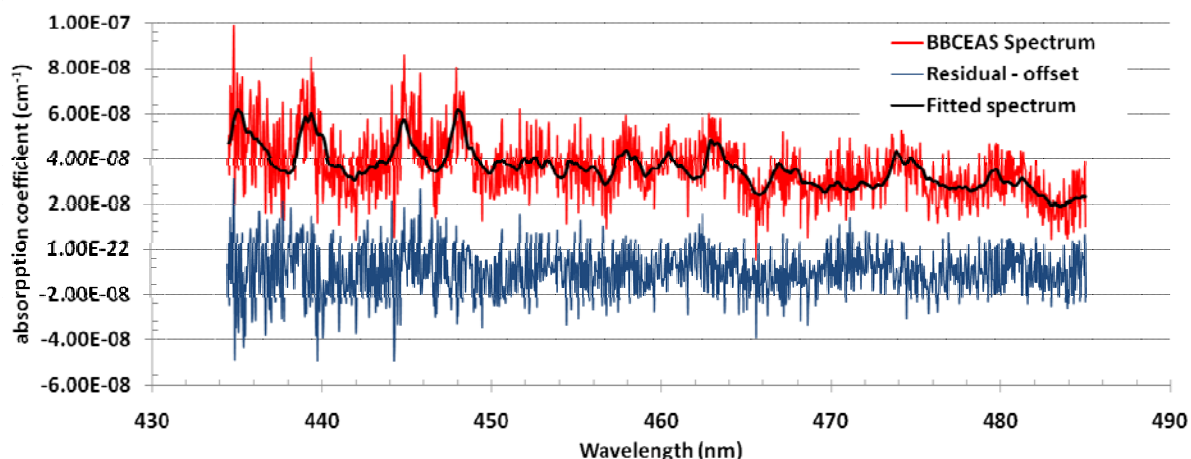


Figure 6.21. BBCEAS spectrum of ambient NO₂ (red) and spectral fit (black) from the evening of 24th July 2007. This spectrum is #53 in the time series corresponding to 19:25hrs (GMT). The fitted NO₂ amount is 3.38ppb +/- 0.181 ppb. The standard deviation of the residual spectrum is 1.003x10⁻⁸ cm⁻¹ and is shown offset from the BBCEAS spectrum by 1x10⁻⁸ cm⁻¹.

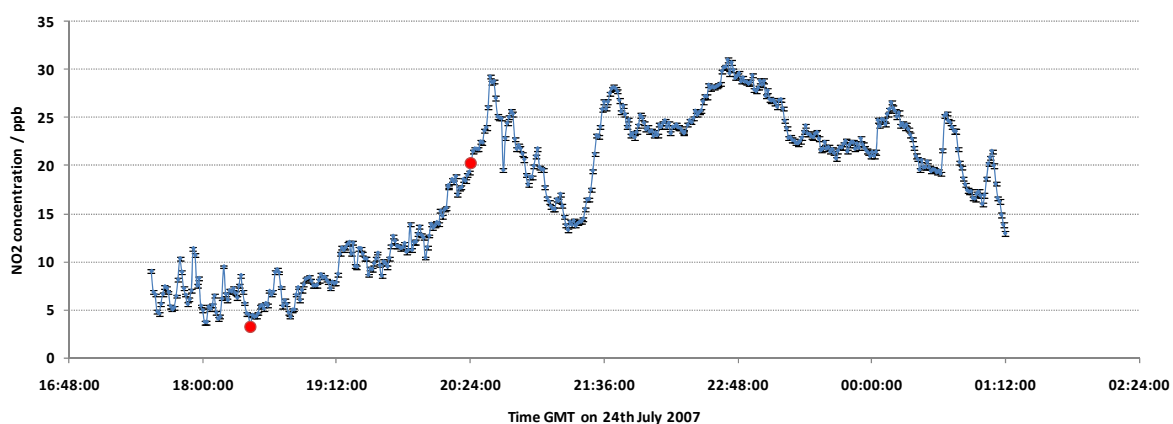


Figure 6.22. Time series from BBCEAS data recorded 24th July 2007. The spectra shown in Spectrum 6.20 and 6.21 correspond to the highlighted red dots.

The total campaign time series of BBCEAS data (analysed at the highest time resolution possible under the constraints of the measurements of 1 minute data frequency) is shown in figure 6.23 and 6.24. The time series illustrates the capability of the BBCEAS

instrument to measure rapidly varying NO₂ concentrations, from low ppbv to several tens of ppbv.

The first two panels (figure 6.23) show the BBCEAS NO₂ concentration alongside the NO_{xy} chemiluminescence instrument's measurements of NO₂ at 10 m sampling height. This subset of the data will be used for direct instrument comparison discussed later in section 6.7. The dark red trace in the remainder of the panels of Figures 6.23 & 6.24 shows the NO_{xy} data sampled at 3 m. This data set is significantly different from the BBCEAS data, and the reasons for these differences are discussed in section 6.8. The grey trace in each panel shows the ozone concentration from the TEI 49C ozone instrument.

A typical diurnal variation of NO₂ is observed in the BBCEAS data, as would be expected in an urban environment. There are additional broad NO₂ concentration peaks which coincide with local commuter times. Short duration spikes of increased NO₂ are also observed throughout the LAMP BBCEAS measurements.

In general the diurnal cycle is driven by shifts in the NO_x photochemical steady state. The NO₂ concentration is generally greatest at night as photolysis is not converting NO₂ to NO; following sunrise (shown by yellow points in figure 6.23) the NO₂ concentration decreases as it is photolysed. NO₂ increases over the course of the day as the ozone concentration builds and the NO + O₃ → NO₂ + O₂ reaction starts to compete with the NO₂ destruction by photolysis. The NO₂ concentration peak during morning rush hour is due to increased traffic emissions of NO₂ coupled with reactions of NO_x species and the regularly observed evening peak in NO₂ is attributed to additional traffic emissions during the evening rush hour.

The short bursts of higher NO₂ concentrations on the minute timescales, seen on top of the broader diurnal cycle, indicate localised sources of NO₂ close to the measurement site. This is observed more clearly by looking at smaller subsets of the time series as shown in figure 6.25. The subsection of the NO₂ time series shown in figure 6.25 highlights some of the more pronounced NO₂ spikes seen during the campaign. These bursts of increased NO₂ concentrations each last for between 5 and 20 minutes and coincide with drops in ozone, indicating these emissions probably contained NO. This NO₂ spiking is observed in both the BBCEAS and NO_{xy} time series indicating the source is local to the measurement site.

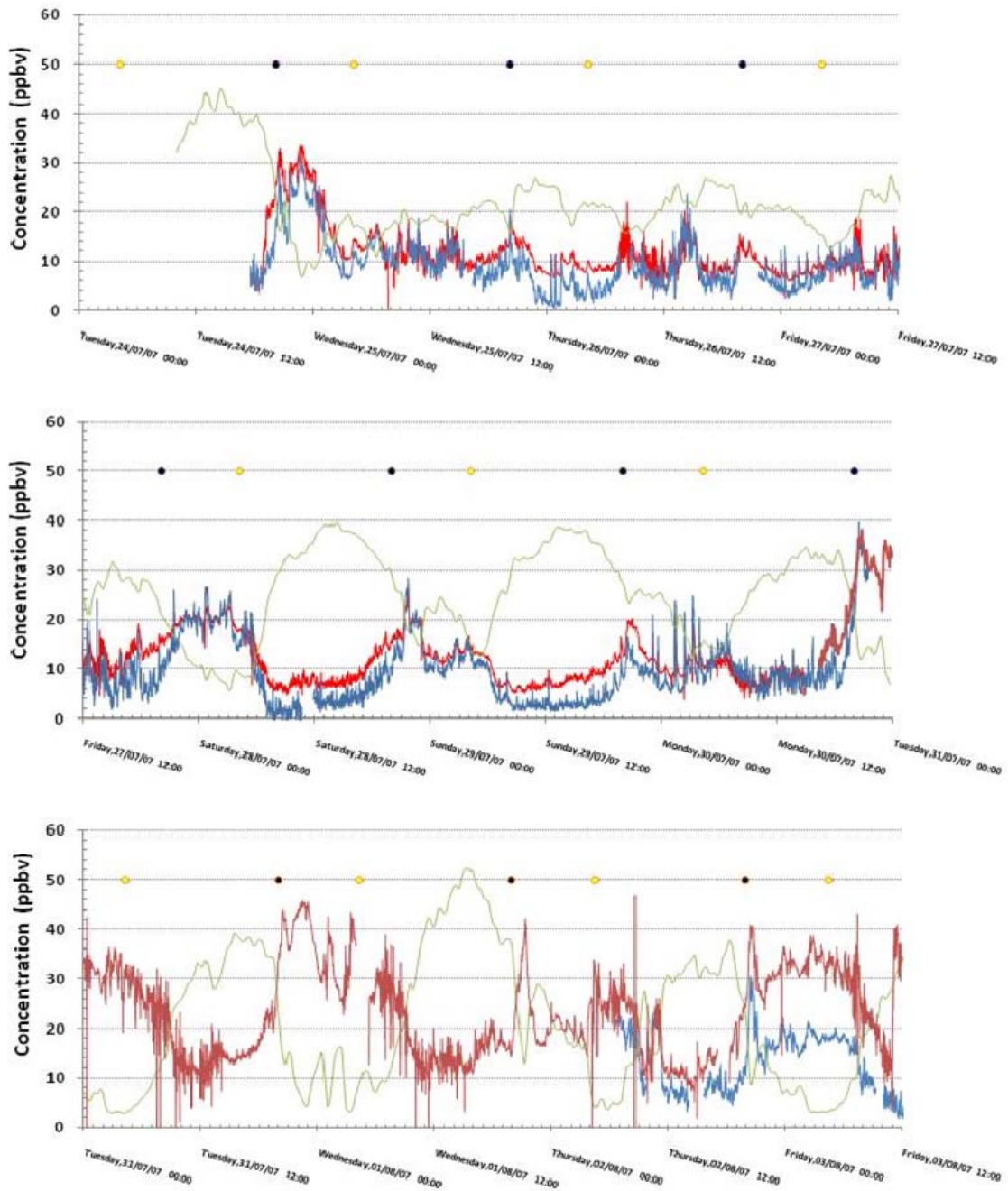


Figure 6.23. LAMP campaign time series for NO₂ and ozone concentrations from 24th July 2007 to 3rd August 2007. BBCEAS NO₂ is shown in blue, the NO_x data sampled at 10m height in bright red and sampled at 3m in dark red. Ozone data are the grey trace.

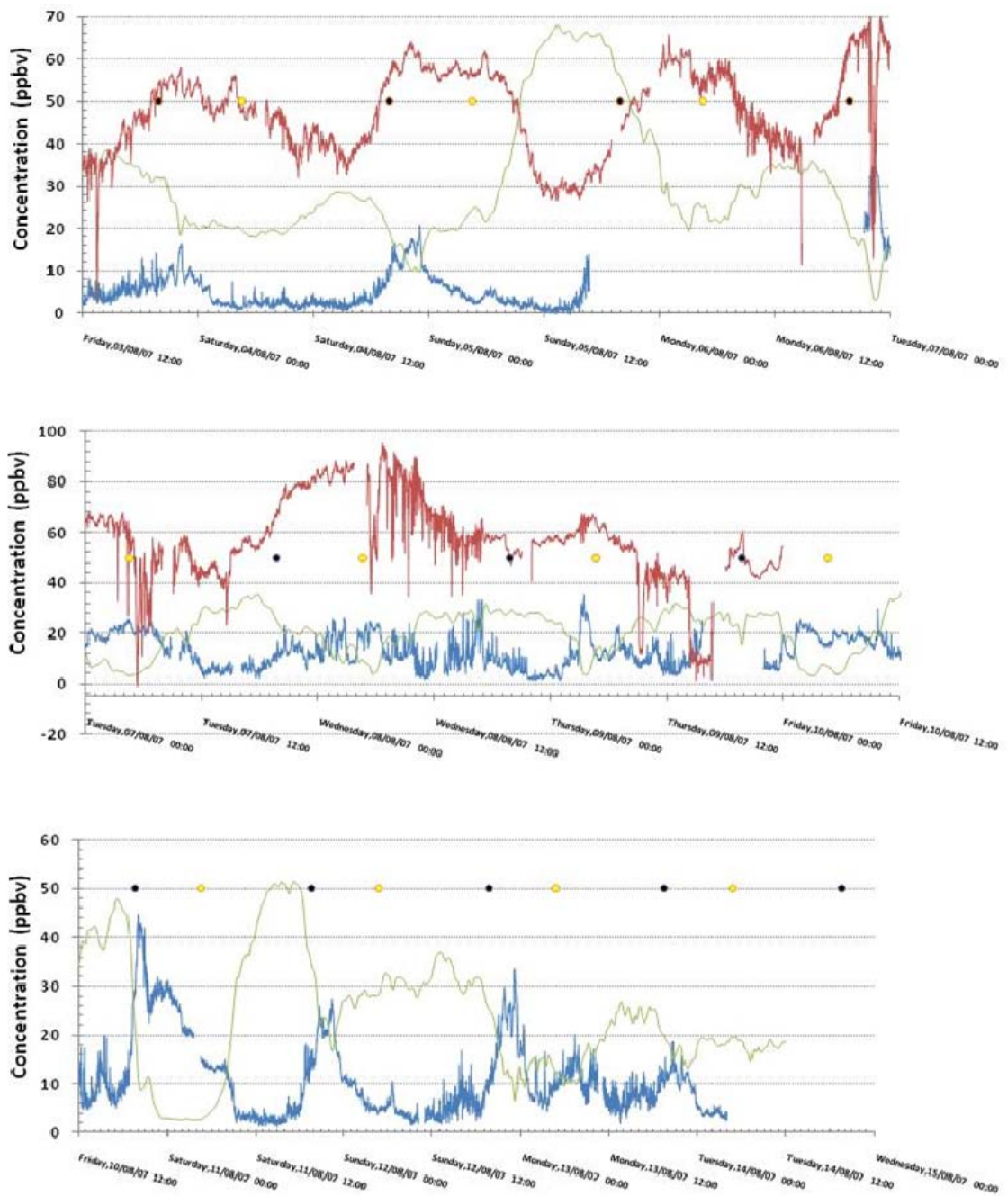


Figure 6.24. LAMP campaign time series for NO₂ and ozone concentrations from 3rd August 2007 to 14th August 2007. BBCEAS NO₂ is shown in blue, the NO_x data sampled at 3 m height in dark red. Ozone data are the grey trace.

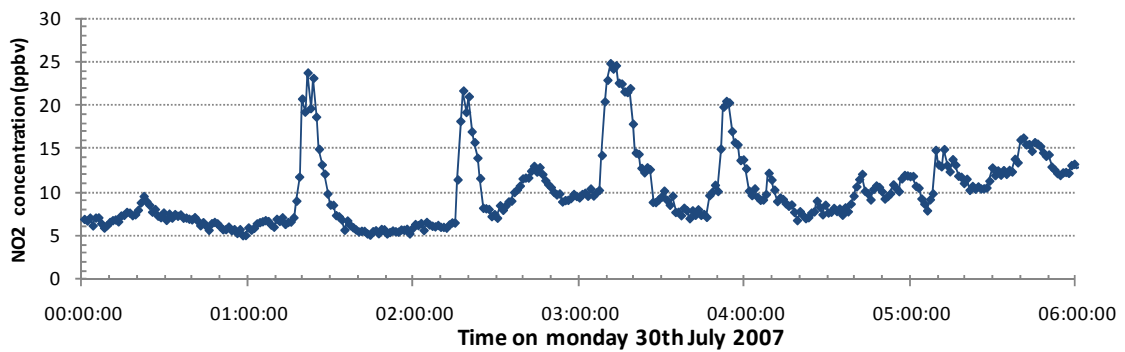


Figure 6.25 Subsection of the BBCEAS NO₂ time series on Monday 30th July 2007.

6.6.1 Weekday and weekend trends in NO₂ concentration

The BBCEAS data is shown in figure 6.26 has been divided according to the days of the week with week 1 of measurements shown by red points, week 2 as blue points and week 3 as green points, in order to identify any regular patterns through the data. Increases in NO₂ due to the photolysis rate decreasing are observed on the majority of evenings peaking between 8pm and 11pm. During the week days the morning rush hour can be observed as broad NO₂ peaks at 20-25 ppbv between 9am and 11am GMT Monday through to Friday, whilst this feature is not apparent in the data for Saturday and Sunday.

Weekend days have a more pronounced minimum NO₂ concentration which is prolonged during the daytime, while weekday trends show more variation and NO₂ spikes on top of the broad trends during the day. In many instances these weekday daytime NO₂ spikes can be as high as the NO₂ levels observed during the night, indicating greater NO_x emissions during the week. The NO₂ levels on Saturdays and Sundays are lower than weekday levels, indicating fewer emissions of NO₂ at the

weekend. The Saturdays match each other and the Sundays match each other far more reproducibly than week days. The greater variability on week days is likely to be due to more and larger emission sources, but those sampled at the LAMP site were likely to depend on many other factors e.g. wind direction.

Data recorded on two Monday's shows very similar patterns and values for NO₂ from 00:00hrs until 19:00hrs GMT, along with the coinciding spikes observed at regular intervals from 00:00 until 07:00hrs GMT. These early morning spikes are seen at similar times on Thursday and Friday during the first week of measurements (red points in figure 6.21). The presence of these spiked peaks during the weekdays only suggests a local source with effects only weekdays.

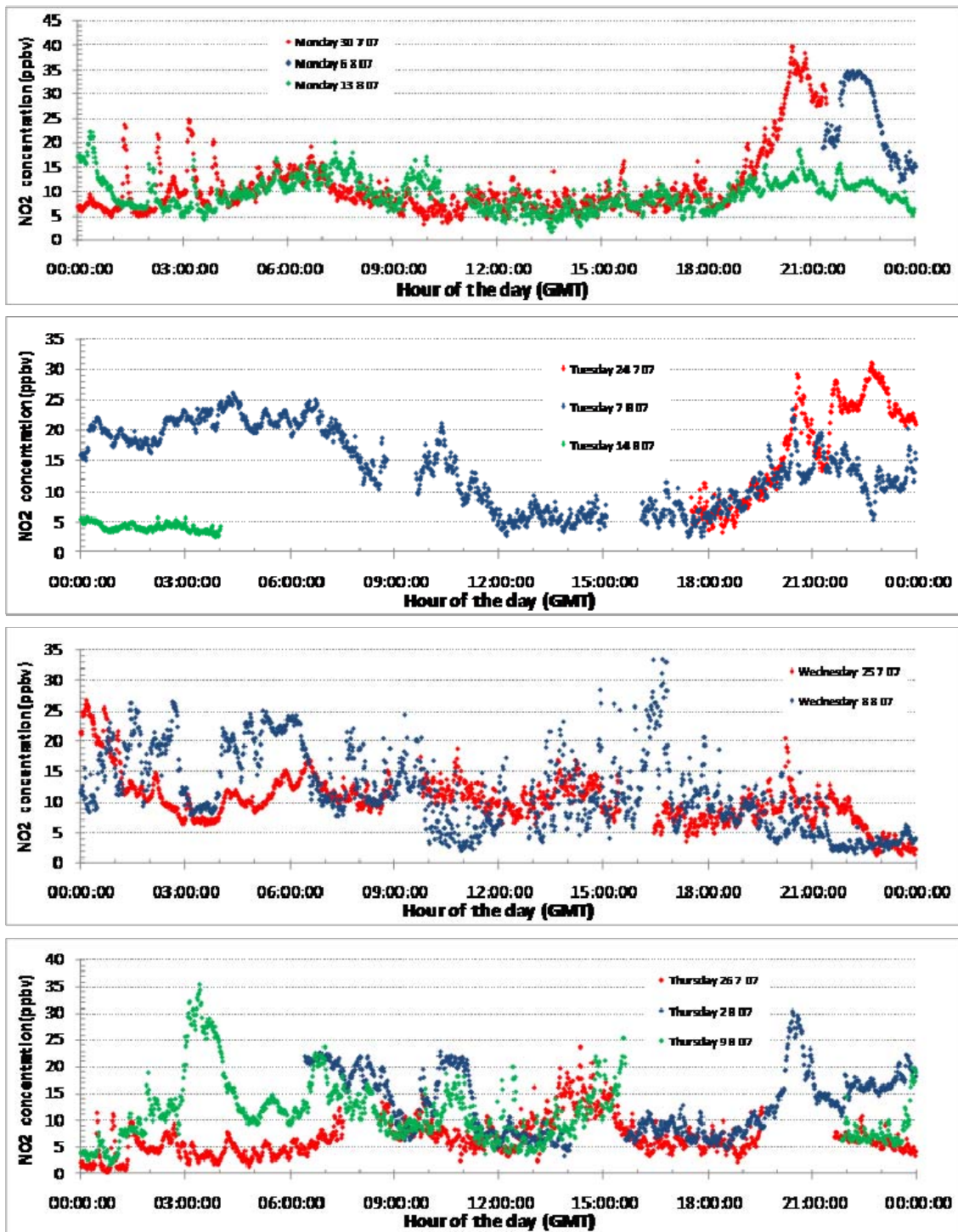


Figure 6.26 (continues over the page).

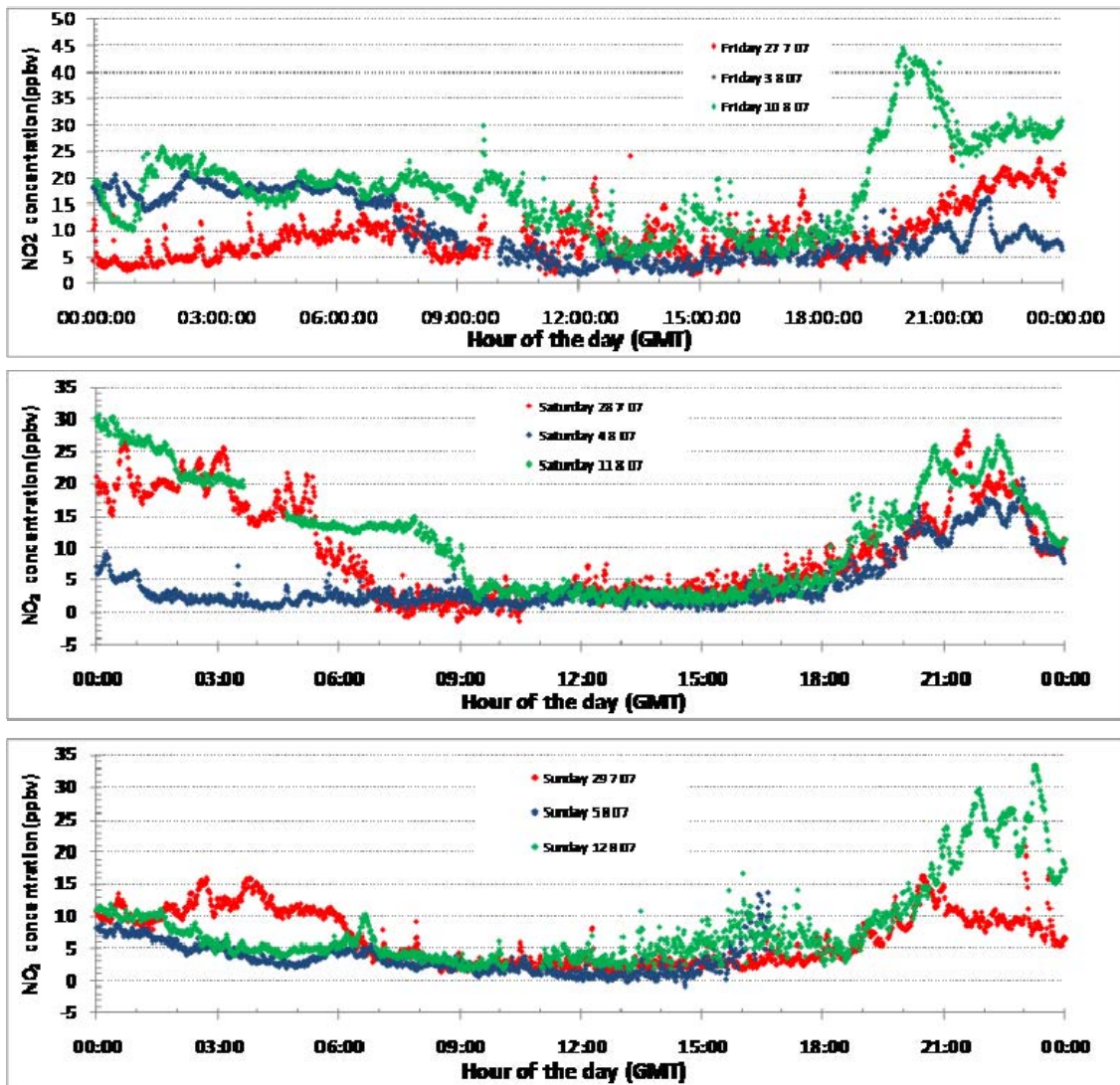


Figure 6.26 BBCEAS NO₂ concentration data plotted according to day of the week. The first week of the BBCEAS measurements are shown in red, the second week in blue and the final week in green points.

6.7 Comparison of NO₂ measurements from BBCEAS and other in situ monitors

Two additional NO₂ data sets are available for comparison with the BBCEAS data; the “state-of-the-art” NO_{xy} photolysis-chemiluminescence instrument (York University) and the commercial chemiluminescence detector from Leicester City Council. The CMAX DOAS data is not available for the time period of the BBCEAS measurements.

6.7.1 Comparison of BBCEAS NO₂ measurements to NO_{xy} photolysis-chemiluminescence instrument NO₂ measurements

The one minute BBCEAS dataset and the NO_{xy} data sampled at 10 m and 3 m height is shown above in figure 6.23. When the two instruments operated simultaneously sampling from a common 10 m height (blue and bright red traces in figure 6.23), the data sets exhibit strong similarities. The importance of co-locating the sampling position for multiple instruments measuring the atmospheric concentrations of short lived species has already been noted in the BIOFLUX II work presented in chapter 5 of this thesis, and it is apparent again here when comparing BBCEAS and NO_{xy} data from LAMP. The close similarities between the BBCEAS and NO_{xy} data is degraded in the second part of LAMP when the NO_{xy} inlet moved to sampling at 3 m (non co located positions) shown by the blue and dark red traces in figure 6.23.

The BBCEAS and NO_{xy} were operated from 24th July 2007 to 30th July 2007 sampling from similar positions as shown in figure 6.12, with the NO_{xy} sampling from the mast at approximately 10 m above ground level. Comparing the data sampled at similar position shows the same trends in NO₂ concentration increase and decrease at the same times and very short timescale spikes in NO₂ concentrations are observed simultaneously. Periods with particularly excellent agreement between the instruments were observed on the 25th, 26th, 27th and 29th July, and these periods are shown in greater detail in figure 6.27.

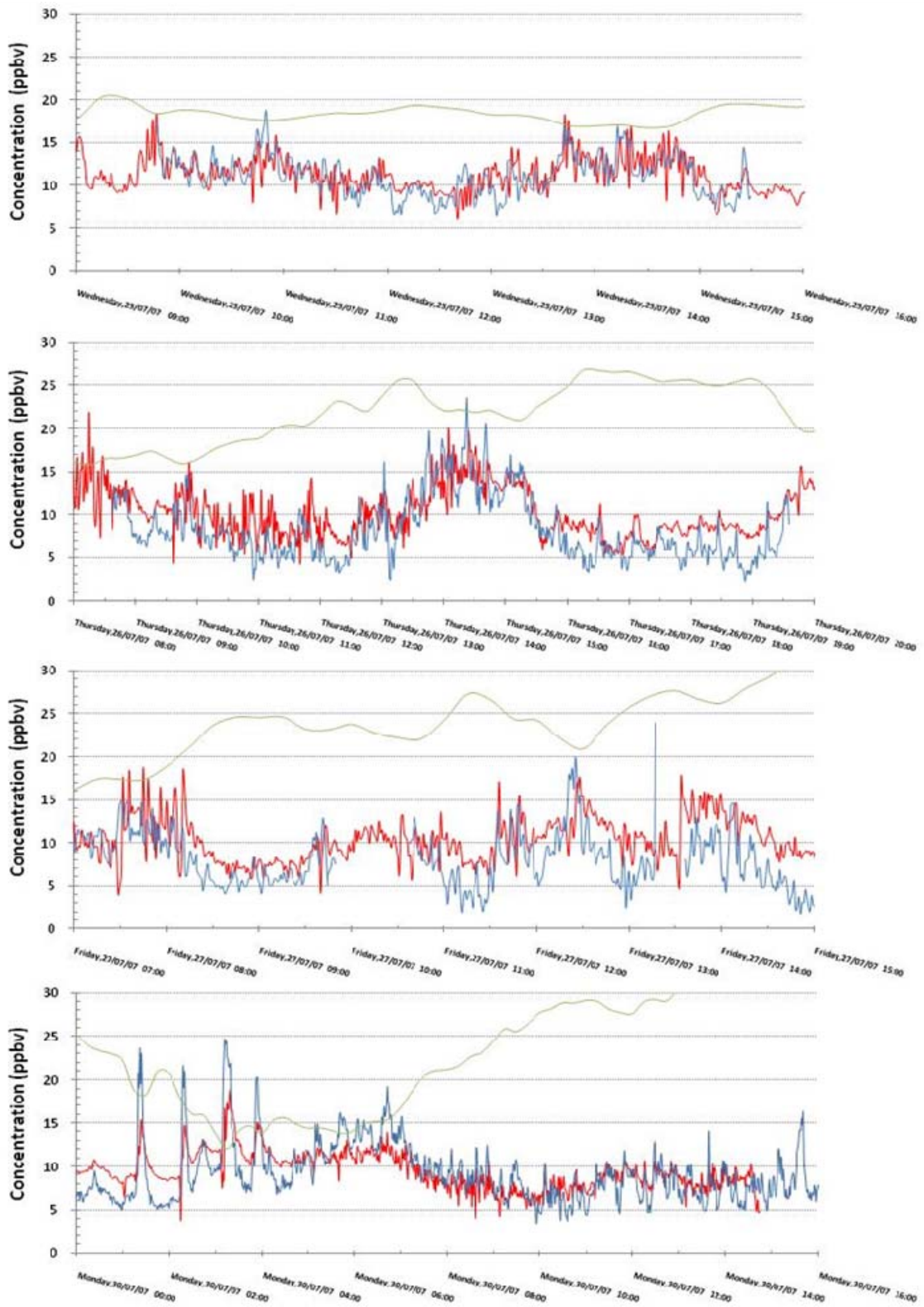


Figure 6.27 LAMP measurements of BBCEAS and NO_{xy} where strong agreement is observed.

BBCEAS is shown by the blue trace and NO_{xy} by the red trace.

This inter comparison period also shows differences in the absolute concentrations over long periods and in the detail of the fast NO₂ spikes. The fast NO₂ spikes in the 1 minute BBCEAS data series are concurrent with spikes in the NO_{xy} data shown in the first two panels of figure 6.24. Particularly obvious NO₂ spikes are observed between 00:00-02:00hrs Thursday 27th July, 22:00hrs 27th July to 06:00hrs on Friday 28th July and from 22:00hrs on Sunday 29th July to 05:00hrs Monday 30th July. The NO₂ spikes during the early hours of Monday the 30th July are shown in greater detail in the bottom panel of figure 6.22. The BBCEAS spikes rise sharply over 2-3 minutes and the NO₂ concentration remains high for 5-10 minutes before falling sharply back to a similar level as just prior to the spike. The NO_{xy} data shows spiking NO₂ at the same time, however the increase occurs over 4-5 minutes and peaks lower than BBCEAS. The shape of the tail of the NO₂ spike in the NO_{xy} data is more prolonged compared to the BBCEAS data, lasting for 10 to 15 minutes. This difference may be caused by the effective response time of the NO_{xy} instrument being less than the BBCEAS instrument. In the NO_{xy} instrument, a photolytic converter dissociates NO₂ to NO before chemiluminescent detection, and the finite residence time for the gas sample to pass through the converter before detection could cause a large, sharp spike in NO₂ concentration to become spread over a longer timescale, e.g. as gas already inside the converter is diluted by the influx of other gas with a vastly different composition. The BBCEAS system operates with the air sample flowing freely across light path of cavity, and ought not to suffer from such effects. Thus the differences observed in the detail of the NO₂ spike features are possibly due to different effective sampling times within the instruments.

There are long periods during the inter comparison dates where the BBCEAS systematically measures lower than the NO_x. One example of this happened on Tuesday 24th July to Wednesday 25th July, as shown in figure 6.28. The instruments agree well at the start and end of this sequence, while the data sets vary during the middle section. This difference is not due to BBCEAS instrument instability (such as the cavity losing and then regaining its alignment) because the continuum absorption retrieved from the BBCEAS spectrum during this time shows a steady small increase. Similar disagreements are observed on the night of the 25th-26th July, 26th – 27th and later parts of 29th July. This suggests that there may be another atmospheric species that is being detected as extra NO₂ in the NO_x instrument, but that is not identifiable by the spectroscopic BBCEAS measurement which is highly specific to NO₂.

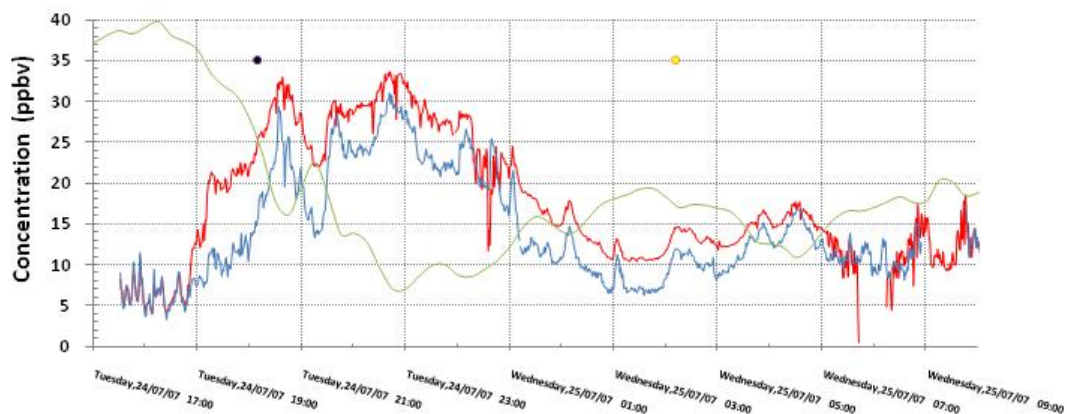


Figure 6.28 BBCEAS data (blue trace) and NO_x data (red trace) for Tuesday 24th July to Wednesday 25th July. Note the excellent agreement at the start and end of this time series, and the rather weaker agreement in between.

A similar observation was made by Dunlea [Dunlea *et al.*, 2007] when comparing spectroscopic (tunable infrared diode laser system) and chemiluminescence

detectors monitoring NO₂. The spectroscopic TDLAS instrument recorded lower NO₂ concentrations compared to the chemiluminescence detectors with discrepancies between 10-20 ppbv [Dunlea et al., 2007]. This is larger than the discrepancies between the BBCEAS and NO_{xy} observed during LAMP which range from 2 -6 ppbv. Dunlea report these discrepancies coincided with high concentrations of NO₂ species (specifically HNO₃ and PAN) which are (partially) converted by the catalytic converter to produce additional NO₂ and hence contribute an extra, false NO₂ signal. There is a possibility that the NO_{xy} instrument's photolytic converter can also produce a false positive, albeit a smaller interference since photolysis ought to be a more discriminating conversion method, and hence provide a reason for the differences observed between the BBCEAS and NO_{xy} techniques. The possibility that similar interference is acting within the NO_{xy} instrument is explored in section 6.7.1.1. The differences in NO₂ mixing ratio between BBCEAS and NO_{xy} are compared to ambient ozone levels in a similar manner as Dunlea [Dunlea et al., 2007].

6.7.1 .1 Exploring the correlation of O₃ with NO_x data.

Previous instrument comparisons for NO_x monitors highlighted that interference can act within chemiluminescence detectors. This interference is observed as a discrepancy between the retrieved NO₂ concentration from chemiluminescence detectors and spectroscopic instruments (Dunlea et al 2007). The interference has been observed regularly (daily) peaking in the afternoon; coinciding with peak ozone concentration. The interference was calculated using the simple metric shown in

equation 6.3, which assumes only the chemiluminescence detector experiences the interference.

$$\text{Interference} = \text{chemiluminescence detector } [NO_2] - \text{Spectroscopic } [NO_2] \quad \text{Equation 6.3}$$

The Dunlea study investigated possible sources for the interference, concluding “a combination of photochemically produced nitric acid and alkyl and multifunctional alkyl nitrates” were the primary cause of the observed interference. The correlation between the interference and ozone is thus due to the photochemical production mechanisms of both ozone and the interfering nitrogen species.

A similar analysis has been applied to LAMP data sets from the NO_{xy} and the BBCEAS determined NO_2 concentration. The data set were averaged to a comparable time scale of 15 minute data acquisitions (shown in figure 6.29). This figure highlights the discrepancies between the two techniques, monitoring the same airflow. The interference was calculated in the same way as the Dunlea study using equation 6.3, with the NO_{xy} data being the chemiluminescence detector and the BBCEAS as the spectroscopic detector. The resulting “interference” is shown alongside ambient ozone levels during the concurrent measurement period of LAMP in figure 6.30, indicating the interference in the NO_{xy} measurement may also be photochemically produced. The correlation between the calculated interference and ambient ozone concentration for the total LAMP measurement period, 24th -30th July 2007, gives a fair correlation ($R^2=0.19$) (see figure 6.31). Whilst correlations of individual days give fair to good correlations ($R^2= 0.176, 0.0018, 0.434, 0.554, 0.547$) as shown in table 6.4.

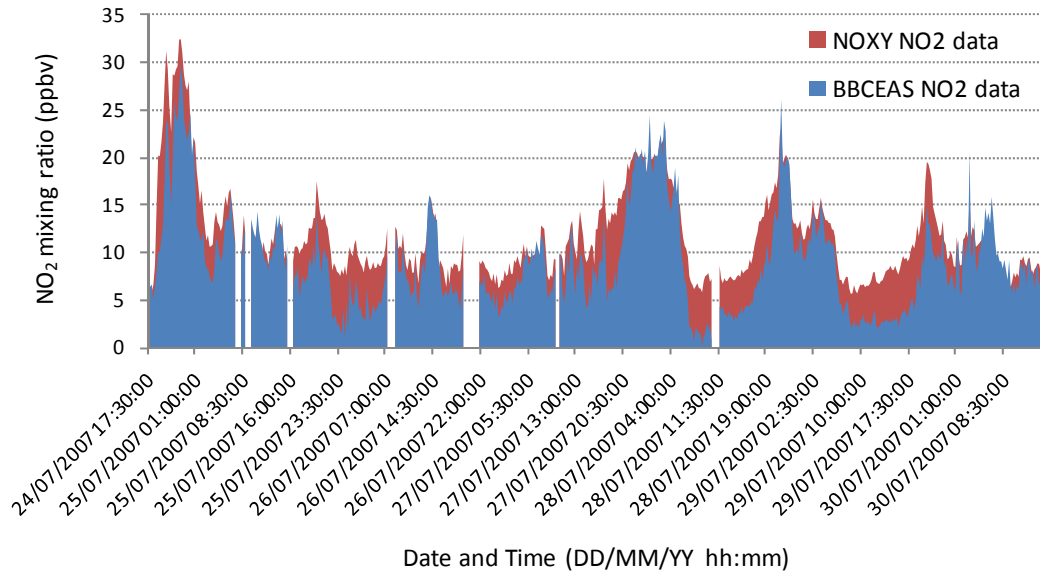


Figure 6.29 Time series of NO₂ measurements by the NO_xy instrument and the BBCEAS instrument during LAMP 2007.

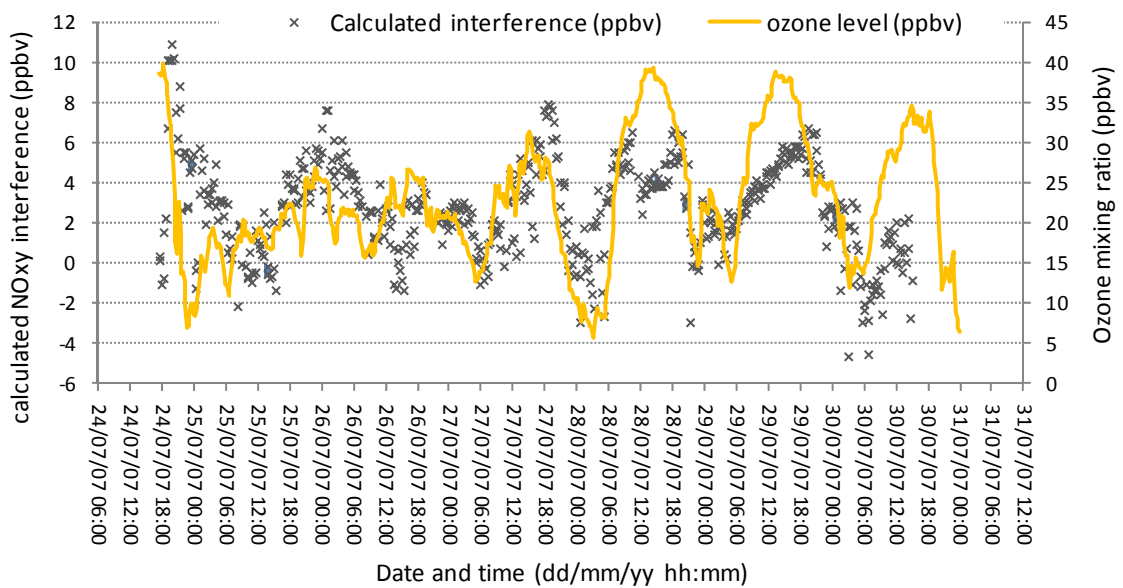


Figure 6.30 the time series of the calculated NO_xy interference (grey) and ambient ozone level (yellow trace)

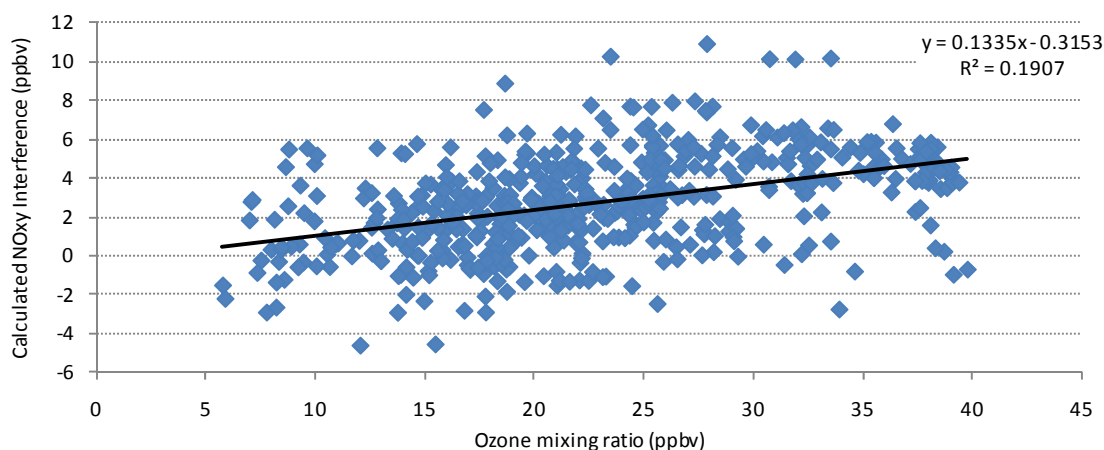


Figure 6.31 Correlation for the interference versus ambient ozone for measurements recorded between 24th and 30th July 2007.

Date of measurements	Slopes of correlation plots of interference versus O ₃ levels. R ² values for fits are given in parentheses.
Wednesday 25 th July 2007	0.208 (0.176)
Thursday 26 th July 2007	0.028 (0.008)
Friday 27 th July 2007	0.262 (0.434)
Saturday 28 th July 2007	0.156 (0.554)
Sunday 28 th July 2007	0.166 (0.547)

Table 6.4 Slopes of daily correlation plots for interference and ozone levels. R² values for fits are given in parentheses.

This interference calculation and comparison of interference with ambient ozone produces correlations similar to those observed by Dunlea during the investigation of possible interference species [Dunlea *et al.*, 2007]. It strongly suggests that similar interference species (nitric acid and alkyl and multifunctional alkyl nitrates) formed photochemically, may act within the NO_x instrument to give higher NO₂ concentrations observed between the 24th and 29th July 2007.

6.7.2 Comparison of BBCEAS NO₂ measurements to the commercial chemiluminescence detector instrument NO₂ measurements

The data from the BBCEAS and NO_{xy} instruments were averaged over 15 minute intervals to allow a direct comparison to be made with NO₂ measurements from Leicester City Council's commercial chemiluminescence monitor that was on the site from 24th-31st July 2007. This time series is shown in figure 6.32. All three data sets shows highly correlated time-dependent trends in NO₂ concentration. But the absolute agreement in the concentrations is better between the NO_{xy} and BBCEAS data, with the Council chemluminescence instrument systematically reporting lower NO₂ amounts. Surprising the chemiluminescence detector has the lowest values of NO₂, likely due to the different instruments sampling different air masses at 3 m for chemiluminescence, 10 m for BBCEAS and 10 m for the NO_{xy} instrument.

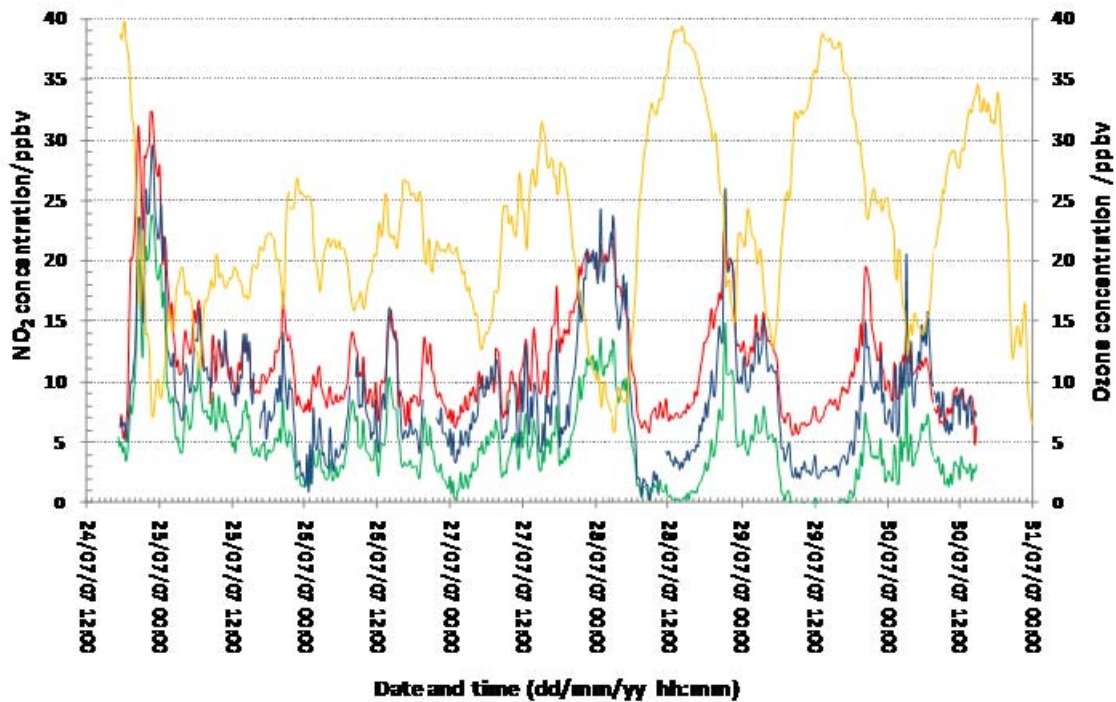


Fig 6.32. Data from BBCEAS instrument (blue trace), NO_x instrument (red trace), chemiluminescence detector (green trace) and Ozone data (yellow trace) averaged to 15 minute timescale.

6.7.3 Correlation of BBCEAS NO₂ with other NO₂ data sets

Correlation plots for the three NO₂ data sets are shown in figure 6.33. The correlation between each of the instruments is very high. The best agreement of NO₂ mixing ratio is between BBCEAS and NO_{xy}, (middle section of figure 6.33) shows a correlation coefficient of 0.79, an offset of -2.38 ppbv and a gradient of 0.9705, with the BBCEAS data retrieving lower concentrations for NO₂. However there is a quite a wide spread of data points around the 1:1 line (R^2 is a disappointing 0.7975), indicative of the higher NO_{xy} measurements during periods of high ozone – middle panel of Fig 6.22.

Regression between both BBCEAS and NO_{xy} to Council measurements produces large positive deviations from the 1:1 line and positive intercepts suggesting the council instrument, for some reason, systematically under-measures NO_2 . The correlation between the BBCEAS and the chemiluminescence instrument (bottom panel figure 6.30) has a correlation coefficient of 0.89 an offset of 3.12 ppbv and a gradient of 1.225 with the BBCEAS retrieving higher NO_2 concentration. The good R^2 value (and relatively good intercept) for the BBCEAS vs Council is fortuitous because the best fit line happens to bisect two distinct arms of data points in the scatter plot. The correlation between the NO_{xy} and chemiluminescence (LCC) measurements is shown on the top panel of figure 6.25 with a correlation coefficient of 0.8447, an offset of 6.44ppbv and a gradient of 1.0958, the NO_{xy} instrument typically retrieving higher concentration than the chemiluminescence detector.

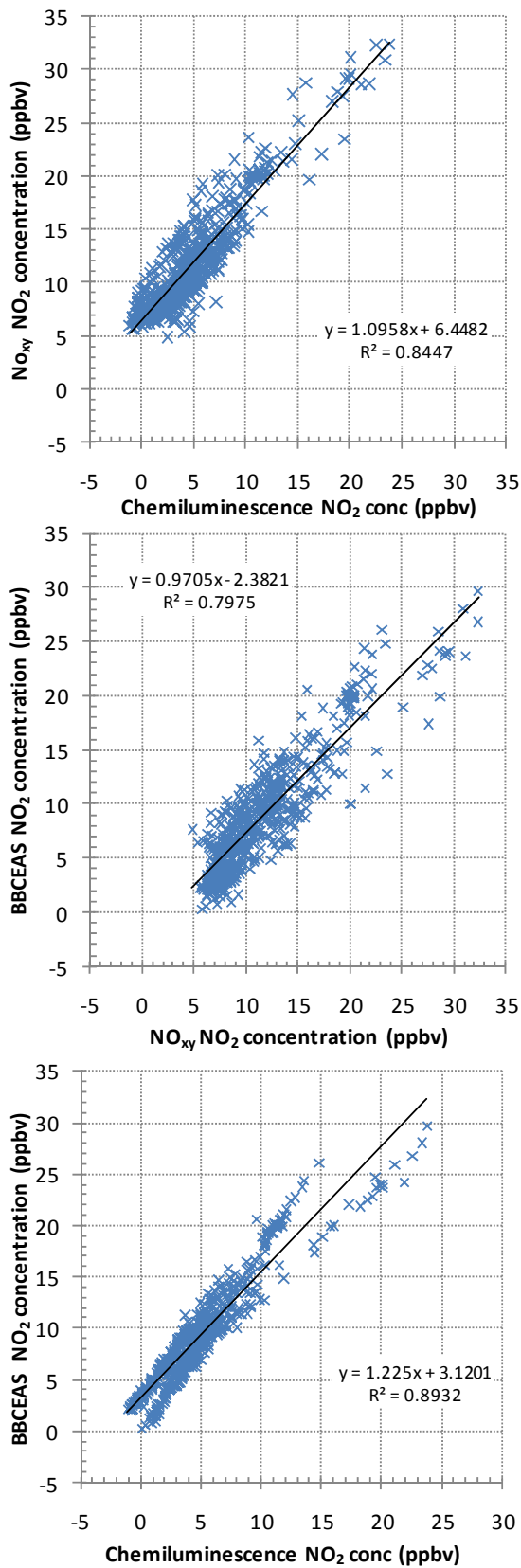


Figure 6.33. The correlation plots of NO₂ measurements made by the BBCEAS, NO_{xy} instrument and the chemiluminescence monitor. The black lines represent the linear regression of the correlation.

6.8 Summary and conclusions

In this chapter the BBCEAS instrument has been shown to be capable of detecting rapidly varying concentrations of NO_2 in the ambient atmosphere on the minute timescale, during measurement campaigns spanning several weeks. The BBCEAS reports NO_2 concentrations that follow the typical diurnal pattern for NO_x in an urban atmosphere. A comparison of NO_2 measurements made between the BBCEAS, NO_{xy} and Leicester City Council chemiluminescence instruments shows a broad general agreement across the three techniques, but systematic differences were also apparent in the LAMP data set. These discrepancies may be due to other nitrogen compounds being converted into NO_2 within instrumentation to produce a false positive NO_2 signal, in similar manner to the discrepancies observed by Dunlea and Ordenez in previous field inter comparisons and attributed to nitric acid and PAN. However, this cannot explain why the LCC commercial chemiluminescence detector consistently reported the lowest NO_2 concentrations of the three instruments. This type of interference is not present in direct spectroscopic observations of NO_2 by techniques such as BBCEAS which offer the “cleanest” measurement method for NO_2 . In order to effectively identify the causes of possible interferences, additional measurements of other oxidised nitrogen species (NO_z) need to be made alongside NO_2 . Also direct quantitative comparisons were only possible for the first week of the LAMP measurements, before the NO_{xy} inlet was moved to sample at a height of 3 m (well below the 10 m roof-top level of the BBCEAS cavity. In any future instrument inter comparisons with BBCEAS, other the instruments’ inlets need to be located as

close as possible to the BBCEAS cavity to provide the optimum comparative opportunity.

6.9 Further work with the LAMP BBCEAS dataset.

Figure 6.17 showed the absorption co-efficient for atmospheric species (at their typical ambient concentrations) that absorb within the bandwidth of the BBCEAS instrument deployed at LAMP. Since BBCEAS records the absorption spectrum of the atmospheric sample, there are potentially signals from other atmospheric absorbers present in the BBCEAS spectra that have yet to be identified. Figure 6.17 shows the two most obvious other absorbers in this wavelength region: water vapour and glyoxal.

Water vapour is not a particularly interesting trace gas from the chemical perspective, and anyway there are more efficient ways to measure ambient water concentrations. However, as used extensively in the last chapter, retrieval of water vapour mixing ratios from BBCEAS spectra that quantitatively match relative humidity measurements from meteorological detectors provides an extra quality assurance and suggests the BBCEAS method is also providing highly quantitative measurements of its other target absorbers. Water vapour's absorption at blue wavelengths is almost an order of magnitude weaker than at the green wavelengths used to detect I_2 , and so fitting of the LAMP spectra for water vapour was not usually performed. However an example of a BBCEAS water vapour spectrum and retrieval is shown in figure 6.26 for a 15 min averaged BBCEAS measurement from the evening of 24th July 2007. Water's band head at 443nm (and to a lesser extent at 470 nm) are clearly visible in the BBCEAS spectrum, and the retrieved water mixing ratio of 1.44% is reasonable for the conditions of the LAMP dataset. Moreover this spectrum give an indication of how

large the absorption signals due to any additional species would have to be for viable retrieval from the BBCEAS data from LAMP. Figure 6.17 shows that the differential spectral structure due to 500 pptv of glyoxal is of a similar size to the differential structure due to approx 1% water vapour that can be seen in BBCEAS spectrum of figure 6.34.

Thus if glyoxal were present above 500 pptv during the LAMP campaign, the BBCEAS instrument (as deployed at LAMP) ought to be capable of quantifying it. Indeed, further development work in the Ball group has demonstrated BBCEAS detection of glyoxal with detection limits of around 50 pptv in 1 minute (under ideal lab conditions). The wholesale re-analysis of the LAMP BBCEAS dataset for glyoxal might make a good undergraduate research project, but is beyond the scope of this thesis. Nevertheless it could be done.

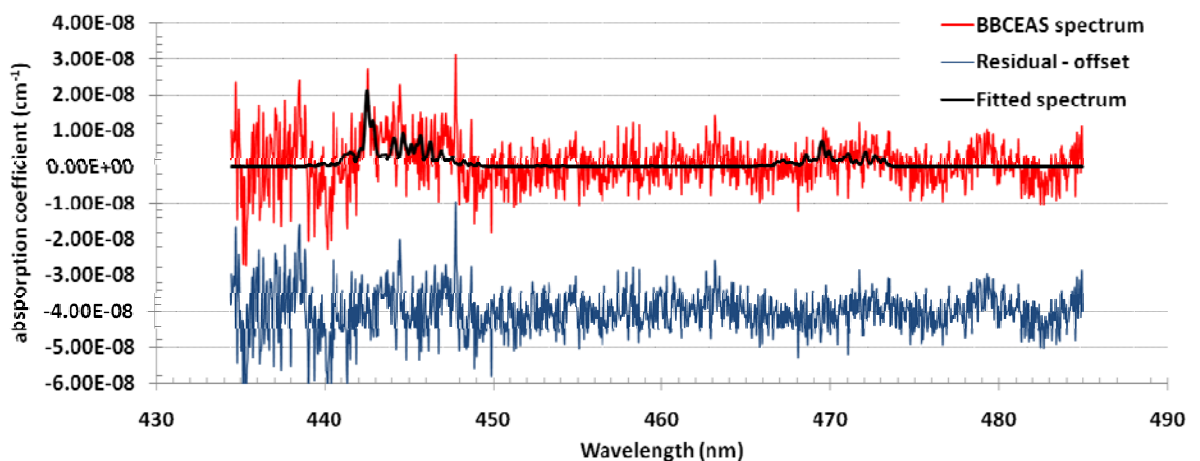


Figure 6.34. BBCEAS spectrum fitted for water vapour (residual spectrum remaining after subtraction of the aerosol continuum fitted NO₂ absorption). 15 min averaged data. Mixing ratio of water vapour = 0.0144 +/- 1.539x10⁻³ from 24th July evening running period. The standard deviation of the residual spectrum is 5.95x10⁻⁹ cm⁻¹, and is shown offset from the BBCEAS spectrum by 4x10⁻⁸ cm⁻¹.

Chapter 7

Conclusions

This work performed in this thesis involved the development and deployment of LED BBCEAS to make direct measurements of trace gas species in the atmosphere. The LED light source provides a compact, energy efficient broadband spectrum enabling measurements to be recorded over wavelength bandwidths of 40-50 nm. The wavelength resolved BBCEAS spectra are analysed using the DOAS method to unambiguously identify absorber species over the bandwidth of the measurements. The *in situ* methods employed to determine the cavity mirror reflectivity for each BBCEAS optical alignment enables the presence of absorbing species to be absolutely quantified.

The instrument development work described in chapter 3 involved investigation into the best possible LED and cavity mirror combinations of those commercially available for monitoring chemically important atmospheric absorbers. The proof-of-principle BBCEAS instrument for measuring HONO was constructed, however the LED and cavity mirrors ($R_{\text{peak}} = 0.995$) available at the time of the work were not efficient enough to produce a viable field instrument. The development of a field LED BBCEAS instrument operating at visible wavelengths to monitor RHS species in the marine boundary layer was successful due to the wider availability of well suited instrument components. The availability of cavity mirrors with very high reflectivity ($R_{\text{peak}} = 0.9995$) and LEDs with bright emission spectra at visible wavelengths where key atmospheric species have absorption structure, enabled the construction of I_2 and NO_2 monitoring BBCEAS.

The first field deployment of the I₂ monitoring BBCEAS onboard RSS Discovery during the D319 cruise, chapter 4, experienced particularly harsh operating conditions, as such the BBCEAS operated at less than optimal sensitivity. The experience proved a valuable learning experience for the operation of the field BBCEAS instrument and led to modifications of the instrument which enabled later field campaigns to be successful, recording high quality data to over extended operating periods.

The modified I₂ monitoring BBCEAS instrument was deployed at Mace head, in 2007 during BIOFLUX II, the measurements are presented in chapter 5, and the main results from the measurements are presented here:

1. The results have demonstrated the LED BBCEAS instrument is capable of monitoring I₂ in the marine boundary layer. Iodine mixing ratios of up to 608 pptv for 2 minute analysis and 280 pptv for 10 minute analyses, observed during the spring tide at night.
2. Elevated I₂ mixing ratios always coincided with night low tides, and no iodine was detected during day time measurements. The absence of daytime iodine was supported by the LIF IO measurements which suggested iodine was photolysed and reacted to form IO before it could be transported to the BBCEAS for detection.
3. The magnitude of the iodine mixing ratios observed during the different parts of the tidal cycle strongly suggest the source of iodine is the seaweeds growing

at the lowest part of the tidal fetch which are only exposed during and close to the spring tides.

4. Comparison of BBCEAS measurements with a concurrently operated LP DOAS showed iodine elevation episodes were observed at similar times for both instruments; however the BBCEAS measured higher mixing ratios and observed iodine on nights when the LP DOAS did not. The difference in observed iodine mixing ratio was due to the different spatial resolutions of the two instruments, and further supports the theory of “hot spots” of iodine emissions from the different types of seaweed growing on the shore line exposed only during the lowest tides.

In chapter 6, the LAMP campaign allowed a comparison between BBCEAS, a NO_{xy} instrument and Leicester City Council’s chemiluminescence instruments. A general agreement across the three techniques was observed, with systematic differences occurring regularly, possibly due to interference from nitrogen compounds being converted into NO_2 within instrumentation, producing false positive NO_2 observations in the non-spectroscopic techniques. The identification of the possible interference species was not possible, as additional measurements of oxidised nitrogen species was not undertaken. There was a strong correlation between the calculated “interference” and ambient ozone during LAMP. This strongly suggests that interference species (nitric acid and alkyl and multifunctional alkyl nitrates) proposed by Dunlea, may act within the NO_{xy} instrument to give higher NO_2 concentrations.

The BBCEAS measurements were capable of monitoring the rapidly varying NO₂ concentration on the minute timescale for a measurement period of 3 weeks, sampling virtually continuously.

The results presented here demonstrated the ability of BBCEAS to retrieve high quality measurements of absorber species in both the marine and urban boundary layer. The improvements to the instrumentation following its first field deployment vastly improved the sensitivity of field measurements; however there is still scope for additional hardware improvements which would lead to even better instrument performance. Further improvements in sensitivity of the BBCEAS operating to monitor I₂, may also enable OIO concentrations to be retrieved from the data sets recorded. The possibility of measuring HONO in the atmosphere has now been realised by the Langridge et al [Langridge et al., 2009] at the University of Cambridge, following improvements in LED light sources at UV wavelengths and more efficient cavity mirror surface coatings.

The LED BBCEAS technique and its application for monitoring atmospheric absorbers has been shown to be accurate and reliable in a number of studies and the technique has potential to be extended into other wavelength bandwidths as the LED and cavity mirrors are developed by manufacturers.

References

- AURN DEFRA (2009), UK Automatic Urban and Rural Network (AURN) website, Available from: <http://aurn.defra.gov.uk/>
- Alicke, B., K. Hebestreit, J. Stutz, and U. Platt (1999), Iodine oxide in the marine boundary layer, *Nature*, *397*, 572-573.
- Allan, J., G. Mcfiggans, and J. M. Plane (2000), Observations of IO in the remote marine boundary layer, *Journal of Geophysical Research*, *105*(D11), 14363-14369.
- Baker, a. R., C. Tunnicliffe, and T. D. Jickells (2001), Iodine speciation and deposition fluxes from the marine atmosphere, *Journal of Geophysical Research*, *106*(D22), 28743-28749.
- Ball, S. M., A. M. Hollingsworth, J. Humbles, C. Leblanc, P. Potin, and G. Mcfiggans (2010), Spectroscopic studies of molecular iodine emitted into the gas phase by seaweed, *Atmospheric Chemistry and Physics*, (2004), 6237-6254.
- Ball, S. M., J. M. Langridge, and R. L. Jones (2004), Broadband cavity enhanced absorption spectroscopy using light emitting diodes, *Chemical Physics Letters*, *398* (1-3), 68-74, doi:10.1016/j.cplett.2004.08.144.
- Ball, S. M., and R. L. Jones (2003), Broad-band cavity ring-down spectroscopy, *Chem. Rev*, *103*, 5239-5262.
- Bitter, M., S. M. Ball, I. M. Povey, and R. L. Jones (2005), A broadband cavity ringdown spectrometer for in-situ measurements of atmospheric trace gases, *Atmospheric Chemistry and Physics*, *5*, 2547-2560.
- Bloss, W. J. et al. (2005), Impact of halogen monoxide chemistry upon boundary layer OH and HO₂ concentrations at a coastal site, *Geophys, Geophysical Research Letters*, *32*, L06814.
- Brown, S. S. (2003), Absorption spectroscopy in high-finesse cavities for atmospheric studies, *Chem. Rev*, *103*, 5219-5238.
- Burkholder, J. B., J. Curtius, A. R. Ravishankara, E. R. Lovejoy, and N. Oceanic (2004), Laboratory studies of the homogeneous nucleation of iodine oxides, *Atmospheric Chemistry and Physics*, *4*, 19-34.
- Carpenter, L. J. (2003), Iodine in the Marine Boundary Layer, *Chemical Reviews*, *103*(12), 4953-4962.
- Carpenter, L. J., K. Hebestreit, U. Platt, and P. Liss (2001), Coastal zone production of IO precursors: A 2-dimensional study, *Atmos. Chem. Phys.*, *1*, 9-18.

Coe, H. et al. (2006), Chemical and physical characteristics of aerosol particles at a remote coastal location, Mace Head, Ireland, during NAMBLEX, *Atmospheric Chemistry and Physics*, 3289-3301.

DEFRA (2010), DEFRA 2010, Available from:
<http://www.defra.gov.uk/environment/quality/air/airquality/eu-int/conventions/gothenburg.htm>

Davis, D., J. Crawford, S. Liu, S. McKeen, A. Bandy, D. Thornton, F. Rowland, and D. Blake (1996), Potential impact of iodine on tropospheric levels of ozone and other critical oxidants, *Journal of Geophysical Research*, 101, 2135-2147.

Daykin, E. P., and P. H. Wine (1990), Rate of Reaction of IO Radicals With Dimethylsulfide, *Journal of Geophysical Research*, 95(D11), 18547-18553.

Dixneuf, S., A. A. Ruth, S. Vaughan, R. M. Varma, and J. Orphal (2009), The time dependence of molecular iodine emission from *Laminaria digitata*, *Atmospheric Chemistry and Physics*, 9, 823-829.

Dunlea, E. J. et al. (2007), Evaluation of nitrogen dioxide chemiluminescence monitors in a polluted urban environment, *Atmospheric Chemistry and Physics*, 7, 2691-2704.

Engeln, R., G. Berden, R. Peeters, and G. Meijer (1998), Cavity enhanced absorption and cavity enhanced magnetic rotation spectroscopy, *Review of Scientific Instruments*, 69 (11), 3763-3769.

European Commission Environment (2010), European Commission Environment, [online] Available from:
http://ec.europa.eu/environment/air/index_en.htm

Febo, A., C. Perrino, M. Gherardi, and R. Sparapani (1995), Evaluation of a high-purity and high stability continuous generation system for nitrous acid., *Environmental Science & Technology*, 29, 2390-2395.

Fiedler, S. (2003), Incoherent broad-band cavity-enhanced absorption spectroscopy, *Chemical Physics Letters*, 371(3-4), 284-294.

Gall, E. A., F. C. Kupper, and B. Kloareg (2004), A survey of iodine content in *Laminaria digitata*, *Botanica Marina*, 47, 30-37.

Garland, J. a., and H. Curtis (1981), Emission of Iodine From the Sea Surface in the Presence of Ozone, *Journal of Geophysical Research*, 86(C4), 3183-3186.

Gherman, T., S. Venables, S. Vaughan, J. Orphal, and A. A. Ruth (2004), Incoherent broad band cavity enhanced absorption spectroscopy in the near UV: application to HONO and NO₂, *Environmental Science & Technology*, 42, 890-895.

Gravestock, T., M. a. Blitz, and D. E. Heard (2005), Kinetics study of the reaction of iodine monoxide radicals with dimethyl sulfide, *Physical Chemistry Chemical Physics*, 7(10), 2173

Gwynn, R., R. Burnett, and G. Thruston (2000), Time-Series Analysis of Acidic Particulate Matter and Daily Mortality, *Environmental Health*, 108(2), 125-133.

Heard, D. E. et al. (2006), The North Atlantic Marine Boundary Layer Experiment (NAMBLEX). Overview of the campaign held at Mace Head, Ireland, in summer 2002, *Atmospheric Chemistry and Physics*, 2241-2272.

Hermans, C. (2008), Measurement of absorption cross sections and spectroscopic molecular parameters: O₂ and its collision induced absorption, *Belgian Institute for Space Aeronomy*, <http://spectrolab.aeronomie.be/o2.htm>.

Hoffmann, T., C. D. O'Dowd, and J. H. Seinfeld (2001), Iodine oxide homogeneous nucleation: An explanation for coastal new particle production, *Geophysical Research Letters*, 28(10), 1949.

Kebabian, P. L., S. C. Herndon, and A. Freedman (2005), Detection of nitrogen dioxide by cavity attenuated phase shift spectroscopy, *Anal. Chem*, 77, 724-728.

Kley, D., J. W. Drummond, M. McFarland, and S. Liu (1981), Tropospheric Profiles of NO_x, *Journal of Geophysical Research*, 86, 3153-3161.

Küpper, F. C. et al. (2008), Iodide accumulation provides kelp with an inorganic antioxidant impacting atmospheric chemistry., *Proceedings of the National Academy of Sciences of the United States of America*, 105(19), 6954-8.

Küpper, F. C., N. Schweigert, E. Ar Gall, J. Legendre, H. Vilter, and B. Kloareg (1998), Iodine uptake in Laminariales involves extracellular, haloperoxidase-mediated oxidation of iodide, *Planta*, 207(2), 163-171.

Langridge, J. M., R. J. Gustafsson, P. T. Griffiths, R. A. Cox, R. M. Lambert, and R. L. Jones (2009), Solar driven nitrous acid formation on building material surfaces containing titanium dioxide: A concern for air quality in urban areas?, *Atmospheric Environment*, 43, 5128-5131.

Langridge, J. M., S. M. Ball, and R. L. Jones (2004), *Development of an led-based broadband cavity enhanced absorption spectrometer for atmospheric studies*.

Langridge, J. M., S. M. Ball, and R. L. Jones (2006), A compact broadband cavity enhanced absorption spectrometer for detection of atmospheric NO₂ using light emitting diodes., *The Analyst*, 131(8), 916-22.

Lee, J. D. et al. (2009), Reactive Halogens in the Marine Boundary Layer (RHAMBLe): the tropical North Atlantic experiments, *Atmospheric Chemistry and Physics Discussions*, 9, 21717-21783.

Leigh, R. J. et al. (2009), Measurements and modelling of molecular iodine emissions, transport and photodestruction in the coastal region around Roscoff, *Atmos. Chem. Phys. Discuss*, 9, 21165-21198.

Li, Y. Q. (2004), Measurement of formaldehyde, nitrogen dioxide, and sulfur dioxide at Whiteface Mountain using a dual tunable diode laser system, *Journal of Geophysical Research*, 109(D16), 1-11.

Mahajan, A. S., H. Oetjen, A. Saiz-Lopez, J. D. Lee, G. B. McFiggans, and J. M. Plane (2009), Reactive iodine species in a semi-polluted environment, *Geophysical Research Letters*, 36(16), 6-11.

Marley, J. S. Gaffney, R. V. White, L. Rodriguez-Cuadra, S. E. Herndon, E. Dunlea, R. M. Volkamer, L. T. Molina, and M. J. Molina (2004), Fast gas chromatography with luminol chemiluminescence detection for the simultaneous determination of nitrogen dioxide and peroxyacetyl nitrate in the atmosphere, *Review of Scientific Instruments*, 75(11), 4595.

McFiggans, G. et al. (2004), Direct evidence for coastal iodine particles from *Laminaria* macroalgae – linkage to emissions of molecular iodine, *Atmospheric Chemistry and Physics*, (2), 701-713.

McFiggans, G. et al. (2010), Iodine-mediated coastal particle formation: an overview of the Reactive Halogens in the Marine Boundary Layer (RHAMBLe) Roscoff coastal study, *Atmospheric Chemistry and Physics*, 2975-2999.

NUI GALWAY (2009.), Mace Head atmospheric research station website: Atmospheric & Environmental Physics Cluster web site. Available from: <http://www.macehead.org>

Nakano, Y., S. Enami, S. Nakamichi, S. Aloisio, S. Hashimoto, and M. Kawasaki (2003), Temperature and Pressure Dependence Study of the Reaction of IO Radicals with Dimethyl Sulfide by Cavity Ring-Down Laser Spectroscopy, *The Journal of Physical Chemistry A*, 107(33), 6381-6387.

O'Dowd, C. D., J. Jimenez, R. Bahreini, R. Flagan, J. H. Seinfeld, K. Hameri, L. Pirjola, M. Kulmala, S. G. Jennings, and T. Hoffmann (2002), Marine aerosol formation from biogenic iodine emissions, *Nature*, 417(June), 632-635.

O'Dowd, C. D., and T. Hoffmann (2005), Coastal New Particle Formation: A Review of the Current State-Of-The-Art, *Environmental Chemistry*, 2(4), 245.

Ordonez, C., A. Richter, M. Steinbacher, C. Zellweger, H. Nub, J. P. Burrows, and A. S. Prevot (2006), Comparison of 7 years of satellite-borne and ground-based tropospheric NO₂ measurements around Milan, Italy, *Journal of Geophysical Research*, 111(2), D05310.

Osthoff, H. D. et al. (2006), Measurement of Atmospheric NO₂ by pulsed cavity ring-down spectroscopy, *Journal of Geophysical Research*, 111(D12), 1-10.

Pechtl, S., J. Zhang, E. R. Lovejoy, and J. B. Burkholder (2006), Modeling the possible role of iodine oxides in atmospheric new particle formation, *Atmospheric Chemistry and Physics*, 6, 505-523.

Peters, C., S. Pechtl, J. Stutz, K. Hebestreit, K. G. Heumann, A. Schwarz, J. Winterlik, U. Platt, and O. Sciences (2005), Reactive and organic halogen species in three different European coastal environments, *Atmospheric Chemistry and Physics*, 5, 3357-3375.

Saiz-Lopez, A., J. M. Plane, G. Mcfiggans, P. I. Williams, S. M. Ball, M. Bitter, R. L. Jones, C. Hongwei, and T. Hoffmann (2006), Modelling molecular iodine emissions in a coastal marine environment: the link to new particle formation, *Atmos. Chem. Phys.*, 6, 883-895.

Saiz-Lopez, A., R. W. Saunders, D. M. Joseph, S. H. Ashworth, and J. M. Plane (2004), Absolute absorption cross-section and photolysis rate of I₂, *Atmos. Chem. Phys.*, 4, 1443-1450.

Saiz-Lopez, A., and J. M. Plane (2004), Novel iodine chemistry in the marine boundary layer, *Geophys. Geophysical Research Letters*, 31, L04112.

Scherer, J. J., J. B. Paul, A. O. Keefe, and R. J. Saykally (1997), Cavity Ringdown Laser Absorption Spectroscopy: History, Development, and Application to Pulsed Molecular Beams, *Chem. Rev.*, 97, 25-51.

Steinbacher, M., C. Zellweger, B. Schwarzenbach, S. Bugmann, B. Buchmann, C. Ordo, A. S. Prevot, and C. Hueglin (2007), Nitrogen oxide measurements at rural sites in Switzerland: Bias of conventional measurement techniques, *Journal of Geophysical Research*, 112(2), D11307.

Thornton, J. A. (2000), Atmospheric NO₂ : In situ laser-induced fluorescence detection at parts per trillion mixing ratios, *Anal. Chem.*, 72(3), 528-539.

Thornton, J. A. (2003), Comparison of in situ and long path measurements of NO₂ in urban plumes, *Journal of Geophysical Research*, 108(D16), 1-12.

Vandaele, A. C., C. Hermans, P. C. Simon, M. Carleer, R. Colin, and B. Coquart (1998), Measurements of the NO₂ absorption cross section from 42 000 cm⁻¹ to 10 000 cm⁻¹ (238-1000 nm) at 220K and 294K, *J. Quant. Spectrosc. Radiat. transfer*, 59(3-5), 171-184.

World Health Organisation (2010), World Health Organisation, Available from: <http://www.who.int/mediacentre/factsheets/fs313/en/index.html>

Wu, T., W. Zhao, W. Chen, W. Zhang, and X. Gao (2009), Incoherent broadband cavity enhanced absorption spectroscopy for in situ measurements of NO₂ with a blue light emitting diode, *Applied Physics*, (2), 85-94.

Yoon, Y. J. et al. (2007), Seasonal characteristics of the physicochemical properties of North Atlantic marine atmospheric aerosols, *Journal of Geophysical Research*, 112, D04206.

Yoon, Y. J., W. Junkerman, P. Aalto, M. Kulmala, H. Lihavainen, and Y. Viisanen (2007), Airborne measurements of nucleation mode particles I: coastal nucleation and growth rates, *Atmospheric Chemistry and Physics*, 7, 1491-1501.

Zingler, J. (2005), Iodine oxide in the Dead Sea Valley: Evidence for inorganic sources of boundary layer IO, *Journal of Geophysical Research*, 110(D7), 1-10.